GLYCOSPHINGOLIPID PROFILING IN CELLS AND TISSUES USING
FLUORESCENT LC/MS

by

Radhika Chakraberty

A thesis submitted in partial fulfillment of the requirements for the degree of

Master of Science

Department of Chemistry
University of Alberta

ABSTRACT

Glycosphingolipids (GSLs) are a class of glycolipids characterized by two major components; an oligosaccharide chain and a ceramide lipid chain bearing a fatty acid and a sphingosine (Sph) base. Gangliosides belong to the family of GSLs whose distinguishing feature is the presence of one or more sialic acid residues in their glycan. These biomolecules play significant roles in a number of cellular processes and have been associated with the pathology of diseases such as Alzheimer's, Huntington's and type 2 diabetes. There is a need for robust methods to analyze GSLs in various biological samples accurately. A significant amount of research has been conducted to identify the analytical tools for this purpose. Unfortunately, there remain limited techniques to identify and quantify GSLs precisely, due to the structural complexity of these molecules.

This thesis has attempted to address this problem, through development of two complementary methods using enzymes to modify GSLs. The endoglycoceramidase (EGCase) enzyme cleaves the ceramide moiety, while the sphingolipid ceramide *N*-deacylase (SCDase) enzyme cleaves the fatty acid chain in the ceramide moiety to generate a lyso-GSL (*l*-GSL). Both degradation products could be labeled with a fluorophore and analyzed by LC-MS using internal standards to quantify GSL components from a variety of biological samples. The primary strength of our methods is quantification based on fluorescence. Additionally, these two methods are complementary providing information about both the oligosaccharide component of GSLs and the Sph base component in *l*-GSLs. The latter are seldom analyzed, despite studies that have shown differential expression of different Sph chains in tissues.

PREFACE

Chapter 3 is based on unpublished work within our group and collaborative projects with Dr Alexey Pshezhetsky of the Department of Biochemistry, Université de Montréal and Dr Simonetta Sipione of the Department of Pharmacology, University of Alberta. I was responsible for the glycosphingolipid analyses. Manuscripts based on **Sections 3.2, 3.3, 3.4,** and **3.6** are currently inpress, in preparation or under review. They are as follows:

Section 3.2: Demina, E., Pierre, W., Londono, I., Nguyen, A., Reiz, B., Zou, C., Chakraberty, R., Cairo, C.W., Pshezhetsky, A.V., Lodygensky, G., "Persistant reduction in sialylation of cerebral glycoproteins following post-natal inflammatory exposure", **2018**. (in press, J. Neuroinflammation)

Section 3.3: Howlader, M. A., Li, C., Zou, C., Chakraberty, R., Ebesoh, N., Cairo, C.W., "Neuraminidase-3 (NEU3) is a negative regulator of LFA-1 adhesion", **2018**. (in preparation)

Section 3.4: Howlader, M. A., Guo, T., Chakraberty, R., Porter, E., Cairo, C.W., "Isoenzyme-selective inhibitors of human neuraminidases reveal distinct effects on cell migration", **2018**. (in preparation)

Section 3.6: Demina, E., Smutova, V., Fougerat, A., Pan, X., Guo, T., Zou, C., Chakraberty, R., Snarr, B., Sheppard, D., Shiao, C., Roy, R., Orekhov, A. N., Miyagi, T., Laffargue, M., Cairo, C.W., Pshezhetsky, A.V., "Inhibitors of neuraminidases 1 and 3 as potential candidates for treating atherosclerosis", **2018**. (under review)

In loving memory of my late grandfather,

Nirmal Chandra Chakraborti (1931-2018)

I will be eternally grateful to him for his wisdom, tutelage, patience,

kind-heartedness, and for teaching me how to smile even in the face of

adversities.

ACKNOWLEDGEMENTS

There are a number of people I would like to acknowledge, without whom my journey as a graduate student would not have been successful. First and foremost, I would like to extend my gratitude to my supervisor, Dr. Christopher Cairo, for his patience, guidance, encouragement, and constant support over the past three years. I thank him for being such a great mentor, helping me grow both professionally and personally. I would also like to extend my gratitude to my supervisory committee members, Dr. Todd Lowary and Dr. Liang Li, for helpful insights into my research and for providing guidance and support throughout the past three years. Finally, I thank Dr. Florence Williams for taking the time out to be part of my defense committee.

This work would not have been possible without Bela Reiz, who has shown utmost patience while helping me run countless samples every week. Additionally, he has provided scientific input in method development that was required for this work to be successful. I thank Ruixhang (Blake) Zheng for training me in protein production and helping me troubleshoot whenever I ran into problems. I also thank the Waters Corporation Inc., for supplying reagents and providing helpful discussions. Finally, I extend my heartfelt gratitude to Dr. Anna Jordan for her dedication, patience, and friendship over a rigorous month of editing my Thesis.

To all the past and present Cairo lab members, thank you for being such great colleagues and an excellent team to work with. I was lucky to have found a few good

TABLE OF CONTENTS

Chapter 1: Glycosphingolipids Structure, Nomenclature, Biosynthesis, Physiological Roles and Analytical Methods

Chapter 2: Glycan Analysis by Enzymatic Degradation of GSLs Using Endoglycoceramide Enzyme

Chapter 3: Application of Endoglycoceramidase to Glycan Analysis

Chapter 4: Lyso-glycosphingolipids Analysis by Enzymatic Degradation Using Sphingolipid Ceramide *N*-deacylase Enzyme

Chapter 5: Conclusions and Future Directions

LIST OF FIGURES

LIST OF TABLES

LIST OF ABBREVIATIONS

2-AA	2-amino benzoic acid
2-AB	2-amino benzamide
2-AP	2-aminopyridine
3'-SL	3'-sialyllactose
4MU-NANA	2-(4-Methylumbelliferyl)-α-D-N-acetylneuraminic acid
ABEE	Aminobenzoic acid ethyl ester
APCI	Atmospheric pressure chemical ionization
ApoE	Apoliprotein E
Arg	Arginine
Asp	Aspartic acid
Aβ	Amyloid beta
BCA	Bicinchonic acid
BCR	B-cell receptor
BODIPY	4,4-difluoro-4-bora-3α,4α-diaza-s-indacene
CAZymes	Carbohydrate-active enzymes
CID	Collision induced dissociation
Cer	Ceramide
CerS	Ceramide synthase
CMP	Cytidine monophosphate
CNS	Central nervous system
CoA	Co-enzyme A
CT-B	Cholera toxin-B

CytoD	Cytochalasin D
DANA	2,3-didehydro-2-deoxy-N-acetylneuraminic acid
DHCer	Dihydroceramides
DMF	Dimethyl formamide
DMSO	Dimethyl sulfoxide
E. coli	*Eshchericia coli*
EGCase	Endoglycoceramidase
EGFR	Endothelial growth factor receptor
EIC	Extracted ion chromatogram
ER	Endoplasmic reticulum
ES	External Standard
ESI	Electrospray ionization
FBS	Fetal bovine serum
FD	Fabry's disease
FLD	Fluorescence detector
FPLC	Fast protein liquid chromatography
Gal	Galactose
GalCer	Galactosylceramide
GH	Glycoside hydrolase
Glc	Glucose
GlcCer	Glucosylceramide
Glu	Glutamic acid
GMCSF	Granulocyte macrophage colony stimulating factor

GSL	Glycosphingolipid
GU	Glucose units
HD	Huntington's disease
Hex	Hexose
HexNAc	*N*-acetylglucosamine
HILIC	Hydrophilic interaction Liquid chromatography
HMO	Human milk oligosaccharide
hNEU	Human Neuraminidase enzymes
HPLC	High performance liquid chromatography
HPTLC	High performance thin layer chromatography
HR	High resolution
HTT	Huntingtin protein
ICAM	Intercellular adhesion molecule
IFN- γ1b	Interferon-gamma1b
IL-10	Interleukin 10
IL-6	Interleukin 6
IMS	Imaging mass spectrometry
IR	Insulin receptor
IS	Internal Standard
IUPAC	International Union of Pure and Applied Chemistry
LacCer	Lactosylceramide
LC	Liquid chromatography
LDL	Low-density lipoprotein

LFA-1	Lymphocyte function antigen-1
LOD	Limit of detection
LOQ	Limit of quantitation
LPC	Lysophosphatidylcholine
LPS	Lipopolysaccharide
LTQ	Linear trap quadropole
MAG	Myelin associated glycoprotein
MALDI	Matrix assisted laser desorption/ionization
MCSF	Macrophage colony stimulating factor
MRM	Multiple reaction monitoring
MS	Mass Spectrometry
MWCO	Molecular weight cut off
NBD	7-nitrobenzo-2-oxa-1,3-diazole
NEU1	Neuraminidase-1
NEU2	Neuraminidase-2
NEU3	Neuraminidase-3
NEU4	Neuraminidase-4
Neu5Ac	*N*-acetylneuraminic acid
Neu5Gc	*N*-glycolylneuraminic acid
NKT	Natural killer T-cells
NP	Normal phase
OPA	o-phthaldialdehyde
PBS	Phosphate buffer saline

PC	Phosphaditylcholine
PC-3	Prostate cancer cells
PE	Phosphatidylethanolamine
Phyto-SPH	Phyto-sphingosine
PI	Phosphatidylinositol
PMA	Phorbol 12-myristate 13-acetate
PSA	Polysialic acid
Py	Pyloma virus
RCC	Renal cell carcinoma
RP	Reverse phase
RSE	Relative standard error
RT	Room temperature
SCDase	Sphingolipid ceramide *N*-deacylase
SD	Standard deviation
SEM	Standard error of mean
Sia	Sialic acid
SIMS	Secondary ion mass spectrometry
SM	Sphingomyelin
SNFG	Symbol nomenclature for glycans
SPA	Sphinganine
SPE	Solid phase extraction
Sph	Sphingosine
SphK	Sphingosine kinase

SPT	Serine palmitoyltransferase
ST	Sialyltransferase
Stx	Shiga toxin
TGFβ1	Transforming growth factor beta-1
TIC	Total ion chromatogram
TLC	Thin layer chromatography
TLR	Toll like receptor
TNFα	Tumor necrosis factor alpha
TOF	Time of flight
Trp	Tryptophan
UDP	Uridine diphosphate
UV	Ultraviolet
WAX-RP	Weak anion exchange-reverse phase
β-ME	Beta-mercaptoethanol

CHAPTER 1

GLYCOSPHINGOLIPID STRUCTURE, NOMENCLATURE, BIOSYNTHESIS, PHYSIOLOGICAL ROLES AND ANALYTICAL METHODS

1.1 INTRODUCTION

According to the Fluid Mosaic Model, the plasma membrane of all vertebrate cells is a thin structure endowed with a lipid bilayer interspersed with protein molecules.[5] These protein molecules remain afloat within the double lipid layer forming a mosaic pattern; the name "fluid mosaic" was coined based on this property.[2, 5, 7] The lipid bilayer is dominated mostly by phospholipids, along with glycolipids, cholesterol, and lipid rafts in low abundance. Glycolipids bear a carbohydrate moiety along with a lipid chain. Despite constituting only about 5% of membrane lipids, they are essential molecules owing to a variety of different physical and chemical properties that are unique to this class of biomolecules.[2-3]

Glycosphingolipids (GSLs) are the most common form of glycolipids found in vertebrate cell membranes. Structurally they are similar to sphingolipids with their lipid backbone being made up of a ceramide (Cer) moeity, bearing a sphingosine (Sph) base attached to a fatty acid chain via an amide bond.[8-9] Different cells and tissues have variable amounts of GSLs, the highest abundance being in neuronal cells where GSLs occur as gangliosides.[3, 10-11]

Gangliosides are a sub-class of GSLs characterized by the same carbohydrate moiety and ceramide lipid backbone; however, the distinguishing feature between them is the presence of sialic acid residues in gangliosides.[10, 12] Sialic acid was isolated in 1936 from bovine submaxillary mucin[13], and its structure was determined to be an exact match with a sugar containing 9-carbon atoms called *N*-acetylneuraminic acid.[12, 14-15] This characteristic feature makes gangliosides acidic in nature and renders these molecules important players in cell proliferation, cell signaling, and various cell-cell interactions,

which are essential for the proper functioning of a living organism.[16] The structural complexity and variability of GSLs makes their analysis challenging.[17-18] This chapter will outline the structure, biosynthesis, biological roles, and analytical methods employed in order to investigate the biological significance of GSLs and why the scientific community needs better strategies to understand and analyze them.

1.2 MAJOR CLASSES, STRUCTURE AND NOMENCLATURE

As mentioned earlier, GSLs are amphiphilic molecules that possess a polar carbohydrate chain attached to a long hydrophobic Cer lipid backbone. Their carbohydrate moiety can vary in structure, linkage, and anomeric configuration, while the Cer backbone can show variability in chain length and saturation for both the fatty acid and Sph base components.[3] Although there have been instances of 16- and 20-carbon Sph chains, in mammalian systems, D-*erythro*-sphingosine (d18:1) is the most common form of Sph with 18-carbon atoms and one unsaturation in its chain.[19-20] The fatty acid counterparts also are highly variable in chain length (14–30 carbon atoms), saturation, and hydroxylation.[2]

Considering their incredible diversity in structure, GSLs have a very complicated chemical nomenclature. Thus, for the sake of convenience, they are named and categorized based only on their carbohydrate/glycan structure.[21] The IUPAC (International Union of Pure and Applied Chemistry) system of nomenclature classifies GSLs into seven different categories, namely ganglio-, lacto-, neolacto-, globo-, isoglobo- , mollu-, and arthro- series, depending on their sugar/glycan core structure **(Figure 1–2)**. This system takes into account the order of linkages between adjacent monosaccharides

in a complex GSL structure. GSLs possessing the same sugar core are said to belong to a particular series, which is defined by the respective core structure.[2] The official IUPAC system of nomenclature of GSLs is cumbersome and hence is not applied very often.[22] Svennerholm introduced a simplified convention of nomenclature, using abbreviated forms for GSLs according to their order of chromatographic separation. Taking the example of ganglioside Galβ1-3GalNAcβ1-4(Neu5Acα2-3)Galβ1-4GlcβCer, this was designated "GM1", where G indicates the ganglioside series, the second letter indicates the number of sialic acid residues (M for mono, D for di, T for tri etc.), and the number at the end indicates the order of chromatographic separation in a thin-layer chromatography (TLC) experiment i.e. GM1 migrates least, followed by GM2, and GM3 **(Figure 1–1)**.[23]
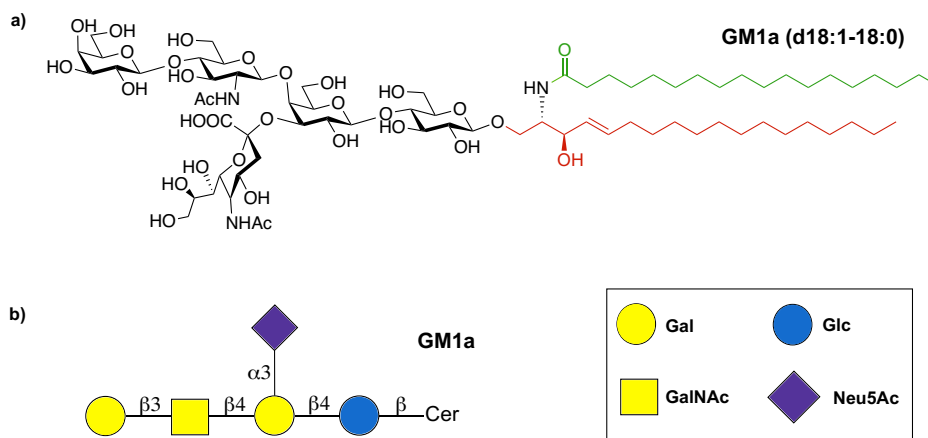
Figure 1– 1. (a) Structure of ganglioside GM1a (d18:1 – 18:0), where d18:1 denotes the 18-carbon sphingosine base with one double bond shown in red, and 18:0 denotes the 18-carbon fatty acid chain with no double bonds shown in green;[24] (b) Symbol nomenclature for glycan (SNFG) representation of GM1[25] (Adapted from the works of Fahy et al [24] and Varki et al [25])

Series	Symbol	Sugar core
Ganglio	Gg	Gal β3 GalNAc β4 Gal β4 Glc
Lacto	Lc	Gal β3 GlcNAc β3 Gal β4 Glc
Neolacto	nLc	Gal β4 GlcNAc β3 Gal β4 Glc
Globo	Gb	GalNAc β3 Gal α4 Gal β4 Glc
Isoglobo	iGb	GalNAc β3 Gal α3 Gal β4 Glc
Mollu	Mu	GlcNAc β2 Man α3 Man β4 Glc
Arthro	At	GalNAc β4 GlcNAc β3 Man β4 Glc

GalNAc   Glc   Gal   GlcNAc   Man
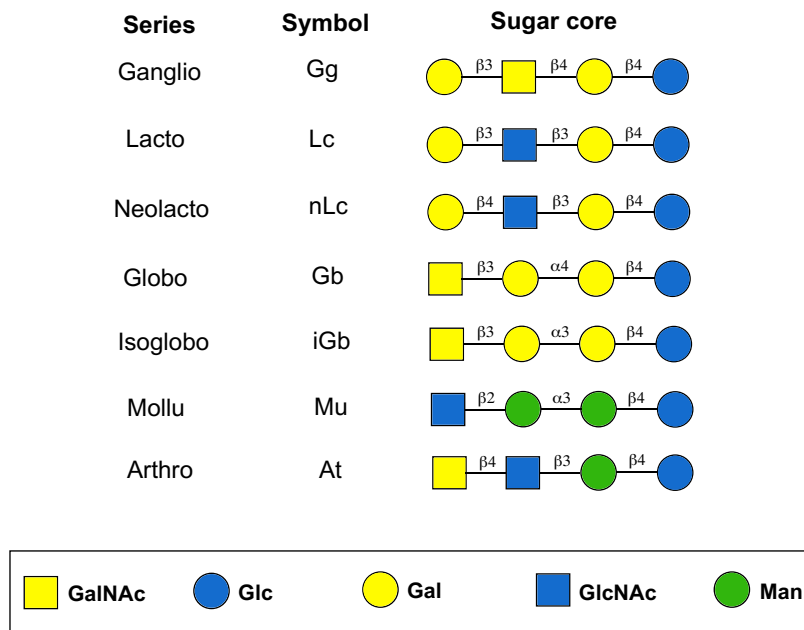
Figure 1– 2. Seven different categories of GSLs found in biological systems, with their respective symbols defined by their unique neutral sugar core structure. The ganglio (Gg) series also have one or more sialic acid residues (Neu5Ac) denoted by a purple diamond, as show in Figure 1–1.[2] (Adapted from the Essentials of Glycobiology[2])

1.3 OCCURRENCE

GSLs are found in a range of different cells, tissues, and bodily fluids depending on the expression of enzymes responsible for their biosynthesis. Gangliosides are enriched primarily in brain cells where they comprise ~12% of the total lipid content with a higher abundance in the gray matter over white matter.[26-27] Studies have shown their expression levels to be different at different stages of brain development. Simpler gangliosides, such as GM3 and GD3, are more prevalent during early stages of development.[28] As the brain ages progressively, complex gangliosides, such as GD1a, GT1a, and GQ1a become more common.[29] These changes contribute to subtle functional consequences, such as,

5

improvement in synaptic activity of neurons in the brain.[30] The ceramide backbone also has shown variable degrees of occurrence and expression in different regions of the brain.[31-32] For example, in mice, C18 Sph chains were widespread in the frontal region of the brain while C20 was more prevalent in the hippocampal region.[33] The fatty acid chains in gangliosides usually are saturated. α-hydroxylated fatty acids are more common in the liver, intestine, and kidneys than in the brain.[34]

The majority of gangliosides found in human serum form part of serum lipoproteins, primarily low-density lipoproteins (LDL).[35] Common gangliosides in human serum include GM3, GD3, GM2, Gb3, Gb4, GM1 and neutral GSL lactosylceramide (LacCer).[1] Food sources, such as egg yolk, milk, and meat are rich in GD3, GM3, and GM4 gangliosides. These not only serve as commercial sources of purified gangliosides for research purposes (Avanti Polar Lipids, Inc.) but if administered to a growing infant, they can prevent infectious diseases.[36-37]

Sialic acid (Sia) residues are the distinguishing feature between neutral GSLs and gangliosides. In vertebrates, Sia exists in two different forms, namely *N*-acetylneuraminic acid (Neu5Ac) and *N*-glycolylneuraminic acid (Neu5Gc), the most prevalent being Neu5Ac.[38] The cytidine monophosphate-N-acetyl-neuraminic acid hydroxylase enzyme, responsible for conversion of CMP-Neu5Ac to CMP-Neu5Gc is inactive in humans.[39] Thus, while human tissues are devoid of glycoconjugates bearing Neu5Gc,[40-41] they are common in other organisms, such as mice, rats, and pigs.[42]

1.4 BIOSYNTHESIS

GSL biosynthesis begins in the endoplasmic reticulum (ER). Later, cellular machinery transfer them to the Golgi apparatus for further modifications.[43] Biosynthesis of GSLs is a step-by-step process of addition of carbohydrate molecules to a lipid molecule, which is facilitated by enzymes such as glycosyl transferases responsible for transferring a monosaccharide from UDP-Glc or UDP-Gal, to a Cer molecule and sialyl transferases (α2-3 and α2-8), which are responsible for transferring one or more sialic acid residues from a sugar nucleotide, i.e., CMP-sialic acid onto the growing sugar chain.[12] The process starts with the addition of a glucose (Glc) and/or galactose (Gal) molecule to Cer, forming glucosylceramide (GlcCer) and/or galactosylceramide (GalCer). Next, GlcCer is converted to lactosylceramide (LacCer) by the addition of a galactose reside from which the more complex GSLs are synthesized further along the pathway. An exception is GM4, which is synthesized directly from GalCer by the addition of one sialic acid residue. LacCer is converted first to GM3 by the addition of one sialic acid by the enzyme LacCer α2-3 sialyltransferase (ST-I), also known as GM3 synthase. Following this, GD3 and GT3 are synthesized by sialic acid addition to GM3 and GD3 by GM3 α2-8 sialyltransferase (ST-II) or GD3 synthase and GD3 α2-8 sialyltransferase (ST-II) or GT3 synthase, respectively. The gangliosides, GM3, GD3, and GT3 are converted to more complex gangliosides bearing two, three, four, and five sialic acid residues by sialyl transferases, generating three distinct ganglioside series, a-, b-, and c- series respectively. The asialo-series of gangliosides, also known as the 0-series, is synthesized following a different pathway taking LacCer as the precursor **(Figure 1–3)**.[2, 9, 16]

The pathway described above explains how the oligosaccharide chains of GSLs are synthesized. The carbohydrate moiety forms only one degree of variability in the structure of GSLs, the other degree of structural variability comes from the ceramide lipid backbone. The biosynthetic pathway for the lipid chain starts with the reaction between serine and palmitoyl-CoA catalyzed by the enzyme serine palmitoyltransferase (SPT), leading to the formation of 3-ketosphinganine.[44] Inhibition of SPT leads to disruption of ceramide biosynthesis, which has been associated with growth abnormalities in mammals eventually leading to death.[45-46] SPT is highly selective towards palmitoyl-CoA bearing 16-carbon atoms (d16:0), which explains why Sph bases of 18- and 20- carbon atoms are most common in mammals,[19, 47] even though studies have reported that fatty acyl-CoA with 16±1 carbons may function as co-substrates as well.[48-49] 3-ketosphinganine is reduced to sphinganine by a reductase enzyme. Sphinganine can either undergo N-acetylation with the preferred fatty acyl-CoA to form dihydroceramides (DHCer) [50] or can be phosphorylated to form sphinganine 1-phosphate.[51] Further along the biosynthetic pathway, action of a variety of different enzymes on DHCers can lead to the synthesis of an array of complex sphingolipids, including GSLs **(Figure 1–4)**.[11]
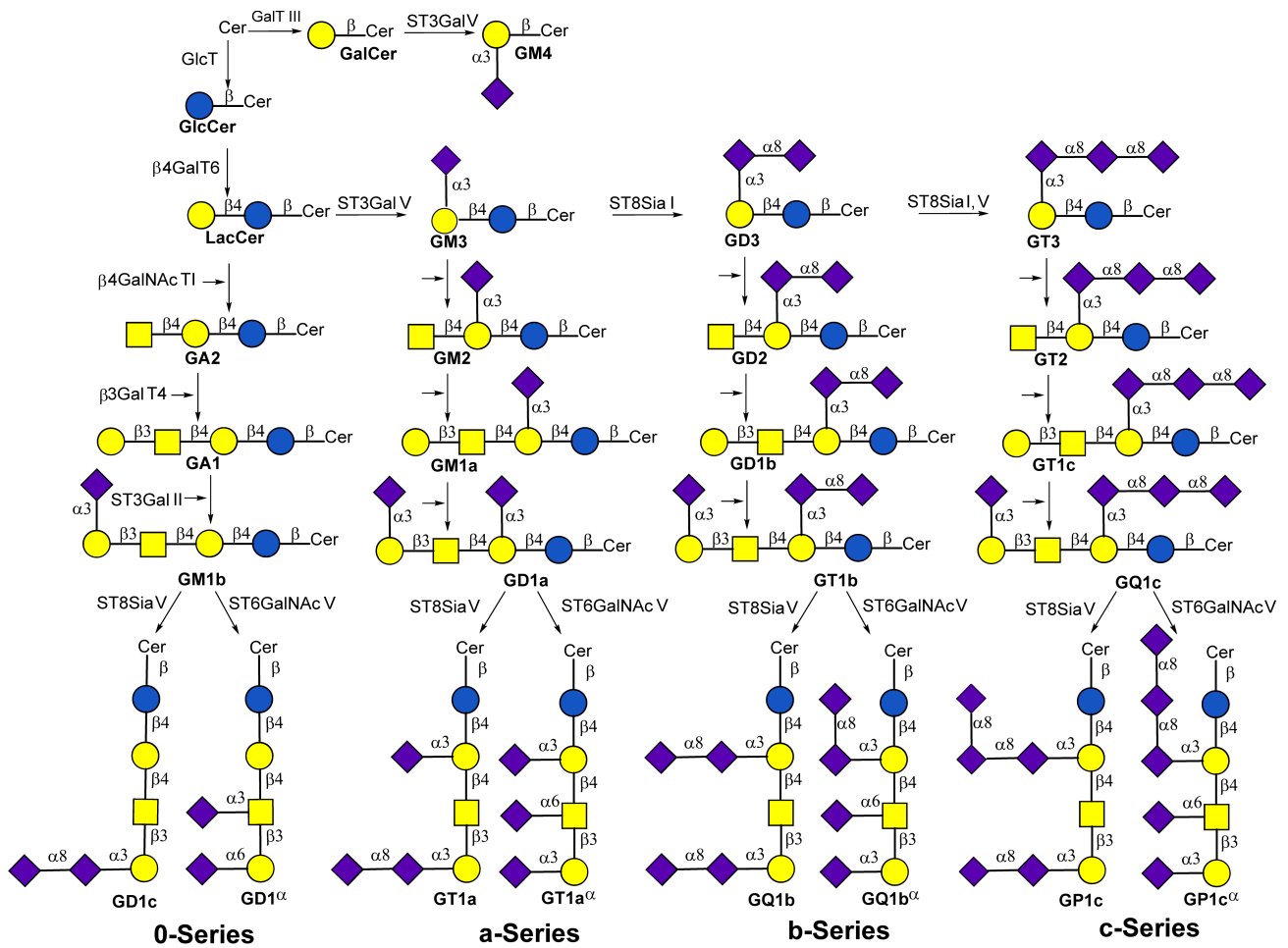
Figure 1– 3. Biosynthetic pathway of gangliosides. Four major ganglioside series, namely 0-Series, a- Series, b-Series, and c-Series are synthesized from precursors LacCer, GM3, GD3, and GT3, respectively. This stepwise synthesis is carried out by sequential addition of carbohydrate residues by the action of specific glycosyltransferases and sialyltransferases [2-3] (Adapted from Essentials of Glycobiology[2] and the works of Groux-Degroote et al[3])

9
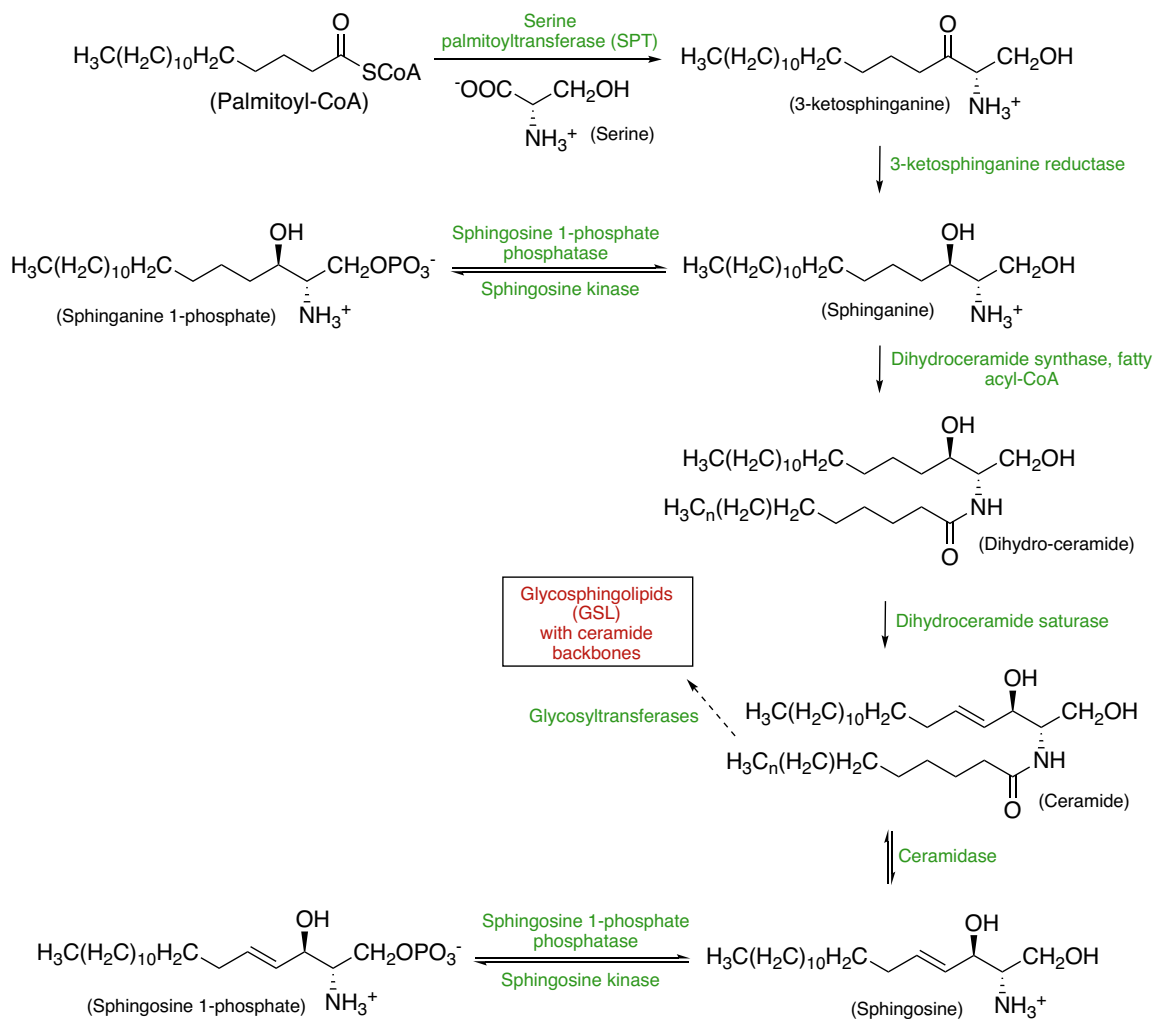
Figure 1– 4. Biosynthetic pathway for sphingolipid bases, ceramides, and complex sphingolipids. The precursors of this pathway are palmitoyl Co-A and serine, which react to form 3-ketosphinganine in the presence of the enzyme serine palmitoyltranferase (SPT). Subsequently, in a stepwise fashion, sphinganine, ceramides, and sphingosines are formed, each step being catalyzed by a specific enzyme shown in green. Ceramides take part in the biosynthesis of complex GSLs utilizing glycosyltransferase enzymes that transfer a sugar residue from sugar nucelotides such as UDP-Gal, UDP-Glc or CMP-Sia onto the acceptor ceramide molecule, as shown in Figure 1–3[11,12,1] (Adapted from the works of Merrill et al[11])

1.5 BIOLOGICAL FUNCTIONS

GSLs are known to play major roles in cell signaling, cell-cell interactions, membrane organization and function. Interestingly, their importance was a matter of debate in some early animal model studies, whereby blocking the biosynthesis of complex GSLs in mice deficient in the GM2/GD2 synthase enzymes showed no major effects on their brain functions.[52] More recently, however, similar experiments with double knock-out mice lacking GM3 and GM2 synthases caused severe neurodegeneration, ultimately leading to death. It was concluded from these experiments that GSLs are in fact essential to a healthy nervous system.[18, 53-54]

The alignment of GSLs on the surface of cell membranes is critical to their biological functions. The long Cer backbone is embedded within the lipid bilayer, while the glycan moiety extends outwardly from the plane of the lipid bilayer of the plasma membrane.[55-56] GSLs in this orientation are enriched in lipid rafts, whose organization is essential for intracellular and intercellular signaling.[18, 57-58] This orientation in lipid rafts also brings kinases and other signal transducers together, leading to the formation of "glycosynapse" or glycan-binding domains.[59-60] Consequently, lateral glycan–glycan interactions as well as glycan–protein interactions occur, thereby facilitating a variety of intercellular signaling pathways and other cellular mechanisms to take place.[59, 61]

There are two molecular mechanisms by which GSLs carry out cellular functions. They are: lateral association of GSLs with proteins on the same plasma membrane or *cis* interactions, and interactions of GSLs on one cell surface with glycan binding proteins on a different cell surface or *trans* interactions.[60-61] An example of *cis* interaction is the binding of ganglioside GM3 with insulin receptor (IR) whereby autophosphorylation and

11

other signaling mechanisms triggered by insulin are disrupted.[62-64] Similar examples of direct ganglioside–protein interactions include binding of GM3 to the endothelial growth factor receptor (EGFR), thereby inactivating the receptor while GD1a binding to EGFR increases the activity of the receptor.[65] An illustration of *trans* interaction is the interaction between glycan binding myelin-associated glycoprotein (MAG) on the inner membrane surface of the myelin sheath with gangliosides on the surface of the respective nerve cell axon that is wrapped by the myelin sheath.[66] It has been observed that complex gangliosides GD1a and GT1b serve as receptors for MAG binding, allowing effective axon-myelin interactions.[67] Knock out mice models devoid of GD1a and GT1b[68] and double knock out mice models lacking both MAG and complex gangliosides[69] suffered axon degeneration[68] and "progressive motor neuropathy". [70]

Gangliosides also function as receptors for binding microorganisms and toxins. For example, GD1a and GT1b on human erythrocytes have been reported to bind to polyoma virus (Py)[71], GM1 expressed on human epithelial cells is known to bind specifically to cholera toxin (CT) B subunit[72], and neutral GSL globotriaosyl ceramide (Gb3) expressed on human epithelial and endothelial cells binds to Shiga toxin (Stx).[73] These binding actions on the surface of the plasma membrane serve as the first step to the initiation of infection in the host cell. Many studies have implicated the involvement of GSLs in immune functions. For example, GSL components of lipid rafts have been shown to play a role in B cell antigen receptor (BCR) signaling[74-75] and neutral GSL α-GalCer has been identified as a ligand that activates natural killer T cells (NKT cells) against multiple diseases, including certain cancers.[76-77]

GSLs and gangliosides have been implicated in several human diseases. Mutations in genes responsible for the production of enzymes involved in GSL degradation lead to lysosomal storage diseases. For example, Gaucher's disease is caused by the mutation in the GlcCer processing enzyme β-glucocerebrosidase; consequences of this disease include accumulation of GlcCer in the liver and spleen.[78] Tay-Sachs disease is another lysosomal storage disease caused by mutations in the GM2 processing enzyme β-hexosaminidase, leading to accumulation of GM2, a condition known as GM2 gangliosidosis.[79]

Gangliosides also have been associated with metabolic disorders, specifically type-2 diabetes.[80] A recent study showed an increase in the overall GM3 content for individuals suffering from metabolic diseases associated with type-2 diabetes. Moreover, this study also identified the particular molecular species of GM3 bearing variable fatty acid chain lengths and/or saturation and hydroxylation, which were elevated in diseased individuals. This highlights the importance of studying the more often than not neglected Cer lipid chains in gangliosides as well.[81]

Sialic acids of gangliosides and glycoproteins serve as receptors for the common influenza virus.[82] In the process of infection, cholera toxin-B (CT-B) subunit and other toxins use gangliosides on the surface of the plasma membrane as their site of attachment to host cells.[2] Specific binding of CT-B to ganglioside GM1 has been used to study the fate of amyloid Aβ dimers associated with Alzheimer's disease in mice.[83] These, along with other *in vivo* studies have shown GM1 to bind very strongly with Aβ dimers[84] and blocking of GM1 reduced the formation of toxic Aβ fibrils associated with Alzheimer's

13

disease.[83] These studies indicate a stimulatory role of ganglioside GM1 in the initiation and progression of Alzheimer's disease.[85]

Gangliosides also have been shown to be involved in another progressive neurodegenerative disease called Huntington's disease (HD). It is caused as a result of a mutation in the gene encoding for the huntingtin (HTT) protein, leading to an elongated polyglutamine chain at the N-terminus.[86-87] *In vitro* studies on ganglioside biosynthesis showed decreased levels of gangliosides in HD neuronal cells compared to normal neuronal cells; especially GM1.[88] Exogenous administration of GM1 into HD mouse models has shown a decrease in mutant HTT toxicity, reduction in neurodegeneration, and reinstitution of normal brain functions.[87] These studies highlight the potential use of GM1 ganglioside in HD therapeutics.

1.6 ANALYSIS OF GLYCOSPHINGOLIPIDS (GSL)

The primary step towards analyzing GSLs is their isolation and purification from biological samples. The lipid composition in biological samples includes not only GSLs but also cholesterol, phospholipids, and other sphingolipids.[89] Traditional methods by Folch or Bligh and Dyer were used in the past for total lipid extraction.[90-91] Recovery of the far more polar gangliosides and GSLs was poor using these methods.[92] Very specific ratios of solvent-to-sample and alcohol-to-non-polar (methanol-to-chloroform) solvent are required in order to achieve maximum efficiency in the extraction protocol to separate GSLs from the remaining cellular components.[93] Additionally, if water is added in small amounts to the extraction solvent, gangliosides and GSLs are much better separated into the polar phase, while the more hydrophobic phospholipids and sphingolipids remain in

the non-polar phase.[94] Svennerholm's classical extraction protocol uses a biphasic system of chloroform:methanol:water in the ratio 4:8:3 (v/v/v) as the extraction solvent. This is the most widely used method of extraction, even though the subsequent purification steps are obsolete and inefficient.[94] Adopting the same extraction protocol as Svennerholm, modifications were made to the purification and recovery steps by using standard SepPak C18 reverse phase cartridges.[93] This, however, was a tedious 18-step purification process and was later improved to a more convenient eight step process by modifying the extraction solvent ratios.[95]

GSLs and gangliosides being such diverse molecules both in structure and function, analytical tools for their precise and accurate analysis are still limited. The following sections list some of the techniques currently in use in ganglioside analytics.

1.6.1 Thin Layer Chromatography (TLC)

Historically, the foundation of detection and analysis of GSLs is thin-layer chromatography (TLC). TLC allows accurate identification of GSLs in biological samples and is an inexpensive way to achieve qualitative separation of GSLs in a complex mixture.[2] Researchers have struggled to find the best possible combination of chromatographic solvents in order to improve GSL separation on a TLC plate.[96] The common solvent systems used nowadays are a combination of the following mobile phases: chloroform:methanol:water (65:35:8), chloroform:methanol:aq.$CaCl_2$ (0.5%) (55:45:10), and acetic acid:n-butanol:aq.$CaCl_2$ (0.25%) (1:2:1)[97-98] Visualizing neutral GSLs and gangliosides after separation on a TLC plate can be achieved by using chemical stains, such as 5% sulfuric acid and orcinol/resorcinol reagents, respectively.[2, 98]

Staining TLC plates with ganglioside specific antibodies[99-100] or bacterial/viral toxins[101] that react specifically with certain gangliosides has improved the sensitivity of this method.[102] This, however, is limited to major gangliosides in the brain for which well defined antibodies and/or toxins are commercially available. For example, CT-B specific for binding to GM1 is easily accessible.[96] Moreover, gangliosides have incredibly diverse structures and multiple isoforms. This makes detection using antibodies and/or toxins even less definitive and inaccurate.[96, 99-100, 103]

TLC experiments also have been used to quantify gangliosides in biological samples. Image densitometry is the technique used for this purpose.[104] Direct scanning of resorcinol stained ganglioside bands on high performance thin layer chromatography (HPTLC) plates was performed using a densitometer to obtain concentrations in the picomolar range.[105-106] Similarly, orcinol stained gangliosides have been analyzed using HPTLC with quantification using ImageJ software.[107] Even though this is a rapid and effective method of quantification, variables in TLC, such as unequal spotting of substrate and reaction products, temperature, and resolving solvent composition, can affect independent runs and thus makes Rf values unreliable.[104] Hence, TLC alone is not an ideal method of quantitation. It is better suited for accurate quantitation of GSLs when used in combination with other advanced tools, such as Mass Spectrometry (MALDI-MS or ESI-MS)[108-110]

1.6.2 Mass Spectrometry (MS)

The field of lipidomics has been taken by a storm with the introduction of Mass Spectrometry (MS). MS essentially involves ionization of the compound of interest into

fragments, which are individually analyzed to provide a comprehensive analysis.[111] Traditional ionization techniques used in MS analysis of GSLs include electrospray ionization (ESI), where the analyte solution is transformed into highly charged droplets under the influence of very high voltages and is then fed into an MS analyzer.[12, 111] It is a very mild ionization technique and is used on most occasions for GSL analysis, such as analyzing the fragmentation pattern of permethylated GSLs[112] or neutral GSLs using collision induced dissociation (CDI)-ESI/MS/MS of fragment ions.[113-114]

Matrix Assisted Laser Desorption Ionization (MALDI) is another classical ionization technique where the analyte, after co-crystallization with a UV-active matrix, is irradiated with a laser that causes ionization of the target analytes along with the matrix molecules.[109, 115] MALDI often is coupled with TLC or HPTLC in an attempt to allow direct analysis of samples from the plates, making TLC reliably quantitative. This has been applied to the analysis of well separated mixtures of phospholipids[116] and identification of Gb3Cer as the GSL responsible for pancreatic cancer in humans,[117] to name a few. Although TLC-MALDI is an attractive strategy to make TLC experiments quantitative, it still is insufficient because it is prone to loss of material while scraping off very closely spaced bands individually or during extraction of target molecules from the TLC plate followed by their transfer onto a MALDI plate.[118]

Atmospheric pressure chemical ionization (APCI) is a complementary technique to ESI where the analyte solution forms droplets under high temperatures and exposure to nitrogen, is sometimes used for GSL analysis.[119] Ionization techniques are coupled with one or more mass analyzers, such as quadrupoles, triple quadrupole, time of flight (TOF),

and ion trap,[111] allowing rapid and comprehensive MS-based structural identification, characterization, profiling, and quantification of GSLs in biological systems.

Even though MS is the most sought-after analytical technique for GSLs, it suffers from inherent drawbacks. The biggest limitation is identifying suitable internal standards that ionize with the same efficiency as all GSL components in a biological sample under the same conditions and can also be recovered maximally along with the target analytes after undergoing robust extraction protocols.[12, 120] The former is far more challenging than the latter. The main criterion for a good internal standard is that it should be identical in structure to the analyte of interest; ensuring same fragmentation patterns for both.[12] However, for this to be implemented, every possible GSL must have a commercially available isotopically labeled version of it.[121] This is not practically possible given the complexity and diversity in the structure of GSLs. Hence, researchers resort to using commonly available lipid standards, even though they do not exactly match the structure of their target analyte. For example, GM1 (d18:1-^{13}C16:0) with ^{13}C labeled carbons on the fatty acid chain has been used to quantify the amounts of GD1b (d20:1-20:0) and GD1b (d20:1-18:0) in porcine brains to understand the affect of fatty acid chain length variations in Alzheimer's disease[122] or phosphatidylinositol (PI) (12:0/13:0) has been used to quantify all molecular species of GM3 carrying variable chain lengths and unsaturation in both the Sph bases and fatty acids.[123] The practice of using standards that do not match the structure of an analyte, is inherently erroneous because it is based on the assumption that these unmatched species will follow the same ionization/fragmentation pattern.

MS alone is limited in its application to separate isomeric and isobaric species of GSLs, and the presence of impurities in a sample can hamper MS analysis due to ionization suppression. To avoid these problems, complementary techniques, such as Liquid Chromatography (LC) can be used in combination with MS.[120] LC can eliminate ionization suppression and can provide favourable chromatographic separation of isomeric and isobaric species.[124-125] Depending on the kind of interactions between the stationary phase and GSLs, the two types of LC separations currently in use are: (a) Reverse phase LC (RP-LC), in which the stationary or bonded phase is less polar than the mobile phase, making this a suitable mode of separation according to the hydrophobic lipid chains of GSLs and (b) Normal phase LC (NP-LC), in which the bonded phase is more polar than the mobile phase and hence can be used to separate GSLs based on their polar carbohydrate moieties.[126] The RP-LC offers several advantages over NP-LC, such as compatibility with ESI, reproducibility between runs, and reduced ionization suppression, making this the preferred separation technique in use today.[127] An interesting application of RP-LC was the use of RP-LC-ESI-MS for complete profiling of GSLs in breast cancer tissues. This was followed by a systematic multiple MS[n] fragmentation to identify and confirm the structure of fucosyl-lactosylceramide (Fuc-Lac) that is overexpressed in breast cancer tissues.[128]

Kirsch and co-workers reported an advanced method of separation and detection of neutral GSLs in human erythrocytes with a nanoflow-HPLC-ESI-QTOF-MS[n] set up, giving femtomolar sensitivities.[129] Subsequently, RP nano-HPLC-Chip QTOF-MS has been used for profiling and characterization of gangliosides in murine brains[130], and more recently in profiling, characterization, and quantification of different molecular species of

GSLs in a human colorectal cell line (Caco-2).[131] The nano-HPLC-Chip is a lab-on-chip analytical tool that is a preferred alternative to traditional LC since it offers better reproducibility and improved chromatographic separation, all with a more convenient set up.[132]

Hydrophilic interaction liquid chromatography (HILIC) is similar to NP-LC but does not suffer from the same drawbacks as NP-LC. Hence, it is used preferably for the separation of polar analytes. It encompasses the characteristics of both RP-LC and NP-LC in a way that the bonded phase for HILIC separations include polar stationary phases, similar to the ones used in NP-LC, i.e., silica, cyano etc;[133] the mobile phases, on the other hand, are usually similar to those used in RP-LC, i.e., high aqueous content mobile phases.[134] This is the characteristic feature of the HILIC mode of separation by which a static aqueous layer is formed between the bonded phase and the mobile phase, allowing hydrogen bonding and electrostatic interactions between this and the analyte solution as it flows through the column.[135] Primary advantages of HILIC over both RP-LC and NP-LC include highly compatible mobile phases for combinatorial HILIC-ESI-MS analysis and excellent separation of amphiphilic molecules.[135-137] In the field of lipidomics, HILIC-ESI/MS has been used to analyze and quantify a range of different sphingolipids, namely, sphingosine (SPH), sphinganine (SPA), phyto-sphingosine (Phyto-SPH), hexocylceramide (HexCer), and lactosylceramide (LacCer), from primary human skin fibroblasts.[138] Holcapek and co-workers used negative-ion HILIC-ESI-MS for chromatographic separation of gangliosides and other polar lipid species, including sphingosine, phosphatidylcholine (PC), phosphatidylinositol (PI), and sphingomyelin (SM) in human kidney, lung, plasma, erythrocytes, and porcine brain.[139] This study,

however, did not use any standards to quantify the lipid species. As an improvement to their existing negative-ion HILIC-ESI-MS/MS protocol, the same group recently quantified major lipid species in normal human kidney tissues and tissues infected with renal cell carcinoma (RCC), using synthetically prepared internal standards bearing shorter fatty acid chains, such as PS (14:0/14:0), SulfoHexCer (18:1/12:0), and GM3 (18:1/12:0).[140] Nano-flow HPLC also has been used in the negative-ion HILIC mode to separate isomeric species of α2-3 and α2-6 linked Sia containing gangliosides in human granulocytes[141] and in the discovery of glycolipids as biomarkers for Barrett's syndrome and high grad dysplasia.[142]

In order to visualize the localization of GSLs in cells or tissues, MS-based imaging techniques, referred to as Imaging Mass Spectrometry (IMS), are employed. An example of IMS is MALDI imaging, where a tissue section placed on a MALDI plate is irradiated with a laser beam, as the plate moves in two-dimensions to acquire data from all possible regions.[143] These MALDI spectra are analyzed by a specific software to generate a colour coded image of the tissue section, representing the spatial distribution of specific m/z values of target ions.[144] This has become an extremely powerful technique in a variety of different clinical applications associated with GSLs. For example, MALDI imaging was used to analyze brain slices from Tay Sachs and Sandhoff disease mouse models that showed differential accumulation of GA2, GM2, and sulfatides in different regions of the cerebellum.[145] Similar studies were performed to investigate the effects of distinctive localization of GM2, GM3, and gangliosides with d20:1 Sph bases in different regions of the brain of Alzheimer's disease rat models.[146] Although MALDI-IMS is a very powerful technique, it still is relatively new and suffers drawbacks such as poor

sensitivity for low mass signals, long acquisition times, and poor resolution due to the application of a matrix.[147]

Secondary ion mass spectrometry (SIMS) is another ionization technique often coupled with IMS. The experimental arrangement of SIMS involves focusing a primary ion beam on the surface of a target in the solid phase, followed by passing the ejected secondary ions through a mass analyzer and acquiring m/z data to determine their elemental composition.[148] The advantages of SIMS over MALDI include high sensitivities in the low mass ranges (m/z = <1000) and no requirement of a matrix. These features can eliminate the problem of poor resolution that MALDI-IMS suffers. However, unlike MALDI, SIMS cannot be used to acquire complete structural information due to fragmentation of analytes during the ionization process.[147] Taking advantage of the complementary features of SIMS and MALDI, Carado et al combined the two techniques in a single MS platform, offering improved performance. With a little bit of refinement and proper instrumentation for implementation of this technique, a SIMS and MALDI combination can be designed for GSL analysis using imaging MS.[149]

1.7 HYPOTHESIS AND OBJECTIVE

GSLs are crucial biomolecules that play significant roles in several cellular processes. Liquid Chromatography and Mass Spectrometry (LC-MS) has been the cornerstone of sphingolipid research; however, as discussed in **Section 1.5.2**, MS based analyses suffer from drawbacks, making comprehensive GSL analysis and quantitation challenging. Moreover, most of the MS analytical methods employed either analyze GSLs as intact molecules or focus on their readily accessible glycan moieties.[1, 150] The Cer lipid

22

backbone is often ignored since the diversity in chain length and saturation makes its analysis difficult. Fatty acid chain variability has been a matter of interest under disease conditions, as has been illustrated earlier.[81] However, there are very few detailed studies about the Sph base and its variability even though many reports have shown differential expression of d18:1 and d20:1 Sph bases in the brain.[151]

Lyso-GSLs (*l*-GSLs) are GSLs with the polar carbohydrate chain and the Sph base but devoid of the *N*-acyl fatty acid. Glucosylsphingosine, galactosylsphingosine and lactosylsphingosine are *l*-GSLs that have been implicated in Gaucher's disease,[152] Krabbe's disease,[153] and certain cancers[154], respectively. Based on these findings, we believe that the Sph base has a functional role to play; therefore, specific analytical tools need to be designed to study *l*-GSLs in detail.

We hypothesize that using specific enzymes for GSL degradation, such as, Endoglycoceramidase (EGCase) and Sphingolipid ceramide *N*-deacylase (SCDase) will help us analyze both the glycan and Sph components of GSLs in a given biological sample. EGCase catalyzes the cleavage of the ceramide lipid backbone, thereby liberating free oligosaccharides from GSLs.[1, 4] SCDase cleaves off the fatty acid chain of the ceramide moiety to produce lyso-GSLs bearing a free amine residue.[6] The degradation products of each enzyme, i.e., reducing glycan and lyso-GSLs could be labeled with the fluorophores, such as, anthranilic acid (2-AA)[4] and Rapifluor-MS, respectively, and analyzed by LC-MS. **(Figure 1–5)**

Traditionally, chemical tools such as osmium catalyzed periodate oxidation[155] or ozonolysis[156] have been used for GSL degradation. The lipid chain is modified most commonly by alkaline treatment to release *N*-acyl fatty acid chains, thereby producing a

23

l-GSLs with a free amine residue.[157] This strategy has been used to generate fluorescently labeled GSLs by tagging the free amine group with NBD dyes, which are applied in assays used to delineate functional roles of gangliosides.[158-159] Although these chemical methods are easily accessible, cost efficient, and can be used routinely, they suffer from inherent problems of low yields, lack of specificity, and long reaction times. Enzymatic strategies of GSL degradation have been able to surpass these problems and hence are a preferred alternative.[18, 160-161] Fluorescent LC-MS (F-LC-MS) has the advantage of higher sensitivity and provides reliable quantification using fluorescently labeled internal or external standards.[162] Accurate quantification using MS alone is confounded by the limited availabilty of approporiately matched standards. Our objective in this study was to incorporate the superior properties of enzymatic GSL degradation and F-LC-MS to design complementary methods of GSL glycan and *l*-GSL analysis.

The analytical techniques discussed in **Section 1.6** of this chapter have their own strengths and weakness. TLCs are a strong technique for identification of GSLs, but TLC bands are challenging to separate and accurately quantify. MS is an excellent method for extensive structural characterization of different classes of GSLs and can also provide relative quantifications for each GSL component. However, MS alone is unable to separate isomeric species of GSLs and cannot provide reliable quantification with the limited number of available standards. Combination of LC and MS can provide a solution to these problems of separation and quantification. The methods designed for this thesis offer advantages of quantification based on fluorescence that are far more reliable than other methods of quantifications mentioned in **Section 1.6**. Moreover, the novelty of the method of *l*-GSL analysis in a complex biological mixture is what makes this method
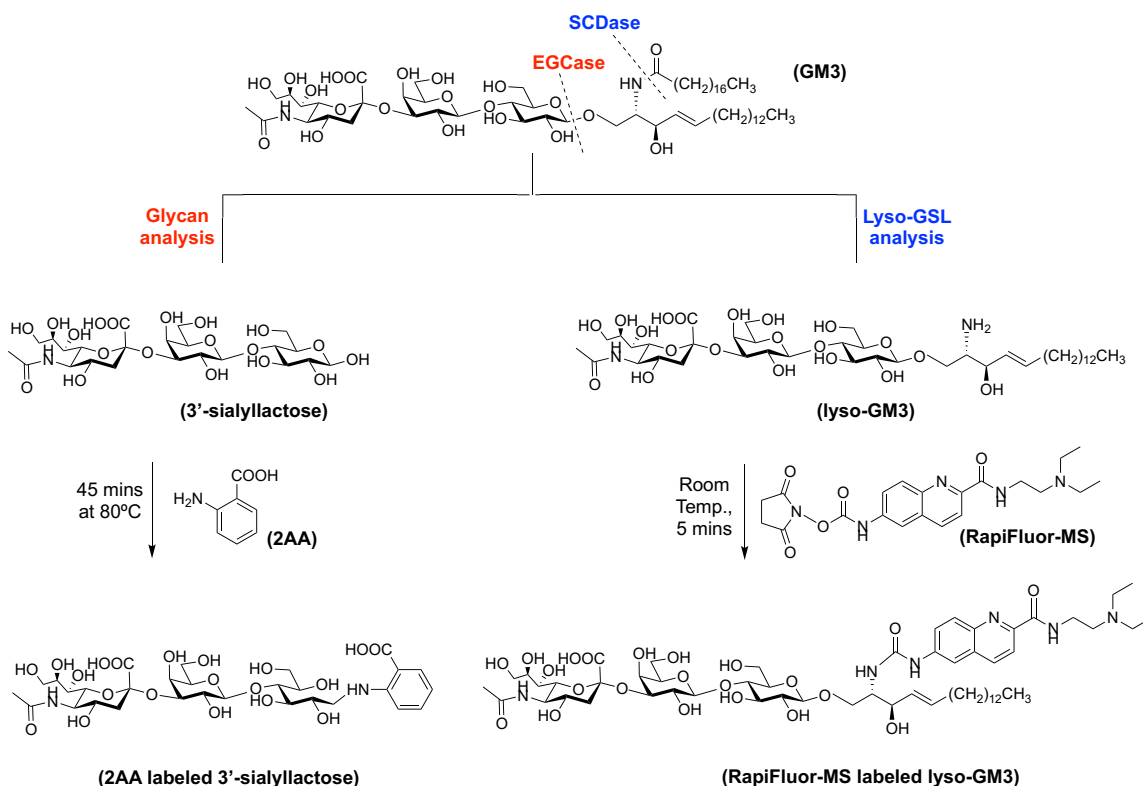
Figure 1– 5. Enzymatic modification of ganglioside GM3 using endoglycoceramidase (EGCase) and sphingolipid ceramide N-deacylase (SCDase). EGCase[1,4] removes the ceramide moiety from GM3, releasing the corresponding glycan 3'-sialyllactose (3'-SL), followed by labeling with a fluorophore 2-AA via reductive amination reaction at the reducing end of the glycan. SCDase[6] removes the N-acyl fatty acid chian from the ceramide moiety, releasing lyso-GM3 with a primary amine residue, which is then labeled with a fluorophore, RapiFluor-MS, via a simple amine coupling reaction. The respective fluorescent products are analyzed by LC-MS thereafter.

unique since this is a problem that has not been given a lot of attention to in the past. With this new method, we hope to provide a starting point in the understanding of possible structural and functional roles of Sph chains of GSLs in the regulation of existing cellular mechanisms; or unravel new mechanisms specific to them.

1.8 REFERENCES

1. Albrecht, S.; Vainauskas, S.; Stockmann, H.; McManus, C.; Taron, C. H.; Rudd, P. M., Comprehensive Profiling of Glycosphingolipid Glycans Using a Novel Broad Specificity Endoglycoceramidase in a High-Throughput Workflow. *Anal Chem* **2016,** *88* (9), 4795-802.

2. In *Essentials of Glycobiology*, rd; Varki, A.; Cummings, R. D.; Esko, J. D.; Stanley, P.; Hart, G. W.; Aebi, M.; Darvill, A. G.; Kinoshita, T.; Packer, N. H.; Prestegard, J. H.; Schnaar, R. L.; Seeberger, P. H., Eds. Cold Spring Harbor (NY), 2015.

3. Groux-Degroote, S.; Guerardel, Y.; Delannoy, P., Gangliosides: Structures, Biosynthesis, Analysis, and Roles in Cancer. *Chembiochem* **2017,** *18* (13), 1146-1154.

4. Neville, D. C.; Coquard, V.; Priestman, D. A.; te Vruchte, D. J.; Sillence, D. J.; Dwek, R. A.; Platt, F. M.; Butters, T. D., Analysis of fluorescently labeled glycosphingolipid-derived oligosaccharides following ceramide glycanase digestion and anthranilic acid labeling. *Anal Biochem* **2004,** *331* (2), 275-82.

5. Nicolson, G. L., The Fluid-Mosaic Model of Membrane Structure: still relevant to understanding the structure, function and dynamics of biological membranes after more than 40 years. *Biochim Biophys Acta* **2014,** *1838* (6), 1451-66.

6. Han, Y. B.; Wu, L.; Rich, J. R.; Huang, F. T.; Withers, S. G.; Feng, Y.; Yang, G. Y., Comprehensive characterization of sphingolipid ceramide N-deacylase for the synthesis and fatty acid remodeling of glycosphingolipids. *Appl Microbiol Biotechnol* **2015,** *99* (16), 6715-26.

7.   Varki, A., Evolutionary forces shaping the Golgi glycosylation machinery: why cell surface glycans are universal to living cells. *Cold Spring Harb Perspect Biol* **2011,** *3* (6).

8.   van Meer, G.; Voelker, D. R.; Feigenson, G. W., Membrane lipids: where they are and how they behave. *Nat Rev Mol Cell Biol* **2008,** *9* (2), 112-24.

9.   Hannun, Y. A.; Obeid, L. M., Sphingolipids and their metabolism in physiology and disease. *Nat Rev Mol Cell Biol* **2018,** *19* (3), 175-191.

10.   D'Angelo, G.; Capasso, S.; Sticco, L.; Russo, D., Glycosphingolipids: synthesis and functions. *FEBS J* **2013,** *280* (24), 6338-53.

11.   Merrill, A. H., Jr., De novo sphingolipid biosynthesis: a necessary, but dangerous, pathway. *J Biol Chem* **2002,** *277* (29), 25843-6.

12.   Merrill, A. H., Jr., Sphingolipid and glycosphingolipid metabolic pathways in the era of sphingolipidomics. *Chem Rev* **2011,** *111* (10), 6387-422.

13.   Blix, G., Über die Kohlenhydratgruppen des Submaxillarismucins. In *Hoppe-Seyler′s Zeitschrift für physiologische Chemie*, 1936; Vol. 240, p 43.

14.   Wickramasinghe, S.; Medrano, J. F., Primer on genes encoding enzymes in sialic acid metabolism in mammals. *Biochimie* **2011,** *93* (10), 1641-1646.

15.   Tiralongo, J., Chapter 29 - Sialic acid-specific microbial lectins. In *Microbial Glycobiology*, Holst, O.; Brennan, P. J.; Itzstein, M. v.; Moran, A. P., Eds. Academic Press: San Diego, 2010; pp 585-598.

16.   Tettamanti, G., Ganglioside/glycosphingolipid turnover: new concepts. *Glycoconj J* **2004,** *20* (5), 301-17.

17. Ariga, T.; McDonald, M. P.; Yu, R. K., Role of ganglioside metabolism in the pathogenesis of Alzheimer's disease--a review. *J Lipid Res* **2008,** *49* (6), 1157-75.

18. Hunter, C. D.; Guo, T.; Daskhan, G.; Richards, M. R.; Cairo, C. W., Synthetic Strategies for Modified Glycosphingolipids and Their Design as Probes. *Chem Rev* **2018**.

19. Futerman, A. H., Chapter 10 - Sphingolipids. In *Biochemistry of Lipids, Lipoproteins and Membranes (Sixth Edition)*, Ridgway, N. D.; McLeod, R. S., Eds. Elsevier: Boston, 2016; pp 297-326.

20. Kopitz, J., Lipid glycosylation: a primer for histochemists and cell biologists. *Histochem Cell Biol* **2017,** *147* (2), 175-198.

21. Yu, R. K.; Tsai, Y. T.; Ariga, T.; Yanagisawa, M., Structures, biosynthesis, and functions of gangliosides--an overview. *J Oleo Sci* **2011,** *60* (10), 537-44.

22. Chester, M. A., IUPAC-IUB Joint Commission on Biochemical Nomenclature (JCBN). Nomenclature of glycolipids--recommendations 1997. *Eur J Biochem* **1998,** *257* (2), 293-8.

23. Svennerholm, L., Designation and schematic structure of gangliosides and allied glycosphingolipids. *Prog Brain Res* **1994,** *101*, XI-XIV.

24. Fahy, E.; Subramaniam, S.; Brown, H. A.; Glass, C. K.; Merrill, A. H., Jr.; Murphy, R. C.; Raetz, C. R.; Russell, D. W.; Seyama, Y.; Shaw, W.; Shimizu, T.; Spener, F.; van Meer, G.; VanNieuwenhze, M. S.; White, S. H.; Witztum, J. L.; Dennis, E. A., A comprehensive classification system for lipids. *J Lipid Res* **2005,** *46* (5), 839-61.

25. Varki, A.; Cummings, R. D.; Aebi, M.; Packer, N. H.; Seeberger, P. H.; Esko, J. D.; Stanley, P.; Hart, G.; Darvill, A.; Kinoshita, T.; Prestegard, J. J.; Schnaar, R. L.; Freeze, H. H.; Marth, J. D.; Bertozzi, C. R.; Etzler, M. E.; Frank, M.; Vliegenthart, J. F.; Lutteke, T.; Perez, S.; Bolton, E.; Rudd, P.; Paulson, J.; Kanehisa, M.; Toukach, P.; Aoki-Kinoshita, K. F.; Dell, A.; Narimatsu, H.; York, W.; Taniguchi, N.; Kornfeld, S., Symbol Nomenclature for Graphical Representations of Glycans. *Glycobiology* **2015,** *25* (12), 1323-4.

26. Kracun, I.; Rosner, H.; Cosovic, C.; Stavljenic, A., Topographical atlas of the gangliosides of the adult human brain. *J Neurochem* **1984,** *43* (4), 979-89.

27. Posse de Chaves, E.; Sipione, S., Sphingolipids and gangliosides of the nervous system in membrane function and dysfunction. *FEBS Lett* **2010,** *584* (9), 1748-59.

28. Yu, R. K.; Nakatani, Y.; Yanagisawa, M., The role of glycosphingolipid metabolism in the developing brain. *J Lipid Res* **2009,** *50 Suppl*, S440-5.

29. Kracun, I.; Rosner, H.; Drnovsek, V.; Heffer-Lauc, M.; Cosovic, C.; Lauc, G., Human brain gangliosides in development, aging and disease. *Int J Dev Biol* **1991,** *35* (3), 289-95.

30. Ando, S., Neuronal dysfunction with aging and its amelioration. *Proc Jpn Acad Ser B Phys Biol Sci* **2012,** *88* (6), 266-82.

31. Sonnino, S.; Chigorno, V., Ganglioside molecular species containing C18- and C20-sphingosine in mammalian nervous tissues and neuronal cell cultures. *Biochim Biophys Acta* **2000,** *1469* (2), 63-77.

32. Ogawa-Goto, K.; Funamoto, N.; Abe, T.; Nagashima, K., Different ceramide compositions of gangliosides between human motor and sensory nerves. *J Neurochem* **1990,** *55* (5), 1486-93.

33. Sugiura, Y.; Shimma, S.; Konishi, Y.; Yamada, M. K.; Setou, M., Imaging mass spectrometry technology and application on ganglioside study; visualization of age-dependent accumulation of C20-ganglioside molecular species in the mouse hippocampus. *PLoS One* **2008,** *3* (9), e3232.

34. Hama, H., Fatty acid 2-Hydroxylation in mammalian sphingolipid biology. *Biochim Biophys Acta* **2010,** *1801* (4), 405-14.

35. Senn, H. J.; Orth, M.; Fitzke, E.; Wieland, H.; Gerok, W., Gangliosides in normal human serum. Concentration, pattern and transport by lipoproteins. *Eur J Biochem* **1989,** *181* (3), 657-62.

36. McJarrow, P.; Schnell, N.; Jumpsen, J.; Clandinin, T., Influence of dietary gangliosides on neonatal brain development. *Nutr Rev* **2009,** *67* (8), 451-63.

37. Rueda, R., The role of dietary gangliosides on immunity and the prevention of infection. *Br J Nutr* **2007,** *98 Suppl 1*, S68-73.

38. Varki, N. M.; Varki, A., Diversity in cell surface sialic acid presentations: implications for biology and disease. *Lab Invest* **2007,** *87* (9), 851-7.

39. Chou, H. H.; Takematsu, H.; Diaz, S.; Iber, J.; Nickerson, E.; Wright, K. L.; Muchmore, E. A.; Nelson, D. L.; Warren, S. T.; Varki, A., A mutation in human CMP-sialic acid hydroxylase occurred after the Homo-Pan divergence. *Proc Natl Acad Sci U S A* **1998,** *95* (20), 11751-6.

40.   Alisson-Silva, F.; Kawanishi, K.; Varki, A., Human risk of diseases associated with red meat intake: Analysis of current theories and proposed role for metabolic incorporation of a non-human sialic acid. *Mol Aspects Med* **2016,** *51*, 16-30.

41.   Tangvoranuntakul, P.; Gagneux, P.; Diaz, S.; Bardor, M.; Varki, N.; Varki, A.; Muchmore, E., Human uptake and incorporation of an immunogenic nonhuman dietary sialic acid. *Proc Natl Acad Sci U S A* **2003,** *100* (21), 12045-50.

42.   Schauer, R.; Srinivasan, G. V.; Coddeville, B.; Zanetta, J. P.; Guerardel, Y., Low incidence of N-glycolylneuraminic acid in birds and reptiles and its absence in the platypus. *Carbohydr Res* **2009,** *344* (12), 1494-500.

43.   Maccioni, H. J., Glycosylation of glycolipids in the Golgi complex. *J Neurochem* **2007,** *103 Suppl 1*, 81-90.

44.   Braun, P. E.; Snell, E. E., The biosynthesis of dihydrosphingosine in cell-free preparations of Hansenula ciferri. *Proc Natl Acad Sci U S A* **1967,** *58* (1), 298-303.

45.   Pinto, W. J.; Srinivasan, B.; Shepherd, S.; Schmidt, A.; Dickson, R. C.; Lester, R. L., Sphingolipid long-chain-base auxotrophs of Saccharomyces cerevisiae: genetics, physiology, and a method for their selection. *J Bacteriol* **1992,** *174* (8), 2565-74.

46.   Hanada, K.; Nishijima, M.; Kiso, M.; Hasegawa, A.; Fujita, S.; Ogawa, T.; Akamatsu, Y., Sphingolipids are essential for the growth of Chinese hamster ovary cells. Restoration of the growth of a mutant defective in sphingoid base biosynthesis by exogenous sphingolipids. *J Biol Chem* **1992,** *267* (33), 23527-33.

47.   Bond, L. M.; Miyazaki, M.; O'Neill, L. M.; Ding, F.; Ntambi, J. M., Chapter 6 - Fatty Acid Desaturation and Elongation in Mammals. In *Biochemistry of Lipids, Lipoproteins and Membranes (Sixth Edition)*, Ridgway, N. D.; McLeod, R. S., Eds. Elsevier: Boston, 2016; pp 185-208.

48.   Williams, R. D.; Wang, E.; Merrill, A. H., Jr., Enzymology of long-chain base synthesis by liver: characterization of serine palmitoyltransferase in rat liver microsomes. *Arch Biochem Biophys* **1984,** *228* (1), 282-91.

49.   Hanada, K.; Hara, T.; Nishijima, M., Purification of the serine palmitoyltransferase complex responsible for sphingoid base synthesis by using affinity peptide chromatography techniques. *J Biol Chem* **2000,** *275* (12), 8409-15.

50.   Levy, M.; Futerman, A. H., Mammalian ceramide synthases. *IUBMB Life* **2010,** *62* (5), 347-56.

51.   Maceyka, M.; Sankala, H.; Hait, N. C.; Le Stunff, H.; Liu, H.; Toman, R.; Collier, C.; Zhang, M.; Satin, L. S.; Merrill, A. H., Jr.; Milstien, S.; Spiegel, S., SphK1 and SphK2, sphingosine kinase isoenzymes with opposing functions in sphingolipid metabolism. *J Biol Chem* **2005,** *280* (44), 37118-29.

52.   Takamiya, K.; Yamamoto, A.; Furukawa, K.; Yamashiro, S.; Shin, M.; Okada, M.; Fukumoto, S.; Haraguchi, M.; Takeda, N.; Fujimura, K.; Sakae, M.; Kishikawa, M.; Shiku, H.; Furukawa, K.; Aizawa, S., Mice with disrupted GM2/GD2 synthase gene lack complex gangliosides but exhibit only subtle defects in their nervous system. *Proc Natl Acad Sci U S A* **1996,** *93* (20), 10662-7.

53. Schengrund, C. L., Gangliosides: glycosphingolipids essential for normal neural development and function. *Trends Biochem Sci* **2015,** *40* (7), 397-406.

54. Yamashita, T.; Wu, Y. P.; Sandhoff, R.; Werth, N.; Mizukami, H.; Ellis, J. M.; Dupree, J. L.; Geyer, R.; Sandhoff, K.; Proia, R. L., Interruption of ganglioside synthesis produces central nervous system degeneration and altered axon-glial interactions. *Proc Natl Acad Sci U S A* **2005,** *102* (8), 2725-30.

55. Aureli, M.; Mauri, L.; Ciampa, M. G.; Prinetti, A.; Toffano, G.; Secchieri, C.; Sonnino, S., GM1 Ganglioside: Past Studies and Future Potential. *Mol Neurobiol* **2016,** *53* (3), 1824-1842.

56. DeMarco, M. L.; Woods, R. J., Atomic-resolution conformational analysis of the GM3 ganglioside in a lipid bilayer and its implications for ganglioside-protein recognition at membrane surfaces. *Glycobiology* **2009,** *19* (4), 344-55.

57. Lichtenberg, D.; Goni, F. M.; Heerklotz, H., Detergent-resistant membranes should not be identified with membrane rafts. *Trends Biochem Sci* **2005,** *30* (8), 430-6.

58. Lingwood, D.; Simons, K., Lipid rafts as a membrane-organizing principle. *Science* **2010,** *327* (5961), 46-50.

59. Gu, R. X.; Ingolfsson, H. I.; de Vries, A. H.; Marrink, S. J.; Tieleman, D. P., Ganglioside-Lipid and Ganglioside-Protein Interactions Revealed by Coarse-Grained and Atomistic Molecular Dynamics Simulations. *J Phys Chem B* **2017,** *121* (15), 3262-3275.

60. Hakomori Si, S. I., The glycosynapse. *Proc Natl Acad Sci U S A* **2002,** *99* (1), 225-32.

61. Regina Todeschini, A.; Hakomori, S. I., Functional role of glycosphingolipids and gangliosides in control of cell adhesion, motility, and growth, through glycosynaptic microdomains. *Biochim Biophys Acta* **2008,** *1780* (3), 421-33.

62. Lipina, C.; Hundal, H. S., Ganglioside GM3 as a gatekeeper of obesity-associated insulin resistance: Evidence and mechanisms. *FEBS Lett* **2015,** *589* (21), 3221-7.

63. Kabayama, K.; Sato, T.; Saito, K.; Loberto, N.; Prinetti, A.; Sonnino, S.; Kinjo, M.; Igarashi, Y.; Inokuchi, J., Dissociation of the insulin receptor and caveolin-1 complex by ganglioside GM3 in the state of insulin resistance. *Proc Natl Acad Sci U S A* **2007,** *104* (34), 13678-83.

64. Yamashita, T.; Hashiramoto, A.; Haluzik, M.; Mizukami, H.; Beck, S.; Norton, A.; Kono, M.; Tsuji, S.; Daniotti, J. L.; Werth, N.; Sandhoff, R.; Sandhoff, K.; Proia, R. L., Enhanced insulin sensitivity in mice lacking ganglioside GM3. *Proc Natl Acad Sci U S A* **2003,** *100* (6), 3445-9.

65. Liu, Y.; Li, R.; Ladisch, S., Exogenous ganglioside GD1a enhances epidermal growth factor receptor binding and dimerization. *J Biol Chem* **2004,** *279* (35), 36481-9.

66. Schnaar, R. L., Brain gangliosides in axon-myelin stability and axon regeneration. *FEBS Lett* **2010,** *584* (9), 1741-7.

67. Yang, L. J.; Zeller, C. B.; Shaper, N. L.; Kiso, M.; Hasegawa, A.; Shapiro, R. E.; Schnaar, R. L., Gangliosides are neuronal ligands for myelin-associated glycoprotein. *Proc Natl Acad Sci U S A* **1996,** *93* (2), 814-8.

68. Sheikh, K. A.; Sun, J.; Liu, Y.; Kawai, H.; Crawford, T. O.; Proia, R. L.; Griffin, J. W.; Schnaar, R. L., Mice lacking complex gangliosides develop Wallerian

degeneration and myelination defects. *Proc Natl Acad Sci U S A* **1999,** *96* (13), 7532-7.

69.   Pan, B.; Fromholt, S. E.; Hess, E. J.; Crawford, T. O.; Griffin, J. W.; Sheikh, K. A.; Schnaar, R. L., Myelin-associated glycoprotein and complementary axonal ligands, gangliosides, mediate axon stability in the CNS and PNS: neuropathology and behavioral deficits in single- and double-null mice. *Exp Neurol* **2005,** *195* (1), 208-17.

70.   Chiavegatto, S.; Sun, J.; Nelson, R. J.; Schnaar, R. L., A functional role for complex gangliosides: motor deficits in GM2/GD2 synthase knockout mice. *Exp Neurol* **2000,** *166* (2), 227-34.

71.   Tsai, B.; Gilbert, J. M.; Stehle, T.; Lencer, W.; Benjamin, T. L.; Rapoport, T. A., Gangliosides are receptors for murine polyoma virus and SV40. *EMBO J* **2003,** *22* (17), 4346-55.

72.   Cuatrecasas, P., Gangliosides and membrane receptors for cholera toxin. *Biochemistry* **1973,** *12* (18), 3558-66.

73.   Takenouchi, H.; Kiyokawa, N.; Taguchi, T.; Matsui, J.; Katagiri, Y. U.; Okita, H.; Okuda, K.; Fujimoto, J., Shiga toxin binding to globotriaosyl ceramide induces intracellular signals that mediate cytoskeleton remodeling in human renal carcinoma-derived cells. *J Cell Sci* **2004,** *117* (Pt 17), 3911-22.

74.   Minguet, S.; Klasener, K.; Schaffer, A. M.; Fiala, G. J.; Osteso-Ibanez, T.; Raute, K.; Navarro-Lerida, I.; Hartl, F. A.; Seidl, M.; Reth, M.; Del Pozo, M. A., Caveolin-1-dependent nanoscale organization of the BCR regulates B cell tolerance. *Nat Immunol* **2017,** *18* (10), 1150-1159.

75. Shrestha, D.; Exley, M. A.; Vereb, G.; Szollosi, J.; Jenei, A., CD1d favors MHC neighborhood, GM1 ganglioside proximity and low detergent sensitive membrane regions on the surface of B lymphocytes. *Biochim Biophys Acta* **2014,** *1840* (1), 667-80.

76. Kawano, T.; Cui, J.; Koezuka, Y.; Toura, I.; Kaneko, Y.; Sato, H.; Kondo, E.; Harada, M.; Koseki, H.; Nakayama, T.; Tanaka, Y.; Taniguchi, M., Natural killer-like nonspecific tumor cell lysis mediated by specific ligand-activated Valpha14 NKT cells. *Proc Natl Acad Sci U S A* **1998,** *95* (10), 5690-3.

77. Rossjohn, J.; Pellicci, D. G.; Patel, O.; Gapin, L.; Godfrey, D. I., Recognition of CD1d-restricted antigens by natural killer T cells. *Nat Rev Immunol* **2012,** *12* (12), 845-57.

78. Benito, J. M.; Garcia Fernandez, J. M.; Ortiz Mellet, C., Pharmacological chaperone therapy for Gaucher disease: a patent review. *Expert Opin Ther Pat* **2011,** *21* (6), 885-903.

79. Sango, K.; Yamanaka, S.; Hoffmann, A.; Okuda, Y.; Grinberg, A.; Westphal, H.; McDonald, M. P.; Crawley, J. N.; Sandhoff, K.; Suzuki, K.; Proia, R. L., Mouse models of Tay-Sachs and Sandhoff diseases differ in neurologic phenotype and ganglioside metabolism. *Nat Genet* **1995,** *11* (2), 170-6.

80. Inokuchi, J., Membrane microdomains and insulin resistance. *FEBS Lett* **2010,** *584* (9), 1864-71.

81. Veillon, L.; Go, S.; Matsuyama, W.; Suzuki, A.; Nagasaki, M.; Yatomi, Y.; Inokuchi, J., Identification of Ganglioside GM3 Molecular Species in Human

Serum Associated with Risk Factors of Metabolic Syndrome. *PLoS One* **2015,** *10* (6), e0129645.

82. Suzuki, Y., Sialobiology of influenza: molecular mechanism of host range variation of influenza viruses. *Biol Pharm Bull* **2005,** *28* (3), 399-408.

83. Hong, S.; Ostaszewski, B. L.; Yang, T.; O'Malley, T. T.; Jin, M.; Yanagisawa, K.; Li, S.; Bartels, T.; Selkoe, D. J., Soluble Abeta oligomers are rapidly sequestered from brain ISF in vivo and bind GM1 ganglioside on cellular membranes. *Neuron* **2014,** *82* (2), 308-19.

84. Ikeda, K.; Yamaguchi, T.; Fukunaga, S.; Hoshino, M.; Matsuzaki, K., Mechanism of amyloid beta-protein aggregation mediated by GM1 ganglioside clusters. *Biochemistry* **2011,** *50* (29), 6433-40.

85. Yanagisawa, K., GM1 ganglioside and Alzheimer's disease. *Glycoconj J* **2015,** *32* (3-4), 87-91.

86. Imarisio, S.; Carmichael, J.; Korolchuk, V.; Chen, C. W.; Saiki, S.; Rose, C.; Krishna, G.; Davies, J. E.; Ttofi, E.; Underwood, B. R.; Rubinsztein, D. C., Huntington's disease: from pathology and genetics to potential therapies. *Biochem J* **2008,** *412* (2), 191-209.

87. Alpaugh, M.; Galleguillos, D.; Forero, J.; Morales, L. C.; Lackey, S. W.; Kar, P.; Di Pardo, A.; Holt, A.; Kerr, B. J.; Todd, K. G.; Baker, G. B.; Fouad, K.; Sipione, S., Disease-modifying effects of ganglioside GM1 in Huntington's disease models. *EMBO Mol Med* **2017,** *9* (11), 1537-1557.

88.   Maglione, V.; Marchi, P.; Di Pardo, A.; Lingrell, S.; Horkey, M.; Tidmarsh, E.; Sipione, S., Impaired ganglioside metabolism in Huntington's disease and neuroprotective role of GM1. *J Neurosci* **2010,** *30* (11), 4072-80.

89.   Spector, A. A.; Yorek, M. A., Membrane lipid composition and cellular function. *J Lipid Res* **1985,** *26* (9), 1015-35.

90.   Folch, J.; Lees, M.; Sloane Stanley, G. H., A simple method for the isolation and purification of total lipides from animal tissues. *J Biol Chem* **1957,** *226* (1), 497-509.

91.   Bligh, E. G.; Dyer, W. J., A RAPID METHOD OF TOTAL LIPID EXTRACTION AND PURIFICATION. *Canadian Journal of Biochemistry and Physiology* **1959,** *37* (8), 911-917.

92.   Wang, W. Q.; Gustafson, A., Ganglioside extraction from erythrocytes: a comparison study. *Acta Chem Scand* **1995,** *49* (12), 929-36.

93.   Schnaar, R. L., Isolation of glycosphingolipids. *Methods Enzymol* **1994,** *230*, 348-70.

94.   Svennerholm, L.; Fredman, P., A procedure for the quantitative isolation of brain gangliosides. *Biochim Biophys Acta* **1980,** *617* (1), 97-109.

95.   Sturgill, E. R.; Aoki, K.; Lopez, P. H.; Colacurcio, D.; Vajn, K.; Lorenzini, I.; Majic, S.; Yang, W. H.; Heffer, M.; Tiemeyer, M.; Marth, J. D.; Schnaar, R. L., Biosynthesis of the major brain gangliosides GD1a and GT1b. *Glycobiology* **2012,** *22* (10), 1289-301.

96.   Scandroglio, F.; Loberto, N.; Valsecchi, M.; Chigorno, V.; Prinetti, A.; Sonnino, S., Thin layer chromatography of gangliosides. *Glycoconj J* **2009,** *26* (8), 961-73.

97. Tanaka, K.; Miyazawa, M.; Mikami, M.; Aoki, D.; Kiguchi, K.; Iwamori, M., Enhanced expression of unique gangliosides with GM2-determinant in human uterine cervical carcinoma-derived cell lines. *Glycoconj J* **2016,** *33* (5), 745-54.

98. Li, C.; Key, J. A.; Jia, F.; Dandapat, A.; Hur, S.; Cairo, C. W., Practical labeling methodology for choline-derived lipids and applications in live cell fluorescence imaging. *Photochem Photobiol* **2014,** *90* (3), 686-95.

99. Kotani, M.; Ozawa, H.; Kawashima, I.; Ando, S.; Tai, T., Generation of one set of monoclonal antibodies specific for a-pathway ganglio-series gangliosides. *Biochim Biophys Acta* **1992,** *1117* (1), 97-103.

100. Schnaar, R. L.; Fromholt, S. E.; Gong, Y.; Vyas, A. A.; Laroy, W.; Wayman, D. M.; Heffer-Lauc, M.; Ito, H.; Ishida, H.; Kiso, M.; Griffin, J. W.; Shiekh, K. A., Immunoglobulin G-class mouse monoclonal antibodies to major brain gangliosides. *Anal Biochem* **2002,** *302* (2), 276-84.

101. Angstrom, J.; Teneberg, S.; Karlsson, K. A., Delineation and comparison of ganglioside-binding epitopes for the toxins of Vibrio cholerae, Escherichia coli, and Clostridium tetani: evidence for overlapping epitopes. *Proc Natl Acad Sci U S A* **1994,** *91* (25), 11859-63.

102. Lopez, P. H.; Aja, S.; Aoki, K.; Seldin, M. M.; Lei, X.; Ronnett, G. V.; Wong, G. W.; Schnaar, R. L., Mice lacking sialyltransferase ST3Gal-II develop late-onset obesity and insulin resistance. *Glycobiology* **2017,** *27* (2), 129-139.

103. Ozawa, H.; Kotani, M.; Kawashima, I.; Tai, T., Generation of one set of monoclonal antibodies specific for b-pathway ganglio-series gangliosides. *Biochim Biophys Acta* **1992,** *1123* (2), 184-90.

104. Muthing, J., High-resolution thin-layer chromatography of gangliosides. *J Chromatogr A* **1996,** *720* (1-2), 3-25.

105. Ando, S.; Chang, N. C.; Yu, R. K., High-performance thin-layer chromatography and densitometric determination of brain ganglioside compositions of several species. *Anal Biochem* **1978,** *89* (2), 437-50.

106. Mullin, B. R.; Poore, C. M. B.; Rupp, B. H., Quantitation of gangliosides in the picomolar range. *Journal of Chromatography B: Biomedical Sciences and Applications* **1984,** *305* (C), 512-513.

107. Howlader, M. A., Li, C., Zou, C., Chakraberty, R., Ebesoh, N., Cairo, C.W., Neuraminidase-3 (NEU3) is a negative regulator of LFA-1 adhesion. 2018.

108. Torretta, E.; Vasso, M.; Fania, C.; Capitanio, D.; Bergante, S.; Piccoli, M.; Tettamanti, G.; Anastasia, L.; Gelfi, C., Application of direct HPTLC-MALDI for the qualitative and quantitative profiling of neutral and acidic glycosphingolipids: the case of NEU3 overexpressing C2C12 murine myoblasts. *Electrophoresis* **2014,** *35* (9), 1319-28.

109. Goto-Inoue, N.; Hayasaka, T.; Taki, T.; Gonzalez, T. V.; Setou, M., A new lipidomics approach by thin-layer chromatography-blot-matrix-assisted laser desorption/ionization imaging mass spectrometry for analyzing detailed patterns of phospholipid molecular species. *J Chromatogr A* **2009,** *1216* (42), 7096-101.

110. Park, H.; Zhou, Y.; Costello, C. E., Direct analysis of sialylated or sulfated glycosphingolipids and other polar and neutral lipids using TLC-MS interfaces. *J Lipid Res* **2014,** *55* (4), 773-81.

111. El-Aneed, A.; Cohen, A.; Banoub, J., Mass Spectrometry, Review of the Basics: Electrospray, MALDI, and Commonly Used Mass Analyzers. *Applied Spectroscopy Reviews* **2009,** *44* (3), 210-230.

112. Farwanah, H.; Kolter, T.; Sandhoff, K., Mass spectrometric analysis of neutral sphingolipids: methods, applications, and limitations. *Biochim Biophys Acta* **2011,** *1811* (11), 854-60.

113. Olling, A.; Breimer, M. E.; Peltomaa, E.; Samuelsson, B. E.; Ghardashkhani, S., Electrospray ionization and collision-induced dissociation time-of-flight mass spectrometry of neutral glycosphingolipids. *Rapid Commun Mass Spectrom* **1998,** *12* (10), 637-45.

114. Hsu, F. F.; Turk, J., Structural determination of glycosphingolipids as lithiated adducts by electrospray ionization mass spectrometry using low-energy collisional-activated dissociation on a triple stage quadrupole instrument. *J Am Soc Mass Spectrom* **2001,** *12* (1), 61-79.

115. Bou Khalil, M.; Hou, W.; Zhou, H.; Elisma, F.; Swayne, L. A.; Blanchard, A. P.; Yao, Z.; Bennett, S. A.; Figeys, D., Lipidomics era: accomplishments and challenges. *Mass Spectrom Rev* **2010,** *29* (6), 877-929.

116. Rohlfing, A.; Muthing, J.; Pohlentz, G.; Distler, U.; Peter-Katalinic, J.; Berkenkamp, S.; Dreisewerd, K., IR-MALDI-MS analysis of HPTLC-separated phospholipid mixtures directly from the TLC plate. *Anal Chem* **2007,** *79* (15), 5793-808.

117. Distler, U.; Hulsewig, M.; Souady, J.; Dreisewerd, K.; Haier, J.; Senninger, N.; Friedrich, A. W.; Karch, H.; Hillenkamp, F.; Berkenkamp, S.; Peter-Katalinic, J.;

Muthing, J., Matching IR-MALDI-o-TOF mass spectrometry with the TLC overlay binding assay and its clinical application for tracing tumor-associated glycosphingolipids in hepatocellular and pancreatic cancer. *Anal Chem* **2008,** *80* (6), 1835-46.

118.   Dreisewerd, K.; Muthing, J.; Rohlfing, A.; Meisen, I.; Vukelic, Z.; Peter-Katalinic, J.; Hillenkamp, F.; Berkenkamp, S., Analysis of gangliosides directly from thin-layer chromatography plates by infrared matrix-assisted laser desorption/ionization orthogonal time-of-flight mass spectrometry with a glycerol matrix. *Anal Chem* **2005,** *77* (13), 4098-107.

119.   Farwanah, H.; Pierstorff, B.; Schmelzer, C. E.; Raith, K.; Neubert, R. H.; Kolter, T.; Sandhoff, K., Separation and mass spectrometric characterization of covalently bound skin ceramides using LC/APCI-MS and Nano-ESI-MS/MS. *J Chromatogr B Analyt Technol Biomed Life Sci* **2007,** *852* (1-2), 562-70.

120.   Sullards, M. C.; Allegood, J. C.; Kelly, S.; Wang, E.; Haynes, C. A.; Park, H.; Chen, Y.; Merrill, A. H., Jr., Structure-specific, quantitative methods for analysis of sphingolipids by liquid chromatography-tandem mass spectrometry: "inside-out" sphingolipidomics. *Methods Enzymol* **2007,** *432*, 83-115.

121.   Shaner, R. L.; Allegood, J. C.; Park, H.; Wang, E.; Kelly, S.; Haynes, C. A.; Sullards, M. C.; Merrill, A. H., Jr., Quantitative analysis of sphingolipids for lipidomics using triple quadrupole and quadrupole linear ion trap mass spectrometers. *J Lipid Res* **2009,** *50* (8), 1692-707.

122.   Oikawa, N.; Matsubara, T.; Fukuda, R.; Yasumori, H.; Hatsuta, H.; Murayama, S.; Sato, T.; Suzuki, A.; Yanagisawa, K., Imbalance in fatty-acid-chain length of

gangliosides triggers Alzheimer amyloid deposition in the precuneus. *PLoS One* **2015,** *10* (3), e0121356.

123. Chan, R. B.; Perotte, A. J.; Zhou, B.; Liong, C.; Shorr, E. J.; Marder, K. S.; Kang, U. J.; Waters, C. H.; Levy, O. A.; Xu, Y.; Shim, H. B.; Pe'er, I.; Di Paolo, G.; Alcalay, R. N., Elevated GM3 plasma concentration in idiopathic Parkinson's disease: A lipidomic analysis. *PLoS One* **2017,** *12* (2), e0172348.

124. Sommer, U.; Herscovitz, H.; Welty, F. K.; Costello, C. E., LC-MS-based method for the qualitative and quantitative analysis of complex lipid mixtures. *J Lipid Res* **2006,** *47* (4), 804-14.

125. Merrill, A. H., Jr.; Sullards, M. C.; Allegood, J. C.; Kelly, S.; Wang, E., Sphingolipidomics: high-throughput, structure-specific, and quantitative analysis of sphingolipids by liquid chromatography tandem mass spectrometry. *Methods* **2005,** *36* (2), 207-24.

126. Zhang, T.; Watson, D. G., A short review of applications of liquid chromatography mass spectrometry based metabolomics techniques to the analysis of human urine. *Analyst* **2015,** *140* (9), 2907-15.

127. Demopoulos, C. A.; Kyrili, M.; Antonopoulou, S.; Andrikopoulos, N. K., Separation of Several Main Glycolipids into Classes and Partially into Species by HPLC and UV-Detection. *Journal of Liquid Chromatography & Related Technologies* **1996,** *19* (5), 771-781.

128. Zhu, T.; Xu, L.; Xu, X.; Wang, Z.; Zhu, J.; Xie, Q.; Zhang, B.; Wang, Y.; Ju, L.; He, Y.; Ye, X.; Zhou, D.; Li, Y., Analysis of breast cancer-associated

glycosphingolipids using electrospray ionization-linear ion trap quadrupole mass spectrometry. *Carbohydr Res* **2015,** *402*, 189-99.

129.   Kirsch, S.; Zarei, M.; Cindric, M.; Muthing, J.; Bindila, L.; Peter-Katalinic, J., On-line nano-HPLC/ESI QTOF MS and tandem MS for separation, detection, and structural elucidation of human erythrocytes neutral glycosphingolipid mixture. *Anal Chem* **2008,** *80* (12), 4711-22.

130.   Lee, H.; Lerno, L. A., Jr.; Choe, Y.; Chu, C. S.; Gillies, L. A.; Grimm, R.; Lebrilla, C. B.; German, J. B., Multiple precursor ion scanning of gangliosides and sulfatides with a reversed-phase microfluidic chip and quadrupole time-of-flight mass spectrometry. *Anal Chem* **2012,** *84* (14), 5905-12.

131.   Wong, M.; Xu, G.; Park, D.; Barboza, M.; Lebrilla, C. B., Intact glycosphingolipidomic analysis of the cell membrane during differentiation yields extensive glycan and lipid changes. *Sci Rep* **2018,** *8* (1), 10993.

132.   Bindila, L.; Peter-Katalinic, J., Chip-mass spectrometry for glycomic studies. *Mass Spectrom Rev* **2009,** *28* (2), 223-53.

133.   Olsen, B. A., Hydrophilic interaction chromatography using amino and silica columns for the determination of polar pharmaceuticals and impurities. *J Chromatogr A* **2001,** *913* (1-2), 113-22.

134.   Jandera, P., Stationary and mobile phases in hydrophilic interaction chromatography: a review. *Anal Chim Acta* **2011,** *692* (1-2), 1-25.

135.   Buszewski, B.; Noga, S., Hydrophilic interaction liquid chromatography (HILIC)-a powerful separation technique. *Anal Bioanal Chem* **2012,** *402* (1), 231-47.

136. Vlckova, H.; Jezkova, K.; Stetkova, K.; Tomsikova, H.; Solich, P.; Novakova, L., Study of the retention behavior of small polar molecules on different types of stationary phases used in hydrophilic interaction liquid chromatography. *J Sep Sci* **2014,** *37* (11), 1297-307.

137. Garbis, S. D.; Melse-Boonstra, A.; West, C. E.; van Breemen, R. B., Determination of folates in human plasma using hydrophilic interaction chromatography-tandem mass spectrometry. *Anal Chem* **2001,** *73* (22), 5358-64.

138. Scherer, M.; Leuthauser-Jaschinski, K.; Ecker, J.; Schmitz, G.; Liebisch, G., A rapid and quantitative LC-MS/MS method to profile sphingolipids. *J Lipid Res* **2010,** *51* (7), 2001-11.

139. Hajek, R.; Jirasko, R.; Lisa, M.; Cifkova, E.; Holcapek, M., Hydrophilic Interaction Liquid Chromatography-Mass Spectrometry Characterization of Gangliosides in Biological Samples. *Anal Chem* **2017,** *89* (22), 12425-12432.

140. Hajek, R.; Lisa, M.; Khalikova, M.; Jirasko, R.; Cifkova, E.; Student, V., Jr.; Vrana, D.; Opalka, L.; Vavrova, K.; Matzenauer, M.; Melichar, B.; Holcapek, M., HILIC/ESI-MS determination of gangliosides and other polar lipid classes in renal cell carcinoma and surrounding normal tissues. *Anal Bioanal Chem* **2018**.

141. Kirsch, S.; Muthing, J.; Peter-Katalinic, J.; Bindila, L., On-line nano-HPLC/ESI QTOF MS monitoring of alpha2-3 and alpha2-6 sialylation in granulocyte glycosphingolipidome. *Biol Chem* **2009,** *390* (7), 657-72.

142. Garcia, A. D.; Chavez, J. L.; Mechref, Y., Rapid and sensitive LC-ESI-MS of gangliosides. *J Chromatogr B Analyt Technol Biomed Life Sci* **2014,** *947-948*, 1-7.

143.   Chen, Y.; Liu, Y.; Sullards, M. C.; Merrill, A. H., Jr., An introduction to sphingolipid metabolism and analysis by new technologies. *Neuromolecular Med* **2010,** *12* (4), 306-19.

144.   Winograd, N.; Garrison, B. J., Biological cluster mass spectrometry. *Annu Rev Phys Chem* **2010,** *61*, 305-22.

145.   Chen, Y.; Allegood, J.; Liu, Y.; Wang, E.; Cachon-Gonzalez, B.; Cox, T. M.; Merrill, A. H., Jr.; Sullards, M. C., Imaging MALDI mass spectrometry using an oscillating capillary nebulizer matrix coating system and its application to analysis of lipids in brain from a mouse model of Tay-Sachs/Sandhoff disease. *Anal Chem* **2008,** *80* (8), 2780-8.

146.   Caughlin, S.; Maheshwari, S.; Agca, Y.; Agca, C.; Harris, A. J.; Jurcic, K.; Yeung, K. K.; Cechetto, D. F.; Whitehead, S. N., Membrane-lipid homeostasis in a prodromal rat model of Alzheimer's disease: Characteristic profiles in ganglioside distributions during aging detected using MALDI imaging mass spectrometry. *Biochim Biophys Acta* **2018,** *1862* (6), 1327-1338.

147.   Touboul, D.; Brunelle, A.; Laprevote, O., Mass spectrometry imaging: Towards a lipid microscope? *Biochimie* **2011,** *93* (1), 113-9.

148.   Gamble, L. J.; Anderton, C. R., Secondary Ion Mass Spectrometry Imaging of Tissues, Cells, and Microbial Systems. *Micros Today* **2016,** *24* (2), 24-31.

149.   Carado, A.; Passarelli, M. K.; Kozole, J.; Wingate, J. E.; Winograd, N.; Loboda, A. V., C60 secondary ion mass spectrometry with a hybrid-quadrupole orthogonal time-of-flight mass spectrometer. *Anal Chem* **2008,** *80* (21), 7921-9.

150. Zhang, Y.; Wang, J.; Liu, J.; Han, J.; Xiong, S.; Yong, W.; Zhao, Z., Combination of ESI and MALDI mass spectrometry for qualitative, semi-quantitative and in situ analysis of gangliosides in brain. *Sci Rep* **2016,** *6*, 25289.

151. Weishaupt, N.; Caughlin, S.; Yeung, K. K.; Whitehead, S. N., Differential Anatomical Expression of Ganglioside GM1 Species Containing d18:1 or d20:1 Sphingosine Detected by MALDI Imaging Mass Spectrometry in Mature Rat Brain. *Front Neuroanat* **2015,** *9*, 155.

152. Nilsson, O.; Svennerholm, L., Accumulation of glucosylceramide and glucosylsphingosine (psychosine) in cerebrum and cerebellum in infantile and juvenile Gaucher disease. *J Neurochem* **1982,** *39* (3), 709-18.

153. Hikita, T.; Tadano-Aritomi, K.; Iida-Tanaka, N.; Levery, S. B.; Ishizuka, I.; Hakomori, S., Cationic glycosphingolipids in neuronal tissues and their possible biological significance. *Neurochem Res* **2002,** *27* (7-8), 575-81.

154. Jozwiak, W.; Koscielak, J., Lactosylsphingosine-reactive antibody and CEA in patients with colorectal cancer. *Eur J Cancer Clin Oncol* **1982,** *18* (7), 617-21.

155. Hakomori, S. I., Release of carbohydrates from sphingoglycolipid by osmium-catalyzed periodate oxidation followed by treatment with mild alkali. *J Lipid Res* **1966,** *7* (6), 789-92.

156. Song, X.; Ju, H.; Lasanajak, Y.; Kudelka, M. R.; Smith, D. F.; Cummings, R. D., Oxidative release of natural glycans for functional glycomics. *Nat Methods* **2016,** *13* (6), 528-34.

157. Neuenhofer, S.; Schwarzmann, G.; Egge, H.; Sandhoff, K., Synthesis of lysogangliosides. *Biochemistry* **1985,** *24* (2), 525-532.

158. Schwarzmann, G.; Wendeler, M.; Sandhoff, K., Synthesis of novel NBD-GM1 and NBD-GM2 for the transfer activity of GM2-activator protein by a FRET-based assay system. *Glycobiology* **2005,** *15* (12), 1302-11.

159. Rao, C. S.; Lin, X.; Pike, H. M.; Molotkovsky, J. G.; Brown, R. E., Glycolipid transfer protein mediated transfer of glycosphingolipids between membranes: a model for action based on kinetic and thermodynamic analyses. *Biochemistry* **2004,** *43* (43), 13805-15.

160. Seyrantepe, V.; Lema, P.; Caqueret, A.; Dridi, L.; Bel Hadj, S.; Carpentier, S.; Boucher, F.; Levade, T.; Carmant, L.; Gravel, R. A.; Hamel, E.; Vachon, P.; Di Cristo, G.; Michaud, J. L.; Morales, C. R.; Pshezhetsky, A. V., Mice doubly-deficient in lysosomal hexosaminidase A and neuraminidase 4 show epileptic crises and rapid neuronal loss. *PLoS Genet* **2010,** *6* (9), e1001118.

161. Yu, R. K.; Schengrund, C.-L., *Glycobiology of the nervous system*. New York, NY : Springer, 2014.: 2014.

162. Kushwah, D.; Patel, H. B.; Sinha, P. K.; Jana, P. K., Practical Approach for the Determination of Response Factors of Impurities in Drugs by HPLC. *E-Journal of Chemistry* **2011,** *8* (4), 1504-1511.

CHAPTER 2

GLYCAN ANALYSIS BY ENZYMATIC DEGRADATION

OF GSLs USING ENDOGLYCOCERAMIDASE ENZYME

2.1 INTRODUCTION

Endoglycosidases are glycoside hydrolase (GH) enzymes that cleave non-terminal glycosidic bonds to liberate the oligosaccharides or glycans from glycolipids and glycoproteins.[1] These enzymes can act by a retaining mechanism or an inverting mechanism. In the retaining mechanism, the anomeric carbon of the reaction product is identical in stereochemistry to that of the substrate. In the inverting mechanism, the anomeric carbon of the reaction product and substrate are stereochemically different.[2-3] **(Figure 2–1)**
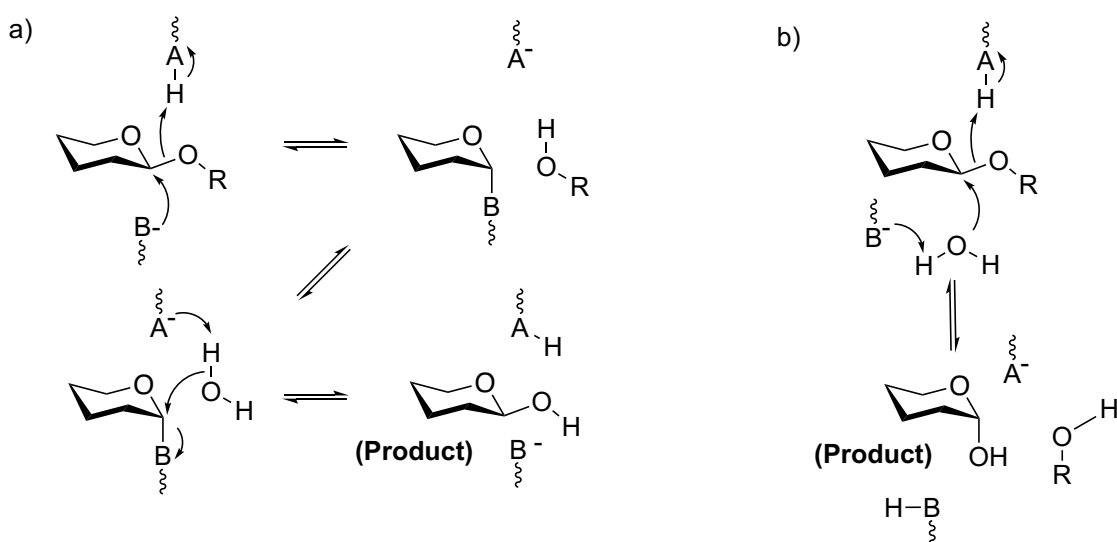
Figure 2–1. Mechanism of action of glyosyl hydrolase enzymes. (a) A retaining mechanism in which the glycosidic oxygen, activated by acid catalyst (AH), is attacked by the nucleophilic base (B-). The reaction intermediate undergoes nucleophilic substitution by a water molecule, leading to the formation of a product with the same anomeric configuration as the substrate; (b) An inverting mechanism is a one-step process involving protonation of the anomeric oxygen by AH and nucleophilic acid by an activated water molecule assisted by the base (B-), finally forming a product with the opposite anomeric configuration to the substrate.[2-3]

Endoglycoceramidases (EGCases), or ceramide glycanases, are a class of endoglycosidase enzymes that act specifically on GSLs, cleaving the ceramide lipid backbone to release the respective glycans.[4] Early on, EGCases were considered to fall under the large family of glycoside hydrolases, i.e., GH5 that show a strict preference towards cleavage of β-glycosidic bonds in only polar sugars, such as cellulose, xylan, etc.[5] However, detailed studies of the substrate recognition of these enzymes found that the active site contains a wide polar cavity suited for binding the oligosaccharide headgroup in GSLs and a narrower hydrophobic cavity that binds the ceramide lipid chain; these enzymes were found to bind amphiphilic substrates with both hydrophobic and hydrophilic moeities much better than strictly polar substrates, unlike other enzymes within the GH5 family.[6-7] Thus, EGCases were rendered as a new sub-category of the GH5 family of carbohydrate-active enzymes (CAZymes).[7]

EGCase enzymes have been isolated from a number of different organisms, namely prokaryotes, eukaryotes, and invertebrates including leeches, earthworms, and jellyfish.[8-10] Among these, enzymes identified in a certain strain of the bacteria *Rhodococcus sp.*[7] and a species of leech called *Macrobdella decora* [11] have been used most often. Three isoenzymes of EGCases were isolated from the M-750 strain of *Rhodococcus sp.*, EGCase I, II, and III. Each of these has its own set of specificities towards certain GSL substrates.[12] For example, EGCase III has the narrowest specificity, acting only on neogalatriaosylceramides (Galβ1-6Galβ1-6Galβ1-1'Cer) or the 6-gala series GSLs,[13] and EGCase II acts on a wide range of GSLs, except for the globo-series and fucosylated GSLs.[14] EGCase I has the broadest specificity and is most widely used for the purpose of GSL analysis.[14] Recently, two new EGCase I sequences, showing

excellent catalytic activity and extremely high expression in *Eshchericia coli* (*E. coli*), were isolated and characterized from *Rhodococcus equi* [7] and *Rhodococcus triatomea*. [15]

Platt and co-workers popularized the use of ceramide glycanase enzymes for the quantitative analysis of GSLs in the early 2000s. The aim of their study was to develop an assay that provided better identification, quantitation, and reproducibility than traditional TLC experiments. [16] The method of detection used for this assay was fluorescent labeling of oligosaccharide products with 2-aminobenzamide (2-AB) via a reductive amination, whereby the aldehyde at the reducing end of a monosaccharide reacts with an amine containing fluorophore to generate a Schiff base/imine intermediate that is reduced further by a reducing agent to a secondary amine. [17] These products were analyzed by High performance liquid chromatography (HPLC) with detection sensitivities of 1 pmol from tissue samples. [18] Their fluorophore of choice, 2-AB, was selected carefully after taking other glycan labeling fluorophores, such as aminobenzoic acid ethyl ester (ABEE)[17] and 2-aminopyridine (2-AP), into consideration. [19] The 2-AB fluorophore was selected as it was the most sensitive among these. The assay was applied to profiling and quantifying GSLs in mouse liver, brains, and human plasma. [18]

Using 2-aminobenzoic acid (2-AA) as the fluorophore instead of 2-AB required less than half the time, and was found to be more efficient for profiling and quantification of GSLs in mouse brain and liver samples. [11] The mode of chromatography used for HPLC separation was Hydrophilic Interaction Liquid Chromatography (HILIC), which has been the preferred mode for such amphiphilic molecules, allowing excellent resolution of neutral GSLs, simple, and complex GSLs. [15]

Even though the EGCase method of GSL profiling offers superior quantitation by analysis of fluorescently labeled products compared to the more frequently used MS based analytical methods **(Chapter 1)**, there are limited reports of this assay being used. The primary reason for this is that GSLs in general are a complex class of glycolipids that are difficult to analyze due to their structural diversity.[20] Additionally, it can be challenging to get quantitative results after extraction, purification, and recovery of GSLs from biological samples. Another possible reason for this assay being seldom used is that, although it is quantitative, it comes at a cost because it only provides information about the glycan component of GSLs with no information about the ceramide lipid counterpart.[21] For our group, however, this was an appealing feature of this assay since our goal was to develop two complementary methods for GSL analysis, which would provide information about the glycan and ceramide lipid components independently. This chapter outlines in detail the implementation of the EGCase method, adapted from the original work by Platt and co-workers, using the same fluorescent label (2-AA) and the same mode of chromatographic separation, i.e., HILIC using an amide-HILIC column (ThermoFisher, Accucore-150-Amide-HILIC, 2.6 μm, 2.1x150mm). We implemented this assay with slight modifications to labeling conditions and chromatographic separation gradients. We also used an improved form of EGCase I reported by Albrecht *et al.*[15] Applications of this assay in quantitative profiling of GSLs in porcine brains, mammalian cells, and human serum from Huntington's disease patients also have been outlined below.

2.2 RESULTS AND DISCUSSION

2.2.1 Expression and Purification of Endoglycoceramidase (EGCase I)

When this project was started, the EGCase enzyme initially was purchased from commercial sources. However, this enzyme was not sufficiently active and was abandoned. We decided to produce a recombinant form of the enzyme, following a recent study by Rudd and co-workers.[15] The gene identified was for EGCase I, which originates from the bacterial strain *Rhodococcus triatomea (R.triatomea)* and shows broad substrate specificity towards both neutral GSLs and acidic gangliosides. The gene encoding EGCase I with an N-terminal polyhistidine tag (His-tag) was synthesized, the protein was expressed in *E.coli*, and it was purified using a Fast Protein Liquid Chromatography (FPLC) instrument on a Ni-NTA agarose column. The detailed protocol is outlined in the **Materials and Methods** Section.

2.2.2 Optimization of Conditions for EGCase I Treatment

The reaction conditions for EGCase digestion were selected carefully after conducting pilot experiments with a mixture of LacCer and GM3. The mixture was digested with EGCase I, and the products were labeled with 2-AA at 80 °C for 45 min and analyzed by an LC-MS instrument coupled to a fluorescent detector. All chromatographic separations were carried out on an amide-HILIC column (Thermo, Accucore-150-Amide-HILIC, 2.6 μm, 2.1x150mm) since this is the most widely used mode of separation of glycans, affording excellent retention of complex glycans and excellent peak resolution as well.[11, 15, 18] Fluorescence was monitored at an excitation wavelength of 320 nm and an emission wavelength of 420 nm. EGCase I digestion was performed over a range of different

temperatures and incubation times, shown in **Figure 2–2**. The enzyme showed optimum activity at 37 °C by 15 h. Based on these data, all reactions were carried out at 37 °C for 18 h in the presence of a reaction buffer composed of 50 mM sodium acetate (pH 5.2) and 1 mg/mL sodium cholate. Because of the amphiphilic nature of GSLs, like any other GSL degrading enzyme, EGCase I also requires the presence of a detergent in the reaction buffer to maximize the cleavage of glycan headgroups.[15] Sodium cholate[18], sodium taurodeoxycholate [11], and Triton X-100 [15] are some common detergents in use. Triton X-100 was avoided since the polyethylene oxide chains interfere with Mass spectrometry (MS) analysis. We selected sodium cholate for this assay.

The first step in the process of characterizing EGCase I is calculating its activity. A commercially available standard ganglioside GM3 was used as the substrate for TLC experiments to test the activity of the enzyme qualitatively. It was chosen because its reaction product from EGCase is 3'-sialyllactose (3'-SL), a human milk oligosaccharide (HMO) that is readily available. The substrate, reaction mixture, and product were spotted on TLC plates, and bands were visualized using Orcinol stain.[22] A plate reader assay was used to determine the activity of EGCase I. Serial dilutions of 3'-SL were taken, labeled with 2-AA, and fluorescence was measured by monitoring at an excitation wavelength of 320 nm and an emission wavelength of 420 nm to obtain a calibration curve of Fluorescence intensity vs concentration of 3'-SL. **(Appendix A, Figure A–1)** An unknown concentration (x) of GM3 was digested with a certain amount of EGCase (calculated from the concentration of protein expressed in μg/μL) at 37 °C for 1 h, followed by 2-AA labeling at 80 °C for 45 min[11], and the fluorescence signal obtained was plotted on the calibration curve. The concentration (expressed in mg/mL) was

extrapolated from the x-axis to obtain the total amount of 3'-SL produced from the GM3 sample in 1 h. The activity of EGCase was expressed in units/mL or U/mL, where U is µmol/min, i.e., one unit is defined as the amount of enzyme required to hydrolyze 1 µmol of GM3 per min at 37 °C.
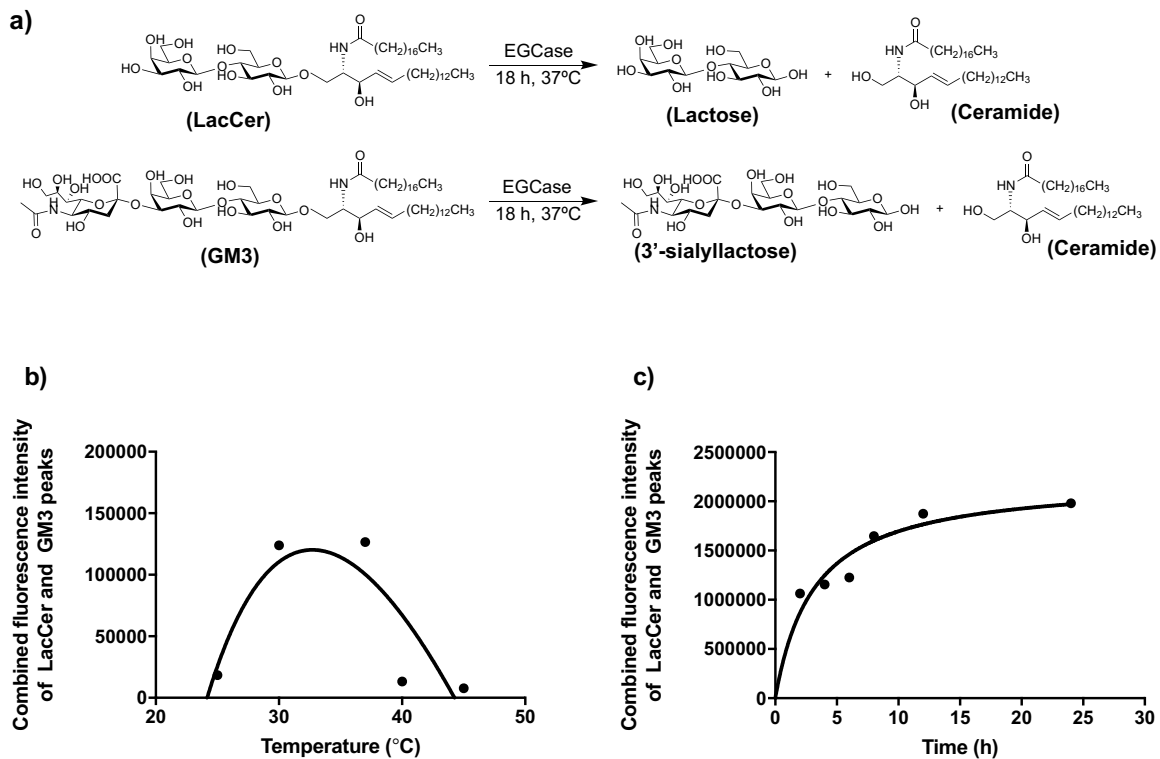
Figure 2–2. Optimization of temperature and incubation time conditions for EGCase reaction. (a) Reaction scheme showing action of EGCase on GSLs LacCer and GM3, to generate corresponding glycans Lactose and 3'-sialyllactose, respectively. (b) Standard mixtures of LacCer and GM3 were incubated at 25–45 °C for 24 h, followed by 2AA-labeling and fluorescence intensity was monitored on LC-MS to show maximum intensity was obtained at 37 °C; (c) Standard mixtures of LacCer and GM3 were incubated with EGCase at 37 °C for 2–24 h, followed by 2-AA labeling and fluorescence intensity was monitored to show maximum intensity between 15-24 h. Optimum enzyme activity conditions were selected as 37 °C and 18 h incubation time. Curve fits were based on Michaelis Menten binding saturation curves. Curves are shown to guide the eye and were not used for quantitative interpretation.

To confirm that the appropriate amounts of enzyme were being used to allow maximum glycan release from GSLs, titration experiments were performed using increasing amounts of EGCase I. A standard of ganglioside GM1 was digested with increasing amounts (in milliunits or mU) of EGCase I (2–11 mU) at 37 °C for 18 h. These were labeled with 2-AA at 80 °C for 45 min and analyzed by fluorescent LC-MS (F-LC-MS). The fluorescence intensity was plotted against the volume of enzyme added for each run. A sharp increase in response from 2 to 4 mU was observed, after which it plateaued until 7 mU, and gradually decreased slightly at 9 and 11 mU. From these results, we concluded that the optimal concentration for glycan release was 4–7 mU of EGCase I **(Figure 2–3)**.
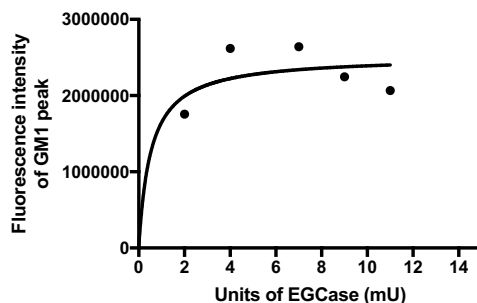
Figure 2–3. Optimization of EGCase I activity. The optimization of enzyme concentration was performed using commercially available standard ganglioside GM1 as the substrate. Serial dilutions of EGCase I were taken i.e. 2–11 mU, and a fixed amount of GM1 was subjected to digestion at 37 °C for 18 h in the presence of a reaction buffer (50 mM sodium acetate at pH 5.0, containing 1 mg/mL sodium cholate). The dynamic range of concentration that afforded optimum glycan cleavage was between 4 and 7 mU of EGCase I. Curve fits were based on Michaelis Menten binding saturation curves. Curves are shown to guide the eye and were not used for quantitative interpretation.

2.2.3 Optimization of 2AA Labeling Conditions

Components of the anthranilic acid (2-AA) labeling reaction mixture used in this study were boric acid, sodium acetate, sodium cyanoborohydride, and 2-AA.[18] Sodium cyanoborohydride serves as the reducing agent. The labeling reaction was carried out at 80 °C for 45 min according to established protocols.[11, 15, 18]

The labeling solution was maintained at pH 5.3. This falls within the range of pH 4–10, which is best suited for such reductive amination reactions with sodium cyanoborohydride.[23] Sialic acids are hydrolyzed readily under acidic pH. Considering this, it was important to make sure that gangliosides would not be desialylated under the labeling conditions. This was confirmed by subjecting ganglioside standard GM1 to EGCase digestion (6 mU) and 2-AA labeling (80 μL) conditions, and the labeled product was analyzed by F-LC-MS (fluorescence monitored at an excitation wavelength 320 nm and an emission wavelength 420 nm). It was confirmed from the fluorescence trace under the given labeling conditions that there was no additional peak corresponding to asialo-GM1, as shown in **Figure 2–4**. Additionally, the same experiment was conducted taking other temperature and time combinations, including 60 °C for 2 h [24] and 65 °C for 3 h (as used by Sigma-Aldrich or Ludger) to see if there were differences in the results. We observed no change to the final results, GM1 was seen always as a single peak in the fluorescence chromatogram, indicating no loss of sialic acid under any of the conditions. Hence, 80 °C for 45 min was used for labeling conditions.[17] **(Appendix A, Figure A–2).**

In order to confirm that reaction products of EGCase I digestion were labeled completely with 2-AA, titration experiments were conducted. In these experiments, a fixed quantity of standard GM1 and GM3 (~ 5 μg) in a mixture were digested with 6 mU

of enzyme and labeled with four different volumes of the fluorophore mixture (5, 20, 40, and 60 μL), followed by analysis on LC-MS. The fluorescence intensity was plotted against the volume of 2-AA added to the reaction mixture for each run. A sharp increase in fluorescence response was observed going from 5 to 20 μL for both GM3 and GM1. After this, the response increased slightly at 40 μL and remained constant up to 60 μL for GM1; however, for GM3, the response dropped slightly at 60 μL (**Figure 2–5).** Thus, 40 μL of fluorophore mixture was taken as the amount for optimum labeling.
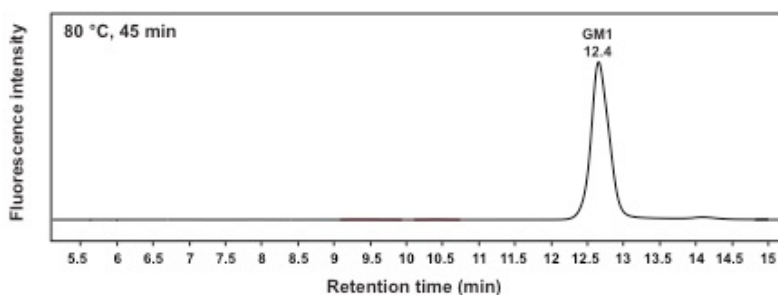
Figure 2–4. Chromatogram showing 2-AA labeled GM1-glycan. Standard ganglioside GM1 was subjected to EGCase digestion at 37 °C for 18 h in a reaction buffer (pH 5.2), followed by 2-AA labeling of GM1-glycan at 80 °C for 45 min. Only one peak was observed for GM1-glycan, confirming no loss of sialic acid under digestion and labeling conditions. A loss of sialic acid would reduce polarity, thereby decreasing the retention time on a HILIC column.

The final step in the labeling process was the post-labeling cleanup to remove unreacted fluorophore. According to previous reports, the Discovery DPA-6S column, which is an amide-HILIC cartridge, offers better profiles and better recovery of all gangliosides compared to other commonly used solid phase extraction (SPE) cartridges for this purpose.[11, 18] Hence, we proceeded with the DPA-6S cartridge for post labeling cleanup.
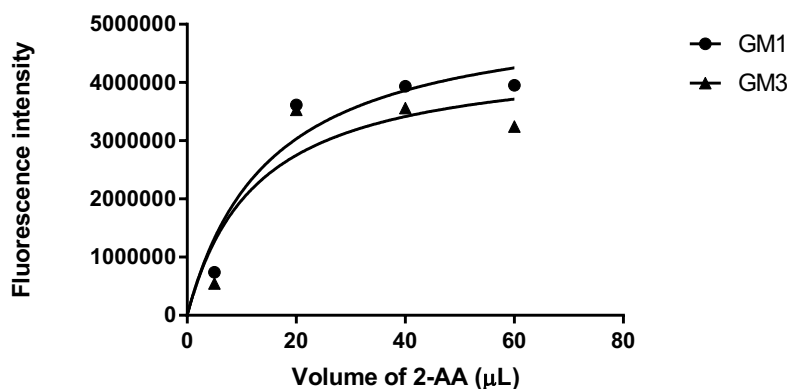
Figure 2– 5. Optimization of 2-AA labeling conditions. A fixed amount of gangliosides GM1 and GM3 in a mixture were subjected to digestion with 6 mU EGCase I, followed by labeling with 5, 20, 40, and 60 µL of 2-AA. The fluorescence intensity of GM1 and GM3 peaks, individually plotted against volume of 2-AA, shows a stark rise from 5 to 20 µL, after which it gets saturated until 60 µL for GM1 and slightly drops for GM3. The optimum volume of 2-AA that affords maximum labeling efficiency was identified to be 40 µL from these experiments. Curve fits were based on Michaelis Menten binding saturation curves. Curves are shown to guide the eye and were not used for quantitative interpretation.

2.2.4 Recovery of GSLs after Extraction, Purification, and 2-AA Labeling

Extraction of GSLs from biological samples such as tissues, cells, or plasma, is a critical step for accurate profiling and quantitation. Specific ratios of organic solvents, such as chloroform and methanol, along with a certain ratio of water, are required for the development of a robust extraction protocol. The widely accepted extraction solvent, chloroform:methanol:water in the ratio 4:8:3 was used for our assay.[25] The final volume of water added is the key to ganglioside partitioning into the upper phase, facilitating better ganglioside purity and recovery from proteins and other lipid components. To enhance the purity of extracted gangliosides from a biological sample a Sep Pak C18

cartridge was used to purify gangliosides from any undesired peptides, salts, and other impurities.[26]

This process of GSL analysis from extraction to digestion with EGCase I and finally labeling oligosaccharides with 2-AA includes passing the reaction mixture through two columns, SepPak C18 and DPA-6S amide-HILIC cartridges. In order to check the recovery of gangliosides from these columns, two different sets of samples containing a mixture of standard GSLs, lactosylceramide (LacCer), GM3, GM1, and GD3, were subjected to EGCase I digestion and 2-AA labeling under the optimum conditions outlined in **Sections 2.2.2 and 2.2.3**. Between the two sets, one was a sample mixture subjected to both SepPak C18 and DPA-6S amide-HILIC (C18 + HILIC) and the other was only a DPA-6S amide-HILIC (HILIC) cleanup. The relative percentage of each GSL was calculated taking the sum of all fluorescence peak areas from the chromatogram and expressing that as a percent of the total peak area **(Figure 2–6).** From the data in **Table 2–1**, it can be seen that the ratios of recovery of individual GSLs in the mixture are consistent between the two conditions. The C18+HILIC condition gave slightly better recoveries of GM3 and GD3. These results confirmed that the relative recovery was not affected by extraction and purification steps and there is reasonable correlation in the recovery percentages between the two procedures **(Figure 2–6b)**. The chromatographic profiles corresponding to each condition are shown in **Appendix A (Figure A–3 and A-4)**.
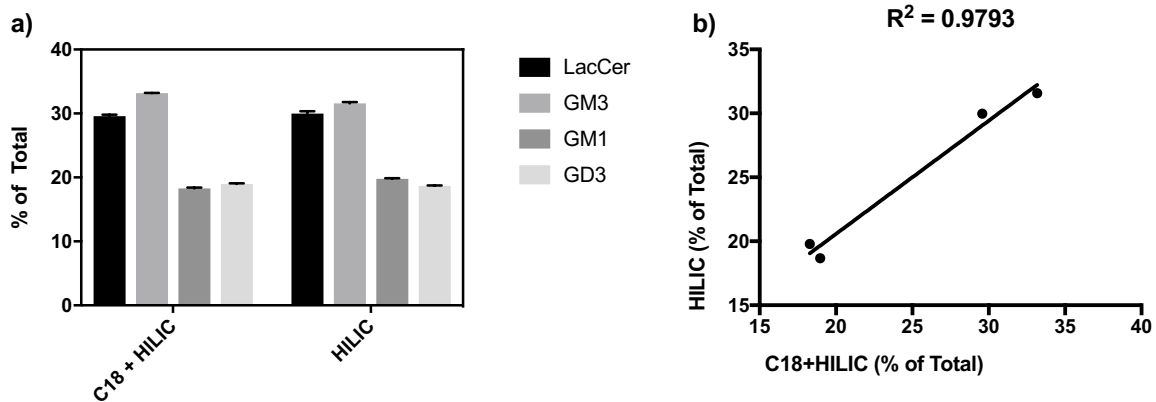
Figure 2–6. Percent recovery of a standard GSL mixture containing LacCer, GM3, GM1, and GD3.
(a) A mixture of LacCer, GM3, GM1, and GD3 was subjected to EGCase I digestion at 37 °C for 18 h, followed by 2-AA labeling. Two sets of samples were analyzed: SepPak C18 and Discovery DPA-6S amide-HILIC clean up (C18 + HILIC) and only Discovery DPA-6S amide-HILIC clean up. Ratios of the recovery of each GSL were consistent for both sets of samples. The fluorescent peak areas of each GSL are represented as a percent of the total fluorescence peak area of all GSLs in the mixture. Values represent mean ± standard error of mean (SEM) of triplicate measurements (n = 3). (b) Plot of average % compositions of GSL glycans recovered from C18+HILIC and only HILIC clean ups shows good correlation with R^2 = 0.9793.

Table 2– 1. Percent recovery of GSL glycans. Relative percentage recoveries of standard GSLs LacCer, GM3, GM1, and GD3 subjected to SepPak C18+HILIC and only HILIC post labeling clean ups. Values represent mean ± standard error of mean (SEM) of triplicate measurements (n = 3).

	LacCer	GM3	GM1	GD3
C18 + HILIC	29.6 ± 0.1	33.17 ± 0.03	18.28 ± 0.08	18.9 ± 0.1
Only HILIC	29.9 ± 0.2	31.6 ± 0.1	19.78 ± 0.06	18.7 ± 0.1

Sources of error affecting these data may include preparation of standard solutions. The concentration of stock solutions of each GSL used in this assay was 1 mg/mL, which was prepared by gravimetric analysis. From each stock solution, 5 μL was used, which corresponds to 5 μg of each GSL used as the substrate for EGCase I.

Inaccuracy in balances would affect the final concentration of the solution. Pipettes used to take aliquots of standard solutions may be a source of error. Additionally, the enzyme may show preferential reactivity towards certain GSLs, cleaving one more efficiently over another. This may lead to unequal recovery between each GSL. Keeping all these issues in mind, when interpreting the results of these recovery experiments, it was reasonable to look for consistency in the ratios of recovery between the two different conditions.

2.2.5 Determination of Limit of Detection (LOD) and Limit of Quantitation (LOQ)

Limit of detection (LOD) is defined as the lowest concentration of analyte that can be differentiated clearly from the baseline and is suitable for detection. Limit of Quantitation (LOQ) is defined as the lowest concentration of analyte that can not only be detected but be quantified precisely as well.[27] LOD and LOQ for this assay were calculated by the method of linear regression, whereby a linear calibration curve is obtained for instrument response (fluorescence intensity in our case) versus a series of low concentrations of the analyte. The value of LOQ is usually higher than the value of LOD. The formula used for calculating LOD and LOQ are given as follows:

$$LOD = \frac{3S_a}{m}, \ LOQ = \frac{10S_a}{m},$$

where S_a is the standard deviation of the response and m is the slope of the calibration curve expressed in the form of the equation $y = mx + c$.[27]

The calibration curve of fluorescence intensity vs amounts of GM3 (in ng) obtained for our assay, when the glycan moiety (3'-SL) was released by the action of 6

mU EGCase I and labeled with 2-AA, is shown in **Figure 2–7**. A sample of GM3 from a stock solution (~1 mg/mL), was diluted to a range of concentrations. The liberated 3'-SL was labeled with 2-AA according to the established labeling protocol outlined in **Section 2.2.3**. The response generated was linear over the entire range of concentrations considered. From the linear calibration curve, the slope was obtained by linear regression. The value of S_a was obtained from Excel using the STEYX function, and LOD was found to be 2.55 ng, which is approximately 2 pmol. This was comparable to previous studies that have achieved sensitivities in the pmol scale for this assay.[18]
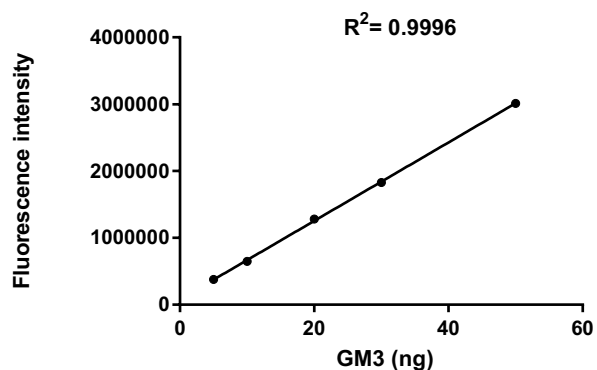
Figure 2–7. Determination of Limit of Detection (LOD). Substrate GM3 (in ng scale) was subjected to EGCase I digestion, followed by 2-AA labeling of the released glycan moiety (3'-SL) and monitoring of fluorescence intensity of the GM3 peak. The response was linear over the range of GM3 concentrations considered. From the calibration curve, the y-intercept and slope were found to be 81039 units and 58651, respectively. The LOD was calculated to be 2.55 ng

The LOQ was found to be 8.50 ng, which is approximately 6.70 pmol. The numbers obtained from this experiment are based on the following assumptions: (a) GM3 was assumed to be a single spcies of molecular weight 1267.849 g/mol for GM3 (d18:1-18:0); (b) the stock solution of GM3 was prepared gravimetrically; and (c) the absolute

number for LOD also may be variable for different GSLs based on recovery and molecular weight **(Section 2.2.4)**. However, based on previous reports, it can be said that the dynamic range of analyte concentrations within which the calibration curve maintains its linearity is consistent for a variety of simple and complex gangliosides.[11, 18] Considering these issues, we considered the sensitivity of our assay to be in the nanogram or picomole range.

2.2.6 Selection of An Internal Standard for Quantification

In order for this assay to be used quantitatively, an internal standard was required. The main criteria for the selection of an internal standard was that it would be well separated from all possible GSLs in a complex biological sample, it would have structural similarities with GSLs, it would be recovered with equal efficiency when subjected to purification conditions, and it would be readily available. Since this assay analyzes only glycan moieties of GSLs, it was reasonable to search for suitable oligosaccharides that could be used as standards. Using any of the GSL glycans was not feasible since the standard peak would overlap with the analyte peak. Focusing our search on bulkier oligosaccharides seemed practical because they are very polar and would retain longer on the amide-HILIC column that was being used for chromatographic separation of GSLs. N, N', N'', N'''- tetraacetyl chitotetraose or chitotetraose (GlcNAcβ1-4GlcNAcβ1-4GlcNAcβ1-4GlcNAc) bearing acetylated forms of four N-Acetylglucosamine residues was the first tetrasaccharide that was tested to serve as an internal standard. After EGCase I digestion of a standard mixture of LacCer, GM3, GM1, and GD3, prior to 2-AA labeling, chitotetraose was spiked into the mixture. This way, glycans released from the

GSL mixture along with chitotetraose would be subjected to the same labeling conditions and post labeling clean-up. The peak for chitotetraose was seen between GM3 and LacCer **(Appendix A, Figure A–5)**.

Further testing for polysaccharides bulkier than chitotetraose that would retain longer on the HILIC column was not fruitful because they are difficult to synthesize, and the ones that are commercially available are expensive. We evaluated smaller sugars, monosaccharides or disaccharides, which would elute earliest. Excellent chromatographic separation was achieved for glucose. However, glucosylceramide (GlcCer) could be present in biological samples. This would release glucose after EGCase I digestion, the fluorescence peak of which would overlap with the glucose standard peak. This limits the applicability of glucose as a standard. Next, a disaccharide maltose was found to be readily distinguishable from LacCer, as well as the other peaks, for complex GSLs in the mixture **(Figure 2–8)**. Thus, maltose was chosen as the internal standard for our assay.
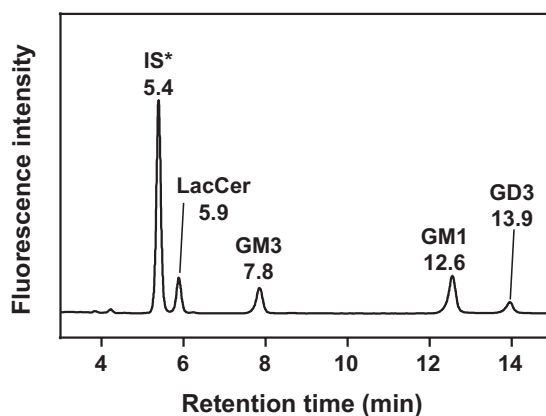
Figure 2– 8. Selection of the internal standard. A standard mixture of commercially available GLSs LacCer, GM3, GM1, and GD3 was subjected to EGCase digestion at 37 °C for 18 h, followed by 2-AA labeling at 80 °C for 45 min. Prior to labeling, maltose was added as an internal standard (IS*). The maltose peak eluted at ~ 5.4 min and was well resolved.

2.2.7 Method Validation using Porcine Brain

Gangliosides typically are enriched in the brain; thus, the applicability of this method was tested first on brains from juvenile pigs. Brain tissues were homogenized and aliquots were frozen. To maintain consistency between replicate runs, identical amounts of brain homogenate (10 μL corresponding to ~ 2 mg of wet tissue weight, and 2.079 mg/mL protein concentration) were used for extraction. Extraction of GSLs from these aliquots generated 0.3–0.5 mg of dry GSL that were subjected to EGCase I digestion, followed by labeling with 2-AA, and analysis by F-LC-MS using an amide-HILIC column. An internal standard (IS*) of maltose was spiked in (0.05–0.15 μg/mL).

A representative GSL profile in porcine brains is shown in **Figure 2–9**. LacCer (6.3 min), GM3 (7.9 min), GM2 (9.6 min), GM1 (12.6 min), Fucosyl-GM1 (14.2 min), GD1a (15.8 min), GD1b (17.9 min), Fucosyl-GD1 (19.2 min), and GT1 (20.4 min) were identified and quantified as absolute concentration based on the IS*. To investigate inter-assay variability, three different brain homogenate aliquots of the same volume were subjected to an identical protocol. All three GSL profiles and corresponding quantitation are shown in detail in **Appendix A, Figure A–6**. Results of these experiments show a relative standard error (RSE) within 10% for the composition of each GSL between runs, except for GM3 and GT1, which show a RSE close to 15%.
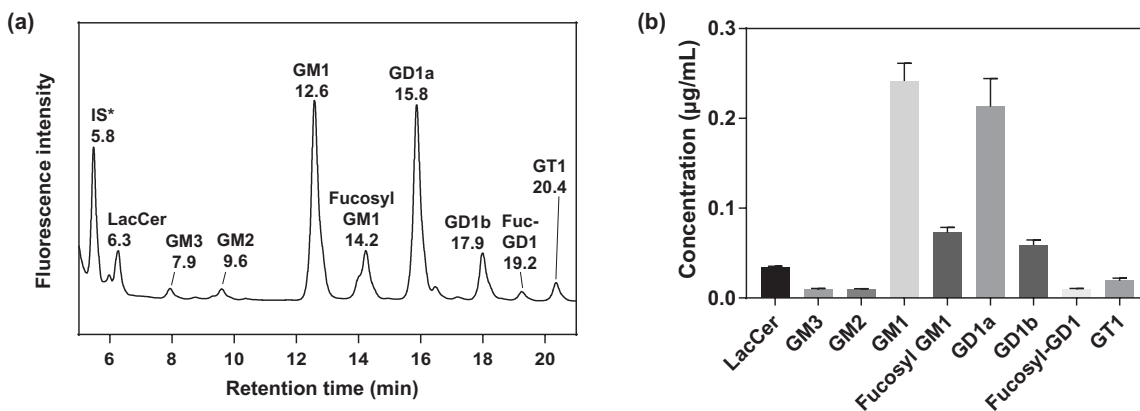
Figure 2–9. Glycosphingolipid (GSL) profiling in porcine brain. (a) HPLC separation of 2-AA labeled oligosaccharides generated from EGCase digestion of GSLs extracted from porcine brain. The GSLs identified were LacCer, GM3, GM2, GM1, Fucosyl-GM1, GD1a, GD1b, Fucosyl-GD1, and GT1. Peak assignment was based on commercially available standards (Figure 2–8), and confirmed by HR-ESI-MS (b) Concentration of individual GSLs in porcine brain based on the peak area of internal standard (IS*) maltose. Values represent mean ± standard error of mean of triplicate measurements, n = 3.

The peaks for LacCer, GM3, and GM1 could be assigned based on the retention times observed from standard mixtures **(Figure 2–8)**. The remaining GSL peaks were assigned by High Resolution Electrospray Ionization Mass Spectrometry (HR-ESI-MS), as outlined in **Materials and Methods**. A full list of target and identified masses is provided in **Appendix A**. Masses were assigned to four decimal places for accuracy. The form of MS used in our assay cannot distinguish between isomeric forms of GD1 (GD1a and GD1b); hence, they were assigned based on previous reports of chromatographic separation of these gangliosides on a HILIC column, whereby the 'a' isomers are expected to elute before the 'b' isomers.[11, 28] Only one peak each for Fucosyl-GD1 and GT1 was observed, suggesting the presence of either of the two isomers, 'a' or 'b', for each; however, these were not assigned.

68

Table 2– 2. Concentrations of individual GSLs in porcine brain. Quantification was based on the known concentration of internal standard (IS*) maltose added.[1]

Retention time (min)	Glycosphingolipid (GSL)	µg/mL
6.3	LacCer	0.034 ± 0.002
7.9	GM3	0.009 ± 0.001
9.6	GM2	0.009 ± 0.001
12.6	GM1	0.24 ± 0.02
14.2	Fucosyl-GM1	0.07 ± 0.01
15.8	GD1a	0.21 ± 0.03
17.9	GD1b	0.059 ± 0.005
19.2	Fucosyl-GD1	0.009 ± 0.001
20.4	GT1	0.019 ± 0.002

To investigate the validity of our assay, it was important to understand how this assay compared to other methods already in use for the purpose of GSL analysis. Literature reports on porcine brain gangliosides have shown the presence of GM1, GD1a, GD1b, GT1a, and GT1b as the major gangliosides consistently, which is comparable to the results of our assay.[28-30] Fucosyl-GM1 was a surprise since it is resistant to cleavage against a particular EGCase enzyme from a different species of the *Rhodococcus* bacteria. However, its presence in porcine brain, along with the presence of Fucosyl-GD1 has been reported previously.[31-32] The sulfated form of galactocerebroside was not observed in our assay, even though it is said to be abundant in brain gangliosides.[33] This is likely because EGCase enzymes are known to be unreactive towards them.[12] Methods which rely on MS/MS techniques can characterize the structure of unknown GSLs precisely based on their fragmentation pattern but cannot quantify the absolute concentrations accurately.[34] Some studies have utilized combinations of Liquid chromatography and Mass

---

[1] Values represent mean ± standard error of mean (SEM) of triplicate measurements (n = 3)

Spectrometry, such as LC-ESI-MS/MS, to analyze GSLs in complex mixtures like porcine brain.[28] However, these methods offered poor resolution of individual GSL peaks, and as a result quantification based on individual peak areas could not be performed. Moreover, MS-based assays for analysis of total lipid components in biological samples do not always include data on GSLs. This is likely because of the limited availability of suitable MS standards for GSLs, thereby hampering accurate identification and quantification.[35] The strategy of chemical modifications of gangliosides also has been employed in this respect, but their inherent drawbacks of incomplete reactions and requirements of large amounts of starting material limits their application in quantitative profiling of GSLs.[29, 32]

From the results of our assay and previous reports on ganglioside profiling in porcine brain, we concluded that our method was comparable to previous reports. Absence of gangliosides such as GQ1 or GT3 in our juvenile pig brain samples, which have been seen in previous reports[28], can be attributed to the fact that the expression level of GSLs is age dependent and that different regions of the brain show a prevalence of certain gangliosides over others.[36-37] Our assay offers a superior method of quantitation because it is based on fluorescence.

2.2.8 Method Validation using Jurkat T Cells

Knowing that our method was sensitive enough to work on tissues, we were interested to find out whether we could apply this to mammalian cells. A mammalian T cell line, Jurkat (Clone E6-1, ATCC TIB-152), was tested for quantitative profiling of GSLs because GSL profiles in these cells have been rarely studied. The first hurdle in designing

experiments was picking the right amount of material that would be sensitive enough for our assay since we had no point of reference to refer to with limited reports of gangliosides in Jurkat T cells. Based on the amount of dry extract used for brain tissues, 0.3–0.5 mg, cell numbers within the range 0.2–1 x 10^6 (with protein concentration 1.36 mg/mL) were able to provide dried GSL extracts within the desired range. The dried extracts were subjected to EGCase I digestion, followed by 2AA labeling after addition of an appropriate amount of IS* within a range of 0.1–0.25 µg/mL.

A complete GSL profile for Jurkat T cells is shown in **Figure 2–10**, indicating the presence of LacCer (5.9 min), GM3 (8.2 min), GM2 (9.6 min), GM1 (12.9 min), GD3 (14.3 min), and GD1 (16.2 min). GM3 and GM2 are the gangliosides that dominate the total GSL composition in these cells, with GM3 taking up over 90% of the composition. The GSL peaks were quantified by taking the fluorescent peak area of internal standard maltose as 100% and representing each GSL as a percentage of this. Then, the absolute numbers were calculated from the known concentration of maltose added. Taking three different samples containing the same number of cells, inter-assay variability was tested. All three GSL profiles and corresponding quantitation are shown in **Appendix A, Figure A–7**. The results of these experiments show an RSE within 10% for the composition of each GSL between runs, except for the RSE of GD1a, which was 18%.
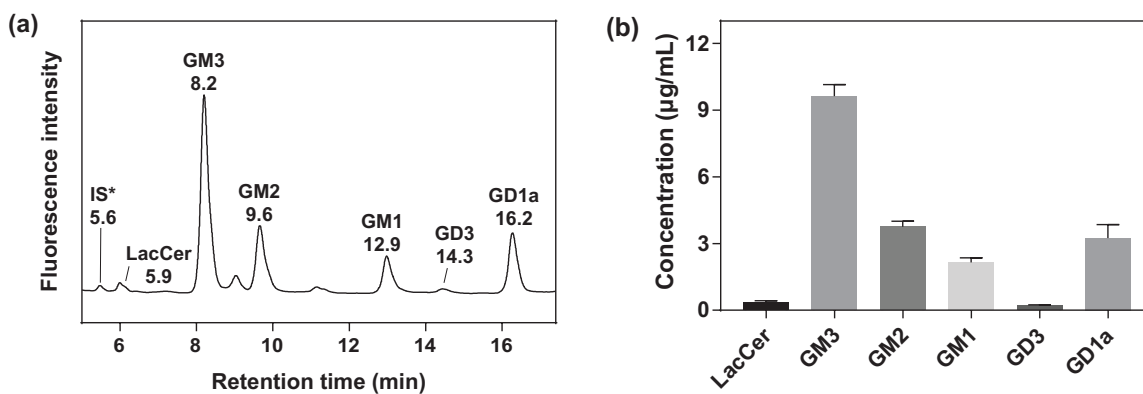
Figure 2– 10. Glycosphingolipid (GSL) profiling in Jurkat T cells. (a) HPLC separation of 2-AA labeled oligosaccharides generated from EGCase digestion of GSLs extracted from Jurkat T cells. The GSLs identified were LacCer, GM3, GM2, GM1, GD3, and GD1a. (b) Concentration of individual GSLs in Jurkat T cells. Quantification was performed based on the peak area of internal standard (IS*) maltose. Values represent mean ± standard error of mean of triplicate measurements, n = 3.

LacCer, GM3, GM1, and GD3 peaks were assigned by comparing the retention times to the standard runs performed earlier, shown in **Figure 2–8**. GM2 and GD1a standards were not available and were assigned by High Resolution Electrospray ionization Mass Spectrometry (HR-ESI-MS). The single GD1 peak at 16.2 min was assigned as GD1a.

Complete lipid profiles in multiple mammalian cell lines, including Jurkat T-cells, have been reported, however, these generally lack data on GSL. These studies choose to analyze lipid classes, such as phosphatidylcholine (PC), lysophosphatidylcholine (LPC), phosphatidylethanoamine (PE), sphingomyelin (SM), and cholesterol.[38-39] These analyses are carried out using LC-MS, and relative quantification is performed based on MS only, which are usually not sensitive and accurate enough to analyze this complex class of

72

glycolipids.[40] Van der Spoel reported a GSL profile in Jurkat T cells previously, utilizing the same method reported by Platt. According to this study, the major GSLs identified were LacCer, GM3, GM2, and GM1, which is in close agreement with our data. Our assay also detected GD3 and GD1a as well. The authors assigned GSL peaks based on glucose units (GU) obtained from a 2-AA labeled glucose oligomer ladder, however, they did not use an internal standard to provide absolute quantifications, and the cell numbers used for this assay were much higher (3×10^6).[41] Other reports also have confirmed the presence of GM1 and GM2 in Jurkat T-cells using qualitative analytical methods.[42]

Table 2– 3. Concentrations of individual GSLs in Jurkat T-cells. Quantification was based on the known concentration of internal standard (IS*) maltose added.[2]

Retention time (min)	Glycosphingolipid (GSL)	μg/mL
5.9	LacCer	0.34 ± 0.01
8.2	GM3	9.6 ± 0.5
9.6	GM2	3.8 ± 0.3
12.9	GM1	2.1 ± 0.2
14.3	GD3	0.23 ± 0.02
16.2	GD1a	3.2 ± 0.6

From these results, we concluded that our method was consistent and more sensitive than previous reports. Our assay was able to identify two new GSL components in these cells, i.e., GD1a and GD3, it was three times more sensitive in terms of material used than the previous study based on the same method,[41] and provided a superior absolute quantification method based on fluorescence.

---

[2] Values represent mean ± standard error of mean (SEM) of triplicate measurements (n = 3).

2.2.9 GSL Profiling in Human Serum from Huntington's Disease Patients

Previous literature reports about the pathology of Huntington's disease (HD) have shown the involvement of ganglioside GM1 and the therapeutic effects of exogenous addition of GM1 in HD mouse models.[43-44] With our assay, we were interested to find out whether changes in other gangliosides are observed in human patients suffering from HD by analyzing serum from these individuals. Levels of gangliosides would need to be compared to normal human serum using our GSL profiling method.

Ganglioside profiling in human serum has been a subject of interest for quite some time, primarily because of the association of gangliosides with diseases like Sandhoff [45], Tay-Sachs [45], Alzheimer's [46], and Huntington's [44]. Gangliosides in serum are in complex with lipoproteins, primarily low-density lipoproteins (LDL). Previous reports have used large volumes of serum, (e.g. 1 mL or 0.6 mL) [47-48] for thin layer chromatography (TLC) and high performance thin layer chromatography (HPTLC) assays. Later studies have used volumes in the microliter scale (180 μL),[15] with the EGCase method on an automated UPLC-HILIC-FLD instrument. In our protocol, 50 μL of serum was enough to afford equal sensitivity as the porcine brain and Jurkat T cell assays.

With our assay, the major GSLs in human serum were identified to be LacCer (6.1 min), GM3 (8.1 min), Gb3 (6.7 min), GM1 (13.8 min), GA1 (9.4 min), GD1b (18.1 min), GD3 (14.3 min), GA2 (6.3 min), and GM2 (9.9 min), with GM3 being dominant. This is in close correlation with other literature reports.[49] Additionally, some reports have suggested the presence of neo-lacto series GSLs, such as nLc4, and lacto series GSL, such as nLc6, in extremely low abundance.[15] The amounts of these GSLs are extremely

Table 2– 4. Concentrations of individual GSLs in serum from normal individuals and Huntington's disease patients. Quantification was based on the known concentration of internal standard (IS*) maltose added.[3]

Retention time (min)	Glycosphingolipids (GSLs)	Control (µg/mL)	Huntington's (HD) (µg/mL)
6.1	LacCer	0.06 ± 0.01	0.08 ± 0.02
6.3	GA2	0.053 ± 0.002	0.08 ± 0.01
6.8	Gb3	0.012 ± 0.002	0.012 ± 0.001
8.1	GM3	0.4 ± 0.1	0.5 ± 0.1
8.6	GM2	0.017 ± 0.005	0.023 ± 0.004
8.9	GA1	0.025 ± 0.006	0.022 ± 0.005
12.8	GM1	0.028 ± 0.006	0.05 ± 0.02
14.0	GD3	0.024 ± 0.005	0.1 ± 0.1
15.3	diF(2,4)-Lc4	0.043 ± 0.004	0.04 ± 0.01
18.0	GD1b	0.02 ± 0.01	0.015 ± 0.004

low and are likely below the LOD/LOQ requirements of our assay. Also, the GSL/ganglioside expression levels are variable depending on age or differences in GSL biosynthesis.[20] The GSL di-Fuc(2,4)-Lc4 was a surprise since it was not detected in any other biological samples that were analyzed. But this finding is consistent with previous data on GSL analysis in human serum.[15] Peak assignments were made based on retention times of commercially available standards and also by High Resolution Electrospray ionization Mass Spectrometry (HR-ESI-MS), details of which are outlined in the **Materials and Methods** Section. Comparing the profiles of normal human serum and serum from Huntington's patients, we found only minor changes of no significance in any of the GSLs. The absolute concentrations between the two groups were compared using a student's t-test, but we did not observe any significant differences.

---

[3] Values represent mean ± standard error of mean (SEM) of triplicate measurements (n = 3)
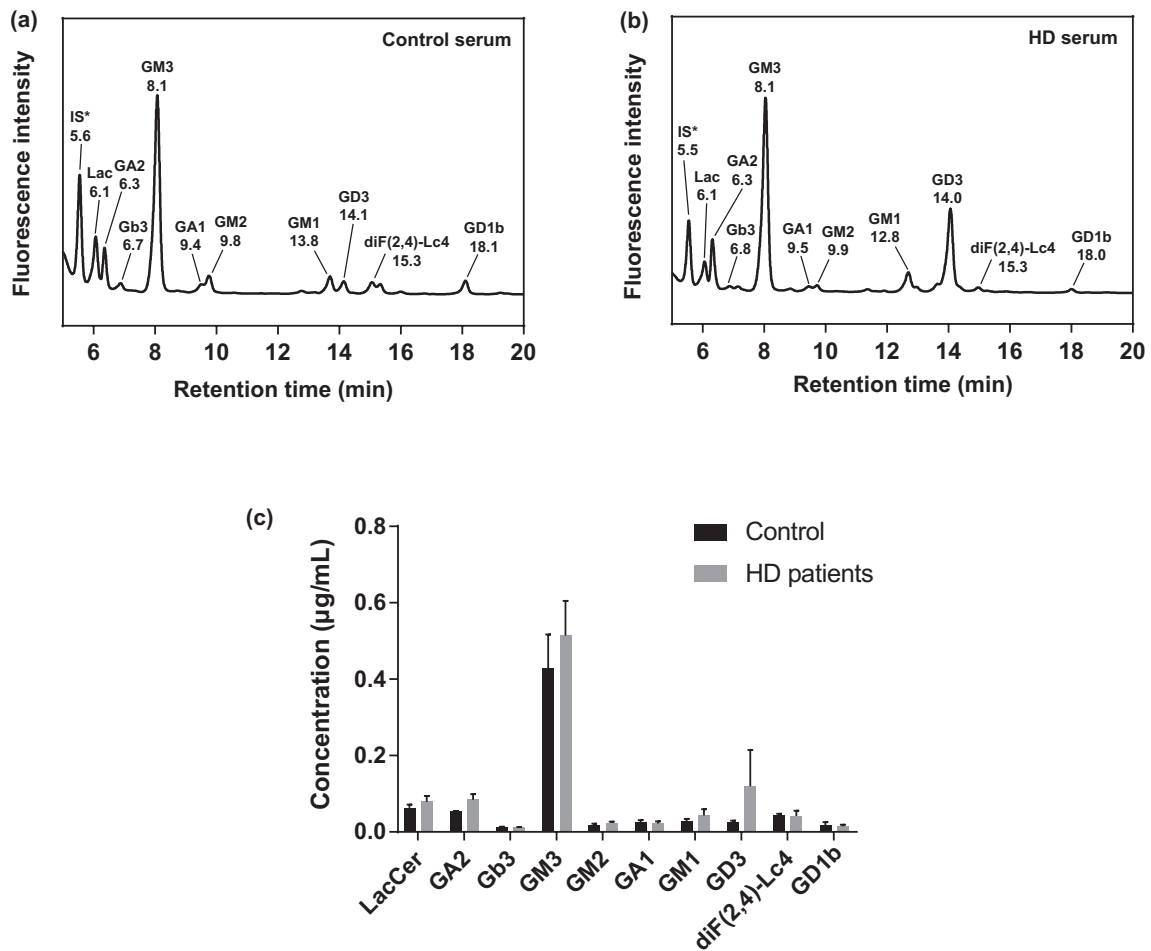
Figure 2– 11. Glycosphingolipid profiling in normal human serum and serum from Huntington's disease patients. HPLC separation of 2-AA labeled oligosaccharides generated from EGCase digestion of GSLs extracted from (a) normal human serum and (b) serum from Huntington's disease (HD) patients. The GSLs identified were LacCer, GA2, Gb3, GM3, GM2, GA1, GM1, GD3, diF(2,4)-Lc4, and GD1b. Peak assignment was performed based on commercially available standards, shown in Figure 2–8, and further confirmed by HR-ESI-MS. (c) Concentration of individual GSLs in control and HD patient serum. Quantification was based on the internal standard (IS*) maltose. Values represent mean ± standard error of mean of triplicate measurements for each group, n = 3.

Surprisingly, GM1, which is said to decrease in HD patients, was seen to increase slightly in our assay. We did observe significant variability between HD samples, which may suggest that additional replicates are needed [**Figure 2–11 (b)**].

This assay gives information only on the glycan moieties, while the lipid chain of GSLs for these patients were not analyzed. **Chapter 4** investigates the lipid chains of these GSLs identified in HD patients.

2.3 CONCLUSIONS

This chapter describes the development of a GSL profiling and quantitation method based on a previously established protocol by Neville et al.[11] An improved enzyme endoglycoceramidase (EGCase I) was used to modify GSLs. A robust extraction protocol has been utilized to extract GSLs from biological samples, such as cells, tissues, and human serum. GSL derived glycans were analyzed quantitatively via F-LC-MS after fluorescent labeling with 2-AA. This method has been validated with analysis of mammalian cells and brain tissues from pigs showing sensitivies in the low picomolar range. The strength of MS based techniques currently in use for GSL analysis lies in the fact that they are capable of extensive structural characterization and identification of a large number of GSLs in a given sample. However, quantification is a challenge due to limited availability of suitable standards that show identical fragmentation patterns as the analyte. This is the fundamental basis of MS based assays as has been highlighted in detail in **Chapter 1**. The EGCase assay is able to simplify quantitation by restricting analysis to the glycan moiety of each GSL component and offers a superior method of quantitation based on fluorescence.

2.4 MATERIALS AND METHODS

2.4.1 Materials

All reagents were purchased from Sigma-Aldrich (Oakville, Ontario, Canada), except for the following: GSL standards LacCer, GM3, GM1, and GD3 were purchased from Avanti Polar Lipids Inc. (Alabaster, Alabama, USA); EGCase I genes from GenScript (Piscataway, NJ, USA); Accucore-150-Amide-HILIC, 2.6 mm, 2.1 x 150 mm from Thermo Fisher Scientific (Mississauga, Ontario, Canada), Amicon Ultra-centrifugation filters from Thermo Fisher Scientific (Mississauga, Ontario, Canada), and SepPak C18 cartridge from Waters Corporation (Milford, MA, USA). Porcine brains were obtained from the Swine Research and Technology Centre at the University of Alberta, and human serum samples (normal and Huntington's disease) were a generous donation from Dr. Simonetta Sipione of the Department of Pharmacology at the University of Alberta.

2.4.2 Jurkat T Cell Culture

Jurkat T cells (Clone E6-1, ATCC TIB-152) were purchased from ATCC (Mannassas, VA). They were cultured in RPMI 1640 media containing fetal bovine serum (FBS) (10%, v/v) and penicillin (10 units mL^{-1}) in a humidified incubator with 5% CO_2 at 37 °C. All experiments were performed with cells in passage numbers P4–P5.

2.4.3 Preparation of Porcine Brain Homogenates

Brains from juvenile pigs were obtained from the Swine Research and Technology Centre at the University of Alberta. A sample of brain tissue was cut from a full porcine brain. This was homogenized in a solvent containing 4 mL methanol, 2 mL chloroform,

and 1.5 mL water, in the ratio 1:5 (w/v) using a mechanical homogenizer. Aliquots of homogenates were stored in -80 °C.

2.4.4 Endoglycoceramidase (EGCase I) Expression and Purification

Expression and purification of EGCase was performed based on the reports of Albrecht et al[15], where a gene encoding recombinant EGCase I was identified and synthesized (Genscript), with a pET30 vector. Protein expression was performed by culturing *E. coli* carrying the pET30 vector overnight, followed by 1:100 dilution into 1 litre of LB medium supplemented with 25 mg/mL Kanamycin. This was grown until OD reached to ~ 0.8 at 37 °C, followed by IPTG induction at 0.1 mM final concentration by shaking at 16 °C for 18–20 h. Then, cells were centrifuged, followed by re-suspension in 45 mL of 300 mM NaCl buffer (pH 7.5) containing 0.1% Triton X-100, 10 mM imidazole, and 50 mM Tris-Cl. Finally, cells were lysed by using a cell disruptor. Prior to purification on an AKTA Prime Plus FPLC instrument, centrifugation was performed to remove any cell debris. For protein purification, a Ni-NTA superflow column (2 mL) was prepared. Elution was performed using an elution buffer (300 mM NaCl, 250 mM imidazole, 50 mM Tris-Cl, pH 7.5) All the fractions were pooled together and concentrated using molecular weight cut-off ultracentrifugation filters (30 kDa MWCO). Protein concentration was measured at 280 nm and protein was stored in 4 °C.

2.4.5 Testing EGCase I Activity

The activity of EGCase I was tested qualitatively on a TLC plate using ganglioside substrate GM3. GM3 substrate and a reaction mixture of GM3+EGCase were spotted on

a TLC plate that was developed with a solvent system of acetic acid:n-butanol:0.25% CaCl$_2$ (1:2:1, v/v/v) and stained with Orcinol stain to visualize GSL-glycan spots. Specific activity was measured from a calibration curve of serial dilutions of 2-AA labeled 3'sialyllactose (3'-SL). One unit of EGCase I is defined as the amount of enzyme that hydrolyzed 1 µmol of GM3 per min at 37 °C.

2.4.6 Extraction and Purification of GSLs from Jurkat T Cells, Porcine Brain, and Human Serum

GSL extraction and purification was performed based on the reports of Schnaar and co-workers,.[26] Essentially, 10 µL brain homogenates, 50 µL of blood plasma, or cell lysates containing ~ 1 x 10^6 cells were diluted with ice cold water (4 mL/g based on wet weight of sample). After vigorously homogenizing this mixture, methanol and chloroform were added to make the final chloroform:methanol:water ratio 4:8:3 (v/v/v). This mixture was subjected to centrifugation at 1500 RPM for 15 min. The upper phase was recovered, the volume recorded carefully, and it was diluted with 0.173 volumes of water. After mixing, the suspension was subjected to centrifugation again at 1500 RPM for 15 min. The upper phase containing ~ 80% of the total volume was recovered and transferred to a fresh tube. This was purified on a Waters SepPak C18 cartridge, evaporated to dryness under nitrogen gas, and re-dissolved in methanol at a volume of 100 µL/mg of dried extract.

2.4.7 EGCase I Digestion

The final methanol extract was dried under nitrogen and in a 50 mM sodium acetate buffer (pH 5.2) containing 1 mg mL^{-1} sodium cholate. For commercially available

standards, a mixture of standard LacCer, GM3, GM1, and GD3 were taken from original stock solutions of concentration ~ 1 mg/mL each. Then the GSLs were incubated for 18 h at 37 °C with 6 mU EGCase to release the corresponding glycans.

2.4.8 Fluorescent Labeling of Glycans

Glycans liberated after EGCase digestion were labeled with 40 µL of fluorescent mixture (30 mg anthranilic acid, 20 mg boric acid, 40 mg sodium acetate.3H$_2$O, and 45 mg sodium cyanoborohydride in methanol) at 80 °C for 45 min after an appropriate concentration of internal standard maltose was spiked in. To this, 1 mL acetonitrile:water (97:3, v/v) was added and purified on a discovery DPA-6S amide-HILIC column, as described[11]. After equilibration of the Discovery DPA-6S with 2 x 1 mL of 100% acetonitrile, samples were loaded on to them. Then, they were washed with 4 x 1 mL of acetonitrile:water (99:1) and 0.5 mL of acetonitrile:water (97:3). Finally, 2 x 0.6 mL of pure water was used to elute labeled glycans. They were reduced under vacuum before LC-MS analysis.

2.4.9 LC-MS Analysis of 2AA-Labeled Glycans

Labeled glycans were analyzed by LC-MS using an Agilent 1200 SL HPLC system and a normal-phase column (Accucore-150-Amide-HILIC, 2.6 mm, 2.1 x 150 mm, Thermo Fisher). Dried samples were re-solubilized in water:DMF:acetonitrile in a 1:1:2 ratio and 2 µL (commercially available standards) and 15 µL (cells, brain homogenates and plasma) were injected. The fluorescence detector monitored at an excitation of 320 nm and an emission of 420 nm. All chromatography was performed on an amide-HILIC

column at 40 °C. The binary solvent system followed a linear gradient with a flow rate of 0.4 mL min^{-1} (Solvent A: 100 mM ammonium formate, pH 4.45; Solvent B: acetonitrile). Quantification of relative glycan concentrations was done by taking the fluorescence peak area of the internal standard (maltose) and calculating the absolute concentrations based on the initial amount of maltose added. Mass spectra were acquired in negative mode using an Agilent 6220 Accurate-Mass TOF HPLC/MS system with a dual spray electrospray ionization source, along with a secondary reference sprayer for a reference mass solution.

2.4.10 Data Analysis using Agilent MassHunter Qualitative Analysis Software Package Version B.07.01

Mass Spectrometry data was analyzed using the Agilent MassHunter Qualitative Analysis software. An extensive database was created for all possible 2-AA labeled GSL derived glycans, with their molecular formula and neutral masses. This database was fed into the software, based on which peaks were identified according to singly and doubly charged species of GSL glycans. Masses were reported correct to four decimal places for accuracy. Some peaks could not be assigned to a particular mass by the software. For those, by manually walking across the total ion chromatogram (TIC), major mass peaks were identified. The extracted ion chromatograms (EIC) for these major mass peaks were checked to confirm the assignment.

2.5 REFERENCES

1.   Kobata, A., Exo- and endoglycosidases revisited. *Proc Jpn Acad Ser B Phys Biol Sci* **2013,** *89* (3), 97-117.

2.   Davies, G.; Henrissat, B., Structures and mechanisms of glycosyl hydrolases. *Structure* **1995,** *3* (9), 853-9.

3.   Piszkiewicz, D.; Bruice, T. C., Glycoside hydrolysis. II. Intramolecular carboxyl and acetamido group catalysis in .beta.-glycoside hydrolysis. *Journal of the American Chemical Society* **1968,** *90* (8), 2156-2163.

4.   Ito, M.; Yamagata, T., A novel glycosphingolipid-degrading enzyme cleaves the linkage between the oligosaccharide and ceramide of neutral and acidic glycosphingolipids. *J Biol Chem* **1986,** *261* (30), 14278-82.

5.   Aspeborg, H.; Coutinho, P. M.; Wang, Y.; Brumer, H.; Henrissat, B., Evolution, substrate specificity and subfamily classification of glycoside hydrolase family 5 (GH5). *BMC Evolutionary Biology* **2012,** *12* (1), 186.

6.   Caines, M. E.; Vaughan, M. D.; Tarling, C. A.; Hancock, S. M.; Warren, R. A.; Withers, S. G.; Strynadka, N. C., Structural and mechanistic analyses of endo-glycoceramidase II, a membrane-associated family 5 glycosidase in the Apo and GM3 ganglioside-bound forms. *J Biol Chem* **2007,** *282* (19), 14300-8.

7.   Han, Y. B.; Chen, L. Q.; Li, Z.; Tan, Y. M.; Feng, Y.; Yang, G. Y., Structural Insights into the Broad Substrate Specificity of a Novel Endoglycoceramidase I Belonging to a New Subfamily of GH5 Glycosidases. *J Biol Chem* **2017,** *292* (12), 4789-4800.

8.	Li, S. C.; DeGasperi, R.; Muldrey, J. E.; Li, Y. T., A unique glycosphingolipid-splitting enzyme (ceramide-glycanase from leech) cleaves the linkage between the oligosaccharide and the ceramide. *Biochem Biophys Res Commun* **1986,** *141* (1), 346-52.

9.	Li, Y. T.; Ishikawa, Y.; Li, S. C., Occurrence of ceramide-glycanase in the earthworm, Lumbricus terrestris. *Biochem Biophys Res Commun* **1987,** *149* (1), 167-72.

10.	Horibata, Y.; Okino, N.; Ichinose, S.; Omori, A.; Ito, M., Purification, characterization, and cDNA cloning of a novel acidic endoglycoceramidase from the jellyfish, Cyanea nozakii. *J Biol Chem* **2000,** *275* (40), 31297-304.

11.	Neville, D. C.; Coquard, V.; Priestman, D. A.; te Vruchte, D. J.; Sillence, D. J.; Dwek, R. A.; Platt, F. M.; Butters, T. D., Analysis of fluorescently labeled glycosphingolipid-derived oligosaccharides following ceramide glycanase digestion and anthranilic acid labeling. *Anal Biochem* **2004,** *331* (2), 275-82.

12.	Ito, M.; Yamagata, T., Purification and characterization of glycosphingolipid-specific endoglycosidases (endoglycoceramidases) from a mutant strain of Rhodococcus sp. Evidence for three molecular species of endoglycoceramidase with different specificities. *J Biol Chem* **1989,** *264* (16), 9510-9.

13.	Ishibashi, Y.; Nakasone, T.; Kiyohara, M.; Horibata, Y.; Sakaguchi, K.; Hijikata, A.; Ichinose, S.; Omori, A.; Yasui, Y.; Imamura, A.; Ishida, H.; Kiso, M.; Okino, N.; Ito, M., A novel endoglycoceramidase hydrolyzes oligogalactosylceramides to produce galactooligosaccharides and ceramides. *J Biol Chem* **2007,** *282* (15), 11386-96.

14. Ishibashi, Y.; Kobayashi, U.; Hijikata, A.; Sakaguchi, K.; Goda, H. M.; Tamura, T.; Okino, N.; Ito, M., Preparation and characterization of EGCase I, applicable to the comprehensive analysis of GSLs, using a rhodococcal expression system. *J Lipid Res* **2012,** *53* (10), 2242-51.

15. Albrecht, S.; Vainauskas, S.; Stockmann, H.; McManus, C.; Taron, C. H.; Rudd, P. M., Comprehensive Profiling of Glycosphingolipid Glycans Using a Novel Broad Specificity Endoglycoceramidase in a High-Throughput Workflow. *Anal Chem* **2016,** *88* (9), 4795-802.

16. Higashi, H.; Hirabayashi, Y.; Ito, M.; Yamagata, T.; Matsumoto, M.; Ueda, S.; Kato, S., Immunostaining on thin-layer chromatograms of oligosaccharides released from gangliosides by endoglycoceramidase. *J Biochem* **1987,** *102* (2), 291-6.

17. Ruhaak, L. R.; Zauner, G.; Huhn, C.; Bruggink, C.; Deelder, A. M.; Wuhrer, M., Glycan labeling strategies and their use in identification and quantification. *Anal Bioanal Chem* **2010,** *397* (8), 3457-81.

18. Wing, D. R.; Garner, B.; Hunnam, V.; Reinkensmeier, G.; Andersson, U.; Harvey, D. J.; Dwek, R. A.; Platt, F. M.; Butters, T. D., High-performance liquid chromatography analysis of ganglioside carbohydrates at the picomole level after ceramide glycanase digestion and fluorescent labeling with 2-aminobenzamide. *Anal Biochem* **2001,** *298* (2), 207-17.

19. Ohara, K.; Sano, M.; Kondo, A.; Kato, I., Two-dimensional mapping by high-performance liquid chromatography of pyridylamino oligosaccharides from various glycosphingolipids. *J Chromatogr* **1991,** *586* (1), 35-41.

20. In *Essentials of Glycobiology*, rd; Varki, A.; Cummings, R. D.; Esko, J. D.; Stanley, P.; Hart, G. W.; Aebi, M.; Darvill, A. G.; Kinoshita, T.; Packer, N. H.; Prestegard, J. H.; Schnaar, R. L.; Seeberger, P. H., Eds. Cold Spring Harbor (NY), 2015.

21. Smith, J.; Mittermayr, S.; Varadi, C.; Bones, J., Quantitative glycomics using liquid phase separations coupled to mass spectrometry. *Analyst* **2017,** *142* (5), 700-720.

22. Fahr, C.; Schauer, R., Detection of Sialic Acids and Gangliosides with Special Reference to 9-O-Acetylated Species in Basaliomas and Normal Human Skin. *Journal of Investigative Dermatology* **2001,** *116* (2), 254-260.

23. Borch, R. F.; Bernstein, M. D.; Durst, H. D., Cyanohydridoborate anion as a selective reducing agent. *Journal of the American Chemical Society* **1971,** *93* (12), 2897-2904.

24. Bigge, J. C.; Patel, T. P.; Bruce, J. A.; Goulding, P. N.; Charles, S. M.; Parekh, R. B., Nonselective and efficient fluorescent labeling of glycans using 2-amino benzamide and anthranilic acid. *Anal Biochem* **1995,** *230* (2), 229-38.

25. Svennerholm, L.; Fredman, P., A procedure for the quantitative isolation of brain gangliosides. *Biochim Biophys Acta* **1980,** *617* (1), 97-109.

26. Sturgill, E. R.; Aoki, K.; Lopez, P. H.; Colacurcio, D.; Vajn, K.; Lorenzini, I.; Majic, S.; Yang, W. H.; Heffer, M.; Tiemeyer, M.; Marth, J. D.; Schnaar, R. L., Biosynthesis of the major brain gangliosides GD1a and GT1b. *Glycobiology* **2012,** *22* (10), 1289-301.

27. Armbruster, D. A.; Pry, T., Limit of blank, limit of detection and limit of quantitation. *Clin Biochem Rev* **2008,** *29 Suppl 1*, S49-52.

28. Hajek, R.; Jirasko, R.; Lisa, M.; Cifkova, E.; Holcapek, M., Hydrophilic Interaction Liquid Chromatography-Mass Spectrometry Characterization of Gangliosides in Biological Samples. *Anal Chem* **2017,** *89* (22), 12425-12432.

29. Barrientos, R. C.; Zhang, Q., Isobaric Labeling of Intact Gangliosides toward Multiplexed LC-MS/MS-Based Quantitative Analysis. *Anal Chem* **2018,** *90* (4), 2578-2586.

30. Li, J.; Han, L.; Li, J.; Kitova, E. N.; Xiong, Z. J.; Prive, G. G.; Klassen, J. S., Detecting Protein-Glycolipid Interactions Using CaR-ESI-MS and Model Membranes: Comparison of Pre-loaded and Passively Loaded Picodiscs. *J Am Soc Mass Spectrom* **2018,** *29* (7), 1493-1504.

31. Xu, X.; Monjusho, H.; Inagaki, M.; Hama, Y.; Yamaguchi, K.; Sakaguchi, K.; Iwamori, M.; Okino, N.; Ito, M., Fucosyl-GM1a, an endoglycoceramidase-resistant ganglioside of porcine brain. *J Biochem* **2007,** *141* (1), 1-7.

32. Song, X.; Ju, H.; Lasanajak, Y.; Kudelka, M. R.; Smith, D. F.; Cummings, R. D., Oxidative release of natural glycans for functional glycomics. *Nat Methods* **2016,** *13* (6), 528-34.

33. Grassi, S.; Prioni, S.; Cabitta, L.; Aureli, M.; Sonnino, S.; Prinetti, A., The Role of 3-O-Sulfogalactosylceramide, Sulfatide, in the Lateral Organization of Myelin Membrane. *Neurochem Res* **2016,** *41* (1-2), 130-43.

34. O'Brien, J. P.; Brodbelt, J. S., Structural characterization of gangliosides and glycolipids via ultraviolet photodissociation mass spectrometry. *Anal Chem* **2013,** *85* (21), 10399-407.

35. Lisa, M.; Holcapek, M., High-Throughput and Comprehensive Lipidomic Analysis Using Ultrahigh-Performance Supercritical Fluid Chromatography-Mass Spectrometry. *Anal Chem* **2015,** *87* (14), 7187-95.

36. Kracun, I.; Rosner, H.; Drnovsek, V.; Heffer-Lauc, M.; Cosovic, C.; Lauc, G., Human brain gangliosides in development, aging and disease. *Int J Dev Biol* **1991,** *35* (3), 289-95.

37. Posse de Chaves, E.; Sipione, S., Sphingolipids and gangliosides of the nervous system in membrane function and dysfunction. *FEBS Lett* **2010,** *584* (9), 1748-59.

38. Ulmer, C. Z.; Yost, R. A.; Chen, J.; Mathews, C. E.; Garrett, T. J., Liquid Chromatography-Mass Spectrometry Metabolic and Lipidomic Sample Preparation Workflow for Suspension-Cultured Mammalian Cells using Jurkat T lymphocyte Cells. *J Proteomics Bioinform* **2015,** *8* (6), 126-132.

39. Ulmer, C. Z.; Patterson, R. E.; Koelmel, J. P.; Garrett, T. J.; Yost, R. A., A Robust Lipidomics Workflow for Mammalian Cells, Plasma, and Tissue Using Liquid-Chromatography High-Resolution Tandem Mass Spectrometry. *Methods Mol Biol* **2017,** *1609*, 91-106.

40. Tu, J.; Yin, Y.; Xu, M.; Wang, R.; Zhu, Z.-J., Absolute quantitative lipidomics reveals lipidome-wide alterations in aging brain. *Metabolomics* **2017,** *14* (1), 5.

41.   Vieira, D. B.; Thur, K.; Sultana, S.; Priestman, D.; van der Spoel, A. C., Verification and refinement of cellular glycosphingolipid profiles using HPLC. *Biochem Cell Biol* **2015,** *93* (6), 581-6.

42.   Novak, J.; Kriston-Pal, E.; Czibula, A.; Deak, M.; Kovacs, L.; Monostori, E.; Fajka-Boja, R., GM1 controlled lateral segregation of tyrosine kinase Lck predispose T-cells to cell-derived galectin-1-induced apoptosis. *Mol Immunol* **2014,** *57* (2), 302-9.

43.   Maglione, V.; Marchi, P.; Di Pardo, A.; Lingrell, S.; Horkey, M.; Tidmarsh, E.; Sipione, S., Impaired ganglioside metabolism in Huntington's disease and neuroprotective role of GM1. *J Neurosci* **2010,** *30* (11), 4072-80.

44.   Alpaugh, M.; Galleguillos, D.; Forero, J.; Morales, L. C.; Lackey, S. W.; Kar, P.; Di Pardo, A.; Holt, A.; Kerr, B. J.; Todd, K. G.; Baker, G. B.; Fouad, K.; Sipione, S., Disease-modifying effects of ganglioside GM1 in Huntington's disease models. *EMBO Mol Med* **2017,** *9* (11), 1537-1557.

45.   Sango, K.; Yamanaka, S.; Hoffmann, A.; Okuda, Y.; Grinberg, A.; Westphal, H.; McDonald, M. P.; Crawley, J. N.; Sandhoff, K.; Suzuki, K.; Proia, R. L., Mouse models of Tay-Sachs and Sandhoff diseases differ in neurologic phenotype and ganglioside metabolism. *Nat Genet* **1995,** *11* (2), 170-6.

46.   Ariga, T.; McDonald, M. P.; Yu, R. K., Role of ganglioside metabolism in the pathogenesis of Alzheimer's disease--a review. *J Lipid Res* **2008,** *49* (6), 1157-75.

47.   Negroni, E.; Chigorno, V.; Tettamanti, G.; Sonnino, S., Evaluation of the efficiency of an assay procedure for gangliosides in human serum. *Glycoconj J* **1996,** *13* (3), 347-52.

48.   Leenders, R. G.; de Jong, J. G.; Wevers, R. A., Extraction and purification of gangliosides from plasma and fibroblasts before analysis by thin layer chromatography. *Ann Clin Biochem* **1995,** *32 (Pt 1)*, 68-73.

49.   Yoshida, Y.; Furukawa, J. I.; Naito, S.; Higashino, K.; Numata, Y.; Shinohara, Y., Quantitative analysis of total serum glycome in human and mouse. *Proteomics* **2016,** *16* (21), 2747-2758.

CHAPTER 3

APPLICATIONS OF ENDOGLYCOCERAMIDASE TO

GLYCAN ANALYSIS

Sections 3.2[1], 3.3[2], 3.4[3] and 3.6[4] of this Chapter are part of the following manuscripts currently under review or in preparation:

[1] Demina, E., Pierre, W., Londono, I., Nguyen, A., Reiz, B., Zou, C., Chakraberty, R., Cairo, C.W., Pshezhetsky, A.V., Lodygensky, G., "Persistant reduction in sialylation of cerebral glycoproteins following post-natal inflammatory exposure", **2018**. (in press)

[2] Howlader, M. A., Li, C., Zou, C., Chakraberty, R., Ebesoh, N., Cairo, C.W., "Neuraminidase-3 (NEU3) is a negative regulator of LFA-1 adhesion", **2018**. (in preparation)

[3] Howlader, M. A., Guo, T., Chakraberty, R., Porter, E., Cairo, C.W., "Isoenzyme-selective inhibitors of human neuraminidases reveal distinct effects on cell migration", **2018**. (in preparation)

[4] Demina, E., Smutova, V., Fougerat, A., Pan, X., Guo, T., Zou, C., Chakraberty, R., Snarr, B., Sheppard, D., Shiao, C., Roy, R., Orekhov, A. N., Miyagi, T., Laffargue, M., Cairo, C.W., Pshezhetsky, A.V., "Inhibitors of neuraminidases 1 and 3 as potential candidates for treatment of atherosclerosis", **2018**. (under review)

Mouse microglia lysates for Section 3.5 were obtained from Dr Simonetta Sipione, Department of Pharmacology, University of Alberta.

3.1 INTRODUCTION

Chapter 2 described the establishment of a GSL profiling method using endoglycoceramidase enzymes (EGCase I) that cleaves the ceramide lipid backbone of GSLs, generating the respective glycans/oligosaccharides. We have applied this to a number of different projects, detailed in this Chapter. Projects included the analysis of mouse brains under conditions of inflammation, changes in GSL composition in mammalian cells treated with human neuraminidase enzymes or inhibitors, and the study of ganglioside profiles of cultured mouse microglia. This Chapter will describe the GSL analysis performed for these projects and highlight the relevant details of the GSL analysis.

3.2. PERSISTENT REDUCTION IN SIALYLATION IN CEREBRAL GLYCOPROTEIN FOLLOWING POST-NATAL INFLAMMATORY EXPOSURE[1]

Gangliosides and polysialic acid (PSA) containing glycoproteins are sialylated glycoconjugates found abundantly in mammalian neuronal cells. Their involvement in cellular signaling pathways, cell differentiation, growth, and endocytosis has been explored in a number of detailed studies.[5] In the central nervous system (CNS), these glycoconjugates play essential roles in myelination of nerve fibres, axon growth, and nerve impulse transmission.[6]

A study conducted by our collaborators at the Université de Montréal tried to delineate the fate of ganglioside and PSA glycoproteins in neuronal cells under pro-inflammatory conditions. Two neuro-inflammatory rat models treated with the pro-inflammatory agent, lipopolysaccharide (LPS), were used for this study. Animals were sacrificed at twenty fours hours (P4) post injection or twenty-one days (P24) post injection. From immunohistochemical and Reverse Transcription Polymerase Chain Reaction (RT-PCR) experiments, both rat models showed an unexpected increase in human neuraminidase (NEU1) activity under these conditions.[1] To understand further whether there were major changes in the sialylation and polysialylation of glycoconjugates, ganglioside and glycoprotein analyses were performed. We used the EGCase method to analyze and quantify gangliosides in both groups of rats, i.e., P4 and P24, under neuronal inflammation conditions.

3.2.1 Results and Discussion

Gangliosides were extracted from brain homogenates of P4 and P24 rat models under LPS and Sham (saline) treatment conditions. These experiments were performed before we had established an internal standard. Hence, for this study, only relative quantities of gangliosides were considered.

Summing the integrated peak areas of each ganglioside from the fluorescent chromatogram and representing each as a percentage of the total ganglioside composition in a given sample provided relative quantitation. The gangliosides identified in both age groups were LacCer (5.9 min), GM3 (8.0 min), GM1 (12.7 min), GD3 (14.2), GD1a (16.1 min), GD1b (18.2 min), GT1a (19.5 min), and GT1b (20.6 min), with GQ1 (23.3 min) found only in the P4 age group, as shown in **Figure 3–1**. This is consistent with previous reports of major gangliosides common in rat brains.[7-9] The slight differences in amounts of gangliosides between the two age groups may be due to the differential expression associated with neuronal development, as has been reported previously.[10-11]

Peaks for LacCer, GM3, GM1, and GD3 were assigned by comparing retention times of commercially available standards. The remaining major peaks were assigned by High Resolution Electrospray Ionization Mass Spectrometry (HR-ESI-MS). Some minor peaks remained unassigned if they could not be identified by the MS software or by manual evaluation of the total ion chromatogram (TIC). The peak at ~22 min may be GQ1a, considering that the next peak at 23.3 min matched GQ1, which could be GQ1b. Since the MS data could not be used to assign isomers, the peak at 23.3 min was taken to
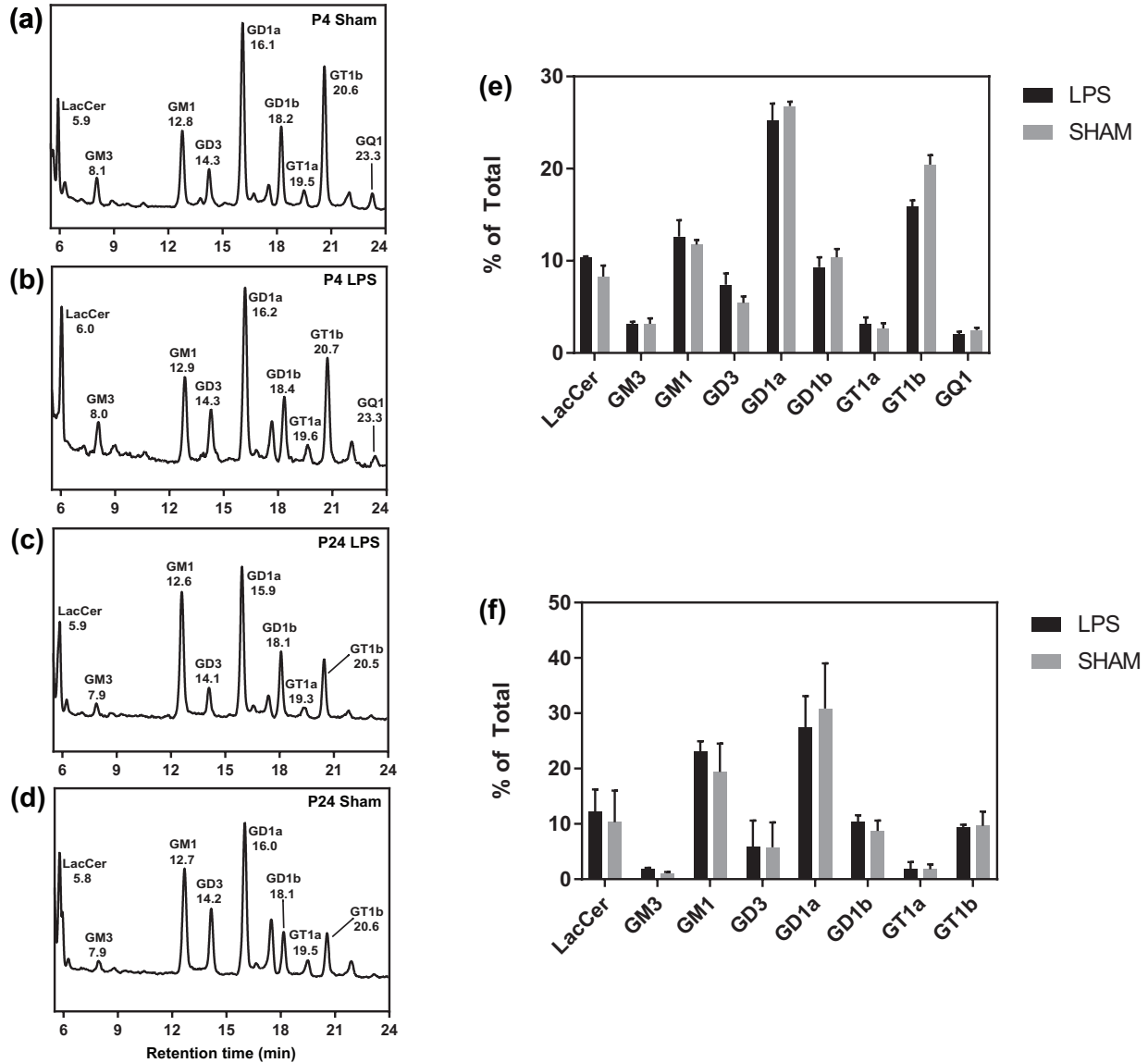
Figure 3– 1. Ganglioside profiling in P4 and P24 rat brains. Representative fluorescence chromatograms of P4 rat brains under (a) Sham (saline) treatment and (b) LPS treatment and P24 rat brains under (c) LPS treatment and (d) Sham (saline) treatment conditions, showing complete ganglioside profiles in each age group. (e, f) Relative percentage compositions of gangliosides showing comparison of levels of LacCer, GM3, GM1, GD3, GD1a, GD1b, GT1a, GT1b, and GQ1 between (e) P4 LPS and Sham conditions, and comparison of levels of LacCer, GM3, GM1, GD3, GD1a, GD1b, GT1a, and GT1b between (f) P24 LPS and Sham conditions. Values represent mean and standard error of mean for n = 2 for P4 and n = 3 for P24 measurements.

be GQ1.

Although there were subtle changes in ganglioside composition between the LPS-treated and Sham brains in both age groups, none were significant. These results indicate that LPS-induced NEU1 elevation did not alter the sialylation of gangliosides in neurons. This is consistent with previous reports that showed no abnormalities in ganglioside content in NEU1 knockout mice.[12] Glycoproteins, on the other hand, showed consistent desialylation after LPS injection across both age groups, with higher effects in the P24 age group (data not shown). Desialylation of glycoproteins possibly could hamper biological processes that are regulated by sialic acid, including neurotransmission and synaptic plasticity.[6] This study highlighted the potential of NEU1 as a therapeutic target for conditions such as epilepsy or bipolar disorder that are associated with sialic acid disregulation.[13]

3.3 NEURAMINIDASE-3 (NEU3) IS A NEGATIVE REGULATOR OF LFA-1 ADHESION[2]

The inflammation cascade is the process by which leukocytes are recruited to sites of inflammation.[14] This pathway consists of the following steps: (a) leukocyte rolling, which is regulated by the interaction of selectin proteins with their ligands on the host cell membrane, (b) leukocyte activation by signaling proteins called chemokines, (c) firm adhesion of leukocytes to the host endothelial cells regulated by integrin proteins, and finally (d) transmigration of leukocytes.[15] The stages of firm adhesion and transmigration are modulated by the interaction of integrin receptors and their ligands. The interaction between the β2-integrin, lymphocyte function antigen-1 (LFA-1) receptor, and its ligand

intercellular adhesion molecule-1 (ICAM-1) is the critical transitioning step from slow rolling to firm adhesion and also the driving force behind subsequent interactions of integrins with other ligands that promote transmigration of leukocytes to the site of infection.[16-17]

Since our group's primary research is on sialic acids and sialic acid bearing glycoconjugates, our interest in the leukocyte adhesion cascade stems from the fact that variability in sialic acid composition in lymphocytes has been reported during cell development and infection.[18] We hypothesized that changes in glycoproteins or glycolipids modulated by hNEU enzymes could regulate this process.[19] Our primary interest was to understand the role of neuraminidase-3 (NEU3) in the process of LFA-1/ICAM-1 adhesion. NEU3 was picked among the four hNEU enzymes since it is a strong player in cell signaling events[20-21] and shows preference towards glycosphingolipid (GSL) targets,[22-23] which have been associated with activation of integrins in lymphocytes.[24-25] In order to investigate changes in GSL composition, high-performance thin layer chromatography (HPTLC) experiments initially were performed, the results of which were corroborated later with the quantitative EGCase glycan analysis method.

3.3.1 Results and Discussion

To investigate the changes in GSL composition, Jurkat T cells were used for analysis. Cells were treated with phorbol 12-myristate 13-acetate (PMA), which activates protein kinase C,[26] and cytochalasin D (cytoD), which disrupts the cytoskeleton.[27] These treatments were chosen since they are expected to change the function of integrin.[28] In

order to understand the effects of NEU enzymes on GSL composition, cells were treated with a recombinant form of NEU3 and a bacterial NEU enzyme, NanI. After these treatments, GSLs were extracted from these cells and analyzed by HPTLC. From the results of these experiments, shown in **Figure 3–2**, it was observed that there was a significant decrease in the levels of GM3 with an increase in LacCer (the asialo form of GM3) under NEU3 treatment, while none of the other treatments showed any significant changes. Thus, NanI treatment afforded no detectable changes in GSL composition, whereas NEU3 treatment specifically altered GSL composition. GM3 is a good substrate for NEU3, hence these results are consistent with what has been reported previously in the literature.[29]

Quantification by HPTLC experiments was performed by image densitometry, where the intensities of orcinol stained bands for GM3 and LacCer were processed by ImageJ software, and a ratio of these intensities was taken for LacCer and GM3. This ratio was normalized to the ratios in control samples and compared using a student's t-test. This method of quantitation is not very accurate due to a number of variables, including LOD, unequal spotting for each condition, and variations in solvent composition or temperature that may affect the Rf values. We implemented our EGCase analysis to provide a more quantitative analysis. The most interesting feature of this method is the fact that by using smaller amounts of starting material (number of cells) four replicates were enough to observe changes in GSL composition, while in the case of HPTLC experiments, twenty-four replicates with a higher amount of starting material were performed, but only very small changes (~5%) were observed.
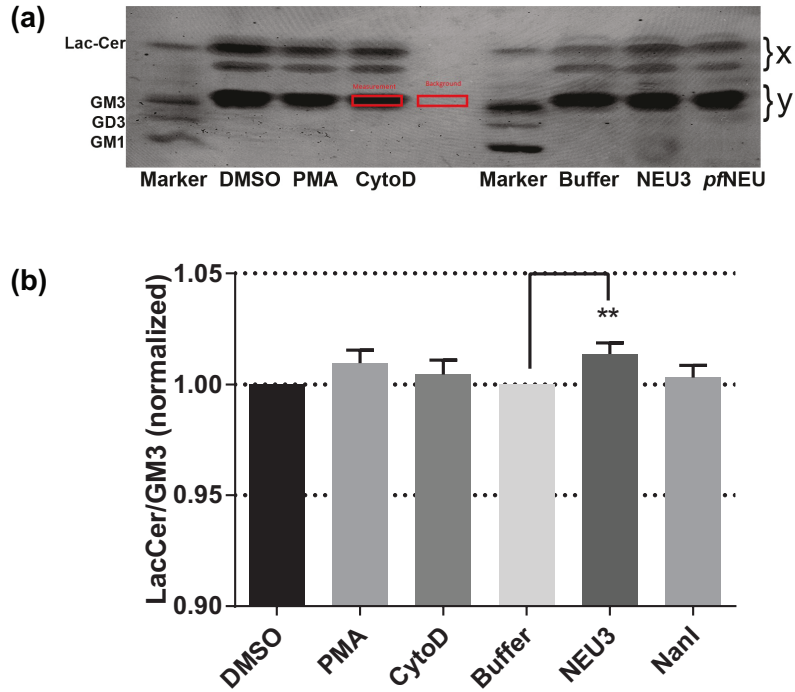
Figure 3– 2. HPTLC analysis showing change in GSL concentrations in Jurkat T cells. GSLs were extracted from control and treated Jurkat T cells and analyzed by HPTLC. (a) A representative HPTLC plate showing bands for LacCer and GM3, which were quantified using image densitometry and processed by the software ImageJ. (b) Ratios of LacCer/GM3 under six different treatment conditions of DMSO, PMA, CytoD, Buffer, NEU3, and NanI. This ratio was determined by taking ratios of intensities of the respective bands, i.e., by calculating x/y, where x and y correspond to areas indicated in red in the Figure (a). PMA and CytoD data were compared to the DMSO control, while NEU3 and NanI were compared to the Buffer control, both using a t-test. A significant loss of GM3 was observed under NEU3 treatment. Values represent mean and standard errors of the mean of n = 24 measurements; p-values were determined from t-tests, **, $p \leq 0.05$. (HPTLC experiments were performed by Dr. Caishun Li, University of Alberta.)

Jurkat T cells were subjected to the same treatments of PMA, CytoD, NEU3, and NanI, as were performed for the HPTLC studies. From the GSL profile, LacCer, GM3, GM2, GD3, and GD1a were identified, and peaks were assigned by comparing with the retention times of commercially available standard gangliosides. The remaining peaks were assigned by High Resolution Electrospray Ionization Mass Spectrometry (HR-ESI-

MS). The results from these experiments confirmed our findings from the HPTLC studies, i.e., there was an increase in the LacCer/GM3 ratio under NEU 3 treatment, while no major changes were seen for the other conditions. These results also clearly highlight the advantages in sensitivity for the EGCase method **(Figure 3–3b)**.

The EGCase analysis allowed us to evaluate other gangliosides. The MS data did not show additional peaks for GA2, the asialo-form of GM2. GD1a with one sialic acid removed would form GM1, hence we checked for any changes in GM1/GD1a ratios under the treatment conditions. Even though subtle variability was observed in the treatment conditions, none of them were significant **(Figure 3–3c)**.

From these data, we were able to conclude that NEU3 altered the GSL composition on cells, particularly the compositions of GM3 and LacCer. This, along with other experimental results, helped us to propose a mechanism by which NEU3 affects LFA-1/ICAM-1 adhesion. We hypothesized that NEU3 activity increased the concentration of asialo-GSLs, which brings about a conformational change in LFA-1, making it inactive. Additionally, some data from adhesion assays have shown decreased binding of LFA-1 to ICAM-1 in cells treated with NEU3. Together, these data suggest that NEU3 plays a key role acting as a regulator of LFA-1 adhesion by modulating the glycolipid composition of cell surfaces.
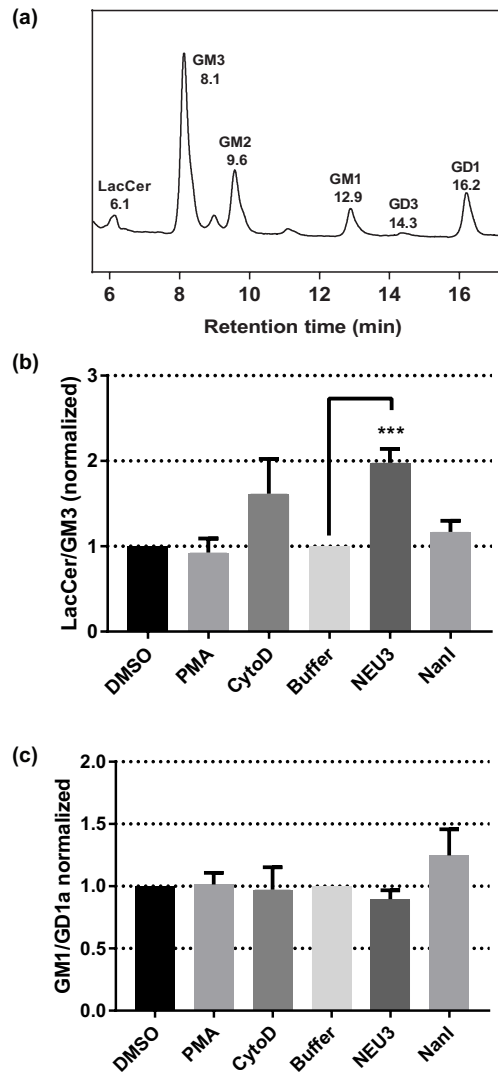
Figure 3– 3. LC-MS analysis showing change in GSL concentrations in Jurkat T cells. GSLs were extracted from control and treated Jurkat T cells, digested with EGCase I enzyme, followed by 2-AA labeling and analysis by LC-MS. (a) Representative HPLC chromatogram showing complete GSL profile in Jurkat T cells (b, c) Ratios of LacCer/GM3 (b) and GM1/GD1a (c) under six different treatment conditions of DMSO, PMA, CytoD, Buffer, NEU3, and NanI. This ratio was determined by taking ratios of fluorescence peak areas of LacCer/GM3 and GM1/GD1a. PMA and CytoD data were compared to the DMSO control, while NEU3 and NanI were compared to the Buffer control, both using a student's t-test. A significant loss of GM3 was observed under NEU3 treatment, while no changes in GM1/GD1 ratios were observed. Values represent mean and standard errors of the mean of n = 4 measurements; p-values were determined from student's t-tests, ***, $p \leq 0.005$.

3.4   ISOENZYME-SELECTIVE   INHIBITORS   OF   HUMAN NEURAMINIDASES REVEAL DISTINCT EFFECTS ON CELL MIGRATION[3]

Glycoproteins and glycolipids have been reported to regulate cell migration, and specific human neuraminidase (hNEU) enzymes show activity towards both these glycoconjugates by removing their terminal sialic acids. NEU3 and NEU4 are known to prefer glycolipids, while NEU1 is known to prefer glycoproteins *in vitro*.[30] The diversity in function of the four human neuraminidase (hNEU) isoenzymes, NEU1, NEU2, NEU3, and NEU4, can be exemplified further by their role in cell migration and cancer metastasis.[30-31] For example, studies have shown NEU1 being the driving force behind decreased cell migration in human lung cancer cells, thereby decreasing metastasis,[31] while NEU2 and NEU3 have been reported to increase cell proliferation and survival in prostate cancer cells.[32-33] Our group was interested in the mechanism by which specific hNEU enzymes affect cell migration.

We hypothesized that one of the mechanisms by which hNEU enzymes may be regulating cell migration and other processes is by acting on glycolipids and changing their composition on the cell surface. To investigate this we studied the effects of treatment of mammalian cells with specific inhibitors of these enzymes on the composition of glycolipids. The EGCase assay was applied to prostate cancer cells (PC-3) after treating them with specific hNEU inhibitors as follows: DANA (non-specific inhibitor active against all hNEU enzymes)[34]; two NEU1 specific inhibitors, C9-butyl *N*-amide derivative of DANA or C9-BA-DANA[35] and II-59 (a NEU1 inhibitors, unpublished data from our group); C9-4HMT-DANA[36] (NEU4 specific); and finally II-

26 [37] (NEU3 specific). A prostate cancer cell line (PC-3) was chosen because, from previous experiments within this study, this cell line was identified as being the most sensitive to hNEU inhibitors.

3.4.1 Results and Discussion

Gangliosides were extracted from PC-3 cells ($\sim$1 x 10^6 cells) after their treatment with the aforementioned hNEU enzyme inhibitors. Cells were treated under serum-free conditions as a precautionary measure against contamination from gangliosides in serum.

A representative profile of GSLs in PC-3 cells is shown in **Figure 3–4a**. LacCer ($\sim$6.1 min), GA2 ($\sim$ 6.5 min), GM3 ($\sim$8.1 min), GM2 ($\sim$9.6 min), GM2-Neu5Gc ($\sim$11.3 min), GM1 ($\sim$13.9 min), GM1-Neu5Gc ($\sim$15.3 min), GD1a ($\sim$17.8 min), Fucosyl-GT1 ($\sim$21.6 min), and Fucosyl-GQ1 ($\sim$23.3 min) were the identified GSLs. Peaks were identified by comparing retention times with commercially available standard GSLs and confirmed by HR-ESI-MS. Although there were a couple of peaks that could not be assigned by the MS software, we were able to identify the majority of GSLs. In comparing our findings to some previous reports in the literature, the major GSLs identified in prostate cancer cells are GM3, GM2, and GM1, which is consistent with our data.[38] Some studies also have shown the presence of GD1a in these cells,[39] while some have shown GD3.[40] All these reports are based on TLC and HPTLC experiments. Differences in GSL composition could be due to differences in cell samples or growth conditions. The appearance of other GSLs, which are in lower abundance than the major ones, appropriately highlights the sensitivity of the EGCase assay.

Similar GSL profiles were observed for PC-3 cells treated with hNEU inhibitors, with subtle differences in composition under treatment conditions. Quantification was performed based on the concentration of internal standard added. A student's test was performed to compare the GSL composition between untreated (control) and treated samples. We observed a significant increase in GM2 under treatment of II-26 (NEU3 specific inhibitor), consistent decrease in LacCer and GA2 across all inhibitor treatments, and overall subtle increases in GSL composition across all inhibitor treated samples **(Figure 3–4)**.

From the EGCase assay, it was not clear that inhibition of the hNEU enzymes was affecting the glycolipid composition in the cells; however, we did observe a subtle increase across all complex GSLs under inhibitor treatment, coupled with a consistent decrease in neutral GSLs LacCer and GA2. LacCer is the neutral GSL formed when hNEUs progressively remove sialic acids from complex gangliosides, while GA2 is the asialo-form of GM2. This does suggest that the hNEUs may be modulating the complex GSL composition on the cell surface, and this is a contributing factor towards the differences in cell migration revealed from other experiments in our study. Inhibition of the NEU1 specific inhibitor II-59 caused increases in GM2 and evidently high levels of other complex gangliosides, such as GM3, GM1, and GM1Gc. This was unexpected since NEU1 is said to be inactive towards glycolipids, although that is only under *in vitro* conditions.[30]
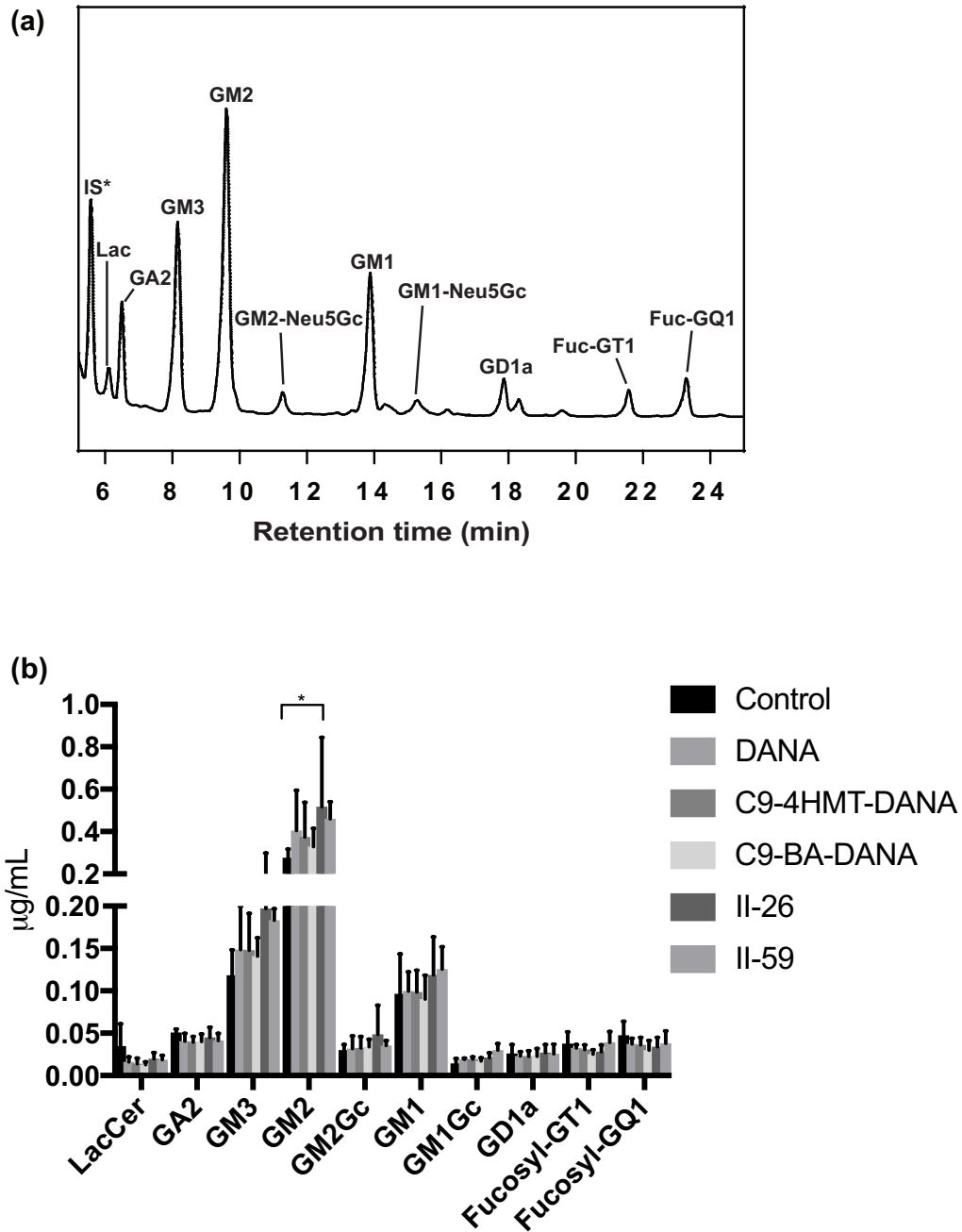
Figure 3– 4. LC-MS analysis showing changes in GSL composition in PC-3 cells. GSLs were extracted from control and treated PC-3 cells, digested with EGCase I enzyme, followed by 2-AA labeling and analysis by LC-MS. (a) Representative HPLC chromatogram showing complete GSL profile in PC-3 cells. (b) GSL composition in untreated PC-3 cells and PC-3 cells treated with specific hNEU inhibitors C9-4HMT (NEU4), C9-BA (NEU1), II-26 (NEU3), II-59 (NEU1), and non-specific inhibitor DANA.

Significant changes were observed in levels of GM2 when treated with II-26. Overall, there were subtle increases in complex gangliosides in the case of inhibitor treated cells, with a consistent decrease in the levels of LacCer and GA2. Values represent mean and standard deviations of n = 3 measurements; p-values were determined from a student's t-test, *, p ≤ 0.05.

For some of the GSLs, it was also observed that even though the changes between treated and untreated conditions seemed large, variability was too high to show significance. For example, for GM3, the increase was quite large for all inhibitor treated samples, but none of the changes were significant. Similar results were observed for GM2 in the case of DANA, C9-4HMT-DANA, II-59 treatments, and for GM1 in the case of II-26 and II-59 treatments.

3.5 DIFFERENTIAL EXPRESSION OF GANGLIOSIDES ACROSS MULTIPLE MICROGLIA PHENOTYPES

Microglia are known as the resident macrophages of the Central Nervous System (CNS), which play a major role in CNS immunity.[41] Typically dormant under healthy conditions, they become activated when exposed to infection or injury, which helps them contribute to the normal functioning and development of the CNS.[42] Additionally, these cells are involved in the development of plasticity and synapses and in providing support for learning and memory.[43]

Neuronal cells are abundant in glycosphingolipids (GSLs), which are responsible for a number of cellular processes in the CNS, including neuronal growth, differentiation, and signaling pathways. They also have been implicated in a number of neuronal diseases, such as Alzheimer's and Huntington's, [44] and have been reported to play a role

in the elevation of pro-inflammatory cytokines *in vitro* and *in vivo* in microglia and astrocytes.[45] Given the potential of GSLs in maintaining such a wide range of cellular activities in the brain, it could be hypothesized that GSLs play a role in microglia biology and modulation of immune response.

In this study, cultured mouse microglia were exposed to various polarizing conditions and the levels of GSLs under each condition were investigated. For each polarization condition microglia were exposed to different cocktails of cytokines, which induce specific phenotypes in the cells. The conditions were as follows: M0, which is similar to an adult microglia in a healthy brain;[46] M1, which is similar to microglia mounting an inflammatory response and showing high expression of pro-inflammatory cytokines, such as tumor necrosis factor-alpha (TNFα), interleukin 6 (IL-6), and interleukin 10 (IL-10),[47] and M2, which corresponds to cells engaged in a reparative process once inflammation has subsided.[48] The GSL levels in each of these states were tested first using GSL-specific antibodies. This, however, was limited to gangliosides GM1 and GD1a, for which there are commercially available antibodies. Glycan analysis using the EGCase method could provide more quantitative data on changes in levels of GSLs present in microglia. To the best of our knowledge, a complete GSL profile in mouse microglia has not been reported in the literature.

3.5.1 Results and Discussion

We received aliquots of treated microglia cell lysates in M0, M1, and M2 states. The protein concentration of each aliquot was calculated and used for normalization across all samples. Microglia cell lysates (equivalent to 40 µg protein) were used for extraction of

GSLs. Dried GSL extracts from each sample were subjected to EGCase I digestion and 2-AA labeling, followed by LC-MS analysis of the labeled products.

Quantification was performed with an internal standard (maltose). Common GSLs identified in each of the three conditions were LacCer (~6.0 min), Gb3 (~6.2 min), GM3 (~8.0 min), GM2 (~9.8 min), GA1 (~10.8 min), GM1 (~13.2 min), GD3 (~14.2 min), GD1a (~16.1 min) and GD1b (~18.2 min). Additionally, GM2-Neu5Gc (~11.4 min) could be seen only in the M0 condition. The absence of GM2-Neu5Gc in M1 and M2 states could be due to the increased activity of neuraminidase enzymes or changes in biosynthesis. These peaks were assigned by comparing retention times of standard GSLs, as mentioned in **Chapter 2** and by High Resolution Electrospray Ionization Mass Spectrometry (HR-ESI-MS). The GSL peaks identified from our assay were in close agreement with a previous study, where the authors were interested in the in situ expression levels of gangliosides (GM3, GM2, GM1, GD1a, GD1b, GT1b, GQ1b, acetyl-GM3, GD2, and GD3) in human glial and neuronal cells both in the gray and white matter. Immunohistochemistry was used to detect the presence of GM3, GM2, GD1a, GD1b, GM1, GD3, and GD2 in white matter but only GM1 and GD2 in the gray matter.[49] We can see an overall consistency between our data and previous reports in terms of the different GSLs that were identified. Small discrepancies, such as the presence of GD2 in their assay and the absence of the same in ours, can be attributed to variability associated with two different sources of glial cells (e.g. human and mouse).

Representative chromatographic profiles of three replicate runs of microglia under M0, M1, and M2 conditions are shown in **Figure 3–5 (a), (b), and (c),** respectively. **Figure 3–5 (d)** shows a comparison of GSL composition under M0, M1, and M2

conditions; a student's t-test was used for comparisons. Comparing M0 and M1 conditions, all the major gangliosides, GM3, GM2, GM1, and GD3, with a significant increase seen only in the case of GM1. Comparing changes between M1 (expressing inflammatory response phenotype) and M2 (expressing a reparative state phenotype), it can be seen that there is a significant decrease in GM1 and GM3 when going from M1 to M2, which might be an expected result, considering that M2 is a state of repair post inflammation and that any increase in gangliosides in the M1 state would decrease gradually once into the M2 state.

Gangliosides have been associated with inflammation and subsequent neurodegeneration in previous studies.[50] Inflammatory reactions in the CNS have been detected in knockout mice lacking GM2/GD2 synthase[51] and GD3 synthase.[52] While these studies highlight the involvement of gangliosides in the regulation of inflammation and associated diseases in the brain,[53] they do not shed any light on the mechanism by which gangliosides act. A study by Park and co-workers, taking primary mouse microglia and astrocytes, has proposed a possible mechanism by which ganglioside-triggered inflammatory reactions can be explained.[43] According to this study, the toll-like receptor 4 (TLR4), which belongs to the class of TLR proteins involved in protecting the host cell from pathogens, regulates inflammatory signals produced by ganglioside expression. The authors proposed that damage to neuronal cells caused gangliosides to be released into the extracellular space. TLR4 receptors expressed on the cell surface along with other cellular machinery recognize this as a state of injury. This, in turn, activates other downstream processes including increased expression of pro-inflammatory cytokines,

such as, TNF-α and IL-6; or an increased production of nitric oxide, which are hallmarks of inflammatory diseases that cause subsequent neurodegeneration.[43]

The M1 cells over-expressed pro-inflammatory cytokines, such as IL-10, IL-6, and TNF-α. Based on the abovementioned mechanism, an increased expression of such cytokines would indicate an increased expression of gangliosides, which is caused as a result of brain injury. Looking at the results of our assay, this is consistent with M1 and M0 states when comparing most identified gangliosides. Though subtle, there was an increase in LacCer, GM3, GM2, GA1, and GM1. GD3 did not show much of a change, while GD1a and GD1b showed a slight decrease. Accumulation of gangliosides such as GM2, GM3, and GD3 have been associated with activation of glial cells and, consequently, with brain injury.[54] Park and co-workers [43] proposed that ganglioside levels would decrease in a reparative state. This is consistent for the major gangliosides in the M2 (post-inflammation) state, i.e., decrease in GM3, GM2, GM1, GD3, Gb3, and a slight decrease in GD1a as well. The most significant changes were observed in GM1 and GM3.
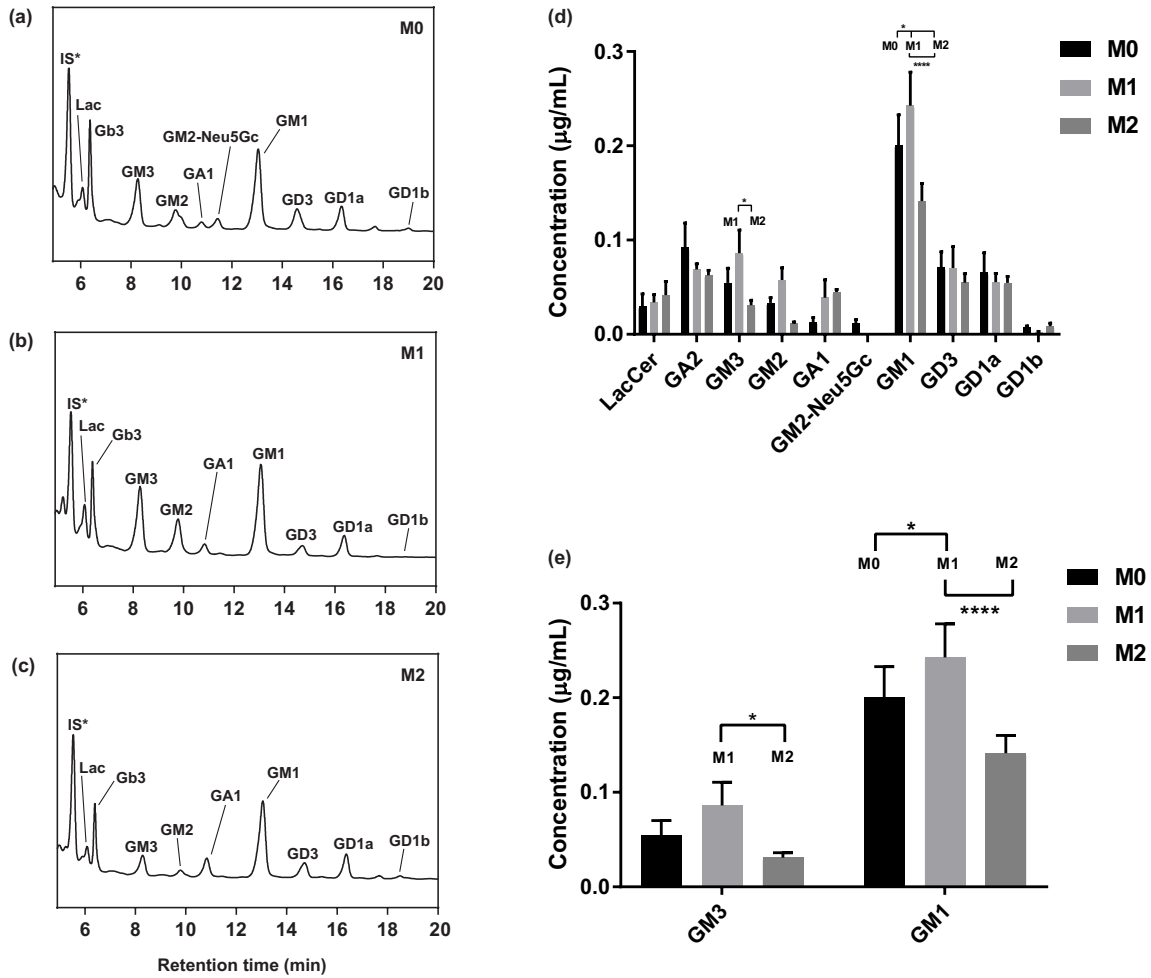
Figure 3– 5. Representative fluorescence chromatograms of cultured mouse microglia. The polarization conditions are as follows: (a) M0 (representing a resting state of microglia), (b) M1 (expressing an inflammatory response phenotype), and (c) M2 (expressing a reparative state phenotype). (d) Concentration of GSLs in microglia showing comparison of levels of LacCer, Gb3, GM3, GM2, GA1, GM2-Neu5Gc, GM1, GD3, GD1a and GD1b, GT1a, GT1b, and GQ1 between M0, M1, and M2 polarization conditions. GM3 and GM1 showed significant differences in composition. (e) Changes in composition of GM3 and GM1 between M0, M1, and M2 states. Values represent mean and standard deviations of n = 3 measurements; p-values were determined from student's t-tests, ****, $p \leq 0.0005$; *, $p \leq 0.05$.

111

3.6 INHIBITORS OF NEURAMINIDASE 1 AND 3 AS POTENTIAL CANDIDATES FOR TREATMENT OF ATHEROSCLEROSIS [4]

Atherosclerosis is an inflammatory disease affecting the arteries, leading to reduction in blood flow to the heart.[55] Smoking, hypertension, obesity, and hyperlipidemia are some of the most common contributing factors to the disease.[56] Although common risk factors causing atherosclerosis have been identified, work to understand the specific mechanisms by which this disease manifests itself is still ongoing. Some studies have proposed the activation of the inflammatory cascade as a mechanism of progression of atherosclerosis.[57] This leads to migration and adhesion of leukocytes or white blood cells that develop into macrophages in the later stages. Low-density lipoproteins (LDL), which are the vehicles for cholesterol transport in the blood, are taken up by these macrophages. Consequently, there occurs an accumulation of cholesterol in the arteries, thereby eliciting a series of other immune responses together leading to atherosclerosis.[58]

Interestingly, studies have shown that elevated levels of LDL in the blood is not the only trigger for atherosclerosis.[59] Chemical modifications of LDL particles are known to increase the susceptibility of LDL uptake by macrophages and are considered triggers of this disease.[60] There are many unexplored LDL modifications playing important roles in this process.[61-62] This study was designed to investigate the role of desialylation (removal of terminal sialic acids or N-acetyl neuraminic acids) of LDL glycoproteins and glycolipids in atherosclerosis. Desialylation is a natural modification of LDL particles, and it has been shown that patients suffering from atherosclerosis or other cardiovascular diseases have a lower sialic acid content in LDL particles than healthy individuals.[63]

Desialylation is facilitated by the action of human neuraminidase (hNEU) enzymes NEU1, NEU2, NEU3, and NEU4, which cleave off terminal sialic acids from sialylated glycoconjugates, such as glycoproteins and glycolipids.[64] The primary goal of this study was to test the hypothesis that hNEUs present in plasma or endothelial cells of arteries are triggering atherosclerosis by removing sialic acids from glycoproteins and glycolipids. We applied the EGCase method to serum samples from a common atherosclerosis murine model, Apoliprotein E knockout (KO) mice (ApoE). To test the role of individual hNEU enzymes, ApoE/NEU3 (ApoE mice with NEU3 deficiency), ApoE/NEU4 (ApoE mice with NEU4 deficiency), and ApoE_Neo-in (knockdown ApoE mice with ~10% NEU1 activity) were generated, and plasma from each animal model was tested for glycolipid content.

3.6.1 Results and Discussion

We received 50 μL aliquots of serum samples from ApoE, ApoE/NEU3, ApoE/NEU4, and ApoE_Neo-in animals. GSLs were extracted from two aliquots of each animal model. Dried GSL extracts from each sample were subjected to EGCase I digestion and 2-AA labeling, followed by LC-MS analysis of the labeled products.

A representative chromatographic profile of GSLs identified in each animal model is shown in **Figure 3–6**. The major GSL identified consistently in all samples was GM2 ganglioside containing a Neu5Gc sialic acid (~10.6–11.2 min). GM2-Neu5Gc takes up over 90% of the total GSL composition in mouse plasma, consistent with previously reported data.[65] LacCer (~6.1 min), GA2, (~6.4 min), GM3 (~8.0 min), GM2 (~8.8 min), GM3-Neu5Gc (~9.8 min), and GM1 (~14.5 min) were the other minor GSLs observed.

We note that GM2 was not observed in ApoE_Neo-in animals. LacCer, GM3, and GM1 peaks were assigned based on retention times of commercially available standard GSLs. The remaining GSL peaks were assigned by High Resolution Electrospray Ionization Mass Spectrometry (HR-ESI-MS). Quantification was performed with the internal standard maltose.

The results of these experiments show similar GSL compositions in ApoE, ApoE/ NEU3, and ApoE/NEU4 mice. The ApoE_Neo-in animal showed significant decreases in GM2-Neu5Gc, GM3, GM1, and GA2. There were small but insignificant changes in GM2-Neu5Gc and GM1 for the ApoE/NEU3 animal, while one of the two replicates of ApoE/NEU4 animals showed a stark increase in LacCer and small decreases in GA2 and GM1. The absence of GM2 and a small amount of GA2 (asialo-GM2) in these animals could be due to the activity of native NEU3 and NEU4 in plasma that desialylate GM2 to GA2.

Considering that there are direct reports of increased expression of NEU1 in macrophages of human carotid arteries with atherosclerosis,[66] the negligible changes in NEU3 (ApoE/NEU3) and NEU4 (ApoE/NEU4) deficient mice, along with significant changes in the NEU1 deficient mice (ApoE_Neo-in), suggest that the hNEU enzymes perhaps could be working together in a synergistic manner to regulate the GSL composition in these atherosclerosis mouse models. More detailed studies are required in order to investigate this hypothesis.

Other experiments in this study showed a direct relationship between desialylation of LDL glycoproteins (Apoliprotein B or ApoB100) by NEU1 and NEU3 enzymes and progressions of atherosclerotic plaques *in vitro* and *in vivo*. Furthermore, inhibition of

114

these enzymes, also leads to a gradual decrease in characteristic atherosclerotic lesions in mice. These results suggest that specific inhibitors of NEU1 and NEU3 enzymes could have potential therapeutic benefits in the prevention and/or treatment of atherosclerosis.
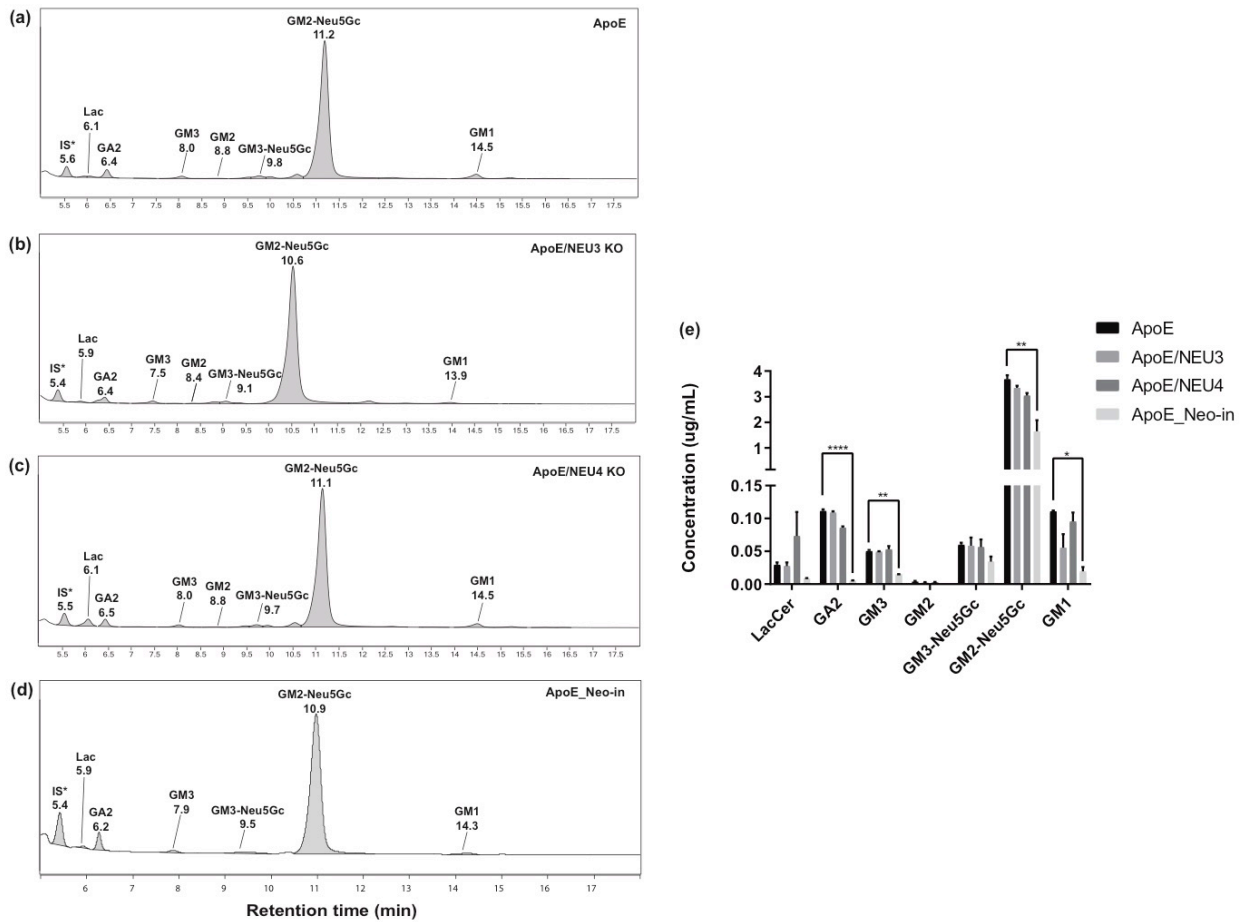
Figure 3– 6. Glycolipid composition of ApoE mouse serum by LC-MS. Representative chromatograms of glycolipid profiling in plasma from atherosclerosis mouse models (a) ApoE, (b) NEU3 knockout ApoE mice or ApoE/NEU3, (c) NEU4 knockout ApoE mice or ApoE/NEU4, and (d) NEU1 deficient ApoE mice or ApoE_Neo-in. (e) Ganglioside composition in mouse plasma from respective ApoE mice. Values represent mean and standard deviation of duplicate measurements (n = 2). The major ganglioside observed in all three cases is GM2-Neu5Gc, with other minor gangliosides LacCer, GM3, GM2, GA2, GM3-Neu5Gc, and GM1. Values were compared to relevant controls using a student's t-test, and p values are summarized as *, p<0.05, **; p<0.01; ***, p<0.005; ****, p<0.0001.

116

3.7 MATERIALS AND METHODS

3.7.1 Treatment of P4 and P24 Rats with Lipopolysaccharide (LPS)

Our collaborators in Montreal performed treatment of P4 and P24 rat brains with LPS, followed by brain homogenization. Briefly, rats in both litters were anesthetized, and 0.5 µl of LPS (*Escherichia coli*, serotype 055:B5; Sigma, St Louis, MO; 1 mg/mL suspension in sterile saline) was injected into the left corpus callosum. For the Sham litter, the same volume of sterile serum was injected into the left corpus callosum. The rats from each litter group were sacrificed and brains were cut, adjusting the cuts to the site of injection. Each piece of the brain was weighed, 5 volumes of water added and sonicated on ice. Aliquots of the brain homogenate were made and stored in -80 °C.

3.7.2 Treatment of Jurkat T cells with Cytochalasin D (CytoD), Phorbol 12-Myristate 13-Acetate (PMA), Recombinant Human Neuraminidase-3 (NEU3) and Bacterial Neuraminindase (NanI)

Jurkat T cells (E6.1 clone) were cultured in RPMI 1640 medium containing 10% fetal bovine serum (FBS) and 1% Penicillin, at 37 °C under 5% CO_2. Phorbol 12-myristate 13-acetate (PMA) (Sigma-Aldrich. Oakville, Ontario, Canada) and cytochalasin D (CytoD) (ENZO Life Sciences, Farmingdale, NY, USA) were dissolved in dimethyl sulphoxide (DMSO) (Sigma-Aldrich, Oakville, Ontario, Canada) to prepare stock solutions of 50 µg mL^{-1} and 5 mg mL^{-1} concentrations, respectively. NanI (Sigma-Aldrich, Oakville, Ontario, Canada) and human neuraminidase 3 (NEU3) were stored in the same NEU3 buffer (0.2 M NaCl; 10% Glycerol; 10 mM Maltose; 20 mM MOPS; pH 7.2).

Cell treatments were performed on a suspension of 1×10^6 Jurkat T cells from the culture flask. The medium was discarded, and the cells were washed three times with 1 mL of PBS buffer by spinning at 1200 rpm for 2 min on a desktop centrifuge. For DMSO control, PMA, and CytoD conditions, cells were suspended in 1 mL of PBS buffer containing 0.05% (final concentration) DMSO, the same buffer with DMSO containing PMA (200 ng ml^{-1}), and the same buffer with DMSO containing CytoD (2.5 μg mL^{-1}). Then, samples were incubated at 37 °C for 30 min. For buffer (PBS) control, NanI and NEU3 treated samples cells were suspended in 100 μL of PBS (pH 7.2), 100 μL of PBS containing 0.018 U of NEU3, and 100 μL of PBS containing 0.018 U of NanI, respectively; one unit of enzyme was defined as the amount of enzyme that cleaved 1 μmol 4MU-NANA substrate per min at pH 4.5. Next, enzyme treated samples were incubated at 37 °C for 3 h. After incubation, all treated samples were washed three times with PBS before GSL extraction and subsequent analyses. All experiments were performed with cells of passage 5.

3.7.3 Treatment of PC3 Cells with Specific Neuraminidase Inhibitors

PC-3 cells were cultured in Ham's F-12k medium supplemented by 10% FBS and 1% penicillin-streptomycin in 5% CO_2 at 37 °C in an incubator. Cell treatments were performed with 1×10^6 cells for each run. PC-3 cells were treated with hNEU inhibitors at 100 μM concentration each and incubated for 21 h at 37 °C under serum free conditions. After 21 h, cells were harvested and washed thrice with PBS before GSL extraction and subsequent analysis. All experiments were performed with cells of passage 5, 9, and 13.

3.7.4 Polarization Conditions of Mouse Microglia.

Microglial cell aliquots were received from the Sipione Lab in the Department of Pharmacology at the University of Alberta. Microglia were grown in a DMEM/F12 medium supplemented with 5% FBS, 1% sodium pyruvate, and 50 μM β-mercaptoethanol (β ME). M0 polarized microglia were generated by growing cells in a microglia medium containing mouse recombinant carrier-free macrophage colony stimulating factor (MCSF) (R&D Systems) and human recombinant transforming growth factor β1 (TGFβ1) (Miltenyi Biotec) for 5 days. M1 polarized microglia were generated by treating cells with granulocyte macrophage colony stimulating factor (GM-CSF), first with half a dose for 48 h and then a full dose for 48–72 h. Finally, cells were activated with interferon-γ1b (IFN- γ1b) for 1 h, followed by lipopolysaccharide (LPS) stimulation for 24–48 h. M2 polarized microglia were generated in the same way as M1, but instead of GM-CSF, M-CSF was used. To activate the cells, they were treated with interleukins (IL-4 and IL-13) twice for 24 h at a time.

3.7.5 Generation of Knockout (KO) Strains Using ApoE Atherosclerosis Models

B6.129P2-Apoetm1Unc/J JAX stock #002052 ($ApoE^{-/-}$), denoted as ApoE in this chapter is a commonly used mouse model of atherosclerosis. This model was the subject of this study as well. The ApoE mice have increased levels of total cholesterol and LDL cholesterol in their bloodstream. ApoE mice were crossed with NEU3 KO ($Neu3^{-/-}$), NEU4 KO ($Neu4^{-/-}$) mice, or *CathA* hypomorph mice with ~10 % residual NEU1 activity in tissues ($CathA^{S190A-Neo}$) to generate ApoE mice with NEU3 (ApoE/NEU3), NEU4 (ApoE/NEU4), and NEU1 (ApoE_Neo-in) deficiencies, respectively. We received two 50

119

µL samples of plasma for GSL analysis from each of the animal strains. All animal work was performed in Dr. Alexey V. Pshezhetsky's lab in the Department of Biochemistry, Université du Québec à Montréal, Montréal, Quebec, Canada.

3.7.6 Analysis of GSLs Extracted from Rat Brains, Jurkat T Cells, PC3 Cells, Microglia, and Mouse Plasma

LC-MS analysis of GSLs from rat brains, cells, and mouse plasma was carried out following the methods in **Chapter 2**. Briefly, a recombinant form of endoglycoceramidase or EGCase I was expressed in *E. coli* following the recent works of Albrecht et al.[67] Samples of cells, tissues, or serum were used for GSL extraction and purification following the protocol reported by Schnaar and co-workers.[68] GSLs extracts were incubated with EGCase for 18 h at 37 °C with 0.08–0.09 U EGCase and labeled with 2-anthranilic acid (2-AA). An Agilent 1200 SL HPLC system was used to analyze labeled glycans. Chromatography was performed on a normal-phase column (Accucore-150-Amide-HILIC, 2.6 mm, 2.1 x 150 mm, Thermo Fisher) at 40 °C. Fluorescence was monitored at an excitation of 320 nm and an emission of 420 nm. Relative quantities of GSLs were calculated by normalizing the peak areas of each GSL to the peak area of the internal standard. An Agilent 6220 Accurate-Mass TOF HPLC/MS system was used for Mass Spectra acquisition, and data analysis was performed using the Agilent MassHunter Qualitative Analysis software package version B.07.01.

3.8 CONCLUSIONS

This chapter highlights the utility of the glycan analysis method using EGCase in an array of applications. We also provide evidence that the EGCase method is more convenient to use and a superior method of quantitation as compared to usual methods of GSL analysis, such as HPTLC. Work is still ongoing in the microglia project, while the others may be revisited later for further studies.

3.9 REFERENCES

1.   Demina, E., Pierre, W., Londono, I., Nguyen, A., Reiz, B., Zou, C., Chakraberty, R., Cairo, C.W., Pshezhetsky, A.V., Lodygensky, G., Persistant reduction in sialylation of cerebral glycoproteins following post-natal inflammatory exposure. 2018.

2.   Howlader, M. A., Li, C., Zou, C., Chakraberty, R., Ebesoh, N., Cairo, C.W., Neuraminidase-3 (NEU3) is a negative regulator of LFA-1 adhesion. 2018.

3.   Howlader, M. A., Guo, T., Chakraberty, R., Porter, E., Cairo, C.W., Isoenzyme-selective inhibitors of human neuraminidases reveal distinct effects on cell migration **2018**.

4.   Demina, E., Smutova, V., Fougerat, A., Pan, X., Guo, T., Zou, C., Chakraberty, R., Snarr, B., Sheppard, D., Shiao, C., Roy, R., Orekhov, A. N., Miyagi, T., Laffargue, M., Cairo, C.W., Pshezhetsky, A.V., Inhibitors of neuraminidases 1 and 3 as potential candidates for treatment of atherosclerosis. **2018**.

5.   Allende, M. L.; Proia, R. L., Lubricating cell signaling pathways with gangliosides. *Curr Opin Struct Biol* **2002,** *12* (5), 587-92.

6.   Schnaar, R. L.; Gerardy-Schahn, R.; Hildebrandt, H., Sialic acids in the brain: gangliosides and polysialic acid in nervous system development, stability, disease, and regeneration. *Physiol Rev* **2014,** *94* (2), 461-518.

7.   Kotani, M.; Kawashima, I.; Ozawa, H.; Terashima, T.; Tai, T., Differential distribution of major gangliosides in rat central nervous system detected by specific monoclonal antibodies. *Glycobiology* **1993,** *3* (2), 137-46.

8.   Pyo, H.; Joe, E.; Jung, S.; Lee, S. H.; Jou, I., Gangliosides activate cultured rat brain microglia. *J Biol Chem* **1999,** *274* (49), 34584-9.

9.   Saito, M.; Sugiyama, K., Characterization of nuclear gangliosides in rat brain: concentration, composition, and developmental changes. *Arch Biochem Biophys* **2002,** *398* (2), 153-9.

10.   Palmano, K.; Rowan, A.; Guillermo, R.; Guan, J.; McJarrow, P., The role of gangliosides in neurodevelopment. *Nutrients* **2015,** *7* (5), 3891-913.

11.   Yu, R. K.; Macala, L. J.; Taki, T.; Weinfield, H. M.; Yu, F. S., Developmental changes in ganglioside composition and synthesis in embryonic rat brain. *J Neurochem* **1988,** *50* (6), 1825-9.

12.   Pan, X.; De Aragao, C. B. P.; Velasco-Martin, J. P.; Priestman, D. A.; Wu, H. Y.; Takahashi, K.; Yamaguchi, K.; Sturiale, L.; Garozzo, D.; Platt, F. M.; Lamarche-Vane, N.; Morales, C. R.; Miyagi, T.; Pshezhetsky, A. V., Neuraminidases 3 and 4 regulate neuronal function by catabolizing brain gangliosides. *FASEB J* **2017,** *31* (8), 3467-3483.

13.   Vawter, M. P., Dysregulation of the neural cell adhesion molecule and neuropsychiatric disorders. *Eur J Pharmacol* **2000,** *405* (1-3), 385-95.

14.   Wells, T. N. C.; Proudfoot, A. E. I.; Power, C. A., Chemokine receptors and their role in leukocyte activation. *Immunology Letters* **1999,** *65* (1), 35-40.

15.   Hogg, N.; Smith, A.; McDowall, A.; Giles, K.; Stanley, P.; Laschinger, M.; Henderson, R., How T cells use LFA-1 to attach and migrate. *Immunol Lett* **2004,** *92* (1-2), 51-4.

16.   Zarbock, A.; Lowell, C. A.; Ley, K., Spleen tyrosine kinase Syk is necessary for E-selectin-induced alpha(L)beta(2) integrin-mediated rolling on intercellular adhesion molecule-1. *Immunity* **2007,** *26* (6), 773-83.

17.   Salas, A.; Shimaoka, M.; Kogan, A. N.; Harwood, C.; von Andrian, U. H.; Springer, T. A., Rolling adhesion through an extended conformation of integrin alphaLbeta2 and relation to alpha I and beta I-like domain interaction. *Immunity* **2004,** *20* (4), 393-406.

18.   Bi, S.; Baum, L. G., Sialic acids in T cell development and function. *Biochim Biophys Acta* **2009,** *1790* (12), 1599-610.

19.   Tauber, R.; Park, C. S.; Reutter, W., Intramolecular heterogeneity of degradation in plasma membrane glycoproteins: evidence for a general characteristic. *Proc Natl Acad Sci U S A* **1983,** *80* (13), 4026-9.

20.   Wang, P.; Zhang, J.; Bian, H.; Wu, P.; Kuvelkar, R.; Kung, T. T.; Crawley, Y.; Egan, R. W.; Billah, M. M., Induction of lysosomal and plasma membrane-bound sialidases in human T-cells via T-cell receptor. *Biochem J* **2004,** *380* (Pt 2), 425-33.

21. Wang, Y.; Yamaguchi, K.; Wada, T.; Hata, K.; Zhao, X.; Fujimoto, T.; Miyagi, T., A close association of the ganglioside-specific sialidase Neu3 with caveolin in membrane microdomains. *J Biol Chem* **2002,** *277* (29), 26252-9.

22. Seyrantepe, V.; Landry, K.; Trudel, S.; Hassan, J. A.; Morales, C. R.; Pshezhetsky, A. V., Neu4, a novel human lysosomal lumen sialidase, confers normal phenotype to sialidosis and galactosialidosis cells. *J Biol Chem* **2004,** *279* (35), 37021-9.

23. Zanchetti, G.; Colombi, P.; Manzoni, M.; Anastasia, L.; Caimi, L.; Borsani, G.; Venerando, B.; Tettamanti, G.; Preti, A.; Monti, E.; Bresciani, R., Sialidase NEU3 is a peripheral membrane protein localized on the cell surface and in endosomal structures. *Biochem J* **2007,** *408* (2), 211-9.

24. Sharma, D. K.; Brown, J. C.; Cheng, Z.; Holicky, E. L.; Marks, D. L.; Pagano, R. E., The glycosphingolipid, lactosylceramide, regulates beta1-integrin clustering and endocytosis. *Cancer Res* **2005,** *65* (18), 8233-41.

25. Pande, G., The role of membrane lipids in regulation of integrin functions. *Curr Opin Cell Biol* **2000,** *12* (5), 569-74.

26. Smith, R. J.; Justen, J. M.; Sam, L. M., Function and stimulus-specific effects of phorbol 12-myristate 13-acetate on human polymorphonuclear neutrophils: autoregulatory role for protein kinase C in signal transduction. *Inflammation* **1988,** *12* (6), 597-611.

27. Mortensen, K.; Larsson, L. I., Effects of cytochalasin D on the actin cytoskeleton: association of neoformed actin aggregates with proteins involved in signaling and endocytosis. *Cell Mol Life Sci* **2003,** *60* (5), 1007-12.

28.   van Kooyk, Y.; Figdor, C. G., Avidity regulation of integrins: the driving force in leukocyte adhesion. *Curr Opin Cell Biol* **2000,** *12* (5), 542-7.

29.   Sandbhor, M. S.; Soya, N.; Albohy, A.; Zheng, R. B.; Cartmell, J.; Bundle, D. R.; Klassen, J. S.; Cairo, C. W., Substrate recognition of the membrane-associated sialidase NEU3 requires a hydrophobic aglycone. *Biochemistry* **2011,** *50* (32), 6753-62.

30.   Miyagi, T.; Yamaguchi, K., Mammalian sialidases: physiological and pathological roles in cellular functions. *Glycobiology* **2012,** *22* (7), 880-96.

31.   Cross, A. S.; Hyun, S. W.; Miranda-Ribera, A.; Feng, C.; Liu, A.; Nguyen, C.; Zhang, L.; Luzina, I. G.; Atamas, S. P.; Twaddell, W. S.; Guang, W.; Lillehoj, E. P.; Puche, A. C.; Huang, W.; Wang, L. X.; Passaniti, A.; Goldblum, S. E., NEU1 and NEU3 sialidase activity expressed in human lung microvascular endothelia: NEU1 restrains endothelial cell migration, whereas NEU3 does not. *J Biol Chem* **2012,** *287* (19), 15966-80.

32.   Koseki, K.; Wada, T.; Hosono, M.; Hata, K.; Yamaguchi, K.; Nitta, K.; Miyagi, T., Human cytosolic sialidase NEU2-low general tissue expression but involvement in PC-3 prostate cancer cell survival. *Biochem Biophys Res Commun* **2012,** *428* (1), 142-9.

33.   Hata, K.; Tochigi, T.; Sato, I.; Kawamura, S.; Shiozaki, K.; Wada, T.; Takahashi, K.; Moriya, S.; Yamaguchi, K.; Hosono, M.; Miyagi, T., Increased sialidase activity in serum of cancer patients: Identification of sialidase and inhibitor activities in human serum. *Cancer Sci* **2015,** *106* (4), 383-9.

34. Zhang, Y.; Albohy, A.; Zou, Y.; Smutova, V.; Pshezhetsky, A. V.; Cairo, C. W., Identification of selective inhibitors for human neuraminidase isoenzymes using C4,C7-modified 2-deoxy-2,3-didehydro-N-acetylneuraminic acid (DANA) analogues. *J Med Chem* **2013,** *56* (7), 2948-58.

35. Magesh, S.; Moriya, S.; Suzuki, T.; Miyagi, T.; Ishida, H.; Kiso, M., Design, synthesis, and biological evaluation of human sialidase inhibitors. Part 1: selective inhibitors of lysosomal sialidase (NEU1). *Bioorg Med Chem Lett* **2008,** *18* (2), 532-7.

36. Albohy, A.; Zhang, Y.; Smutova, V.; Pshezhetsky, A. V.; Cairo, C. W., Identification of Selective Nanomolar Inhibitors of the Human Neuraminidase, NEU4. *ACS Med Chem Lett* **2013,** *4* (6), 532-7.

37. Guo, T.; Datwyler, P.; Demina, E.; Richards, M. R.; Ge, P.; Zou, C.; Zheng, R.; Fougerat, A.; Pshezhetsky, A. V.; Ernst, B.; Cairo, C. W., Selective Inhibitors of Human Neuraminidase 3. *J Med Chem* **2018,** *61* (5), 1990-2008.

38. Kwon, K. M.; Chung, T. W.; Kwak, C. H.; Choi, H. J.; Kim, K. W.; Ha, S. H.; Cho, S. H.; Lee, Y. C.; Ha, K. T.; Lee, M. J.; Kim, C. H., Disialyl GD2 ganglioside suppresses ICAM-1-mediated invasiveness in human breast cancer MDA-MB231 cells. *Int J Biol Sci* **2017,** *13* (3), 265-275.

39. Zhuo, D.; Li, X.; Guan, F., Biological Roles of Aberrantly Expressed Glycosphingolipids and Related Enzymes in Human Cancer Development and Progression. *Front Physiol* **2018,** *9*, 466.

40. Hatano, K.; Miyamoto, Y.; Nonomura, N.; Kaneda, Y., Expression of gangliosides, GD1a, and sialyl paragloboside is regulated by NF-kappaB-

dependent transcriptional control of alpha2,3-sialyltransferase I, II, and VI in human castration-resistant prostate cancer cells. *Int J Cancer* **2011,** *129* (8), 1838-47.

41.   Perry, V. H.; Teeling, J., Microglia and macrophages of the central nervous system: the contribution of microglia priming and systemic inflammation to chronic neurodegeneration. *Semin Immunopathol* **2013,** *35* (5), 601-12.

42.   Gomez-Nicola, D.; Perry, V. H., Microglial dynamics and role in the healthy and diseased brain: a paradigm of functional plasticity. *Neuroscientist* **2015,** *21* (2), 169-84.

43.   Jou, I.; Lee, J. H.; Park, S. Y.; Yoon, H. J.; Joe, E. H.; Park, E. J., Gangliosides trigger inflammatory responses via TLR4 in brain glia. *Am J Pathol* **2006,** *168* (5), 1619-30.

44.   In *Essentials of Glycobiology*, rd; Varki, A.; Cummings, R. D.; Esko, J. D.; Stanley, P.; Hart, G. W.; Aebi, M.; Darvill, A. G.; Kinoshita, T.; Packer, N. H.; Prestegard, J. H.; Schnaar, R. L.; Seeberger, P. H., Eds. Cold Spring Harbor (NY), 2015.

45.   Kim, O. S.; Park, E. J.; Joe, E. H.; Jou, I., JAK-STAT signaling mediates gangliosides-induced inflammatory responses in brain microglial cells. *J Biol Chem* **2002,** *277* (43), 40594-601.

46.   Butovsky, O.; Jedrychowski, M. P.; Moore, C. S.; Cialic, R.; Lanser, A. J.; Gabriely, G.; Koeglsperger, T.; Dake, B.; Wu, P. M.; Doykan, C. E.; Fanek, Z.; Liu, L.; Chen, Z.; Rothstein, J. D.; Ransohoff, R. M.; Gygi, S. P.; Antel, J. P.;

Weiner, H. L., Identification of a unique TGF-beta-dependent molecular and functional signature in microglia. *Nat Neurosci* **2014,** *17* (1), 131-43.

47.   Durafourt, B. A.; Moore, C. S.; Zammit, D. A.; Johnson, T. A.; Zaguia, F.; Guiot, M. C.; Bar-Or, A.; Antel, J. P., Comparison of polarization properties of human adult microglia and blood-derived macrophages. *Glia* **2012,** *60* (5), 717-27.

48.   Orihuela, R.; McPherson, C. A.; Harry, G. J., Microglial M1/M2 polarization and metabolic states. *Br J Pharmacol* **2016,** *173* (4), 649-65.

49.   Marconi, S.; De Toni, L.; Lovato, L.; Tedeschi, E.; Gaetti, L.; Acler, M.; Bonetti, B., Expression of gangliosides on glial and neuronal cells in normal and pathological adult human brain. *J Neuroimmunol* **2005,** *170* (1-2), 115-21.

50.   Ohmi, Y.; Ohkawa, Y.; Tajima, O.; Sugiura, Y.; Furukawa, K.; Furukawa, K., Ganglioside deficiency causes inflammation and neurodegeneration via the activation of complement system in the spinal cord. *J Neuroinflammation* **2014,** *11*, 61.

51.   Nagata, Y.; Yamashiro, S.; Yodoi, J.; Lloyd, K. O.; Shiku, H.; Furukawa, K., Expression cloning of beta 1,4 N-acetylgalactosaminyltransferase cDNAs that determine the expression of GM2 and GD2 gangliosides. *J Biol Chem* **1992,** *267* (17), 12082-9.

52.   Nagata, Y.; Yamashiro, S.; Yodoi, J.; Lloyd, K. O.; Shiku, H.; Furukawa, K., Expression cloning of beta 1,4 N-acetylgalactosaminyltransferase cDNAs that determine the expression of GM2 and GD2 gangliosides. *J Biol Chem* **1994,** *269* (9), 7045.

53. Ohmi, Y.; Tajima, O.; Ohkawa, Y.; Yamauchi, Y.; Sugiura, Y.; Furukawa, K.; Furukawa, K., Gangliosides are essential in the protection of inflammation and neurodegeneration via maintenance of lipid rafts: elucidation by a series of ganglioside-deficient mutant mice. *J Neurochem* **2011,** *116* (5), 926-35.

54. Saito, M.; Wu, G.; Hui, M.; Masiello, K.; Dobrenis, K.; Ledeen, R. W.; Saito, M., Ganglioside accumulation in activated glia in the developing brain: comparison between WT and GalNAcT KO mice. *J Lipid Res* **2015,** *56* (8), 1434-48.

55. Lozano, R.; Naghavi, M.; Foreman, K.; Lim, S.; Shibuya, K.; Aboyans, V.; Abraham, J.; Adair, T.; Aggarwal, R.; Ahn, S. Y.; Alvarado, M.; Anderson, H. R.; Anderson, L. M.; Andrews, K. G.; Atkinson, C.; Baddour, L. M.; Barker-Collo, S.; Bartels, D. H.; Bell, M. L.; Benjamin, E. J.; Bennett, D.; Bhalla, K.; Bikbov, B.; Bin Abdulhak, A.; Birbeck, G.; Blyth, F.; Bolliger, I.; Boufous, S.; Bucello, C.; Burch, M.; Burney, P.; Carapetis, J.; Chen, H.; Chou, D.; Chugh, S. S.; Coffeng, L. E.; Colan, S. D.; Colquhoun, S.; Colson, K. E.; Condon, J.; Connor, M. D.; Cooper, L. T.; Corriere, M.; Cortinovis, M.; de Vaccaro, K. C.; Couser, W.; Cowie, B. C.; Criqui, M. H.; Cross, M.; Dabhadkar, K. C.; Dahodwala, N.; De Leo, D.; Degenhardt, L.; Delossantos, A.; Denenberg, J.; Des Jarlais, D. C.; Dharmaratne, S. D.; Dorsey, E. R.; Driscoll, T.; Duber, H.; Ebel, B.; Erwin, P. J.; Espindola, P.; Ezzati, M.; Feigin, V.; Flaxman, A. D.; Forouzanfar, M. H.; Fowkes, F. G.; Franklin, R.; Fransen, M.; Freeman, M. K.; Gabriel, S. E.; Gakidou, E.; Gaspari, F.; Gillum, R. F.; Gonzalez-Medina, D.; Halasa, Y. A.; Haring, D.; Harrison, J. E.; Havmoeller, R.; Hay, R. J.; Hoen, B.; Hotez, P. J.; Hoy, D.; Jacobsen, K. H.; James, S. L.; Jasrasaria, R.; Jayaraman, S.; Johns, N.;

Karthikeyan, G.; Kassebaum, N.; Keren, A.; Khoo, J. P.; Knowlton, L. M.; Kobusingye, O.; Koranteng, A.; Krishnamurthi, R.; Lipnick, M.; Lipshultz, S. E.; Ohno, S. L.; Mabweijano, J.; MacIntyre, M. F.; Mallinger, L.; March, L.; Marks, G. B.; Marks, R.; Matsumori, A.; Matzopoulos, R.; Mayosi, B. M.; McAnulty, J. H.; McDermott, M. M.; McGrath, J.; Mensah, G. A.; Merriman, T. R.; Michaud, C.; Miller, M.; Miller, T. R.; Mock, C.; Mocumbi, A. O.; Mokdad, A. A.; Moran, A.; Mulholland, K.; Nair, M. N.; Naldi, L.; Narayan, K. M.; Nasseri, K.; Norman, P.; O'Donnell, M.; Omer, S. B.; Ortblad, K.; Osborne, R.; Ozgediz, D.; Pahari, B.; Pandian, J. D.; Rivero, A. P.; Padilla, R. P.; Perez-Ruiz, F.; Perico, N.; Phillips, D.; Pierce, K.; Pope, C. A., 3rd; Porrini, E.; Pourmalek, F.; Raju, M.; Ranganathan, D.; Rehm, J. T.; Rein, D. B.; Remuzzi, G.; Rivara, F. P.; Roberts, T.; De Leon, F. R.; Rosenfeld, L. C.; Rushton, L.; Sacco, R. L.; Salomon, J. A.; Sampson, U.; Sanman, E.; Schwebel, D. C.; Segui-Gomez, M.; Shepard, D. S.; Singh, D.; Singleton, J.; Sliwa, K.; Smith, E.; Steer, A.; Taylor, J. A.; Thomas, B.; Tleyjeh, I. M.; Towbin, J. A.; Truelsen, T.; Undurraga, E. A.; Venketasubramanian, N.; Vijayakumar, L.; Vos, T.; Wagner, G. R.; Wang, M.; Wang, W.; Watt, K.; Weinstock, M. A.; Weintraub, R.; Wilkinson, J. D.; Woolf, A. D.; Wulf, S.; Yeh, P. H.; Yip, P.; Zabetian, A.; Zheng, Z. J.; Lopez, A. D.; Murray, C. J.; AlMazroa, M. A.; Memish, Z. A., Global and regional mortality from 235 causes of death for 20 age groups in 1990 and 2010: a systematic analysis for the Global Burden of Disease Study 2010. *Lancet* **2012,** *380* (9859), 2095-128.

56. Kalanuria, A. A.; Nyquist, P.; Ling, G., The prevention and regression of atherosclerotic plaques: emerging treatments. *Vasc Health Risk Manag* **2012,** *8*, 549-61.

57. Pastrana, J. L.; Sha, X.; Virtue, A.; Mai, J.; Cueto, R.; Lee, I. A.; Wang, H.; Yang, X. F., Regulatory T cells and Atherosclerosis. *J Clin Exp Cardiolog* **2012,** *2012* (Suppl 12), 2.

58. Spitz, C.; Winkels, H.; Burger, C.; Weber, C.; Lutgens, E.; Hansson, G. K.; Gerdes, N., Regulatory T cells in atherosclerosis: critical immune regulatory function and therapeutic potential. *Cell Mol Life Sci* **2016,** *73* (5), 901-22.

59. Packard, R. R.; Libby, P., Inflammation in atherosclerosis: from vascular biology to biomarker discovery and risk prediction. *Clin Chem* **2008,** *54* (1), 24-38.

60. Ahotupa, M.; Suomela, J. P.; Vuorimaa, T.; Vasankari, T., Lipoprotein-specific transport of circulating lipid peroxides. *Ann Med* **2010,** *42* (7), 521-9.

61. Millar, J. S., The sialylation of plasma lipoproteins. *Atherosclerosis* **2001,** *154* (1), 1-13.

62. Orekhov, A. N.; Tertov, V. V.; Mukhin, D. N., Desialylated low density lipoprotein--naturally occurring modified lipoprotein with atherogenic potency. *Atherosclerosis* **1991,** *86* (2-3), 153-61.

63. Ruelland, A.; Gallou, G.; Legras, B.; Paillard, F.; Cloarec, L., LDL sialic acid content in patients with coronary artery disease. *Clin Chim Acta* **1993,** *221* (1-2), 127-33.

64.   Pilatte, Y.; Bignon, J.; Lambre, C. R., Sialic acids as important molecules in the regulation of the immune system: pathophysiological implications of sialidases in immunity. *Glycobiology* **1993,** *3* (3), 201-18.

65.   Cotterchio, M.; Seyfried, T. N., Serum gangliosides in mice with metastatic and non-metastatic brain tumors. *J Lipid Res* **1994,** *35* (1), 10-4.

66.   Sieve, I.; Ricke-Hoch, M.; Kasten, M.; Battmer, K.; Stapel, B.; Falk, C. S.; Leisegang, M. S.; Haverich, A.; Scherr, M.; Hilfiker-Kleiner, D., A positive feedback loop between IL-1beta, LPS and NEU1 may promote atherosclerosis by enhancing a pro-inflammatory state in monocytes and macrophages. *Vascul Pharmacol* **2018,** *103-105*, 16-28.

67.   Albrecht, S.; Vainauskas, S.; Stockmann, H.; McManus, C.; Taron, C. H.; Rudd, P. M., Comprehensive Profiling of Glycosphingolipid Glycans Using a Novel Broad Specificity Endoglycoceramidase in a High-Throughput Workflow. *Anal Chem* **2016,** *88* (9), 4795-802.

68.   Sturgill, E. R.; Aoki, K.; Lopez, P. H.; Colacurcio, D.; Vajn, K.; Lorenzini, I.; Majic, S.; Yang, W. H.; Heffer, M.; Tiemeyer, M.; Marth, J. D.; Schnaar, R. L., Biosynthesis of the major brain gangliosides GD1a and GT1b. *Glycobiology* **2012,** *22* (10), 1289-301.

CHAPTER 4

LYSO-GLYCOSPHINGOLIPID ANALYSIS BY ENZYMATIC DEGRADATION USING SPHINGOLIPID CERAMIDE *N*-DEACYLASE ENZYME

[1]Compound 1 described in this chapter was reported in Daskhan, G. C.; Tran, H. T.; Meloncelli, P. J.; Lowary, T. L.; West, L. J.; Cairo, C. W., Construction of Multivalent Homo- and Heterofunctional ABO Blood Group Glycoconjugates Using a Trifunctional Linker Strategy, *Bioconjug Chem* **2018,** *29* (2), 343-362.

[2] RapiFluor-MS labeling kit and the X-Select CSH C18 RP column were provided by Waters Corporation Inc., USA

4.1 INTRODUCTION

Lyso-glycosphingolipids (*l*-GSLs) are a class of GSLs devoid of the fatty acyl chain on the ceramide moiety, characterized by a GSL glycan attached to the sphingosine (Sph) base bearing a primary amine residue **(Figure 4–1)**. Semi-synthesis of *l*-GSLs can be accomplished by alkaline hydrolysis of GSLs, which often results in poor yields of the final product.[2] Alternatively, *l*-GSLs can be prepared by the action of enzymes, such as, sphingolipid ceramide N-deacylase (SCDase), first isolated from *Pseudomonas sp*. TK4.[3] This enzyme is reactive specifically towards GSLs and sphingomyelins.[4] A unique property of SCDase is its ability to perform transacylation reactions, whereby free fatty acids are transferred to *l*-GSLs, forming GSLs.[3-4] This property sometimes complicates the use of SCDase as this equilibrium is an impediment to the synthesis of *l*-GSLs. **Figure 4–1** shows the action of SCDase on glycosylceramide (GlcCer) generating *l*-GlcCer (d18:1), where d18 represents the number of carbon atoms and 1 represents the number of double bonds in the Sph chain.
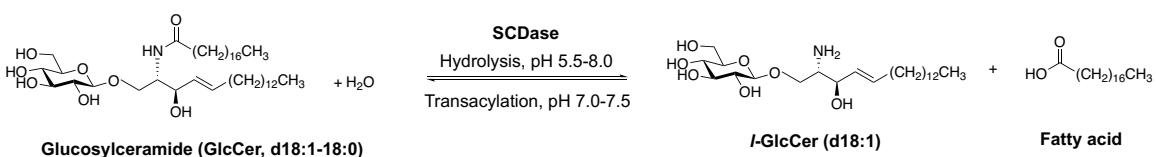
Figure 4– 1. Action of Sphingolipid ceramide N-deacylase (SCDase). Hydrolysis of glucosylceramide or GlcCer (at pH 5.5–8.0) to form *l*-GlcCer bearing an 18-carbon Sph chain and transacylation (at pH 7.0–7.5) catalyzed by SCDase.

Organisms such as *Nocardia sp.*,[5] *Pseudomonas sp.*,[3] and *Streptomyces sp.*[6] are sources of SCDase enzyme variants. The most recent one reported is from *Shewanella alga* G8.[7] These enzymes commonly are not used for the purpose of *l*-GSL semi-synthesis, owing to their poor characterization. A recent enzymatic and synthetic study of this enzyme by Han et al. reported specificities and kinetic properties of SA_SCD (*Shewanella* alga SCDase).[8] The enzyme is most active at a pH of 6.0 for hydrolysis, while its transacylation activity is dominant between pH 7.0 and 7.5. SA_SCD can hydrolyze a wide range of substrates but shows preference towards substrates with large polar head-groups. Transacylation properties of SA_SCD are exhibited more commonly towards glucosylceramide (GlcCer), galactosylceramide (GalCer), and lactosylceramide (LacCer) over other GSLs.[8] The dynamic equilibrium between hydrolysis and transacylation provide a reason why SCDase enzymes are not used frequently for GSL modifications.[9] Efforts have been made to control this problem. An aqueous organic biphasic system has been used by Kurita et al. to remove the fatty acids generated from the reaction mixture, thereby eliminating the possibility of transacylation.[10] Huang et al have used divalent metal cations to precipitate salts formed by reaction with the released fatty acids in the mixture, thereby maximizing the hydrolysis of GSLs and reducing the chances of transacylation in the process.[11]

A crystal structure of the SCDase enzymes has not been reported, making it difficult to pinpoint specific residues in the active site of the enzyme responsible for its action. Studies of critical amino acid residues by chemical modification evaluate their role in enzyme reactivity. Tryptophan (Trp), arginine (Arg), and free carboxyl residues on aspartic acid (Asp) or glutamic acid (Glu) have been identified as the key residues

responsible for the proper functioning of SCDase enzymes.[12] Studies also have suggested that the same active site catalyzes both hydrolytic and synthetic activities.[13]

The primary amine residue of *l*-GSLs serves as a convenient chemical handle for attaching amine reactive fluorophores by amine coupling. Common fluorescent dyes used for this purpose include, cyanine dyes[14], 4,4-difluoro-4-bora-3*a*,4*a*-diaza-*s*-indacene (BODIPY)[15-16], nitrobenzoxadiazole (NBD)[17], and ophthaldialdehyde (OPA).[11] After fluorescent labeling with OPA, SCDase-generated *l*-GSLs have been analyzed by HPLC to separate the different Sph base chains.[8, 11] Similar studies based on fluorescent labeling of *l*-GSLs and their HPLC analysis have been performed to quantify specific GSLs, such as glucosylceramide and galactosylceramide in human fibroblasts and zebra fish.[18]

l-GSLs have been implicated in a number of storage diseases, such as Sandhoff disease, which is characterized by an elevation of *l*-GM2.[19] There are several reports suggesting involvement of *l*-GSLs in cellular activities, such as modulation of the function of the epidermal growth factor receptor (EGFR) in cell growth or inhibition of protein kinase C that leads to sphingolipidosis.[20] Although the importance of *l*-GSLs has been highlighted [21] and they have been analyzed by various techniques, such as HPLC and LC-MS, these studies have focused on *l*-GSLs without considering the effects of chain length and saturation of the Sph base. Reports have shown differential expression of *l*-GM1 containing d18:1 and d20:1 Sph chains in different regions of the brain.[22] These studies suggest that the Sph base, and variability in chain length or saturation may play a role in the function of GSLs. This chapter outlines the development of a method for profiling and quantification of *l*-GSLs from biological samples. As a complementary approach to the EGCase method described in **Chapter 2**, this method aims to identify and

quantify lyso-species of GSLs that already have been identified in a sample utilizing the EGCase method. The method is based on fluorescent LC-MS (F-LC-MS) using an MS-sensitive fluorophore. This approach used fluorescence for quantitation rather than Mass Spectrometry (MS) alone.[23]

4.2 RESULTS AND DISCUSSION

4.2.1 Expression and Purification of Sphingolipid Ceramide *N*-deacylase (SCDase)

Commercial samples of SCDase enzyme that were tested were not sufficiently active to detect the production of *l*-GSLs. Thus, we produced a recombinant form of the enzyme following an established protocol [8] for the SA_SCD originating from the marine algae *Shewanella alga (SA)* with broad substrate specificity towards both neutral GSLs and acidic gangliosides. The gene encoding SA_SCD had 277 C-terminal residues deleted, lacked 38 residues at its N-terminus, and was synthesized (GenScript) with a purification tag (His-tag) attached to its N-terminus. The protein was expressed in *E. coli* and purified using Fast Protein Liquid Chromatography (FPLC) on a Ni-NTA agarose column. The protocol is outlined in **Materials and Methods**. The protein concentration was measured using the bicinchonic acid protein assay (BCA assay), with BSA as a standard.

4.2.2 Separation on a Reverse Phase C8 Column

The biggest challenge we faced with this method was the separation of *l*-GSLs in a complex mixture. Separation needs to resolve both the hydrophilic (polar) oligosaccharide moiety in *l*-GSLs and the hydrophobic (non-polar) moiety of the Sph chain. We first tested a Phenomenex, Kinetex C8, Reverse Phase column (RP).

Commercially available GSL standards LacCer, GM3, GM1, and GD3 were taken individually and in a mixture, after treatment with an appropriate amount of SA_SCD. Based on previous reports, the pH for optimum enzyme activity was taken as 6.0.[7-8] Metal cations and detergents have been shown to increase the hydrolysis of GSLs to *l*-GSLs by SCDase enzymes, hence, CaCl$_2$ and sodium cholate were added to the buffer.[8] Triton X-100 was tested, however, the polyethylene oxide chains interfered with MS analysis, therefore, sodium cholate was used instead. After enzyme treatment, samples were labeled with an appropriate amount of the fluorophore, RapiFluor-MS (Waters Corporation Inc.), at room temperature (RT) for 5 min, and post-labeling cleanup was performed using an HILIC elution plate, as outlined in the GlycoWorks RapiFluor-MS labeling Kit module (Waters Corporation Inc.). Then, labeled samples were analyzed by LC-MS with fluorescence monitored at an excitation wavelength of 265 nm and an emission wavelength of 425 nm. The structure of RapiFluor-MS is shown in **Figure 4–2**; it bears an NHS-carbamate ester group for coupling with primary amines, a quinolinyl fluorophore, and a tertiary amine.
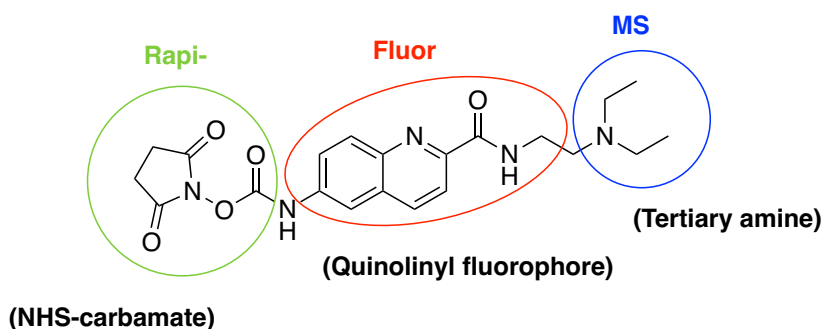
Figure 4– 2. Structure of RapiFluor-MS.

From the results of experiments (**Figure 4–3**) performed on individual standard GSLs, the *l*-GSLs identified for GM3 and GD3 both had d16:1, d17:1, and d18:1 Sph chains, while GM1 had d18:1 and d20:1 Sph chains. LacCer did not show any peak for *l*-LacCer, consistent with the preference of SA_SCD towards acidic and more polar GSLs over neutral GSLs.[8]

The peaks for individual Sph chain lengths were separated well for each *l*-GSL. *l*-GM3 (d16:1) eluted at ~18.5 min, *l*-GM3 (d17:1) eluted at ~21.6 min, and *l*-GM3 (d18:1) eluted at ~24.4 min; *l*-GD3 (d16:1) eluted at ~18.3 min, *l*-GD3 (d17:1) eluted at ~21.4 min, and *l*-GD3 (d18:1) eluted at ~24.4 min; and *l*-GM1 (d18:1) eluted at ~24.0 min, and *l*-GM1 (d20:1) at ~28.8 min. High Resolution Electrospray Ionization Mass Spectrometry (HR-ESI-MS) was employed to assign peaks using a database containing neutral masses of RapiFluor labeled *l*-GSLs (with Sph chains ranging from d12 to d28) from all possible biologically relevant GSLs. The sources for commercial GSLs were identified as bovine milk for GM3 and GD3 and porcine brain for GM1.
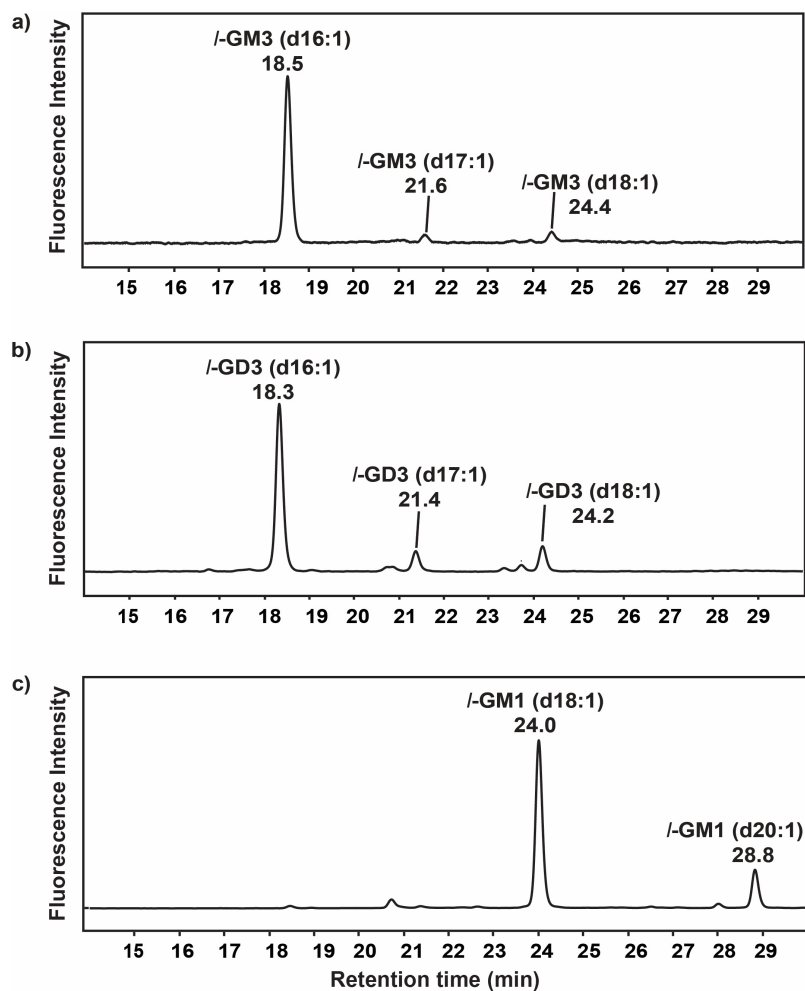
Figure 4– 3. HPLC separation of RapiFluor labeled *l*-GSLs. Separation of RapiFluor labeled (a) *l*-GM3, (b) *l*-GD3, and (c) *l*-GM1 on a Reverse Phase (RP) C8 column. GM3 and GD3, both sourced from bovine milk show peaks for *l*-GSLs with d16:1, d17:1, and d18:1 Sph chains, while GM1, sourced from porcine brain, show d18:1 and d20:1 Sph chains.

Comparing the results of our assay to previous literature reports, the Sph chains of GM3 and GD3 in bovine milk have been reported to be dominated by d16 with small amounts of d18, while Sph chains of GM1 in porcine brain only show d18 and d20 chain lengths.[24] The odd number of carbon atoms in d17:1 for GM3 and GD3 was a surprise, however, literature reports have suggested the incorporation of fatty acyl-CoA bearing 16±1 carbon chains by the enzyme serine palmitoyltransferase (SPT) in its active site

during the biosynthesis of ceramides.[25-26] Additionally, branching in the Sph chain could explain the odd number of carbon atoms.[24] To validate these findings further, MALDI was used to investigate the variability in the ceramide lipid chains in untreated, intact GM3, GM1, and GD3. **(Appendix B, Figure B–1 to B–3)** The results show an incredible variety in the ceramide chains (including odd number chain lengths in the ceramide moiety) for both GM3 and GD3, with GM1 showing less diversity in masses.

The individual *l*-GSLs showed excellent separation on the LC, however, when tested as a mixture, the peak separation was very poor. For a particular chain length, the *l*-GSL peaks were clustered, although well separated from other clusters of peaks bearing different chain lengths. *l*-GD3 (d16:1) and *l*-GM3 (d16:1) eluted at ~18.9 and ~19.1 min, respectively; *l*-GD3 (d17:1) and *l*-GM3 (d17:1) eluted at ~21.9 and ~22.1 min, respectively; and *l*-GM1 (d18:1), *l*-GD3 (d18:1), and *l*-GM3 (d18:1) eluted at ~24.5, ~24.7, ~24.9 min, respectively. As seen from **Figure 4–3 (a)**, the chain lengths were separated well, but the separation based on oligosaccharides in a mixture was very poor. We were unable to achieve improved separation by changing the gradient of the chromatography solvents. Instead, we obtained different retention times, with no positive effects on separation, as shown in **Figure 4–4 (b)**.
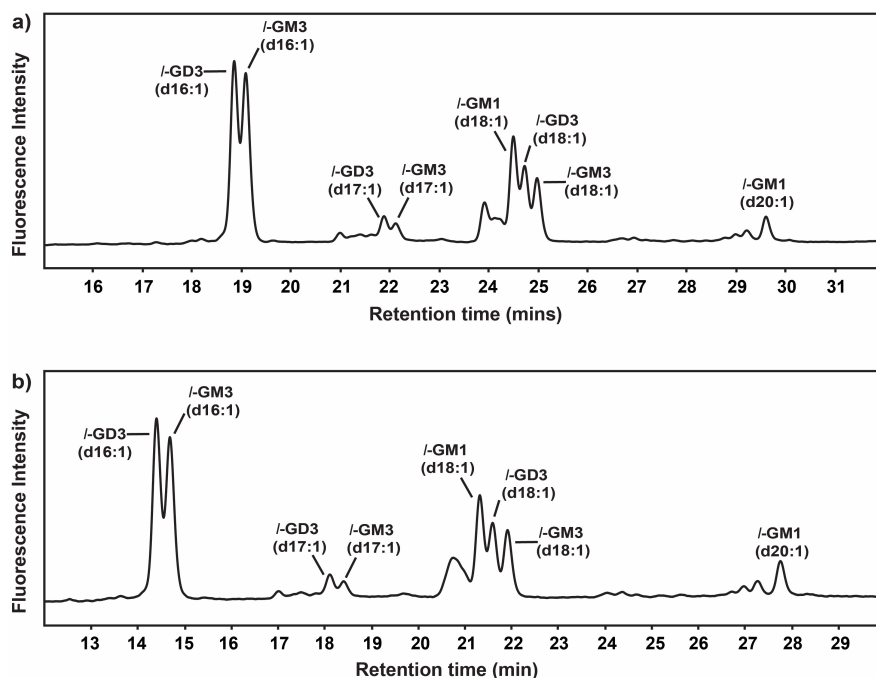
Figure 4– 4. HPLC separation of RapiFluor labeled *l*-GM3, *l*-GD3, and *l*-GM1 in a mixture on a Reverse Phase (RP) C8 column. (a) and (b) show two different gradients, with lower percentage of organic solvent in the mobile phase in (b). The separation of (d16:1) and (d17:1) Sph base chains of *l*-GM3 and *l*-GD3 formed a cluster of peaks at retention times very close to each other, and similar clustering was seen for (d18:1) Sph chains of *l*-GM3, *l*-GD3, and *l*-GM1 as well.

4.2.3 Separation on a reverse phase C18 column

We next tested a reverse phase (RP) Waters X-Select CSH C18 column. This column was tested only on a mixture of LacCer, GM3, GM1, and GD3 digested with SA-SCD at 37 °C for 24 h, followed by labeling with RapiFluor-MS and analysis by F-LC-MS. Peak assignments were made with HR-ESI-MS. As expected, similar results were obtained with clusters of peaks for different Sph chains and no improved separation based on oligosaccharides. **(Figure 4–5)**
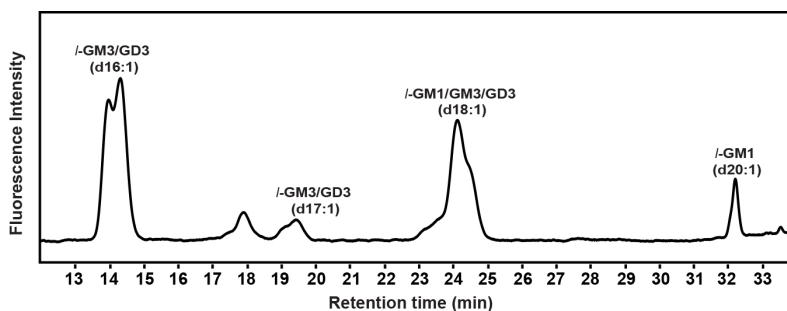
Figure 4– 5. HPLC separation of RapiFluor labeled *l*-GM3, *l*-GD3, and *l*-GM1 in a mixture on the Waters X-Select CSH Reverse Phase C18 column. Peaks for *l*-GM3 (d16:1) and *l*-GD3 (d16:1); *l*-GM3 (d17:1) and *l*-GD3 (d17:1); and *l*-GM3 (d18:1), *l*-GD3 (d18:1), and *l*-GM1 (d18:1) formed clusters, just the way they did for the previously tested C8 column. A change in gradient also did not improve the separation in any way.

4.2.4 Separation on a Weak Anion Exchange-Reverse Phase (WAX-RP) Mixed Mode Column

The problem identified from previous experiments on strictly RP columns was that the separation of *l*-GSL based on oligosaccharides was poor. This can be attributed to the fact that the bonded phase in a RP column is optimized to bind to hydrophobic analytes more than polar analytes. Hence, strongly hydrophobic analytes would be better suited for RP chromatography. *l*-GSLs are amphiphilic, with polar sugars and hydrophobic Sph chains. We next tested this assay on the GlycanPAC AXR-1 column (Kinetex), which is a mixed mode column offering a combination of weak anion exchange and reverse phase (WAX-RP) chromatography. WAX chromatography would offer separation of oligosaccharides in *l*-GSLs, while RP would offer separation of the Sph chains.

Tests of available standards were run on the Glycan-PAC AXR-1 column after SA_SCD digestion and RapiFluor-MS labeling **(Figure 4–6)**. We observed peaks for *l*-GM3 and *l*-GD3 with d16:1, d17:1, and d18:1 Sph chains, while *l*-GM1 had d18:1 and

143

d20:1 Sph chains. LacCer did not show any *l*-GSL peaks. The individual *l*-GSL peaks showed excellent separation, with *l*-GM3 (d16:1) eluting at ~10.9 min, *l*-GM3 (d17:1) eluting at ~14.1 min, and *l*-GM3 (d18:1) eluting at ~17.2 and ~18.2 min; *l*-GD3 (d16:1) eluting at ~14.3 min, *l*-GD3 (d17:1) eluting at ~18.1 min, and *l*-GD3 (d18:1) eluting at ~22.1 and ~23.4 min; and *l*-GM1 (d18:1) eluting at ~17.0 min and *l*-GM1 (d20:1) at ~28.0 min. For both *l*-GM3 and *l*-GD3, there were two peaks that were assigned as (d18:1), one less intense than the other. Since the GlycanPAC AXR-1 column is able to separate analytes based on polarity, branching, and linkage, possible explanations for the existence of two peaks with identical masses either could be the presence of a differently linked sialic acid in GM3 and GD3 i.e. an α(2-6) linked sialic acid generating two isomers of GM3/GD3 (d18:1) or the presence of two double-bond isomers of GM3/GD3 (d18:1) at different positions on the Sph chain. Further studies are required to test these possibilities. **[Figure 4–6 (a–c)]**

When a mixture of GSLs was subjected to the same reaction conditions and run on the mixed mode column, a much better separation was achieved compared to the RP C8 and C18 columns. All major peaks were assigned successfully by MS, with *l*-GM3 (d16:1) eluting at ~10.9 min, *l*-GM3 (d17:1) eluting at ~13.8 min, and *l*-GM3 (d18:1) eluting at ~17.9 min; *l*-GD3 (d16:1) eluting at ~14.9 min, *l*-GD3 (d17:1) eluting at ~19.0 min, and *l*-GD3 (d18:1) eluting at ~24.3 min; and *l*-GM1 (d18:1) eluting at ~16.8 min and *l*- GM1 (d20:1) at ~27.0 min. With these improved results, the GlycanPAC AXR-1 column was chosen for further experiments **[Figure 4–6 (d)].**
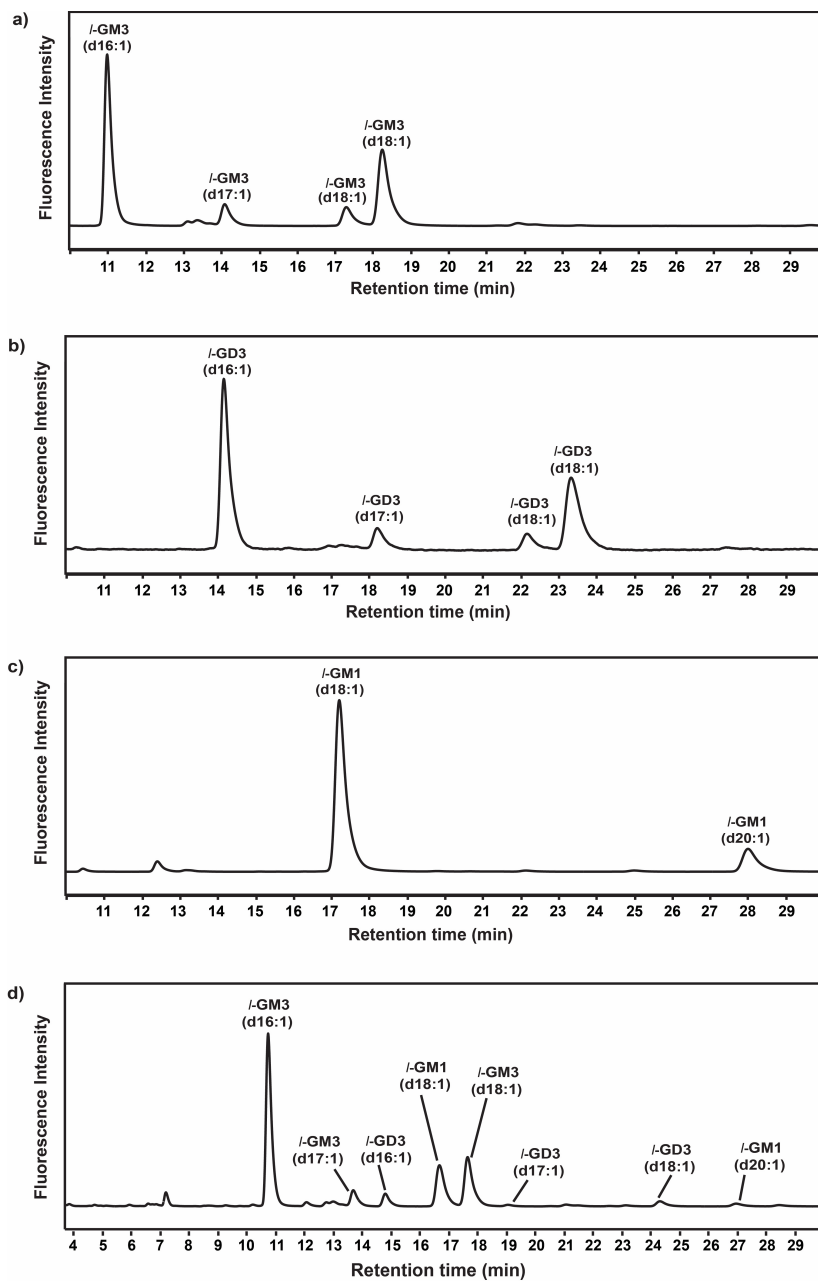
Figure 4– 6. HPLC separation of RapiFluor labeled *l*-GSLs on a mixed mode, weak anion exchange-reverse phase (WAX-RP) GlycanPAC AXR-1 column (a) *l*-GM3, (b) *l*-GD3, (c) *l*-GM1, and (d) a mixture of *l*-GM3, *l*-GD3, and *l*-GM1 on a mixed mode, weak anion exchange-reverse phase (WAX-RP) GlycanPAC AXR-1 column. GM3 and GD3, both sourced from bovine milk, show peaks for *l*-GSLs with d16:1, d17:1, and d18:1 Sph bases, while GM1, sourced from porcine brain, shows d18:1 and d20:1 Sph bases.

4.2.5 Optimizing Conditions for SA_SCD Treatment

Preliminary experiments on the RP C8 and C18 columns were performed after reviewing previous literature reports on SCDase digestion conditions, where incubation at 37 °C for 24 h is typically used.[7, 11-13] After selecting the GlycanPAC AXR-1 column for our assay, we proceeded to scan conditions for SA-SCD to make sure the conditions afforded optimum release of *l*-GSLs. Experiments were conducted by subjecting a mixture of standard GSLs (GM3 and GM1) to SA_SCD digestion at 25, 30, 37, and 45 °C for 24 h, followed by RapiFluor-MS labeling of *lyso*-products and LC-MS analysis. By monitoring the combined fluorescence intensity of each *l*-GSL bearing different Sph chains, it was observed that the optimum enzyme activity was at 37 °C **[Figure 4–7 (b)]**. Incubation times were varied from 2–24 h at 37 °C. The RapiFluor labeled *l*-GSLs were analyzed by LC-MS, and after fluorescence monitoring, it was observed that the response increased from 8 to 14 h, with a gentle decrease until 24 h. Therefore, 14 h was chosen for the incubation time. The conditions for optimum enzyme activity were selected as 37 °C and 14 h of incubation **[Figure 4–7 (c)]**.

146

b)

c)
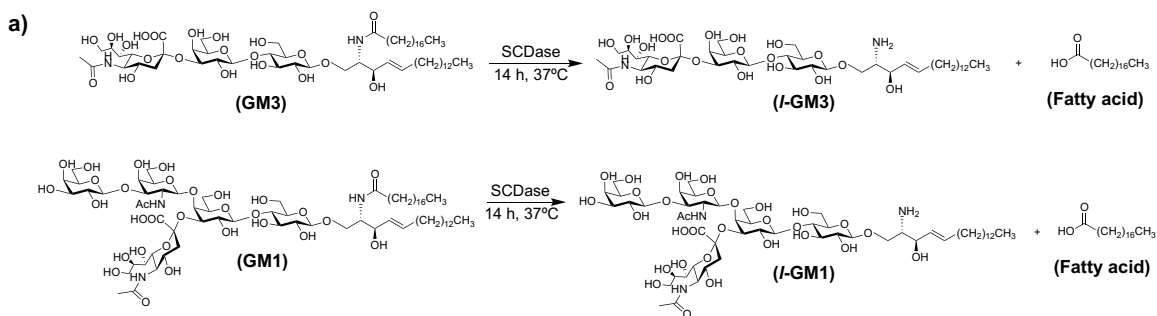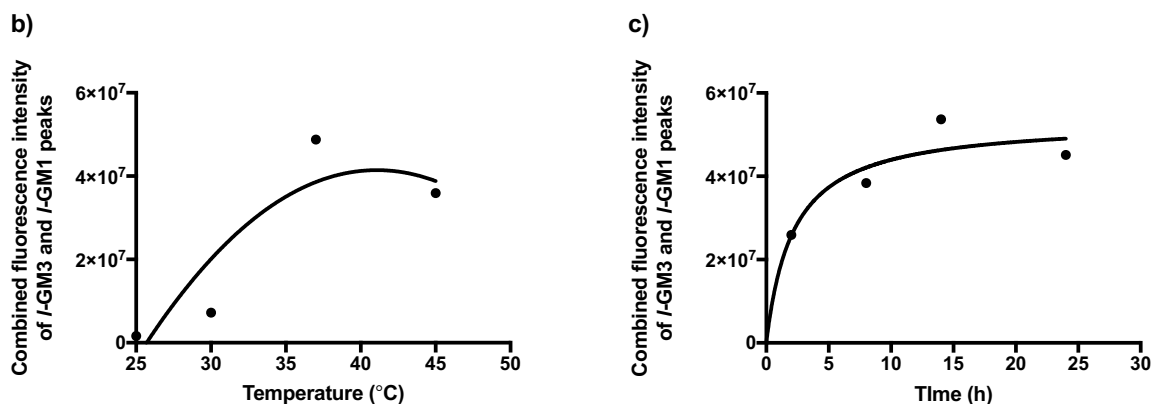
Figure 4– 7. Optimization of temperature and incubation time for SA_SCD digestion of GSLs. (a) Reaction scheme for the action of SCDase on GSLs GM3 and GM1, generating *l*-GM3 and *l*-GM1, respectively. (b) Standard mixtures of GM3 and GM1 were incubated at 25, 30, 37, and 45 °C for 24 h, followed by RapiFluor-labeling. Fluorescence intensities of *l*-GM3 and *l*-GM1 peaks were monitored on LC-MS. (c) Standard mixtures of GM3 and GM1 were incubated with SA_SCD at 37 °C for 2, 8, 14, and 24 h, followed by RapiFluor labeling. Curve fits were based on Michaelis Menten binding saturation curves. Curves are shown to guide the eye and were not used for quantitative interpretation.

4.2.6 Optimizing RapiFluor-MS Labeling Conditions

The labeling protocol followed the one provided by the manufacturer (Waters Corporation Inc.). The solid RapiFluor powder was dissolved in anhydrous dimethyl formamide (DMF), and an aliquot of that was used to label analytes. The labeling mechanism is a simple NHS-ester labeling of amines, requiring neutral-basic pH conditions. Following the protocol, the labeling process was carried out at RT for 5 min, after which the excess labeling reagent was removed using the HILIC elution plate.

To ensure that the volume of labeling reagent recommended in the kit's protocol (12 μL) was sufficient to label analytes of interest, a series of titration experiments were performed. A fixed quantity of standard GM1 (~5 μg) was subjected to digestion with an appropriate amount of SA_SCD at optimized conditions of 37 °C for 14 h and labeled

with increasing volumes (4, 8, 12, 16, and 24 μL) of RapiFluor-MS to be analyzed by LC-MS. The combined fluorescence intensity of *l*-GM1 (d18:1) and *l*-GM1 (d20:1) was plotted against the volume of RapiFluor-MS added to the reaction mixture for each run. There was a gradual increase in response with increasing amounts of labeling reagent added, and maximum response was seen at 24 μL. Thus, we chose 24 μL as the standard labeling reagent required (**Figure 4–8**).
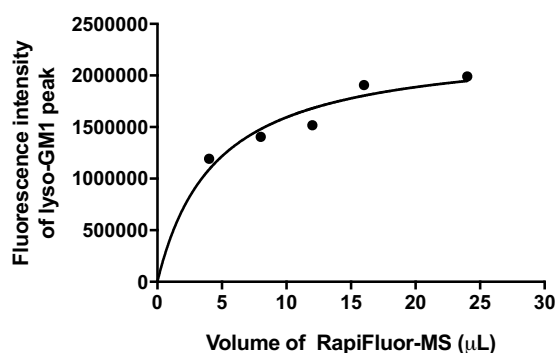
Figure 4– 8. Optimization of RapiFluor-MS labeling conditions. A fixed amount of standard GM1 (~5 μg) was subjected to SA_SCD digestion, followed by labeling with 4, 8, 12, 16, and 24 μL of RapiFluor-MS. The value for Fluorescence Intensity was close to 0 with a negative control experiment; hence saturation curve was fitted starting from 0. Curve fits were based on Michaelis Menten binding saturation curves. Curves are shown to guide the eye and were not used for quantitative interpretation.

4.2.7 Determination of Limit of Detection (LOD) and Limit of Quantitation (LOQ)

The Limit of Detection (LOD) and Limit of Quantitation (LOQ) were determined for SCDase-generated *l*-GSLs similar to our method for EGCase in **Chapter 2**. Essentially, the LOD and LOQ were determined by the method of linear regression, where a linear calibration curve of the instrument response (fluorescence) was plotted against variable

concentrations of the analyte. The values of LOD and LOQ were calculated using the following formulae:

$$LOD = \frac{3Sa}{m} \text{ and } LOQ = \frac{10Sa}{m} \text{ ,}$$

where S_a is the standard deviation of the response and m is the slope of the calibration curve expressed in the form of the equation $y = mx + c$.[27]

Figure 4–9 shows the calibration curve of combined fluorescence intensity vs the amounts of GM1 obtained after GM1 was digested with SA_SCD and *l*-GM1 (d18:1) and *l*-GM1 (d20:1) were labeled with RapiFluor-MS. From a stock solution of GM1 (~1 mg/mL), aliquots were diluted to analyte solutions containing a range of different amounts of GM1. The response generated was linear over the range of concentrations considered for this experiment. The value of S_a was obtained from Excel using the STEYX function, the LOD was found to be 3.04 ng, which is approximately 2 pmol and the LOQ was found to be 9.20 ng, which is approximately 6 pmol.
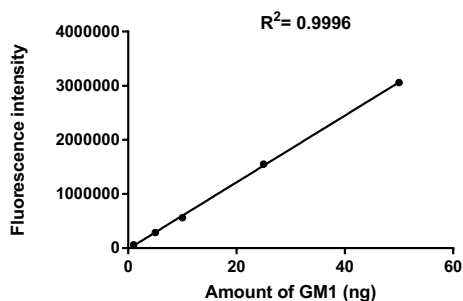
Figure 4–9. Determination of Limit of Detection (LOD) for SCDase. A range of GM1 was subjected to SA_SCD digestion, followed by RapiFluor-MS labeling of *l*-GM1 (d18:1 and d20:1) and monitoring the fluorescence intensities of F-LC-MS peaks. The y-intercept and slope (m) were found to be 17013 units and 61609, respectively. LOD was calculated to be 3.04 ng, or ~ 2 pmol.

The numbers obtained from this experiment were based on the assumption that the molecular weight of GM1 was assumed to be 1546.823 g/mol [GM1 (d18:1-18:0)].

4.2.8 Selection of An Internal/External Standard for Quantification

In the absence of standard *l*-GSLs, the activity of SA_SCD could be determined with the use of an internal or external standard. The main criteria for selecting an internal/external standard was that it would be well separated from all possible *l*-GSLs in a complex mixture, it would share structural similarities with *l*-GSLs, and would be recovered maximally when subjected to the post-labeling cleanup protocols. Since RapiFluor-MS reacts with *l*-GSLs via an amine coupling reaction, our search for internal/external standards started with primary amines, such as ethanolamine, propyl amine, and iso-propyl amine. However, since the post-labeling cleanup involved passing the reaction mixture through a hydrophilic interaction liquid chromatography (HILIC) column on which highly polar analytes are retained very well, hydrophobic or non-polar analytes were not retained. Thus, we changed direction to look for oligosaccharide bearing long chain linker attached to the reducing end of the sugar. These would resemble *l*-GSLs closely in structure and would be retained well on the HILIC column. As a pilot experiment, we tested a representative compound synthesized in our lab, 8-[(2-aminoethyl)thiol)]-1-octyl-β-D-galactopyranosyl-(1→4)-β-D-glucopyranoside or lactose-amine **(Figure 4–10)**, bearing an octyl chain with a primary amine residue at its terminus.[1]
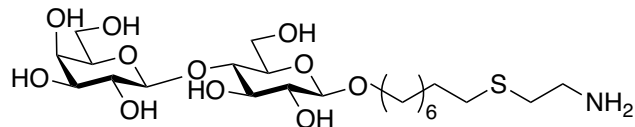
Figure 4– 10. Structure of Compound 1. Compound 1 or 8-[(2-aminoethyl)thiol)]-1-octyl-β-D-galactopyranosyl-(1→4)-β-D-glucopyranoside, bearing a long octyl chain with a primary amine residue at its terminus. The detailed synthetic scheme for this compound has been reported. [1]

Compound **1** was labeled separately with RapiFluor-MS, cleaned up with the HILIC elution plate, and spiked into real samples before they were run on the LC-MS. Thus, Compound **1** served as an external standard. The separation of this standard was tested with a mixture of *l*-GM3, *l*-GM1, and *l*-GD3, shown in **Figure 4–11,** when the labeled form of **1** eluted at 2.5 min.
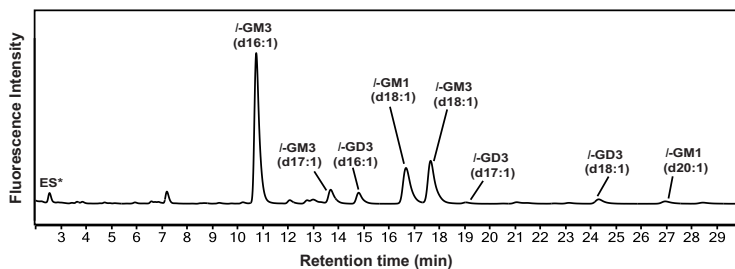
Figure 4– 11. Compound 1 as an external standard. A standard mixture of commercially available GLSs (GM3, GM1, and GD3) was subjected to SA_SCD digestion at 37 °C for 14 h, followed by RapiFluor labeling at RT for 5 min. Then, labeled ES* was spiked in. The ES* peak eluted at ~2.5 min.

4.2.9 Optimizing Activity of SA_SCD

With Compound 1 identified as an appropriate external standard for this assay, the activity of SA_SCD now could be measured by reference. A mixture of standard GM3 and GM1 was digested with an appropriate amount of SA_SCD at optimum conditions of

37 °C over a period of 2, 8, 14, and 24 h. This was followed by RapiFluor-MS labeling of the reaction products and spiking of a known concentration of the external standard lactose-amine before F-LC-MS analysis. At each time point, the absolute concentrations of all forms of *l*-GM3 (d16:1, d17:1, and d18:1) and all forms of *l*-GM1 (d18:1 and d20:1) were calculated from the known concentration of Compound 1 added. A plot was obtained for the absolute concentration (μg/mL) vs time (h) for *l*-GM3 and *l*-GM1, shown in **Figure 4–12**. To calculate the activity of SA_SCD, the concentration at 1 h was extrapolated from this plot and expressed in U/mL, where one Unit was defined as the amount of SA_SCD required to hydrolyze 1 nmol of substrate GM1 or GM3 per minute at 37 °C.
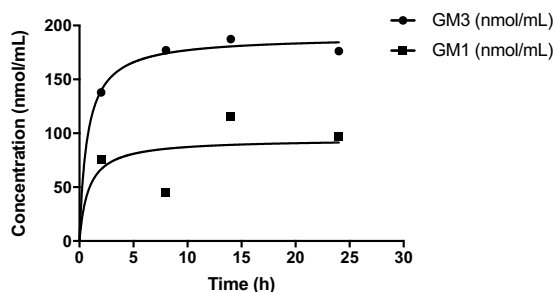
Figure 4– 12. Determination of activity of SA_SCD. A mixture containing approximately equal amounts of standard GSLs (GM3 and GM1) were subjected to SA_SCD digestion at 37 °C for 2, 8, 14, and 24 h, followed by RapiFluor labeling at room temperature for 5 min. Post labeling, a known concentration of labeled external standard Compound 1 was spiked in, and the mixture was analyzed by F-LC-MS. Curve fits were based on Michaelis Menten binding saturation curves. Curves are shown to guide the eye and were not used for quantitative interpretation.

To optimize the SA_SCD concentration, titration experiments were performed. A standard mixture of GM1 and GM3 was digested with increasing amounts (10, 15, 20, 30, and 40 mU) of SA_SCD at 37 °C for 14 h. The released *l*-GSLs were labeled with

RapiFluor-MS and analyzed by LC-MS. **Figure 4-13** shows the plot of the total
fluorescence intensity of all forms of *l*-GSLs from GM3 (d16:1, d17:1, d18:1) and GM1
(d18:1, d20:1) against the amount of enzyme used for each run. The results show a
gradual increase in response from 10–20 mU and a sharp increase at 30 mU, following
which there was a sharp decrease in response. From these results, we picked 25–35 mU
as the range for SA_SCD optimum activity.
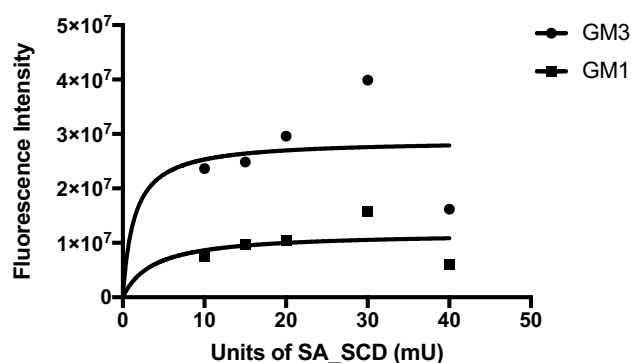
Figure 4– 13. Optimization of SA_SCD activity. The optimization of enzyme cocncentration was
performed using the commercially available standard gangliosides (GM1 and GM3) as substrates in a
mixture. Serial dilutions of SA_SCD were taken, i.e., 10, 15, 20, 30, and 40 mU and a fixed amount of
GM1+GM3 was subjected to digestion at 37 °C for 14 h in the presence of a reaction buffer (25 mM
sodium acetate at pH 6.0, containing 1 mg/mL sodium cholate). Curve fits were based on Michaelis Menten
binding saturation curves. Curves are shown to guide the eye and were not used for quantitative
interpretation.

4.2.10 Recovery of GSLs after Extraction, Purification, and RapiFluor-MS Labeling

As mentioned in **Chapters 1** and **2**, the extraction of GSLs from biological samples is
critical to their accurate profiling and quantitation. Typically, organic solvents together
with water are used for this purpose. We used the most widely accepted and robust

extraction protocol involving the use of chloroform:methanol:water in the ratio 4:8:3. The final GSL extract was subjected to a C18 purification step, where undesirable salts, peptides, proteins, and other impurities are removed to enhance the purity of the extracted GSLs from a complex mixture.[28]

For the purposes of our assay, the entire process of GSL analysis, starting from extraction, purification, SA_SCD digestion, and RapiFluor-MS labeling, involved two critical steps of passing the reaction mixture through purification cartridges (a SepPak C18 cartridge for GSL extract purification and a HILIC elution cartridge for post-labeling cleanup). In order to check the recovery of GSLs from these cartridges, two sets of samples containing standard GSLs, GM3, GM1, and GD3, in a mixture, were subjected to SA_SCD digestion and RapiFluor-MS labeling under optimized conditions outlined in **Sections 4.2.5, 4.2.6, and 4.2.9**. A standard mixture of GM3, GM1 and GD3 was taken in a ratio of 2:2:1. Between the two sets, one was subjected to both SepPak C18 and post-labeling HILIC elution cleanup and the other was set with only an HILIC elution cleanup. The relative percentage of each *l*-GSL was calculated by expressing the fluorescence peak area of each identified *l*-GSLs as a percentage of the total peak area of all *l*-GSLs.

Table 4– 1. Percentage recovery of *l*-GSLs. Relative percentage recoveries of standard GSLs GM3, GM1, and GD3, subjected to SepPak C18+HILIC and Only HILIC elution plate post labeling clean ups.[4]

	(d16:1) GM3	(d17:1) GM3	(d18:1) GM3	(d16:1) GD3	(d17:1) GD3	(d18:1) GD3	(d18:1) GM1	(d20:1) GM1
C18+HILIC	50.8 ± 0.4	6.11 ± 0.03	16.5 ± 0.2	2.27 ± 0.02	4.57 ± 0.03	0.62 ± 0.04	16.8±0.1	2.32 ± 0.04
Only HILIC	47.8 ± 0.4	5.8 ± 0.1	19.4 ± 0.6	2.09 ± 0.06	4.19 ± 0.01	0.67 ± 0.02	17.5±0.1	2.41 ± 0.05

---

[4] Values represent mean ± standard error of mean (SEM) of triplicate measurements (n = 3).

154

From **Figure 4–14** and **Table 4–1**, it can be seen that the ratios of recovery of each of the *l*-GSLs in the mixture are consistent between the two conditions, and they also show good correlation **(Figure 4–14b)**. The C18+HILIC condition gave slightly better recoveries of GM3 and GM1. With these results in hand, we proceeded to the analysis of biological samples. The chromatographic profiles corresponding to each condition are shown in **Appendix B, Figures B–4 and B–5.**
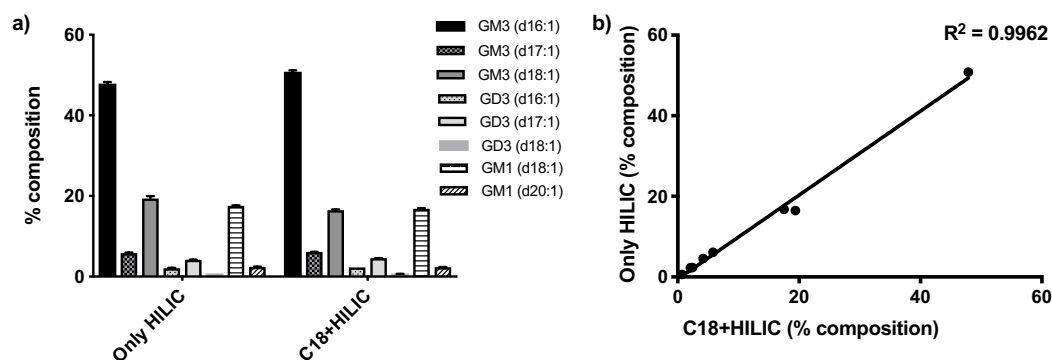
Figure 4– 14. Percent recovery of a standard GSL mixture containing GM3, GM1, and GD3. (a) A mixture of GM3, GM1, and GD3 containing an approximate ratio of 2:2:1 was subjected to SA_SCD digestion at 37 °C for 14 h, followed by RapiFluor labeling. Two sets of samples were analyzed: a SepPak C18 and an HILIC elution plate clean up (C18 + HILIC) and only a HILIC elution plate clean up (Only HILIC). The fluorescent peak areas of *l*-GSLs are represented as a percent of the fluorescence peak area of the ES* added. Values represent mean ± standard error of mean (SEM) of triplicate measurement (n = 3). (b) Plot of average % compositions of *l*-GSLs recovered from C18+HILIC and Only HILIC clean ups showing good correlation, with R^2 = 0.9962.

The overall recovery ratios of *l*-GSLs did not satisfy the (2:2:1) ratio that was used as starting material for these experiments; this can be attributed to the following reasons. As outlined in **Chapter 2**, sources of error affecting these results may include the gravimetric preparation of standard stock solutions and micropipettes used for

dilution. This could lead to unequal recovery of individual *l*-GSL components. Additionally, SA_SCD is known to show preference towards certain GSLs, cleaving charged GSLs more efficiently over neutral and showing a strong preference towards GM3 specifically.[8] This can explain the high percent recovery of *l*-GM3 over *l*-GM1 and *l*-GD3. Since there are no previous reports on the efficiency of SCDase in cleaving GD3 or any other complex gangliosides, we were unable to confirm our findings.

4.2.11 Method Validation using Porcine Brain

The SCDase method provides data complementary to the EGCase assay. The two approaches provide information about the glycan component and the Sph base component of GSLs. We first tested the tissue from brains of juvenile pigs, as was done in **Chapter 2** for the EGCase method. While 10 μL of brain homogenates (corresponding to ~ 2 mg of wet tissue) was an appropriate amount to extract enough GSLs for the EGCase method, the SCDase method required increased amounts of material. This could be attributed to the slightly higher LOD of this method compared to the EGCase method, i.e., 3.05 ng as opposed to 2.15 ng for the EGCase method. Brain homogenate (30 μL, corresponding to ~ 6 mg wet tissue weight) was used for this assay. It generated 1–1.5 mg of dry GSL extract and was subjected to SA_SCD digestion, followed by RapiFluor-MS labeling under optimized conditions. After labeling, an appropriate amount of the external standard **1** was spiked in before the samples were run on the F-LC-MS. Chromatography was carried out on the mixed mode (WAX-SP) GlycanPAC AXR-1 column as above.

A representative profile of RapiFluor-MS labeled *l*-GSLs in juvenile porcine brains is shown in **Figure 4–15**. LacCer could not be identified since SA_SCD shows

very poor reactivity toward neutral GSLs. The *l*-GSL species identified include *l*-GM3 (d16:1) at ~10.0 min and *l*-GM3 (d18:1) at ~17.2 min; *l*-GM1 (d18:2) at ~11.8 min and *l*-GM1 (d18:1) at ~16.8 min; *l*-GD1 (d16:1) at ~14.8 min, *l*-GD1 (d18:1) at ~22.8 and ~23.4 min and *l*-GD1 (d20:1) at ~36.1 min; *l*-GT1 (d18:1) at ~34.5 min; and only *l*-Fuc-GM1 (d18:1) at ~15.2 min. Each *l*-GSL peak was quantified based on the external standard (ES*) Compound 1 **(Table 4–2)**.

Three biological replicates were analyzed to investigate inter-assay variability. Each replicate had identical amounts of starting material subjected to identical extraction, purification, digestion, and labeling conditions. All three *l*-GSL profiles and their corresponding quantifications are shown in detail in **Appendix B (Figure B-6)**. The results of these experiments show a relative standard error (RSE) between each run within 20% for the composition of each *l*-GSL, except for *l*-Fuc-GM1 (d18:1), which was 23.5%.

One of the flaws of this assay in terms of quantitation is the fact that it is based on the automatic integrations performed by the MassHunter software. Notice that the (d18:1) peaks for *l*-Fuc-GM1, GM1, and GM3 are not separated very well. The MassHunter software identifies a common baseline and performs peak integrations based on certain built-in parameters. For comparison, peak heights for all the major chain lengths of the identified *l*-GSLs were also analyzed. Considering peak heights and performing the same quantification using the height of the ES*, the concentrations of all *l*-GSLs were calculated **(Appendix B, Figure B–10)**. **Figure 4–16** shows a correlation plot of *l*-GSL compositions calculated using peak heights vs peak areas. It is clear from the plot that the two analyses show good correlation, providing similar general conclusions. Based on

these data, even though the integrations might be flawed, we favor the peak area analysis for simplicity and because this it is the most widely accepted method of quantitation in such LC-MS assays.
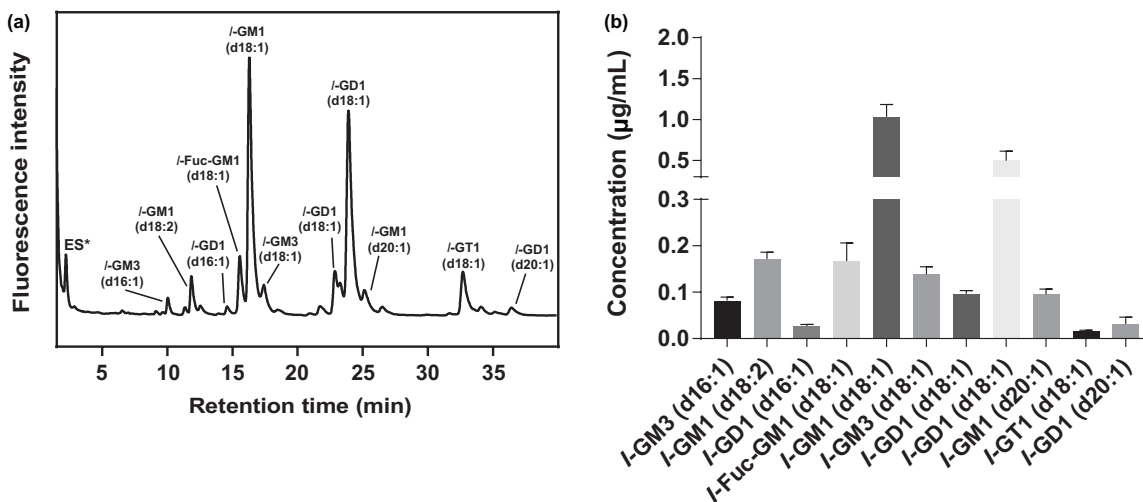
Figure 4– 15. *l*-GSL profiling in porcine brain. (a) HPLC separation of RapiFluor-MS labeled *l*-GSLs generated from SA_SCD digestion of GSLs extracted from porcine brain. The *l*-GSL species identified were *l*-GM3 (d16:1) at ~10.0 min and *l*-GM3 (d18:1) at ~17.2 min; *l*-GM1 (d18:2) at ~11.8 min and *l*-GM1 (d18:1) at ~16.8 min; *l*-GD1 (d16:1) at ~14.8 min, *l*-GD1 (d18:1) at ~22.8 and ~23.4 min, and *l*-GD1 (d20:1) at ~36.1 min; *l*-GT1 (d18:1) at ~34.5 min; and only *l*-Fuc-GM1 (d18:1) at ~15.2 min. Peak assignment was performed based on commercially available standards shown in Figure 4–11 and were confirmed further by HR-ESI-MS (b) The concentration of individual *l*-GSL species in porcine brain. Values represent the mean ± standard error of the mean of triplicate measurements, n = 3.

Table 4– 2. Concentrations of individual *l*-GSLs in porcine brain. Quantification was based on the known concentration of external standard (ES*) Compound 1 added.[5]

Retention time (min)	Lyso-glycosphingolipid (*l*-GSL)	µg/mL
10.0	GM3 (d16:1)	0.082 ± 0.007
11.8	GM1 (d18:2)	0.17 ± 0.02
14.8	GD1 (d16:1)	0.028 ± 0.004
15.2	Fuc-GM1 (d18:1)	0.17 ± 0.04
16.8	GM1 (d18:1)	1.03 ± 0.15
17.2	GM3 (d18:1)	0.14 ± 0.02
22.8	GD1 (d18:1)	0.096 ± 0.007
23.4	GD1 (d18:1)	0.5 ± 0.1
24.8	GM1 (d20:1)	0.09 ± 0.01
34.5	GT1 (d18:1)	0.017 ± 0.001
36.1	GD1 (d20:1)	0.031 ± 0.006

---

[5] Values represent mean ± standard error of mean (SEM) of triplicate measurements (n=3).
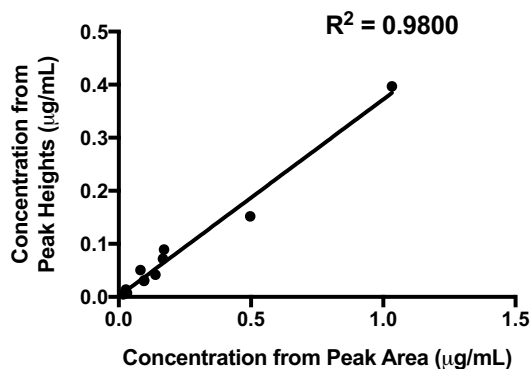
Figure 4– 16. Correlation plot of peak height vs peak area of *l*-GSLs in Porcine brain. Peak heights and peak areas were considered for quantification of *l*-GSLs using ES*. The correlation plot shows good agreement between the two methods of quantification, with $R^2 = 0.9800$.

The peaks for *l*-GM3 and *l*-GM1 were assigned based on the retention times observed when standard mixtures were run, shown in **Figure 4–11**. They also were confirmed by High Resolution Electrospray Ionization Mass Spectrometry (HR-ESI-MS), as was done for the *l*-GD1, *l*-fuc-GM1 and *l*-GT1 peaks. **Figure 4–17** shows an example of how these MS peaks were assigned and identified. Shown in the figure is the fragmentation pattern identified for *l*-Fuc-GM1 (d18:1). The singly charged species of the parent ion is shown in red, with an m/z value of 1738.8430, and its corresponding doubly charged species at 869.4215. The MS spectra show fragments from the parent ion after the loss of a Fuc and Hex at 1389.2314, followed by a loss of HexNAc at 1227.6502 and a sialic acid at 936.9916. Finally, the complete Fuc + Hex + HexNAc fragment is seen at 512.1974, which when added to the fragment at 1227.6502, gives the m/z value for the singly charged species at 1738.8430. This is how each MS peak was identified, checked for fragmentation pattern, and assigned accordingly. A complete list of target and identified masses is provided in **Appendix B (Table B-3)**. Masses were assigned correct to four decimal places for accuracy. Looking at the profile, there are two peaks assigned

160

as *l*-GD1 (d18:1), which is likely the two isomers of GD1 i.e. GD1a and GD1b since the GlycanPAC AXR-1 column is capable of separating based on linkage. Both the isomers were identified in the EGCase assay, as shown in **Chapter 2**. In this method, we cannot assign isomers based on chromatographic separation without a reference.
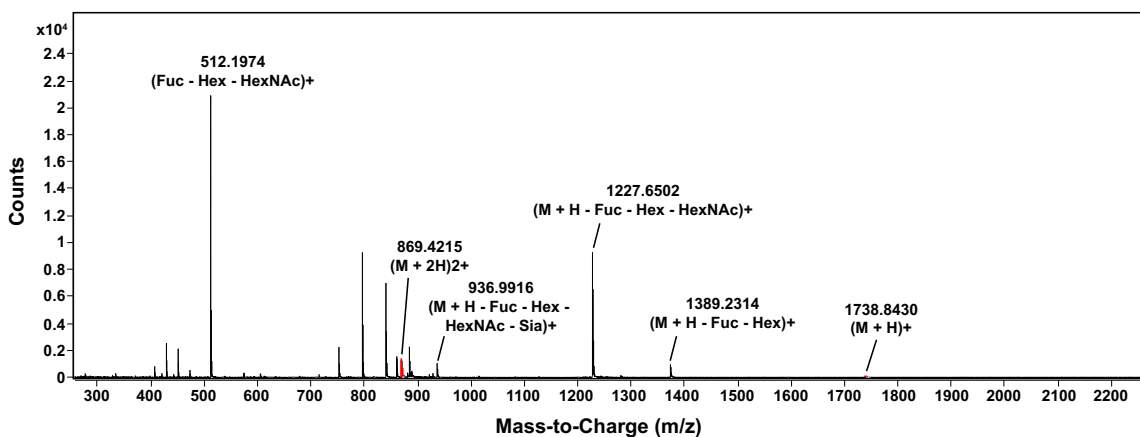
Figure 4– 17. Fragmentation pattern of RapiFluor-MS labeled *l*-Fuc-GM1 (d18:1). It shows the singly charged species of the parent ion with an m/z value of 1738.8430 and its corresponding doubly charged species at 869.4215. Strong fragments of the parent ion were seen after the loss of a fucose (Fuc) and galatcose (Hex) at 1389.2314, followed by a loss of N-acetylglucosamine (HexNAc) at 1227.6502 and a Sialic acid (Sia) at 936.9916. Finally, the complete Fuc + Hex + HexNAc fragment was seen at 512.1974. This is the strongest fragment, which when added to the fragment at 1227.6502, gives the m/z value for the singly charged species at 1738.8430.

Some small peaks were not assigned due to limited instrument sensitivity. For example, in **Figure 4–15**, the unassigned peak at ~21 min possibly could be *l*-Fuc-GD1, considering *l*-Fuc-GM1 eluted right before the *l*-GM1 peak. The MS instrument was not sensitive enough to assign this peak due to very low m/z counts. Alternatives could include multi-stage MS fragmentation,[29] Orbitrap MS instruments,[30] or LC-ESI/MS in a multiple reaction monitoring (MRM) mode.[31] Nevertheless, most of the *l*-forms of each

GSL were separated well, hence easily quantifiable using the ES*. With this method, it is possible now to profile and quantify *l*-GSLs with variable Sph chain lengths in a complex biological mixture.

We next compared the GSLs identified in this method to the ones identified in the EGCase method in **Chapter 2**. From the EGCase method, the GSLs identified were LacCer, GM3, GM2, GM1, Fucosyl-GM1, GD1a, GD1b, Fucosyl-GD1, and GT1b. With the exceptions of LacCer, GM2, and Fucosyl-GD1, all other GSLs were identified in this method as well. LacCer is known to be a poor substrate for SA_SCD.[8] Fucosylated substrates have not been tested with SCDase enzymes. GM2 appeared in very low abundance in the EGCase assay, which may explain why it was not observed here. The sum of all the *l*-forms of individual GSLs identified in this assay was represented as a percentage of total GSL composition and this was compared to the EGCase data from Chapter 2. **(Table 4–3 and Figure 4–18)**. We identified discrepancies between the two data. This was not unexpected because the amount of starting material was different for the two assays, and some of the GSLs identified in the EGCase method were not observed in the SCDase method due to the preferential action of SCDase on particular GSLs over others. But, we note that all the major GSLs identified in the EGCase method were observed in this assay. Thus, we propose to use this method strictly to analyze and quantify the changes in Sph bases of major GSLs in a given biological sample.

162

Table 4– 3. Comparison of percent composition of major GSLs in porcine brain identified independently in the EGCase and SCDase assays. [6]

Glycosphingolipid (GSL)	EGCase (% of total GSL composition)	SCDase (% of total GSL composition)
LacCer	5.2 ± 0.7	n.d.
GM3	1.3 ± 0.1	9.8 ± 1.8
GM2	1.5 ± 0.2	n.d.
GM1	36.3 ± 0.9	55.4 ± 1.7
Fuc-GM1	10.9 ± 0.2	6.9 ± 0.8
GD1 (a/b)	40.5 ± 1.6	27.2 ± 2.4
Fuc-GD1	1.4 ± 0.1	n.d.
GT1	2.9 ± 0.2	0.8 ± 0.1
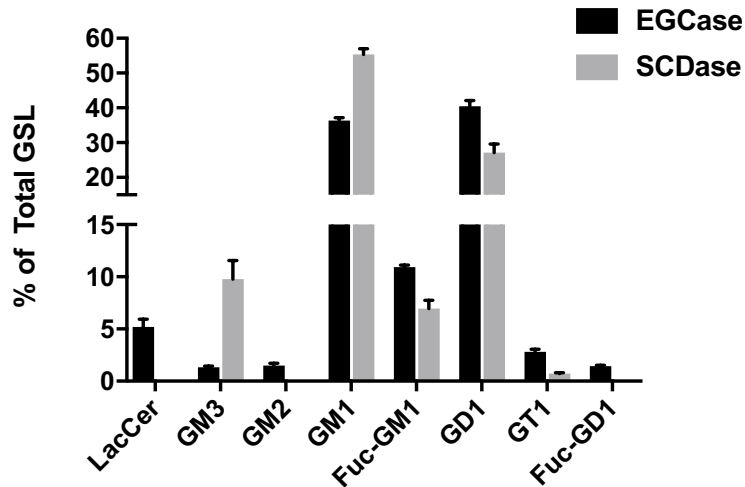
Figure 4– 18. Comparison of percent composition of GSLs identified in porcine brain using EGCase and SCDase methods. Relative percentages of LacCer, GM3, GM3, GM1, Fuc-GM1, GD1, GT1, and Fuc-GD1 identified in porcine brain from glycan analysis (EGCase method) and *l*-GSL analysis (SCDase method). Values represent the mean ± standard error of the mean of triplicate measurements, n = 3.

---

[6] Values represent the mean ± standard error of the mean of triplicate measurements, n = 3; n.d.- Not detected

Using SCDase enzymes on a complex biological sample such as porcine brains, has not been reported previously. The only reports available in the literature are for standard GSLs, and only for a single GSL, not a mixture.[8, 13, 18] There are, however, reports using other methods of GSL analysis, such as simple TLC or more advanced MALDI-IMS, which show a higher prevalence of (d18:1) and (d20:1) Sph chains in pig and mouse brains.[32-33] Drawing a corollary between these studies and our assay, we did see a higher occurrence of (d18:1) Sph in the juvenile brain samples (shown in **Figure 4–15**), with (d20:1) species occurring in small amounts only in GM1 and one of the isomers of GD1, and also a surprising occurrence of (d18:2) species of *l*-GM1 bearing two double bonds on the Sph chain. This *l*-GM1 species with an additional unsaturation in its chain has not been reported in any previous studies on porcine brain. The low abundance of (d20:1) could be attributed to the fact that expression of GSLs is age and tissue specific, and different regions of the brain show a differential expression of Sph chain lengths.[22] It is possible that the active site of SCDase could act preferentially on certain lipid chain lengths over others.

4.2.12 Method Validation Using Jurkat T Cells

To extend our comparison between the EGCase glycan analysis and the SCDase *l*-GSL analysis, we tested Jurkat T cells. While the number of cells required for the EGCase method were $0.2–1 \times 10^6$ cells generating 0.3–0.5 mg of dry extract, these numbers were not sufficient for the SCDase assay. Cell numbers were increased to a range of $1–5 \times 10^7$ to get dried GSL extracts in the 1–1.5 mg range. This was subjected to SA_SCD digestion, followed by RapiFluor-MS labeling under optimized conditions. After

labeling, an appropriate amount of the ES* was spiked in before the samples were run on the LC-MS. Chromatography was carried out on the mixed mode (WAX-SP) GlycanPAC AXR-1 column as above.

A representative profile of RapiFluor-MS labeled *l*-GSLs in Jurkat T cells is shown in **Figure 4–19**. The *l*-GSL species identified include *l*-GM3 (d16:1) at ~10.5 min, *l*-GM3 (d17:1) at ~13.4, *l*-GM3 (d18:1) at ~17.3 min, and *l*-GM3 (d18:2) at ~12.5 min; *l*-GM1 (d16:1) at ~10.0 min, *l*-GM1 (d18:1) at ~16.3 min, and *l*-GM1 (d18:2) at ~11.8 min; *l*-GM2 (d16:1) at ~10.3 min, *l*-GM2 (d18:1) at ~16.8 min, and *l*-GM2 (d18:2) at ~12.2 min; *l*-GD1a (d16:1) at ~14.6 min, and *l*-GD1a (d18:1) at ~23.9 min. Additionally, there were *l*-GSL species for acetylated forms of GM3 (~6.3 min) , GM2 (~6.7 min), and GD1a (~8.3 min) as well, each bearing the d16:1 chain. Concentrations are provided in **Table 4–4.** All three replicate *l*-GSL profiles and their corresponding quantifications are shown in detail in **Appendix B (Figure B-7)**. The results of these experiments show a relative standard error (RSE) between each run within 20% for most of the *l*-GSLs, while the others ranged between 20 and 30%.
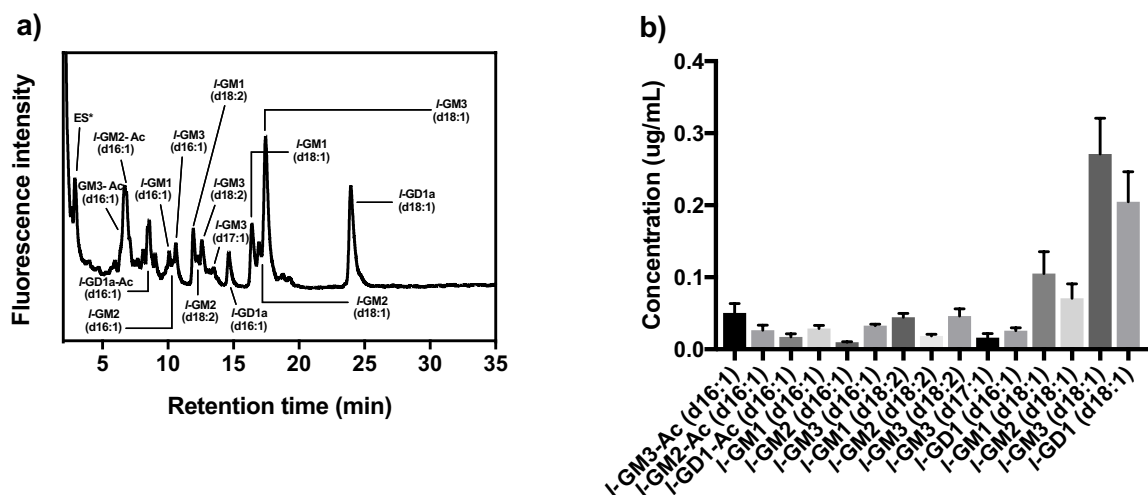
Figure 4– 19. *l*-GSL profiling in Jurkat T cells. (a) HPLC separation of RapiFluor-MS labeled *l*-GSLs generated from SA_SCD digestion of GSLs extracted from Jurkat T cells. The *l*-GSLs identified were (d16:1) species of GM3-Ac, GM2-Ac, GD1a-Ac, GM3, GM1, GM2, and GD1a; (d18:1) species of GM3, GM1, GM2, and GD1a; (d17:1) species of GM3; and (d18:2) species of GM3, GM2, and GM1. (b) The composition of individual *l*-GSL species in Jurkat T cells. Quantification was performed based on the concentration of ES* added to the mixture. Values represent the mean ± standard error of the mean of triplicate measurements, n = 3.

Several peaks, such as, (d16:1), (d18:2), and (d18:1) peaks for *l*-GM1, *l*-GM2, and *l*-GM3 , the (d16:1) peaks for *l*-GM3 and *l*-GM2, and the (d16:1) peaks for acetylated *l*-GM3 and *l*-GM2 are not separated very well. Similar to the pig brain analysis, we compared the peak heights and peak areas. The absolute concentrations from peak heights **(Appendix B, Figure B–11)** and **Figure 4–20** shows that the two analyses again are correlated. Thus, using either methods of quantitation would give us similar results. We propose to use peak areas for simplicity and also because it is common practice for such LC-MS profiling methods.

166

Table 4– 4. Concentrations of individual *l*-GSLs in Jurkat T cells. Quantification was based on the known concentration of external standard (ES*) lactose-amine added. [7]

Retention time (min)	Lyso-glycosphingolipid (*l*-GSL)	µg/mL
6.3	GM3-Ac (d16:1)	0.05 ± 0.01
6.7	GM2-Ac (d16:1)	0.027 ± 0.007
8.3	GD1-Ac (d16:1)	0.017 ± 0.004
10.0	GM1 (d16:1)	0.029 ± 0.004
10.3	GM2 (d16:1)	0.009 ± 0.001
10.5	GM3 (d16:1)	0.033 ± 0.002
11.6	GM1 (d18:2)	0.044 ± 0.005
12.2	GM2 (d18:2)	0.019 ± 0.002
12.5	GM3 (d18:2)	0.05 ± 0.01
13.4	GM3 (d17:1)	0.016 ± 0.005
14.6	GD1 (d16:1)	0.025 ± 0.004
16.3	GM1 (d18:1)	0.11 ± 0.03
16.8	GM2 (d18:1)	0.07 ± 0.02
17.3	GM3 (d18:1)	0.27 ± 0.05
23.9	GD1a (d18:1)	0.21 ± 0.04

[7] Values represent the mean ± standard error of the mean (SEM) of triplicate measurements (n = 3).
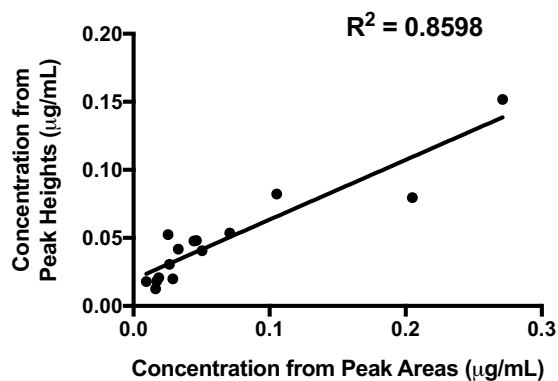
Figure 4– 20. Correlation plot of peak height vs peak area of *l*-GSLs in Jurkat T cells. Peak heights and peak areas were considered for quantification of *l*-GSLs using the ES*. The correlation plot shows reasonable agreement between the two methods of quantification, with $R^2 = 0.8598$.

The peaks for *l*-GM3 and *l*-GM1 were assigned based on the retention times observed when standard mixtures were run, shown in **Figure 4–11**. They also were confirmed by High Resolution Electrospray Ionization Mass Spectrometry (HR-ESI-MS), as was done for the other *l*-GSLs that did not have commercially available standards. **Figure 4–21** shows an example of how these MS peaks were assigned and identified. Shown in the figure is the fragmentation pattern identified for *l*-GM1 (d18:2), with an additional unsaturation in the Sph chain.

Comparing our findings in this assay to the already established EGCase method, with the exception of LacCer and GD3, we were able to identify all other GSLs, i.e., GM3, GM2, GM1, and GD1. LacCer and GD3 both were seen in very low abundance from the EGCase method. This may explain the reason why GD3 could not be identified in a complex mixture where other GSLs were present in much larger quantities, owing to a higher LOD for this assay than EGCase. *l*-GD1 (d18:1) showed only one peak, confirming the presence of the isomer GD1a, as was seen in the EGCase method as well.

168
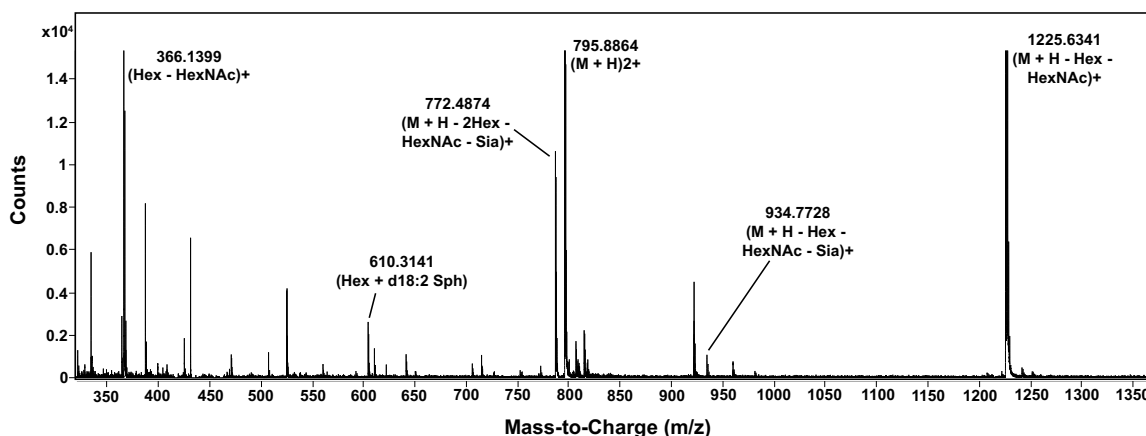
Figure 4– 21. Fragmentation pattern of RapiFluor-MS labeled *l*-GM1 (d18:2). It shows the doubly charged species of the parent ion with an m/z value of 795.8864, its corresponding singly charged species being 1591.7725. Strong fragments of the singly charged parent ion were seen after the loss of a N-acetylglucosamine (HexNAc) and galactose (Hex) at 1225.6341, followed by a loss of Sialic acid (Sia) at 934.7728 and another loss of Hex at 772.4874. Finally, the (d18:2) lipid is seen at an m/z value 610.3141.

The (d17:1) chain length for GM3 was puzzling; as odd number Sph chains are not common in biological samples. We confirmed this peak by comparing the MS fragmentation pattern of *l*-GM3 (d17:1) in Jurkat cells to that observed in a commercially available standard GM3, as shown in **Figure 4–22**.

Similar to the *l*-GSL analysis in porcine brain, for Jurkat T cells, comparisons of percent composition of individual GSLs were made between the EGCase method and the SCDase method. **Table 4–5** and **Figure 4–23** illustrate complete glycan and *l*-GSL analysis by the two methods. From these data, it is clear that even though there are variations in the calculated percentages and some minor unidentified GSLs, the SCDase assay is able to analyze and quantify all major GSL components in cells as well. Hence, this assay can be used complementarily with the EGCase assay to identify differences in Sph chain lengths of major GSLs.
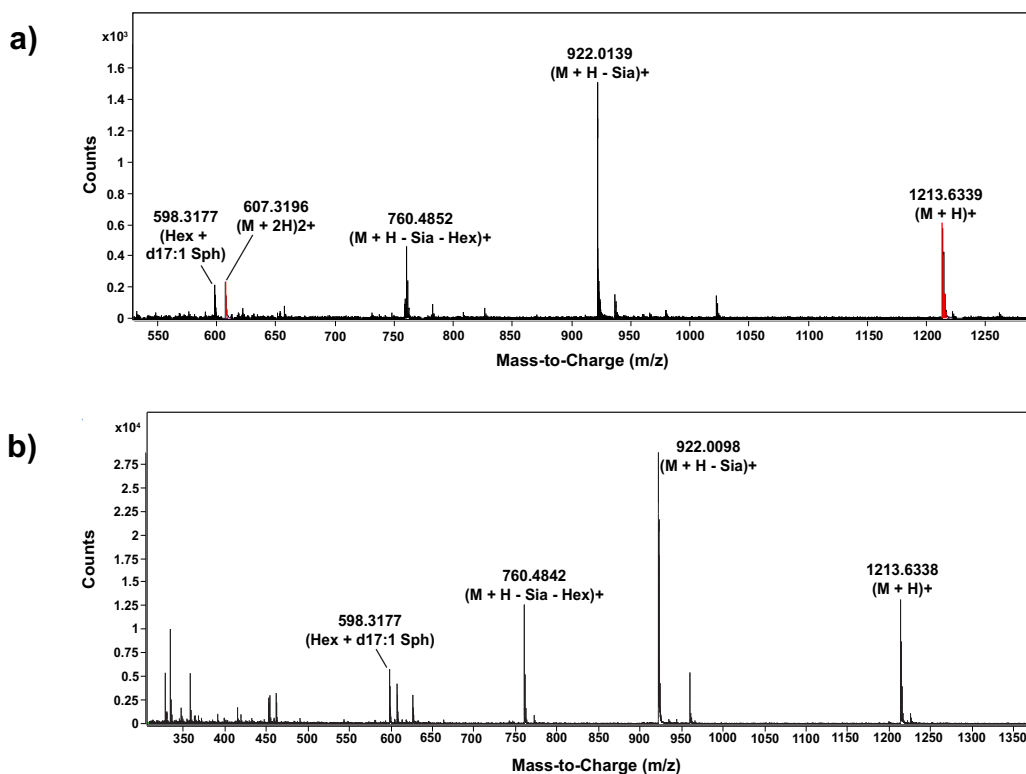
Figure 4– 22. Fragmentation pattern of RapiFluor-MS labeled GM3 (d17:1). (a) Fragmentation of GM3 (d17:1) in Jurkat T cells shows the singly charged parent ion at m/z value of 1213.6339 and its corresponding doubly charged species at an m/z value 607.3196. Strong fragments of the parent ion are seen at 922.0139 due to the loss of a Sialic acid (Sia), followed by a loss of galactose (Hex) at 760.4852. Finally, the (d17:1) Sph chain is seen at 598.3177. This fragmentation pattern was compared to (d17:1) from standard GM3 shown in (b), indicating the same fragmentation pattern. This confirmed that the peak at ~13.4 min was indeed from a (d17:1) Sph chain of *l*-GM3.

Table 4– 5. Comparison of percent composition of major GSLs in Jurkat T cells identified independently in the EGCase and SCDase assays[8]

Glycosphingolipid (GSL)	EGCase (% of total GSL composition)	SCDase (% of total GSL composition)
LacCer	1.8 ± 0.5	n.d.
GM3	49.7 ± 1.4	43.4 ± 1.9
GM2	19.4 ± 0.4	12.9 ± 0.2
GM1	12.9 ± 2.1	18.2 ± 0.9
GD3	1.2 ± 0.1	n.d.
GD1a	16.6 ± 2.1	23.5 ± 1.1
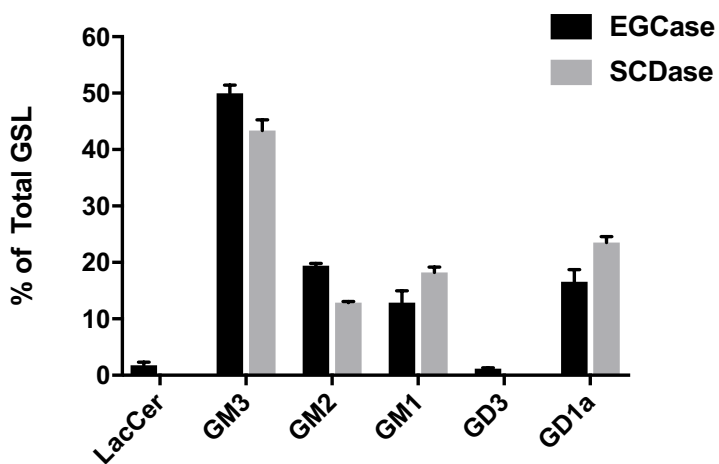
Figure 4– 23. Comparison of percent composition of GSLs identified in Jurkat T cells using EGCase and SCDase methods. Relative percentages of LacCer, GM3, GM2, GM1, GD3, and GD1a identified in Jurkat T cells from glycan analysis (EGCase method) and *l*-GSL analysis (SCDase method). Values represent the mean ± standard error of the mean of triplicate measurements, n = 3.

---

[8] Values represent the mean ± standard error of the mean of triplicate measurements, n = 3; n.d.- Not detected

4.2.13 Lyso-GSL Profiling in Human Serum from Huntington's Disease Patients

Chapter 2 discussed the utility of the EGCase method in profiling and quantification of 2-AA labeled glycans derived from GSLs in normal human serum and serum from patients suffering from Huntington's disease. No information was obtained about the lipid chain in the glycan analysis. With the SCDase assay, we can analyze and identify changes in the Sph base chains of GSLs. For the EGCase method, 50 µL of serum was used, for the SCDase assay we used 150 µL. GSLs were extracted from serum, and the dry extract was subjected to SA_SCD digestion, followed by RapiFluor-MS labeling under optimized conditions. RapiFluor labeled *l*-GSLs were run on the LC-MS after spiking in a known concentration of external standard (ES*). **Figure 4–24** shows a representative chromatogram of the major *l*-GSL forms identified. They were *l*-GM3 (d16:1), *l*-GM2 (d16:1), *l*-GM1 (d16:1), *l*-GD1b (d16:1), and *l*-diF(2,4)-Lc4 (d16:1) at ~10.3 min, ~10.1 min, ~9.1 min, ~14.3 min, and ~6.5 min, respectively; *l*-GM3 (d17:1) at ~13.4 min; *l*-GM3 (d18:1) and *l*-GD3 (d18:1) at ~16.7 min and ~22.9 min, respectively; and *l*-GM1 (d18:2) at ~11.9 min. According to previous reports in the literature, the major Sph chains identified in serum are (d18:1) along with (d16:1). This is in close correlation to what we were able to identify from our assay, (d16:1) being the dominant *l*-form.[34-35] The concentrations of *l*-GSLs in serum were calculated based on the known concentration of external standard added **(Table 4–6)**.
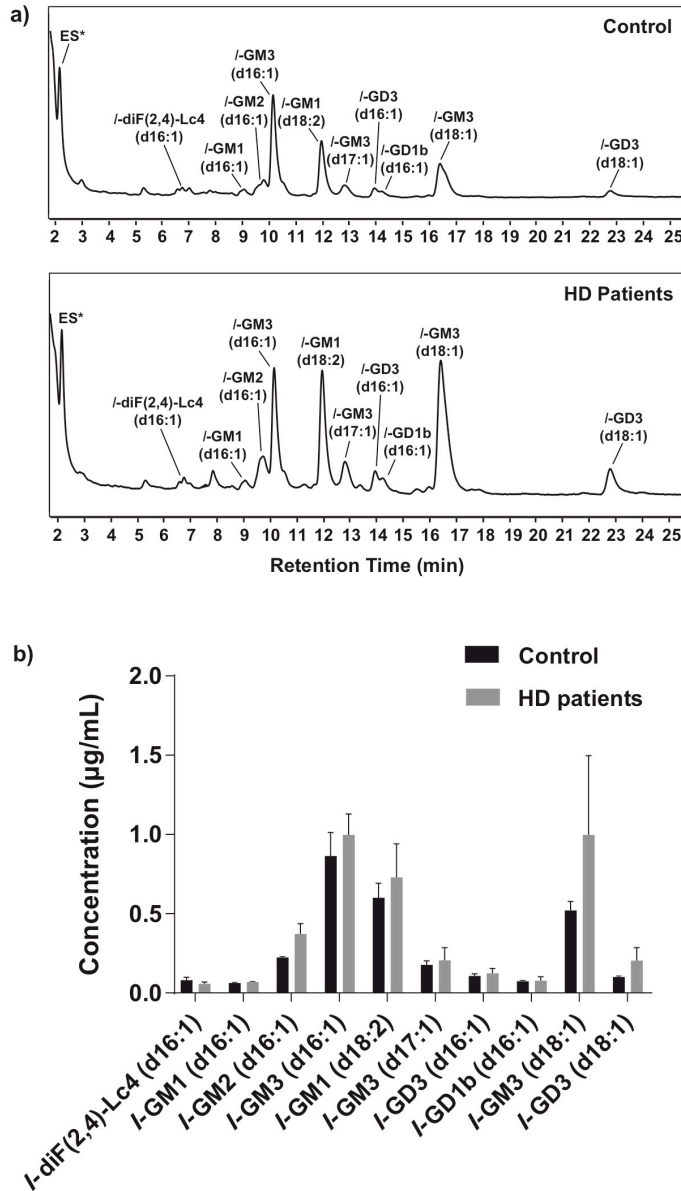
Figure 4– 24. *l*-**GSL profiling in normal human serum and serum from Huntington's disease patients.**

(a) HPLC separation of RapiFluor-MS labeled *l*-GSLs generated from SA_SCD digestion of GSLs extracted from normal human serum and serum from Huntington's disease (HD) patients. The *l* GSLs identified were the (d16:1) forms of diF(2,4)-Lc4, GM3, GM2, GM1, GD1b, and GD3; the (d18:1) forms of GM3 and GD3; the (d17:1) form of GM3, and the (d18:2) form of GM1. (b) The concentration of individual *l*-GSLs in control and HD patient serum. Quantification was performed based on the concentration of ES* added. Values represent the mean ± standard error of the mean of triplicate measurements for each group, n = 3.

Table 4– 6. Concentrations of individual *l*-GSLs in serum from normal individuals and Huntington's disease patients. Quantification was based on the known concentration of external standard (ES*) Compound 1 added.[9]

Retention time (min)	*l*-GSL	Control (µg/mL)	Huntington's (HD) (µg/mL)
6.5	diF(2,4)-Lc4 (d16:1)	0.08 ± 0.02	0.06 ± 0.01
9.1	GM1 (d16:1)	0.063 ± 0.005	0.068 ± 0.004
10.1	GM2 (d16:1)	0.224 ± 0.007	0.37 ± 0.06
10.3	GM3 (d16:1)	0.86 ± 0.15	1.0 ± 0.1
11.9	GM1 (d18:2)	0.6 ± 0.1	0.7 ± 0.2
13.4	GM3 (d17:1)	0.18 ± 0.02	0.2 ± 0.1
14.1	GD3 (d16:1)	0.11 ± 0.01	0.12 ± 0.03
14.4	GD1b (d16:1)	0.075 ± 0.005	0.08 ± 0.02
16.7	GM3 (d18:1)	0.52 ± 0.06	1.0 ± 0.5
22.9	GD3 (d18:1)	0.10 ± 0.01	0.2 ± 0.1

Comparing these results with the EGCase results, LacCer, GA1, GA2, and Gb3 were not identified in this assay. All these GSLs are neutral, smaller in size than complex GSLs, which is likely the reason why the SC_SCD enzyme does not act on them, owing to its selectivity.[7-8] In comparing the percent compositions of GSLs between the two methods, it was found that all major GSLs identified in the EGCase assay were also observed in the SCDase assay (**Appendix B, Figure B–13**). All peaks were assigned based on the retention times of commercially available standards and also High Resolution Electrospray Ionization Mass Spectrometry (HR-ESI-MS). The fragmentation patterns of all *l*-GSLs were followed carefully, and it was possible to identify most of the expected fragments. Shown in **Figure 4–25** is the fragmentation pattern of GD1b (d16:1).

---

[9] Values represent the mean ± standard error of the mean (SEM) of triplicate measurements (n=3).
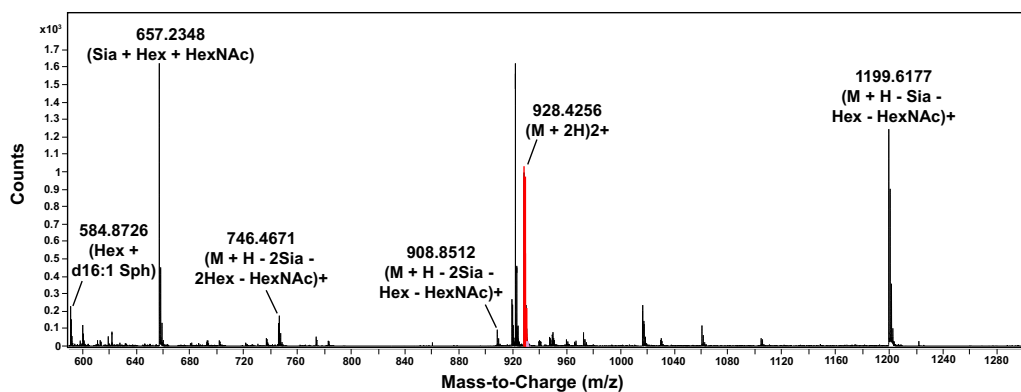
Figure 4– 25. Fragmentation pattern of RapiFluor-MS labeled *l*-GD1b (d16:1). It shows the doubly

charged species of the parent ion with an m/z value of 928.4256. The corresponding singly charged species

would be at 1856.8512. Strong fragments of the singly charged parent ion were seen after the loss of a

Sialic acid (Sia), N-acetylglucosamine (HexNAc), and a galactose (Hex) at 1199.6177. This was followed

by another loss of a Sialic acid (Sia) at 908.8512 and another loss of Hex at 746.4671. Finally, the (d16:1)

Sph chain fragment was seen at m/z value 584.8726. The complete fragment of one Sia, one Hex, and one

HexNAc is seen at 657.2348, which when added to 1199.6177, gives the singly charged parent ion at an

m/z value of 1856.8525.

We were interested to see whether there is a change in the Sph chain length for

any of the major GSLs between normal and Huntington's disease patients. In quantifying

each *l*-GSL peak by normalizing their fluorescence peak area to that of the ES* (absolute

numbers shown in **Table 4–6**), no significant changes were seen in any of the analytes

between the control and HD serum when compared by a student's t-test. We observed a

subtle increase in GM2 (d16:1), GM3 (d16:1), and GM1 (d18:2). There was, however, a

massive increase in GM3 (d18:1) for one of the three patients, which is why even though

the change seems large, the error bars suggest that this is not significant. Similar results

were obtained when the peak height of each *l*-GSL was compared between normal

individuals and HD patients (**Appendix B, Figure B–12**). We wanted to make sure that

this was consistent with the data we had from the EGCase method of glycan analysis, and indeed, the same patient showed higher amounts of total GM3 and GD3 compared to the remaining two. From these experiments, we concluded that there is a consistent increase in the Sph chains of all *l*-GSLs, as shown in **Figure 4–24** and **Figure 4–26**; however, more replicates are needed to identify significant changes.
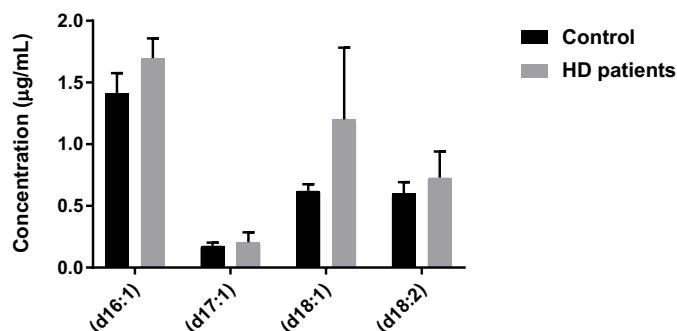
Figure 4– 26. Concentration of (d16:1), (d17:1), (d18:1), and (d18:2) forms of *l*-GSLs in human serum. (d16:1), (d17:1), (d18:1), and (d18:2) forms of *l*-GM3, *l*-GM1, *l*-GM2, *l*-GD3, *l*-GD1, and *l*-diF(2,4)-Lc4 in serum from normal individuals and Huntington's disease patients.

4.3 CONCLUSIONS

This chapter describes the development of a novel GSL profiling and quantitation method that provides information about both the glycan component and the Sph chains of the ceramide component. We use the enzyme, sphingolipid ceramide N-deacylase (SA_SCD), used to cleave the fatty acid part of ceramide moieties. *l*-GSLs generated as a result of the action of this enzyme on complex biological mixtures were analyzed after labeling with RapiFluor-MS. The choice of fluorophore was important since RapiFluor-MS is extremely sensitive to MS analyses, which was our primary method of identification of analytes. With the help of an external standard, this now can function as

a quantitative assay for the analysis of *l*-GSLs, potentially quantifying changes in Sph chain lengths. The assay uses fluorescence to provide quantitaion. We used this method to study changes in the Sph chain lengths of GSLs identified in Huntington's disease patients (Chapter 2) and found a consistent, subtle increase in individual Sph chain lengths across all *l*-GSLs. These changes were not significant, possibly because of a high degree of variability between patients. Analysis of additional replicates will be needed to establish significant changes.

As mentioned in **Chapter 1**, *l*-GSLs are seldom a subject of interest for researchers, despite their proven involvement in several diseases and other physiological conditions.[28,32,35] A few studies focusing on the Sph chains have highlighted their role in aging and have rendered Sph chain lengths to be biomarkers of aging.[22,33] These studies were based on MALDI imaging, which are very sentitive for detection; however, are challenging to quantify. Other MS based techniques have rarely studied Sph chains.[31] Thus, the SCDase assay described in this chapter offers an alternative, more quantitative approach to analyze and accurately quantify Sph chain lengths of different *l*-GSLs. Although preliminary, the data presented in this chapter highlights the potential of this method to become a much more robust strategy compared to other MS based techniques in the field.

4.4 MATERIALS AND METHODS

4.4.1 Materials

All reagents were purchased from Sigma-Aldrich (Oakville, Ontario, Canada), except for the following: GSL standards LacCer, GM3, GM1, and GD3 were purchased from Avanti

Polar Lipids Inc. (Alabaster, Alabama, USA); SA_SCD genes from GenScript (Piscataway, NJ, USA); Reverse Phase C8, 2.1 x 50 mm, 2.6 um, 100 A from Phenomenex (Torrance, CA, USA); GlycanPAC AXR-1, 1.9 um, 2.1 x 150 mm from Thermo Fisher (Mississauga, Ontario, Canada); Amicon Ultra-centrifugation filters from Thermo Fisher Scientific (Mississauga, Ontario, Canada); SepPak C18 cartridge from Waters Corporation (Milford, MA, USA); RapiFluor-MS labeling kit was a generous gift from Waters Corporaation (Milford, MA, USA); porcine brains were obtained from the Swine Research and Technology Centre at the University of Alberta; and human serum samples (normal and Huntington's disease) were a generous donation from Dr. Simonetta Sipione of the Department of Pharmacology at the University of Alberta

4.4.2 Jurkat T Cell Culture

Jurkat T-cells (clone E.61) were purchased form ATCC (Mannassas, VA). They were cultured in RPMI 1640 media containing fetal bovine serum (FBS) (10%, v/v) and penicillin (10 units mL^{-1}) in a humidified incubator with 5% CO_2 at 37 °C. All experiments were performed with cell numbers between passage 7 and passage 9.

4.4.3 Preparation of Porcine Brain Homogenates

Brains from juvenile pigs were obtained from the Swine Research and Technology Centre at the University of Alberta. A certain weight of brain tissue was cut out of a full porcine brain and was homogenized in a solvent containing 4 mL methanol, 2 mL chloroform, and 1.5 mL water, in a ratio of 1:5 (w/v) using a mechanical homogenizer. Aliquots of brain homogenates were stored in -80 °C.

178

4.4.4 Sphingolipid Ceramide N-deacylase (SA_SCD) Expression and Purification

Expression and purification of SA_SCD was performed based on the reports of Han et al[8], where a gene encoding recombinant SA_SCD was identified and synthesized by Genscript, with a pET23b vector. For protein expression, *E. coli* carrying the pET23b vector was cultured overnight, followed by 1:100 dilution into 1 L of LB medium containing 100 mg/mL Ampicillin and 35 mg/mL chloramphenicol. This was grown to ~ 0.8 OD_{600} at 37 °C, followed by IPTG induction at a final concentration of 0.1 mM by shaking at 16 °C for 18–20 h. Cells were then centrifuged, followed by re-suspension in 40 ml of 300 mM NaCl buffer (pH 7.5) containing 0.1% Triton X-100, 10 mM imidazole, and 50 mM Tris-Cl. Finally, cells were lysed by using a cell disruptor. Prior to purification of SA_SCD, centrifugation was performed to remove any cell debris. For protein purification, a Ni-NTA superflow column (2 mL) was prepared. Elution was performed in 50 fractions (1 mL each) using an elution buffer (300 mM NaCl, 250 mM imidazole, 50 mM Trist-Cl, pH 7.5) All the fractions were pooled together and concentrated using molecular weight cut-off ultracentrifugation filters from Amicon (50 kDa MWCO). The purified and concentrated protein was stored in 4 °C.

4.4.5 Testing SA_SCD Activity

The activity of SA_SCD was tested on a TLC plate using the ganglioside substrate GM3. The GM3 substrate and the reaction mixture of GM3 + SA_SCD were spotted on a TLC plate that was developed using a solvent system containing acetic acid:n-butanol:0.25% $CaCl_2$ (1:2:1, v/v/v) and stained with Orcinol stain to visualize *l*-GSL spots. Activity was

measured quantitatively from a fluorescence intensity vs time plot of a mixture of RapiFluor-MS labeled *l*-GM3 and *l*-GM1, generated as a result of SA_SCD digestion at 37 °C for 14 h. One unit of SA_SCD is defined as the amount of enzyme that hydrolyzes 1 μmol of GM3 or GM1 per minute at 37 °C.

4.4.6 Extraction and Purification of Gangliosides from Jurkat T-Cells, Porcine Brain Homogenates and Human Serum

Ganglioside extraction and purification was performed based on the reports of Schnaar and co-workers.[28] Essentially, 30 μL brain homogenates or 150 μL of blood plasma or cell lysates containing ~1 x 10^7 cells were diluted with ice cold water (4 mL/g based on wet weight of sample). After homogenizing this mixture vigorously, methanol was added to make the final ratio of methanol/water to 8:3. Chloroform was added after vigorous mixing of this suspension to make the chloroform/methanol/water mixture in a ratio of 4:8:3 (v/v/v). This mixture was vortexed and subjected to centrifugation at 1500 RPM for 15 min on a tabletop centrifuge. The supernatant was recovered carefully, the volume measured and diluted with 0.173 volumes of water. After mixing, the suspension was subjected to centrifugation again at 1500 RPM for 15 min. The upper phase, containing ~80% of the total volume, was recovered and transferred to a fresh tube. This was purified on a Waters SepPak C18 cartridge, evaporated to dryness under a stream of nitrogen, and re-dissolved in methanol at a volume of 100 μL/mg of dried extract.

4.4.7 SA_SCD Digestion

The final methanol extract was dried under a stream of nitrogen, followed by res-suspension of the residue in a 25 mM sodium acetate buffer (pH 5.0) containing 1 mg mL^{-1} sodium cholate and 100 mM CaCl$_2$. For commercially available standards, a mixture of 10 μL each of standard LacCer, GM3, GM1, and GD3 were taken from the original stock solutions of ~1 mg/mL concentration. Next, the gangliosides were incubated for 14 h at 37 °C with 30 mU SA_SCD to release the corresponding *l*-GSLs.

4.4.8 Fluorescent Labeling of *l*-gangliosides

The SA_SCD released *l*-gangliosides were labeled with 24 μL of fluorescent mixture (1 mg RapiFluor-MS in 14.5 ml DMF) at room temperature for 5 min. After dilution of samples with 100% acetonitrile to a final volume of 400 μL, the labeled *l*-gangliosides were purified using GlycoWorks HILIC μ-elution plate from Waters. Essentially, the columns were pre-washed with 200 μL of water, followed by 200 μL of 85% acetonitrile, and then the samples were loaded on to the columns. Next, the columns were washed with two 600 μL volumes of formic acid/water/acetonitrile in a ratio of 1:9:90 (v/v/v). Finally, the *l*-gangliosides were eluted with three 30 μL volumes of elution buffer containing 200 mM ammonium acetate in 5% acetonitrile.

4.4.9 LC-MS Analysis of RapiFluor Labeled *l*-GSLs on a Phenomenex Kinetex C8 RP Analytical Column

RapiFluor labeled *l*-ganglisoides were analyzed by LC-MS using an Agilent 1200 SL HPLC system and a reverse phase column (Phenomenex, Kinetex C8, 2.1 x 50 mm, 2.6

um, 100 A). Samples in 5% acetonitrile buffer were loaded onto the column in 10 μL injections. The fluorescence detector was set to monitor the excitation at 265 nm and the emission at 465 nm. All chromatography was performed at 50 °C. The binary solvent system followed a linear gradient, with a flow rate of 0.4 mL min^{-1} (Solvent A: 0.1 % formic acid in dd Water; Solvent B: 0.1 % formic acid in methanol). The flow was split ~50:50 between the fluorescence and mass spectrometry (MS) detectors. MS was used to assign and confirm the identity of fluorescent peaks. Mass spectra were acquired in the positive mode using an Agilent 6220 Accurate-Mass TOF HPLC/MS system with a dual spray electrospray ionization source, along with a secondary reference sprayer for a reference mass solution. Data analysis was performed using the Agilent MassHunter Qualitative Analysis software package version B.07.01.

4.4.10 LC-MS Analysis of RapiFluor-labeled *l*-gangliosides on a Mixed Mode Weak Anion Exchange (WAX)-Reverse Phase (RP) GlycanPAC AXR-1 Analytical Column

RapiFluor labeled *l*-ganglisoides were analysed by LC-MS using an Agilent 1200 SL HPLC system and a reverse phase column (Dionex/Thermo Fisher, GlycanPAC AXR-1, 1.9 um, 2.1 x 150 mm). Samples in 5% acetonitrile buffer were loaded onto the column in 15 μL injections. The fluorescence detector was set to monitor the excitation at 265 nm and the emission at 465 nm. All chromatography was performed at 50 °C. The binary solvent system followed a linear gradient with a flow rate of 0.4 mL min^{-1} (Solvent A: dd Water; Solvent B: 50 mM ammonium formate, pH 4.45 in 40:60 water/acetonitrile). The flow was split ~ 50:50 between the fluorescence and mass spectrometry (MS) detectors.

MS was used to assign and confirm the identity of fluorescent peaks. Mass spectra were acquired in the positive mode using an Agilent 6220 Accurate-Mass TOF HPLC/MS system with a dual spray electrospray ionization source, along with a secondary reference sprayer for a reference mass solution. Data analysis was performed using the Agilent MassHunter Qualitative Analysis software package version B.07.01.

4.4.11 Data Analysis using Agilent MassHunter Qualitative Analysis Software Package Version B.07.01

Mass Spectrometry data were analyzed using the Agilent MassHunter Qualitative Analysis software. An extensive database was created for all possible RapiFluor-MS labeled *l*-GSLs with their molecular formula and neutral masses. This database was fed into the software, based on which peaks were identified according to singly and doubly charged species of *l*-GSLs. Masses were reported correct to four decimal places for accuracy. Some peaks could not be assigned to a particular mass by the software. For those, major mass peaks were identified by manually walking across the total ion chromatogram (TIC). The extracted ion chromatograms (EIC) for these major mass peaks were checked to make sure the assignment was correct.

4.5 REFERENCES

1.   Daskhan, G. C.; Tran, H. T.; Meloncelli, P. J.; Lowary, T. L.; West, L. J.; Cairo, C. W., Construction of Multivalent Homo- and Heterofunctional ABO Blood Group Glycoconjugates Using a Trifunctional Linker Strategy. *Bioconjug Chem* **2018,** *29* (2), 343-362.

2.   Taketomi, T.; Hara, A.; Uemura, K.; Sugiyama, E., Rapid method of preparation of lysoglycosphingolipids and their confirmation by delayed extraction matrix-assisted laser desorption ionization time-of-flight mass spectrometry. *J Biochem* **1996,** *120* (3), 573-9.

3.   Ito, M.; Kurita, T.; Kita, K., A novel enzyme that cleaves the N-acyl linkage of ceramides in various glycosphingolipids as well as sphingomyelin to produce their lyso forms. *J Biol Chem* **1995,** *270* (41), 24370-4.

4.   Mitsutake, S.; Kita, K.; Okino, N.; Ito, M., [14C]ceramide synthesis by sphingolipid ceramide N-deacylase: new assay for ceramidase activity detection. *Anal Biochem* **1997,** *247* (1), 52-7.

5.   Hirabayashi, Y.; Kimura, M.; Matsumoto, M.; Yamamoto, K.; Kadowaki, S.; Tochikura, T., A novel glycosphingolipid hydrolyzing enzyme, glycosphingolipid ceramide deacylase, which cleaves the linkage between the fatty acid and sphingosine base in glycosphingolipids. *J Biochem* **1988,** *103* (1), 1-4.

6.   Ashida, H.; Hayashi, S.; Sakamoto, Y.; Tsuji, Y.; Yamamoto, K.; Kumagai, H.; Tochikura, T., Formation of lyso-glycosphingolipids by Streptomyces sp. *Biosci Biotechnol Biochem* **1995,** *59* (11), 2028-32.

7.   Furusato, M.; Sueyoshi, N.; Mitsutake, S.; Sakaguchi, K.; Kita, K.; Okino, N.; Ichinose, S.; Omori, A.; Ito, M., Molecular cloning and characterization of sphingolipid ceramide N-deacylase from a marine bacterium, Shewanella alga G8. *J Biol Chem* **2002,** *277* (19), 17300-7.

8.   Han, Y. B.; Wu, L.; Rich, J. R.; Huang, F. T.; Withers, S. G.; Feng, Y.; Yang, G. Y., Comprehensive characterization of sphingolipid ceramide N-deacylase for the

synthesis and fatty acid remodeling of glycosphingolipids. *Appl Microbiol Biotechnol* **2015,** *99* (16), 6715-26.

9.   Beermann, C.; Rohrig, A. K.; Boehm, G., Chemical and enzymatic transacylation of amide-linked FA of buttermilk gangliosides. *Lipids* **2003,** *38* (8), 855-64.

10.   Kurita, T.; Izu, H.; Sano, M.; Ito, M.; Kato, I., Enhancement of hydrolytic activity of sphingolipid ceramide N-deacylase in the aqueous-organic biphasic system. *J Lipid Res* **2000,** *41* (5), 846-51.

11.   Huang, F. T.; Han, Y. B.; Feng, Y.; Yang, G. Y., A facile method for controlling the reaction equilibrium of sphingolipid ceramide N-deacylase for lyso-glycosphingolipid production. *J Lipid Res* **2015,** *56* (9), 1836-42.

12.   Kita, K.; Okino, N.; Ito, M., Reverse hydrolysis reaction of a recombinant alkaline ceramidase of Pseudomonas aeruginosa. *Biochim Biophys Acta* **2000,** *1485* (2-3), 111-20.

13.   Kita, K.; Kurita, T.; Ito, M., Characterization of the reversible nature of the reaction catalyzed by sphingolipid ceramide N-deacylase. A novel form of reverse hydrolysis reaction. *Eur J Biochem* **2001,** *268* (3), 592-602.

14.   Rockendorf, N.; Bade, S.; Hirst, T. R.; Gorris, H. H.; Frey, A., Synthesis of a fluorescent ganglioside GM1 derivative and screening of a synthetic peptide library for GM1 binding sequence motifs. *Bioconjug Chem* **2007,** *18* (2), 573-8.

15.   Mikhalev, II; Molotkovskii Iu, G., [Synthesis and characteristics of fluorescent BODIPY-labeled gangliosides]. *Bioorg Khim* **2003,** *29* (2), 190-7.

16. Mikhalyov, I.; Gretskaya, N.; Johansson, L. B., Fluorescent BODIPY-labelled GM1 gangliosides designed for exploring lipid membrane properties and specific membrane-target interactions. *Chem Phys Lipids* **2009,** *159* (1), 38-44.

17. Nakagawa, T.; Tani, M.; Kita, K.; Ito, M., Preparation of fluorescence-labeled GM1 and sphingomyelin by the reverse hydrolysis reaction of sphingolipid ceramide N-deacylase as substrates for assay of sphingolipid-degrading enzymes and for detection of sphingolipid-binding proteins. *J Biochem* **1999,** *126* (3), 604-11.

18. Zama, K.; Hayashi, Y.; Ito, S.; Hirabayashi, Y.; Inoue, T.; Ohno, K.; Okino, N.; Ito, M., Simultaneous quantification of glucosylceramide and galactosylceramide by normal-phase HPLC using O-phtalaldehyde derivatives prepared with sphingolipid ceramide N-deacylase. *Glycobiology* **2009,** *19* (7), 767-75.

19. Rosengren, B.; Mansson, J. E.; Svennerholm, L., Composition of gangliosides and neutral glycosphingolipids of brain in classical Tay-Sachs and Sandhoff disease: more lyso-GM2 in Sandhoff disease? *J Neurochem* **1987,** *49* (3), 834-40.

20. Hannun, Y. A.; Bell, R. M., Lysosphingolipids inhibit protein kinase C: implications for the sphingolipidoses. *Science* **1987,** *235* (4789), 670-4.

21. Hesselmark, E.; Bejerot, S., Corrigendum to Biomarkers for diagnosis of Pediatric Acute Neuropsychiatric Syndrome (PANS) - Sensitivity and specificity of the Cunningham Panel [J. Neuroimmunol. 312. (2017) 31-37]. *J Neuroimmunol* **2017,** *313*, 116-117.

22. Weishaupt, N.; Caughlin, S.; Yeung, K. K.; Whitehead, S. N., Differential Anatomical Expression of Ganglioside GM1 Species Containing d18:1 or d20:1

Sphingosine Detected by MALDI Imaging Mass Spectrometry in Mature Rat Brain. *Front Neuroanat* **2015,** *9*, 155.

23.   Gantner, M.; Schwarzmann, G.; Sandhoff, K.; Kolter, T., Partial synthesis of ganglioside and lysoganglioside lipoforms as internal standards for MS quantification. *J Lipid Res* **2014,** *55* (12), 2692-704.

24.   Merrill, A. H., Jr., Sphingolipid and glycosphingolipid metabolic pathways in the era of sphingolipidomics. *Chem Rev* **2011,** *111* (10), 6387-422.

25.   Hanada, K.; Hara, T.; Nishijima, M., Purification of the serine palmitoyltransferase complex responsible for sphingoid base synthesis by using affinity peptide chromatography techniques. *J Biol Chem* **2000,** *275* (12), 8409-15.

26.   Williams, R. D.; Wang, E.; Merrill, A. H., Jr., Enzymology of long-chain base synthesis by liver: characterization of serine palmitoyltransferase in rat liver microsomes. *Arch Biochem Biophys* **1984,** *228* (1), 282-91.

27.   Armbruster, D. A.; Pry, T., Limit of blank, limit of detection and limit of quantitation. *Clin Biochem Rev* **2008,** *29 Suppl 1*, S49-52.

28.   Sturgill, E. R.; Aoki, K.; Lopez, P. H.; Colacurcio, D.; Vajn, K.; Lorenzini, I.; Majic, S.; Yang, W. H.; Heffer, M.; Tiemeyer, M.; Marth, J. D.; Schnaar, R. L., Biosynthesis of the major brain gangliosides GD1a and GT1b. *Glycobiology* **2012,** *22* (10), 1289-301.

29.   Zamfir, A. D.; Vukelic, Z.; Schneider, A.; Sisu, E.; Dinca, N.; Ingendoh, A., A novel approach for ganglioside structural analysis based on electrospray multiple-stage mass spectrometry. *J Biomol Tech* **2007,** *18* (4), 188-93.

30. Fong, B.; Norris, C.; Lowe, E.; McJarrow, P., Liquid chromatography-high-resolution mass spectrometry for quantitative analysis of gangliosides. *Lipids* **2009,** *44* (9), 867-74.

31. Suzuki, A.; Suzuki, M.; Ito, E.; Nitta, T.; Inokuchi, J. I., Mass Spectrometry of Gangliosides. *Methods Mol Biol* **2018,** *1804*, 207-221.

32. Akino, T., Sphingosine base and fatty acid compositions of pig brain sphingolipids. *Tohoku J Exp Med* **1969,** *98* (1), 87-97.

33. Caughlin, S.; Maheshwari, S.; Weishaupt, N.; Yeung, K. K.; Cechetto, D. F.; Whitehead, S. N., Age-dependent and regional heterogeneity in the long-chain base of A-series gangliosides observed in the rat brain using MALDI Imaging. *Sci Rep* **2017,** *7* (1), 16135.

34. Quehenberger, O.; Armando, A. M.; Brown, A. H.; Milne, S. B.; Myers, D. S.; Merrill, A. H.; Bandyopadhyay, S.; Jones, K. N.; Kelly, S.; Shaner, R. L.; Sullards, C. M.; Wang, E.; Murphy, R. C.; Barkley, R. M.; Leiker, T. J.; Raetz, C. R.; Guan, Z.; Laird, G. M.; Six, D. A.; Russell, D. W.; McDonald, J. G.; Subramaniam, S.; Fahy, E.; Dennis, E. A., Lipidomics reveals a remarkable diversity of lipids in human plasma. *J Lipid Res* **2010,** *51* (11), 3299-305.

35. Scherer, M.; Bottcher, A.; Schmitz, G.; Liebisch, G., Sphingolipid profiling of human plasma and FPLC-separated lipoprotein fractions by hydrophilic interaction chromatography tandem mass spectrometry. *Biochim Biophys Acta* **2011,** *1811* (2), 68-75.

CHAPTER 5

CONCLUSIONS AND FUTURE DIRECTIONS

5.1 CONCLUSIONS

An organism's metabolome is a complicated environment consisting of nucleic acids (DNA & RNA), proteins, carbohydrates, and lipids. With "omics" technologies, such as proteomics, genomics, transciptomics, and glycomics, there have been significant advancements in sequencing of proteins, genes, and analysis of carbohydrates.[1] Among all the constituents, lipids show the largest diversity in structure and molecular species, making them the hardest to analyze.[2] In an effort to simplify their characterization and analysis, the LIPID MAPS Consortium has classified lipids into eight different categories. This is a powerful tool in the field of lipidomics that helps study the biology of different lipid species in an organism.[3]

Even though lipidomics is an emerging field, significant research has been carried out to study a section of the entire lipidome in organisms, mainly glycerolipids, glycerophospholipids, sphingolipids, and sterols.[4] The primary subject of this thesis is glycosphingolipids (GSLs), which fall under the category of sphingolipids but are studied less frequently than other members of the class. **Chapter 1** in this thesis provides a detailed description of the biological functions of GSLs, how they play important roles in cellular signaling, and their association with serious diseases, such as Alzheimer's, Huntington's, Gaucher, and Sandhoff. It also describes the challenges researchers have faced over the past few decades to analyze and quantify these biomolecules accurately, owing to the incredible structural diversity of different molecular species that makes analyses more complicated. With the limited analytical tools at our disposal, there still is a need for more convenient techniques to simplify GSLs analysis. This thesis is an

attempt to address this problem by developing two complementary methods of GSL analysis, utilizing convenient enzymatic modifications.

Chapter 2 describes a GSL analysis method originally developed by Dr. Frances Platt and co-workers at the University of Oxford, United Kingdom. The method is based on enzymatic modification of GSLs using endoglycoceramidase (EGCase), which cleaves off the ceramide lipid backbone of GSLs, generating the corresponding glycans. They are fluorescently labeled with anthranilic acid (2-aminobenzoic acid) and analyzed by HPLC. We adapted the same protocol with modifications and an internal standard to quantify GSL components in biological samples accurately using LC-MS. This method gave detailed information about the carbohydrate component of GSLs and was useful when studying GSL composition in complex biological mixtures, such as human serum from individuals suffering from Huntington's disease. With the EGCase method being established successfully and validated using pig brains and mammalian Jurkat T cells, it was applied to a number of different projects both within our group and projects with collaborators, where GSL composition played a crucial role in each of the studies. **Chapter 3** describes each of these individual projects and the role of GSL composition in each of them. These projects included studying changes in GSL composition in mice brains under pro-inflammatory conditions induced by: lipopolysaccharide (LPS) injections in Jurkat T cells when treated with recombinant neuramindase-3 (NEU3) enzyme, which is said to act on gangliosides *in vitro*; in PC3 cells when treated with specific inhibitors of human neuraminidase enzymes to see their effects on cell migration; in mouse microglia exposed to certain polarization conditions that express characteristic

phenotypes; and in mouse plasma from animals in which genes for specific NEU enzymes, i.e., NEU3, NEU4, and NEU1 were knocked out.

Our goal was to design two complementary methods that would provide information not just about the glycan component of GSLs but also about the sphingosine base component of the lipid chain. **Chapter 4** describes a method using the enzyme sphingolipid ceramide *N*-deacylase (SCDase) to cleave the fatty acid chain of the ceramide lipid backbone, generating a *l*-GSL. This was labeled with a fluorophore, RapiFluor-MS, and analyzed by LC-MS; RapiFluor-MS has high sensitivity for MS based analyses. The major challenge with this project was to identify a suitable column to separate lyso-GSLs that have both hydrophilic (sugar) and hydrophobic (sphingosine chain) components in their structure. After trials, we were able to narrow it down to a mixed mode column (Weak Anion Exchange-Reverse Phase), which would help separate both the sugar and sphingosine chain. An internal standard was identified to allow absolute quantification of lyso-GSL components in a complex biological mixture. Even though separation was not ideal for sugars that were structurally related, such as GM1, GM2, and GM3 (differing in structure by just one sugar unit), we were able to achieve improved separation for all the other components that could not be separated on reverse phased columns. Moreover, peak heights (intensity) could be used in these cases where peak areas would not provide accurate quantification due to poor separation. This method was validated using pig brains and mammalian Jurkat T cells, just as was done for the EGCase method to study individual lyso-GSL components in each of these samples. Finally, the SCDase method was put to use as a complementary method of analysis of human serum from the same individuals suffering from Huntington's disease, as were

192

used for the EGCase method, to investigate any changes in sphingosine chains of the GSL components.

5.2 FUTURE DIRECTIONS

We have established the EGCase method of glycan analysis successfully and have demonstrated its success in **Chapter 3** for profiling and quantitation of GSLs in a variety of different studies. This assay will be used in upcoming projects within our group.

We have been successful in designing the new SCDase method for lyso-GSL analysis, with improved peak resolutions and good sensitivities. This method can be made even more robust with more improvements. They are as follows:

i) There were certain peaks that could not be resolved fully with the existing method we designed. These were the lyso-GSL peaks for GM1, GM2, and GM3 of the same sphingosine chain length. Notice that these GSLs differ only by one oligosaccharide residue, i.e., a Hexose (Hex) or a *N*-acetyl hexosamine (HexNAc) residue. In order to address this problem, we propose the use of a different column offering a different mixed mode separation. For example, a mixed mode HILIC and reverse phase (RP) column [Thermo Fisher Acclaim Mixed Mode HILIC-1 LC column] should be tested. This is based on the rationale that the HILIC mode of separation is the most popular mode used to separate oligosaccharides, affording excellent peak resolution, as has been demonstrated in **Chapter 2**.

ii) Due to the sensitivity of our MS instrument, there were some small peaks that remained unassigned in each of the biological samples run using the SCDase method. One way to address this problem would be to perform MS/MS experiments with product

ion scanning. This would delineate the fragmentation pattern of all the peaks and could be used to identify those ambiguous peaks.

iii) Previous reports in the literature have suggested that SCDase shows preference towards certain GSLs over others.[5] This also has been demonstrated in our studies in **Chapter 4**. Mutations of the gene encoding SCDase can be performed to design a suitable mutant that cleaves all GSLs with equal efficiency.

5.3 REFERENCES

1.   Quehenberger, O.; Armando, A. M.; Brown, A. H.; Milne, S. B.; Myers, D. S.; Merrill, A. H.; Bandyopadhyay, S.; Jones, K. N.; Kelly, S.; Shaner, R. L.; Sullards, C. M.; Wang, E.; Murphy, R. C.; Barkley, R. M.; Leiker, T. J.; Raetz, C. R.; Guan, Z.; Laird, G. M.; Six, D. A.; Russell, D. W.; McDonald, J. G.; Subramaniam, S.; Fahy, E.; Dennis, E. A., Lipidomics reveals a remarkable diversity of lipids in human plasma. *J Lipid Res* **2010,** *51* (11), 3299-305.

2.   Fahy, E.; Subramaniam, S.; Brown, H. A.; Glass, C. K.; Merrill, A. H., Jr.; Murphy, R. C.; Raetz, C. R.; Russell, D. W.; Seyama, Y.; Shaw, W.; Shimizu, T.; Spener, F.; van Meer, G.; VanNieuwenhze, M. S.; White, S. H.; Witztum, J. L.; Dennis, E. A., A comprehensive classification system for lipids. *J Lipid Res* **2005,** *46* (5), 839-61.

3.   Schmelzer, K.; Fahy, E.; Subramaniam, S.; Dennis, E. A., The lipid maps initiative in lipidomics. *Methods Enzymol* **2007,** *432*, 171-83.

4.   Tumanov, S.; Kamphorst, J. J., Recent advances in expanding the coverage of the lipidome. *Curr Opin Biotechnol* **2017,** *43*, 127-133.

5. Han, Y. B.; Wu, L.; Rich, J. R.; Huang, F. T.; Withers, S. G.; Feng, Y.; Yang, G. Y., Comprehensive characterization of sphingolipid ceramide N-deacylase for the synthesis and fatty acid remodeling of glycosphingolipids. *Appl Microbiol Biotechnol* **2015,** *99* (16), 6715-26.

BIBLIOGRAPHY

(IN ALPHABETICAL ORDER)

1. Ahotupa, M.; Suomela, J. P.; Vuorimaa, T.; Vasankari, T., Lipoprotein-specific transport of circulating lipid peroxides. *Ann Med* **2010,** *42* (7), 521-9.

2. Akino, T., Sphingosine base and fatty acid compositions of pig brain sphingolipids. *Tohoku J Exp Med* **1969,** *98* (1), 87-97.

3. Albohy, A.; Zhang, Y.; Smutova, V.; Pshezhetsky, A. V.; Cairo, C. W., Identification of Selective Nanomolar Inhibitors of the Human Neuraminidase, NEU4. *ACS Med Chem Lett* **2013,** *4* (6), 532-7.

4. Albrecht, S.; Vainauskas, S.; Stockmann, H.; McManus, C.; Taron, C. H.; Rudd, P. M., Comprehensive Profiling of Glycosphingolipid Glycans Using a Novel Broad Specificity Endoglycoceramidase in a High-Throughput Workflow. *Anal Chem* **2016,** *88* (9), 4795-802.

5. Alisson-Silva, F.; Kawanishi, K.; Varki, A., Human risk of diseases associated with red meat intake: Analysis of current theories and proposed role for metabolic incorporation of a non-human sialic acid. *Mol Aspects Med* **2016,** *51*, 16-30.

6. Allende, M. L.; Proia, R. L., Lubricating cell signaling pathways with gangliosides. *Curr Opin Struct Biol* **2002,** *12* (5), 587-92.

7. Alpaugh, M.; Galleguillos, D.; Forero, J.; Morales, L. C.; Lackey, S. W.; Kar, P.; Di Pardo, A.; Holt, A.; Kerr, B. J.; Todd, K. G.; Baker, G. B.; Fouad, K.; Sipione, S., Disease-modifying effects of ganglioside GM1 in Huntington's disease models. *EMBO Mol Med* **2017,** *9* (11), 1537-1557.

8. Ando, S., Neuronal dysfunction with aging and its amelioration. *Proc Jpn Acad Ser B Phys Biol Sci* **2012,** *88* (6), 266-82.

9. Ando, S.; Chang, N. C.; Yu, R. K., High-performance thin-layer chromatography and densitometric determination of brain ganglioside compositions of several species. *Anal Biochem* **1978,** *89* (2), 437-50.

10. Angstrom, J.; Teneberg, S.; Karlsson, K. A., Delineation and comparison of ganglioside-binding epitopes for the toxins of Vibrio cholerae, Escherichia coli, and Clostridium tetani: evidence for overlapping epitopes. *Proc Natl Acad Sci U S A* **1994,** *91* (25), 11859-63.

11. Ariga, T.; McDonald, M. P.; Yu, R. K., Role of ganglioside metabolism in the pathogenesis of Alzheimer's disease--a review. *J Lipid Res* **2008,** *49* (6), 1157-75.

12. Armbruster, D. A.; Pry, T., Limit of blank, limit of detection and limit of quantitation. *Clin Biochem Rev* **2008,** *29 Suppl 1*, S49-52.

13. Ashida, H.; Hayashi, S.; Sakamoto, Y.; Tsuji, Y.; Yamamoto, K.; Kumagai, H.; Tochikura, T., Formation of lyso-glycosphingolipids by Streptomyces sp. *Biosci Biotechnol Biochem* **1995,** *59* (11), 2028-32.

14. Aspeborg, H.; Coutinho, P. M.; Wang, Y.; Brumer, H.; Henrissat, B., Evolution, substrate specificity and subfamily classification of glycoside hydrolase family 5 (GH5). *BMC Evolutionary Biology* **2012,** *12* (1), 186.

15. Aureli, M.; Mauri, L.; Ciampa, M. G.; Prinetti, A.; Toffano, G.; Secchieri, C.; Sonnino, S., GM1 Ganglioside: Past Studies and Future Potential. *Mol Neurobiol* **2016,** *53* (3), 1824-1842.

16. Barrientos, R. C.; Zhang, Q., Isobaric Labeling of Intact Gangliosides toward Multiplexed LC-MS/MS-Based Quantitative Analysis. *Anal Chem* **2018,** *90* (4), 2578-2586.

17. Beermann, C.; Rohrig, A. K.; Boehm, G., Chemical and enzymatic transacylation of amide-linked FA of buttermilk gangliosides. *Lipids* **2003,** *38* (8), 855-64.

18. Benito, J. M.; Garcia Fernandez, J. M.; Ortiz Mellet, C., Pharmacological chaperone therapy for Gaucher disease: a patent review. *Expert Opin Ther Pat* **2011,** *21* (6), 885-903.

19. Bi, S.; Baum, L. G., Sialic acids in T cell development and function. *Biochim Biophys Acta* **2009,** *1790* (12), 1599-610.

20. Bigge, J. C.; Patel, T. P.; Bruce, J. A.; Goulding, P. N.; Charles, S. M.; Parekh, R. B., Nonselective and efficient fluorescent labeling of glycans using 2-amino benzamide and anthranilic acid. *Anal Biochem* **1995,** *230* (2), 229-38.

21. Bindila, L.; Peter-Katalinic, J., Chip-mass spectrometry for glycomic studies. *Mass Spectrom Rev* **2009,** *28* (2), 223-53.

22. Bligh, E. G.; Dyer, W. J., A RAPID METHOD OF TOTAL LIPID EXTRACTION AND PURIFICATION. *Canadian Journal of Biochemistry and Physiology* **1959,** *37* (8), 911-917.

23. Blix, G., Über die Kohlenhydratgruppen des Submaxillarismucins. In *Hoppe-Seyler´s Zeitschrift für physiologische Chemie*, 1936; Vol. 240, p 43.

24. Bond, L. M.; Miyazaki, M.; O'Neill, L. M.; Ding, F.; Ntambi, J. M., Chapter 6 - Fatty Acid Desaturation and Elongation in Mammals. In *Biochemistry of Lipids, Lipoproteins and Membranes (Sixth Edition)*, Ridgway, N. D.; McLeod, R. S., Eds. Elsevier: Boston, 2016; pp 185-208.

25. Borch, R. F.; Bernstein, M. D.; Durst, H. D., Cyanohydridoborate anion as a selective reducing agent. *Journal of the American Chemical Society* **1971,** *93* (12), 2897-2904.

26. Bou Khalil, M.; Hou, W.; Zhou, H.; Elisma, F.; Swayne, L. A.; Blanchard, A. P.; Yao, Z.; Bennett, S. A.; Figeys, D., Lipidomics era: accomplishments and challenges. *Mass Spectrom Rev* **2010,** *29* (6), 877-929.

27. Braun, P. E.; Snell, E. E., The biosynthesis of dihydrosphingosine in cell-free preparations of Hansenula ciferri. *Proc Natl Acad Sci U S A* **1967,** *58* (1), 298-303.

28. Buszewski, B.; Noga, S., Hydrophilic interaction liquid chromatography (HILIC)--a powerful separation technique. *Anal Bioanal Chem* **2012,** *402* (1), 231-47.

29. Butovsky, O.; Jedrychowski, M. P.; Moore, C. S.; Cialic, R.; Lanser, A. J.; Gabriely, G.; Koeglsperger, T.; Dake, B.; Wu, P. M.; Doykan, C. E.; Fanek, Z.; Liu, L.; Chen, Z.; Rothstein, J. D.; Ransohoff, R. M.; Gygi, S. P.; Antel, J. P.; Weiner, H. L., Identification of a unique TGF-beta-dependent molecular and functional signature in microglia. *Nat Neurosci* **2014,** *17* (1), 131-43.

30. Caines, M. E.; Vaughan, M. D.; Tarling, C. A.; Hancock, S. M.; Warren, R. A.; Withers, S. G.; Strynadka, N. C., Structural and mechanistic analyses of endo-glycoceramidase II, a membrane-associated family 5 glycosidase in the Apo and GM3 ganglioside-bound forms. *J Biol Chem* **2007,** *282* (19), 14300-8.

31. Carado, A.; Passarelli, M. K.; Kozole, J.; Wingate, J. E.; Winograd, N.; Loboda, A. V., C60 secondary ion mass spectrometry with a hybrid-quadrupole orthogonal time-of-flight mass spectrometer. *Anal Chem* **2008,** *80* (21), 7921-9.

32. Caughlin, S.; Maheshwari, S.; Agca, Y.; Agca, C.; Harris, A. J.; Jurcic, K.; Yeung, K. K.; Cechetto, D. F.; Whitehead, S. N., Membrane-lipid homeostasis in a prodromal rat model of Alzheimer's disease: Characteristic profiles in ganglioside distributions during aging detected using MALDI imaging mass spectrometry. *Biochim Biophys Acta* **2018,** *1862* (6), 1327-1338.

33. Caughlin, S.; Maheshwari, S.; Weishaupt, N.; Yeung, K. K.; Cechetto, D. F.; Whitehead, S. N., Age-dependent and regional heterogeneity in the long-chain base of A-series gangliosides observed in the rat brain using MALDI Imaging. *Sci Rep* **2017,** *7* (1), 16135.

34. Chan, R. B.; Perotte, A. J.; Zhou, B.; Liong, C.; Shorr, E. J.; Marder, K. S.; Kang, U. J.; Waters, C. H.; Levy, O. A.; Xu, Y.; Shim, H. B.; Pe'er, I.; Di Paolo, G.; Alcalay, R. N., Elevated GM3 plasma concentration in idiopathic Parkinson's disease: A lipidomic analysis. *PLoS One* **2017,** *12* (2), e0172348.

35. Chen, Y.; Allegood, J.; Liu, Y.; Wang, E.; Cachon-Gonzalez, B.; Cox, T. M.; Merrill, A. H., Jr.; Sullards, M. C., Imaging MALDI mass spectrometry using an oscillating capillary nebulizer matrix coating system and its application to analysis of lipids in brain from a mouse model of Tay-Sachs/Sandhoff disease. *Anal Chem* **2008,** *80* (8), 2780-8.

36. Chen, Y.; Liu, Y.; Sullards, M. C.; Merrill, A. H., Jr., An introduction to sphingolipid metabolism and analysis by new technologies. *Neuromolecular Med* **2010,** *12* (4), 306-19.

37. Chester, M. A., IUPAC-IUB Joint Commission on Biochemical Nomenclature (JCBN). Nomenclature of glycolipids--recommendations 1997. *Eur J Biochem* **1998,** *257* (2), 293-8.

38. Chiavegatto, S.; Sun, J.; Nelson, R. J.; Schnaar, R. L., A functional role for complex gangliosides: motor deficits in GM2/GD2 synthase knockout mice. *Exp Neurol* **2000,** *166* (2), 227-34.

39. Chou, H. H.; Takematsu, H.; Diaz, S.; Iber, J.; Nickerson, E.; Wright, K. L.; Muchmore, E. A.; Nelson, D. L.; Warren, S. T.; Varki, A., A mutation in human CMP-sialic acid hydroxylase occurred after the Homo-Pan divergence. *Proc Natl Acad Sci U S A* **1998,** *95* (20), 11751-6.

40. Cotterchio, M.; Seyfried, T. N., Serum gangliosides in mice with metastatic and non-metastatic brain tumors. *J Lipid Res* **1994,** *35* (1), 10-4.

41. Cross, A. S.; Hyun, S. W.; Miranda-Ribera, A.; Feng, C.; Liu, A.; Nguyen, C.; Zhang, L.; Luzina, I. G.; Atamas, S. P.; Twaddell, W. S.; Guang, W.; Lillehoj, E. P.; Puche, A. C.; Huang, W.; Wang, L. X.; Passaniti, A.; Goldblum, S. E., NEU1 and NEU3 sialidase activity expressed in human lung microvascular endothelia: NEU1 restrains endothelial cell migration, whereas NEU3 does not. *J Biol Chem* **2012,** *287* (19), 15966-80.

42. Cuatrecasas, P., Gangliosides and membrane receptors for cholera toxin. *Biochemistry* **1973,** *12* (18), 3558-66.

43. D'Angelo, G.; Capasso, S.; Sticco, L.; Russo, D., Glycosphingolipids: synthesis and functions. *FEBS J* **2013,** *280* (24), 6338-53.

44. Daskhan, G. C.; Tran, H. T.; Meloncelli, P. J.; Lowary, T. L.; West, L. J.; Cairo, C. W., Construction of Multivalent Homo- and Heterofunctional ABO Blood Group Glycoconjugates Using a Trifunctional Linker Strategy. *Bioconjug Chem* **2018,** *29* (2), 343-362.

45. Davies, G.; Henrissat, B., Structures and mechanisms of glycosyl hydrolases. *Structure* **1995,** *3* (9), 853-9.

46. DeMarco, M. L.; Woods, R. J., Atomic-resolution conformational analysis of the GM3 ganglioside in a lipid bilayer and its implications for ganglioside-protein recognition at membrane surfaces. *Glycobiology* **2009,** *19* (4), 344-55.

47. Demina, E., Pierre, W., Londono, I., Nguyen, A., Reiz, B., Zou, C., Chakraberty, R., Cairo, C.W., Pshezhetsky, A.V., Lodygensky, G., Persistant reduction in sialylation of cerebral glycoproteins following post-natal inflammatory exposure. **2018**.

48. Demina, E., Smutova, V., Fougerat, A., Pan, X., Guo, T., Zou, C., Chakraberty, R., Snarr, B., Sheppard, D., Shiao, C., Roy, R., Orekhov, A. N., Miyagi, T., Laffargue, M., Cairo, C.W., Pshezhetsky, A.V., Inhibitors of neuraminidases 1 and 3 as potential candidates for treating atherosclerosis. **2018**.

49. Demopoulos, C. A.; Kyrili, M.; Antonopoulou, S.; Andrikopoulos, N. K., Separation of Several Main Glycolipids into Classes and Partially into Species by HPLC and UV-Detection. *Journal of Liquid Chromatography & Related Technologies* **1996,** *19* (5), 771-781.

50. Distler, U.; Hulsewig, M.; Souady, J.; Dreisewerd, K.; Haier, J.; Senninger, N.; Friedrich, A. W.; Karch, H.; Hillenkamp, F.; Berkenkamp, S.; Peter-Katalinic, J.;

Muthing, J., Matching IR-MALDI-o-TOF mass spectrometry with the TLC overlay binding assay and its clinical application for tracing tumor-associated glycosphingolipids in hepatocellular and pancreatic cancer. *Anal Chem* **2008,** *80* (6), 1835-46.

51. Dreisewerd, K.; Muthing, J.; Rohlfing, A.; Meisen, I.; Vukelic, Z.; Peter-Katalinic, J.; Hillenkamp, F.; Berkenkamp, S., Analysis of gangliosides directly from thin-layer chromatography plates by infrared matrix-assisted laser desorption/ionization orthogonal time-of-flight mass spectrometry with a glycerol matrix. *Anal Chem* **2005,** *77* (13), 4098-107.

52. Durafourt, B. A.; Moore, C. S.; Zammit, D. A.; Johnson, T. A.; Zaguia, F.; Guiot, M. C.; Bar-Or, A.; Antel, J. P., Comparison of polarization properties of human adult microglia and blood-derived macrophages. *Glia* **2012,** *60* (5), 717-27.

53. El-Aneed, A.; Cohen, A.; Banoub, J., Mass Spectrometry, Review of the Basics: Electrospray, MALDI, and Commonly Used Mass Analyzers. *Applied Spectroscopy Reviews* **2009,** *44* (3), 210-230.

54. Fahr, C.; Schauer, R., Detection of Sialic Acids and Gangliosides with Special Reference to 9-O-Acetylated Species in Basaliomas and Normal Human Skin. *Journal of Investigative Dermatology* **2001,** *116* (2), 254-260.

55. Fahy, E.; Subramaniam, S.; Brown, H. A.; Glass, C. K.; Merrill, A. H., Jr.; Murphy, R. C.; Raetz, C. R.; Russell, D. W.; Seyama, Y.; Shaw, W.; Shimizu, T.; Spener, F.; van Meer, G.; VanNieuwenhze, M. S.; White, S. H.; Witztum, J. L.; Dennis, E. A., A comprehensive classification system for lipids. *J Lipid Res* **2005,** *46* (5), 839-61.

56. Farwanah, H.; Kolter, T.; Sandhoff, K., Mass spectrometric analysis of neutral sphingolipids: methods, applications, and limitations. *Biochim Biophys Acta* **2011,** *1811* (11), 854-60.

57. Farwanah, H.; Pierstorff, B.; Schmelzer, C. E.; Raith, K.; Neubert, R. H.; Kolter, T.; Sandhoff, K., Separation and mass spectrometric characterization of covalently bound skin ceramides using LC/APCI-MS and Nano-ESI-MS/MS. *J Chromatogr B Analyt Technol Biomed Life Sci* **2007,** *852* (1-2), 562-70.

58. Folch, J.; Lees, M.; Sloane Stanley, G. H., A simple method for the isolation and purification of total lipides from animal tissues. *J Biol Chem* **1957,** *226* (1), 497-509.

59. Fong, B.; Norris, C.; Lowe, E.; McJarrow, P., Liquid chromatography-high-resolution mass spectrometry for quantitative analysis of gangliosides. *Lipids* **2009,** *44* (9), 867-74.

60. Furusato, M.; Sueyoshi, N.; Mitsutake, S.; Sakaguchi, K.; Kita, K.; Okino, N.; Ichinose, S.; Omori, A.; Ito, M., Molecular cloning and characterization of sphingolipid ceramide N-deacylase from a marine bacterium, Shewanella alga G8. *J Biol Chem* **2002,** *277* (19), 17300-7.

61. Futerman, A. H., Chapter 10 - Sphingolipids. In *Biochemistry of Lipids, Lipoproteins and Membranes (Sixth Edition)*, Ridgway, N. D.; McLeod, R. S., Eds. Elsevier: Boston, 2016; pp 297-326.

62. Gamble, L. J.; Anderton, C. R., Secondary Ion Mass Spectrometry Imaging of Tissues, Cells, and Microbial Systems. *Micros Today* **2016,** *24* (2), 24-31.

63. Gantner, M.; Schwarzmann, G.; Sandhoff, K.; Kolter, T., Partial synthesis of ganglioside and lysoganglioside lipoforms as internal standards for MS quantification. *J Lipid Res* **2014,** *55* (12), 2692-704.

64. Garbis, S. D.; Melse-Boonstra, A.; West, C. E.; van Breemen, R. B., Determination of folates in human plasma using hydrophilic interaction chromatography-tandem mass spectrometry. *Anal Chem* **2001,** *73* (22), 5358-64.

65. Gomez-Nicola, D.; Perry, V. H., Microglial dynamics and role in the healthy and diseased brain: a paradigm of functional plasticity. *Neuroscientist* **2015,** *21* (2), 169-84.

66. Goto-Inoue, N.; Hayasaka, T.; Taki, T.; Gonzalez, T. V.; Setou, M., A new lipidomics approach by thin-layer chromatography-blot-matrix-assisted laser desorption/ionization imaging mass spectrometry for analyzing detailed patterns of phospholipid molecular species. *J Chromatogr A* **2009,** *1216* (42), 7096-101.

67. Grassi, S.; Prioni, S.; Cabitta, L.; Aureli, M.; Sonnino, S.; Prinetti, A., The Role of 3-O-Sulfogalactosylceramide, Sulfatide, in the Lateral Organization of Myelin Membrane. *Neurochem Res* **2016,** *41* (1-2), 130-43.

68. Groux-Degroote, S.; Guerardel, Y.; Delannoy, P., Gangliosides: Structures, Biosynthesis, Analysis, and Roles in Cancer. *Chembiochem* **2017,** *18* (13), 1146-1154.

69. Gu, R. X.; Ingolfsson, H. I.; de Vries, A. H.; Marrink, S. J.; Tieleman, D. P., Ganglioside-Lipid and Ganglioside-Protein Interactions Revealed by Coarse-Grained and Atomistic Molecular Dynamics Simulations. *J Phys Chem B* **2017,** *121* (15), 3262-3275.

70. Guo, T.; Datwyler, P.; Demina, E.; Richards, M. R.; Ge, P.; Zou, C.; Zheng, R.; Fougerat, A.; Pshezhetsky, A. V.; Ernst, B.; Cairo, C. W., Selective Inhibitors of Human Neuraminidase 3. *J Med Chem* **2018,** *61* (5), 1990-2008.

71. Hajek, R.; Jirasko, R.; Lisa, M.; Cifkova, E.; Holcapek, M., Hydrophilic Interaction Liquid Chromatography-Mass Spectrometry Characterization of Gangliosides in Biological Samples. *Anal Chem* **2017,** *89* (22), 12425-12432.

72. Hajek, R.; Lisa, M.; Khalikova, M.; Jirasko, R.; Cifkova, E.; Student, V., Jr.; Vrana, D.; Opalka, L.; Vavrova, K.; Matzenauer, M.; Melichar, B.; Holcapek, M., HILIC/ESI-MS determination of gangliosides and other polar lipid classes in renal cell carcinoma and surrounding normal tissues. *Anal Bioanal Chem* **2018**.

73. Hakomori Si, S. I., The glycosynapse. *Proc Natl Acad Sci U S A* **2002,** *99* (1), 225-32.

74. Hakomori, S. I., Release of carbohydrates from sphingoglycolipid by osmium-catalyzed periodate oxidation followed by treatment with mild alkali. *J Lipid Res* **1966,** *7* (6), 789-92.

75. Hama, H., Fatty acid 2-Hydroxylation in mammalian sphingolipid biology. *Biochim Biophys Acta* **2010,** *1801* (4), 405-14.

76. Han, Y. B.; Chen, L. Q.; Li, Z.; Tan, Y. M.; Feng, Y.; Yang, G. Y., Structural Insights into the Broad Substrate Specificity of a Novel Endoglycoceramidase I Belonging to a New Subfamily of GH5 Glycosidases. *J Biol Chem* **2017,** *292* (12), 4789-4800.

77. Han, Y. B.; Wu, L.; Rich, J. R.; Huang, F. T.; Withers, S. G.; Feng, Y.; Yang, G. Y., Comprehensive characterization of sphingolipid ceramide N-deacylase for the

synthesis and fatty acid remodeling of glycosphingolipids. *Appl Microbiol Biotechnol* **2015,** *99* (16), 6715-26.

78. Hanada, K.; Hara, T.; Nishijima, M., Purification of the serine palmitoyltransferase complex responsible for sphingoid base synthesis by using affinity peptide chromatography techniques. *J Biol Chem* **2000,** *275* (12), 8409-15.

79. Hanada, K.; Nishijima, M.; Kiso, M.; Hasegawa, A.; Fujita, S.; Ogawa, T.; Akamatsu, Y., Sphingolipids are essential for the growth of Chinese hamster ovary cells. Restoration of the growth of a mutant defective in sphingoid base biosynthesis by exogenous sphingolipids. *J Biol Chem* **1992,** *267* (33), 23527-33.

80. Hannun, Y. A.; Bell, R. M., Lysosphingolipids inhibit protein kinase C: implications for the sphingolipidoses. *Science* **1987,** *235* (4789), 670-4.

81. Hannun, Y. A.; Obeid, L. M., Sphingolipids and their metabolism in physiology and disease. *Nat Rev Mol Cell Biol* **2018,** *19* (3), 175-191.

82. Hata, K.; Tochigi, T.; Sato, I.; Kawamura, S.; Shiozaki, K.; Wada, T.; Takahashi, K.; Moriya, S.; Yamaguchi, K.; Hosono, M.; Miyagi, T., Increased sialidase activity in serum of cancer patients: Identification of sialidase and inhibitor activities in human serum. *Cancer Sci* **2015,** *106* (4), 383-9.

83. Hatano, K.; Miyamoto, Y.; Nonomura, N.; Kaneda, Y., Expression of gangliosides, GD1a, and sialyl paragloboside is regulated by NF-kappaB-dependent transcriptional control of alpha2,3-sialyltransferase I, II, and VI in human castration-resistant prostate cancer cells. *Int J Cancer* **2011,** *129* (8), 1838-47.

84. Hesselmark, E.; Bejerot, S., Corrigendum to Biomarkers for diagnosis of Pediatric Acute Neuropsychiatric Syndrome (PANS) - Sensitivity and specificity of the Cunningham Panel [J. Neuroimmunol. 312. (2017) 31-37]. *J Neuroimmunol* **2017,** *313*, 116-117.

85. Higashi, H.; Hirabayashi, Y.; Ito, M.; Yamagata, T.; Matsumoto, M.; Ueda, S.; Kato, S., Immunostaining on thin-layer chromatograms of oligosaccharides released from gangliosides by endoglycoceramidase. *J Biochem* **1987,** *102* (2), 291-6.

86. Hikita, T.; Tadano-Aritomi, K.; Iida-Tanaka, N.; Levery, S. B.; Ishizuka, I.; Hakomori, S., Cationic glycosphingolipids in neuronal tissues and their possible biological significance. *Neurochem Res* **2002,** *27* (7-8), 575-81.

87. Hirabayashi, Y.; Kimura, M.; Matsumoto, M.; Yamamoto, K.; Kadowaki, S.; Tochikura, T., A novel glycosphingolipid hydrolyzing enzyme, glycosphingolipid ceramide deacylase, which cleaves the linkage between the fatty acid and sphingosine base in glycosphingolipids. *J Biochem* **1988,** *103* (1), 1-4.

88. Hogg, N.; Smith, A.; McDowall, A.; Giles, K.; Stanley, P.; Laschinger, M.; Henderson, R., How T cells use LFA-1 to attach and migrate. *Immunol Lett* **2004,** *92* (1-2), 51-4.

89. Hong, S.; Ostaszewski, B. L.; Yang, T.; O'Malley, T. T.; Jin, M.; Yanagisawa, K.; Li, S.; Bartels, T.; Selkoe, D. J., Soluble Abeta oligomers are rapidly sequestered from brain ISF in vivo and bind GM1 ganglioside on cellular membranes. *Neuron* **2014,** *82* (2), 308-19.

90. Horibata, Y.; Okino, N.; Ichinose, S.; Omori, A.; Ito, M., Purification, characterization, and cDNA cloning of a novel acidic endoglycoceramidase from the jellyfish, Cyanea nozakii. *J Biol Chem* **2000,** *275* (40), 31297-304.

91. Howlader, M. A., Guo, T., Chakraberty, R., Porter, E., Cairo, C.W., Isoenzyme-selective inhibitors of human neuraminidases reveal distinct effects on cell migration **2018**.

92. Howlader, M. A., Li, C., Zou, C., Chakraberty, R., Ebesoh, N., Cairo, C.W., Neuraminidase-3 (NEU3) is a negative regulator of LFA-1 adhesion. **2018**.

93. Hsu, F. F.; Turk, J., Structural determination of glycosphingolipids as lithiated adducts by electrospray ionization mass spectrometry using low-energy collisional-activated dissociation on a triple stage quadrupole instrument. *J Am Soc Mass Spectrom* **2001,** *12* (1), 61-79.

94. Huang, F. T.; Han, Y. B.; Feng, Y.; Yang, G. Y., A facile method for controlling the reaction equilibrium of sphingolipid ceramide N-deacylase for lyso-glycosphingolipid production. *J Lipid Res* **2015,** *56* (9), 1836-42.

95. Hunter, C. D.; Guo, T.; Daskhan, G.; Richards, M. R.; Cairo, C. W., Synthetic Strategies for Modified Glycosphingolipids and Their Design as Probes. *Chem Rev* **2018**.

96. Ikeda, K.; Yamaguchi, T.; Fukunaga, S.; Hoshino, M.; Matsuzaki, K., Mechanism of amyloid beta-protein aggregation mediated by GM1 ganglioside clusters. *Biochemistry* **2011,** *50* (29), 6433-40.

97. Imarisio, S.; Carmichael, J.; Korolchuk, V.; Chen, C. W.; Saiki, S.; Rose, C.; Krishna, G.; Davies, J. E.; Ttofi, E.; Underwood, B. R.; Rubinsztein, D. C.,

Huntington's disease: from pathology and genetics to potential therapies. *Biochem J* **2008,** *412* (2), 191-209.platypus. *Carbohyd Res* **2009,** *344* (12), 1494-500.

98. In *Essentials of Glycobiology*, rd; Varki, A.; Cummings, R. D.; Esko, J. D.; Stanley, P.; Hart, G. W.; Aebi, M.; Darvill, A. G.; Kinoshita, T.; Packer, N. H.; Prestegard, J. H.; Schnaar, R. L.; Seeberger, P. H., Eds. Cold Spring Harbor (NY), 2015.

99. Inokuchi, J., Membrane microdomains and insulin resistance. *FEBS Lett* **2010,** *584* (9), 1864-71.

100. Ishibashi, Y.; Kobayashi, U.; Hijikata, A.; Sakaguchi, K.; Goda, H. M.; Tamura, T.; Okino, N.; Ito, M., Preparation and characterization of EGCase I, applicable to the comprehensive analysis of GSLs, using a rhodococcal expression system. *J Lipid Res* **2012,** *53* (10), 2242-51.

101. Ishibashi, Y.; Nakasone, T.; Kiyohara, M.; Horibata, Y.; Sakaguchi, K.; Hijikata, A.; Ichinose, S.; Omori, A.; Yasui, Y.; Imamura, A.; Ishida, H.; Kiso, M.; Okino, N.; Ito, M., A novel endoglycoceramidase hydrolyzes oligogalactosylceramides to produce galactooligosaccharides and ceramides. *J Biol Chem* **2007,** *282* (15), 11386-96.

102. Ito, M.; Kurita, T.; Kita, K., A novel enzyme that cleaves the N-acyl linkage of ceramides in various glycosphingolipids as well as sphingomyelin to produce their lyso forms. *J Biol Chem* **1995,** *270* (41), 24370-4.

103. Ito, M.; Yamagata, T., A novel glycosphingolipid-degrading enzyme cleaves the linkage between the oligosaccharide and ceramide of neutral and acidic glycosphingolipids. *J Biol Chem* **1986,** *261* (30), 14278-82.

211

104. Ito, M.; Yamagata, T., Purification and characterization of glycosphingolipid-specific endoglycosidases (endoglycoceramidases) from a mutant strain of Rhodococcus sp. Evidence for three molecular species of endoglycoceramidase with different specificities. *J Biol Chem* **1989,** *264* (16), 9510-9.

105. Jandera, P., Stationary and mobile phases in hydrophilic interaction chromatography: a review. *Anal Chim Acta* **2011,** *692* (1-2), 1-25.

106. Jou, I.; Lee, J. H.; Park, S. Y.; Yoon, H. J.; Joe, E. H.; Park, E. J., Gangliosides trigger inflammatory responses via TLR4 in brain glia. *Am J Pathol* **2006,** *168* (5), 1619-30.

107. Jozwiak, W.; Koscielak, J., Lactosylsphingosine-reactive antibody and CEA in patients with colorectal cancer. *Eur J Cancer Clin Oncol* **1982,** *18* (7), 617-21.

108. Kabayama, K.; Sato, T.; Saito, K.; Loberto, N.; Prinetti, A.; Sonnino, S.; Kinjo, M.; Igarashi, Y.; Inokuchi, J., Dissociation of the insulin receptor and caveolin-1 complex by ganglioside GM3 in the state of insulin resistance. *Proc Natl Acad Sci U S A* **2007,** *104* (34), 13678-83.

109. Kalanuria, A. A.; Nyquist, P.; Ling, G., The prevention and regression of atherosclerotic plaques: emerging treatments. *Vasc Health Risk Manag* **2012,** *8*, 549-61.

110. Kawano, T.; Cui, J.; Koezuka, Y.; Toura, I.; Kaneko, Y.; Sato, H.; Kondo, E.; Harada, M.; Koseki, H.; Nakayama, T.; Tanaka, Y.; Taniguchi, M., Natural killer-like nonspecific tumor cell lysis mediated by specific ligand-activated Valpha14 NKT cells. *Proc Natl Acad Sci U S A* **1998,** *95* (10), 5690-3.

111. Kim, O. S.; Park, E. J.; Joe, E. H.; Jou, I., JAK-STAT signaling mediates gangliosides-induced inflammatory responses in brain microglial cells. *J Biol Chem* **2002,** *277* (43), 40594-601.

112. Kirsch, S.; Muthing, J.; Peter-Katalinic, J.; Bindila, L., On-line nano-HPLC/ESI QTOF MS monitoring of alpha2-3 and alpha2-6 sialylation in granulocyte glycosphingolipidome. *Biol Chem* **2009,** *390* (7), 657-72.

113. Kirsch, S.; Zarei, M.; Cindric, M.; Muthing, J.; Bindila, L.; Peter-Katalinic, J., On-line nano-HPLC/ESI QTOF MS and tandem MS for separation, detection, and structural elucidation of human erythrocytes neutral glycosphingolipid mixture. *Anal Chem* **2008,** *80* (12), 4711-22.

114. Kita, K.; Kurita, T.; Ito, M., Characterization of the reversible nature of the reaction catalyzed by sphingolipid ceramide N-deacylase. A novel form of reverse hydrolysis reaction. *Eur J Biochem* **2001,** *268* (3), 592-602.

115. Kita, K.; Okino, N.; Ito, M., Reverse hydrolysis reaction of a recombinant alkaline ceramidase of Pseudomonas aeruginosa. *Biochim Biophys Acta* **2000,** *1485* (2-3), 111-20.

116. Kobata, A., Exo- and endoglycosidases revisited. *Proc Jpn Acad Ser B Phys Biol Sci* **2013,** *89* (3), 97-117.

117. Kopitz, J., Lipid glycosylation: a primer for histochemists and cell biologists. *Histochem Cell Biol* **2017,** *147* (2), 175-198.

118. Koseki, K.; Wada, T.; Hosono, M.; Hata, K.; Yamaguchi, K.; Nitta, K.; Miyagi, T., Human cytosolic sialidase NEU2-low general tissue expression but

involvement in PC-3 prostate cancer cell survival. *Biochem Biophys Res Commun* **2012,** *428* (1), 142-9.

119. Kotani, M.; Kawashima, I.; Ozawa, H.; Terashima, T.; Tai, T., Differential distribution of major gangliosides in rat central nervous system detected by specific monoclonal antibodies. *Glycobiology* **1993,** *3* (2), 137-46.

120. Kotani, M.; Ozawa, H.; Kawashima, I.; Ando, S.; Tai, T., Generation of one set of monoclonal antibodies specific for a-pathway ganglio-series gangliosides. *Biochim Biophys Acta* **1992,** *1117* (1), 97-103.

121. Kracun, I.; Rosner, H.; Cosovic, C.; Stavljenic, A., Topographical atlas of the gangliosides of the adult human brain. *J Neurochem* **1984,** *43* (4), 979-89.

122. Kracun, I.; Rosner, H.; Drnovsek, V.; Heffer-Lauc, M.; Cosovic, C.; Lauc, G., Human brain gangliosides in development, aging and disease. *Int J Dev Biol* **1991,** *35* (3), 289-95.

123. Kurita, T.; Izu, H.; Sano, M.; Ito, M.; Kato, I., Enhancement of hydrolytic activity of sphingolipid ceramide N-deacylase in the aqueous-organic biphasic system. *J Lipid Res* **2000,** *41* (5), 846-51.

124. Kwon, K. M.; Chung, T. W.; Kwak, C. H.; Choi, H. J.; Kim, K. W.; Ha, S. H.; Cho, S. H.; Lee, Y. C.; Ha, K. T.; Lee, M. J.; Kim, C. H., Disialyl GD2 ganglioside suppresses ICAM-1-mediated invasiveness in human breast cancer MDA-MB231 cells. *Int J Biol Sci* **2017,** *13* (3), 265-275.

125. Lee, H.; Lerno, L. A., Jr.; Choe, Y.; Chu, C. S.; Gillies, L. A.; Grimm, R.; Lebrilla, C. B.; German, J. B., Multiple precursor ion scanning of gangliosides

and sulfatides with a reversed-phase microfluidic chip and quadrupole time-of-flight mass spectrometry. *Anal Chem* **2012,** *84* (14), 5905-12.

126. Leenders, R. G.; de Jong, J. G.; Wevers, R. A., Extraction and purification of gangliosides from plasma and fibroblasts before analysis by thin layer chromatography. *Ann Clin Biochem* **1995,** *32 (Pt 1)*, 68-73.

127. Levy, M.; Futerman, A. H., Mammalian ceramide synthases. *IUBMB Life* **2010,** *62* (5), 347-56.

128. Li, C.; Key, J. A.; Jia, F.; Dandapat, A.; Hur, S.; Cairo, C. W., Practical labeling methodology for choline-derived lipids and applications in live cell fluorescence imaging. *Photochem Photobiol* **2014,** *90* (3), 686-95.

129. Li, J.; Han, L.; Li, J.; Kitova, E. N.; Xiong, Z. J.; Prive, G. G.; Klassen, J. S., Detecting Protein-Glycolipid Interactions Using CaR-ESI-MS and Model Membranes: Comparison of Pre-loaded and Passively Loaded Picodiscs. *J Am Soc Mass Spectrom* **2018,** *29* (7), 1493-1504.

130. Li, S. C.; DeGasperi, R.; Muldrey, J. E.; Li, Y. T., A unique glycosphingolipid-splitting enzyme (ceramide-glycanase from leech) cleaves the linkage between the oligosaccharide and the ceramide. *Biochem Biophys Res Commun* **1986,** *141* (1), 346-52.

131. Li, Y. T.; Ishikawa, Y.; Li, S. C., Occurrence of ceramide-glycanase in the earthworm, Lumbricus terrestris. *Biochem Biophys Res Commun* **1987,** *149* (1), 167-72.

132. Lichtenberg, D.; Goni, F. M.; Heerklotz, H., Detergent-resistant membranes should not be identified with membrane rafts. *Trends Biochem Sci* **2005,** *30* (8), 430-6.

133. Lingwood, D.; Simons, K., Lipid rafts as a membrane-organizing principle. *Science* **2010,** *327* (5961), 46-50.

134. Lipina, C.; Hundal, H. S., Ganglioside GM3 as a gatekeeper of obesity-associated insulin resistance: Evidence and mechanisms. *FEBS Lett* **2015,** *589* (21), 3221-7.

135. Lisa, M.; Holcapek, M., High-Throughput and Comprehensive Lipidomic Analysis Using Ultrahigh-Performance Supercritical Fluid Chromatography-Mass Spectrometry. *Anal Chem* **2015,** *87* (14), 7187-95.

136. Liu, Y.; Li, R.; Ladisch, S., Exogenous ganglioside GD1a enhances epidermal growth factor receptor binding and dimerization. *J Biol Chem* **2004,** *279* (35), 36481-9.

137. Lopez, P. H.; Aja, S.; Aoki, K.; Seldin, M. M.; Lei, X.; Ronnett, G. V.; Wong, G. W.; Schnaar, R. L., Mice lacking sialyltransferase ST3Gal-II develop late-onset obesity and insulin resistance. *Glycobiology* **2017,** *27* (2), 129-139.

138. Lozano, R.; Naghavi, M.; Foreman, K.; Lim, S.; Shibuya, K.; Aboyans, V.; Abraham, J.; Adair, T.; Aggarwal, R.; Ahn, S. Y.; Alvarado, M.; Anderson, H. R.; Anderson, L. M.; Andrews, K. G.; Atkinson, C.; Baddour, L. M.; Barker-Collo, S.; Bartels, D. H.; Bell, M. L.; Benjamin, E. J.; Bennett, D.; Bhalla, K.; Bikbov, B.; Bin Abdulhak, A.; Birbeck, G.; Blyth, F.; Bolliger, I.; Boufous, S.; Bucello, C.; Burch, M.; Burney, P.; Carapetis, J.; Chen, H.; Chou, D.; Chugh, S. S.; Coffeng, L. E.; Colan, S. D.; Colquhoun, S.; Colson, K. E.; Condon, J.; Connor,

M. D.; Cooper, L. T.; Corriere, M.; Cortinovis, M.; de Vaccaro, K. C.; Couser, W.; Cowie, B. C.; Criqui, M. H.; Cross, M.; Dabhadkar, K. C.; Dahodwala, N.; De Leo, D.; Degenhardt, L.; Delossantos, A.; Denenberg, J.; Des Jarlais, D. C.; Dharmaratne, S. D.; Dorsey, E. R.; Driscoll, T.; Duber, H.; Ebel, B.; Erwin, P. J.; Espindola, P.; Ezzati, M.; Feigin, V.; Flaxman, A. D.; Forouzanfar, M. H.; Fowkes, F. G.; Franklin, R.; Fransen, M.; Freeman, M. K.; Gabriel, S. E.; Gakidou, E.; Gaspari, F.; Gillum, R. F.; Gonzalez-Medina, D.; Halasa, Y. A.; Haring, D.; Harrison, J. E.; Havmoeller, R.; Hay, R. J.; Hoen, B.; Hotez, P. J.; Hoy, D.; Jacobsen, K. H.; James, S. L.; Jasrasaria, R.; Jayaraman, S.; Johns, N.; Karthikeyan, G.; Kassebaum, N.; Keren, A.; Khoo, J. P.; Knowlton, L. M.; Kobusingye, O.; Koranteng, A.; Krishnamurthi, R.; Lipnick, M.; Lipshultz, S. E.; Ohno, S. L.; Mabweijano, J.; MacIntyre, M. F.; Mallinger, L.; March, L.; Marks, G. B.; Marks, R.; Matsumori, A.; Matzopoulos, R.; Mayosi, B. M.; McAnulty, J. H.; McDermott, M. M.; McGrath, J.; Mensah, G. A.; Merriman, T. R.; Michaud, C.; Miller, M.; Miller, T. R.; Mock, C.; Mocumbi, A. O.; Mokdad, A. A.; Moran, A.; Mulholland, K.; Nair, M. N.; Naldi, L.; Narayan, K. M.; Nasseri, K.; Norman, P.; O'Donnell, M.; Omer, S. B.; Ortblad, K.; Osborne, R.; Ozgediz, D.; Pahari, B.; Pandian, J. D.; Rivero, A. P.; Padilla, R. P.; Perez-Ruiz, F.; Perico, N.; Phillips, D.; Pierce, K.; Pope, C. A., 3rd; Porrini, E.; Pourmalek, F.; Raju, M.; Ranganathan, D.; Rehm, J. T.; Rein, D. B.; Remuzzi, G.; Rivara, F. P.; Roberts, T.; De Leon, F. R.; Rosenfeld, L. C.; Rushton, L.; Sacco, R. L.; Salomon, J. A.; Sampson, U.; Sanman, E.; Schwebel, D. C.; Segui-Gomez, M.; Shepard, D. S.; Singh, D.; Singleton, J.; Sliwa, K.; Smith, E.; Steer, A.; Taylor, J. A.; Thomas, B.;

217

Tleyjeh, I. M.; Towbin, J. A.; Truelsen, T.; Undurraga, E. A.; Venketasubramanian, N.; Vijayakumar, L.; Vos, T.; Wagner, G. R.; Wang, M.; Wang, W.; Watt, K.; Weinstock, M. A.; Weintraub, R.; Wilkinson, J. D.; Woolf, A. D.; Wulf, S.; Yeh, P. H.; Yip, P.; Zabetian, A.; Zheng, Z. J.; Lopez, A. D.; Murray, C. J.; AlMazroa, M. A.; Memish, Z. A., Global and regional mortality from 235 causes of death for 20 age groups in 1990 and 2010: a systematic analysis for the Global Burden of Disease Study 2010. *Lancet* **2012,** *380* (9859), 2095-128.

139. Maccioni, H. J., Glycosylation of glycolipids in the Golgi complex. *J Neurochem* **2007,** *103 Suppl 1*, 81-90.

140. Maceyka, M.; Sankala, H.; Hait, N. C.; Le Stunff, H.; Liu, H.; Toman, R.; Collier, C.; Zhang, M.; Satin, L. S.; Merrill, A. H., Jr.; Milstien, S.; Spiegel, S., SphK1 and SphK2, sphingosine kinase isoenzymes with opposing functions in sphingolipid metabolism. *J Biol Chem* **2005,** *280* (44), 37118-29.

141. Magesh, S.; Moriya, S.; Suzuki, T.; Miyagi, T.; Ishida, H.; Kiso, M., Design, synthesis, and biological evaluation of human sialidase inhibitors. Part 1: selective inhibitors of lysosomal sialidase (NEU1). *Bioorg Med Chem Lett* **2008,** *18* (2), 532-7.

142. Maglione, V.; Marchi, P.; Di Pardo, A.; Lingrell, S.; Horkey, M.; Tidmarsh, E.; Sipione, S., Impaired ganglioside metabolism in Huntington's disease and neuroprotective role of GM1. *J Neurosci* **2010,** *30* (11), 4072-80.

143. Marconi, S.; De Toni, L.; Lovato, L.; Tedeschi, E.; Gaetti, L.; Acler, M.; Bonetti, B., Expression of gangliosides on glial and neuronal cells in normal and pathological adult human brain. *J Neuroimmunol* **2005,** *170* (1-2), 115-21.

144. McJarrow, P.; Schnell, N.; Jumpsen, J.; Clandinin, T., Influence of dietary gangliosides on neonatal brain development. *Nutr Rev* **2009,** *67* (8), 451-63.

145. Merrill, A. H., Jr., De novo sphingolipid biosynthesis: a necessary, but dangerous, pathway. *J Biol Chem* **2002,** *277* (29), 25843-6.

146. Merrill, A. H., Jr., Sphingolipid and glycosphingolipid metabolic pathways in the era of sphingolipidomics. *Chem Rev* **2011,** *111* (10), 6387-422.

147. Merrill, A. H., Jr.; Sullards, M. C.; Allegood, J. C.; Kelly, S.; Wang, E., Sphingolipidomics: high-throughput, structure-specific, and quantitative analysis of sphingolipids by liquid chromatography tandem mass spectrometry. *Methods* **2005,** *36* (2), 207-24.

148. Mikhalev, II; Molotkovskii Iu, G., [Synthesis and characteristics of fluorescent BODIPY-labeled gangliosides]. *Bioorg Khim* **2003,** *29* (2), 190-7.

149. Mikhalyov, I.; Gretskaya, N.; Johansson, L. B., Fluorescent BODIPY-labelled GM1 gangliosides designed for exploring lipid membrane properties and specific membrane-target interactions. *Chem Phys Lipids* **2009,** *159* (1), 38-44.

150. Millar, J. S., The sialylation of plasma lipoproteins. *Atherosclerosis* **2001,** *154* (1), 1-13.

151. Minguet, S.; Klasener, K.; Schaffer, A. M.; Fiala, G. J.; Osteso-Ibanez, T.; Raute, K.; Navarro-Lerida, I.; Hartl, F. A.; Seidl, M.; Reth, M.; Del Pozo, M. A.,

Caveolin-1-dependent nanoscale organization of the BCR regulates B cell tolerance. *Nat Immunol* **2017,** *18* (10), 1150-1159.

152. Mitsutake, S.; Kita, K.; Okino, N.; Ito, M., [14C]ceramide synthesis by sphingolipid ceramide N-deacylase: new assay for ceramidase activity detection. *Anal Biochem* **1997,** *247* (1), 52-7.

153. Miyagi, T.; Yamaguchi, K., Mammalian sialidases: physiological and pathological roles in cellular functions. *Glycobiology* **2012,** *22* (7), 880-96.

154. Mortensen, K.; Larsson, L. I., Effects of cytochalasin D on the actin cytoskeleton: association of neoformed actin aggregates with proteins involved in signaling and endocytosis. *Cell Mol Life Sci* **2003,** *60* (5), 1007-12.

155. Mullin, B. R.; Poore, C. M. B.; Rupp, B. H., Quantitation of gangliosides in the picomolar range. *Journal of Chromatography B: Biomedical Sciences and Applications* **1984,** *305* (C), 512-513.

156. Muthing, J., High-resolution thin-layer chromatography of gangliosides. *J Chromatogr A* **1996,** *720* (1-2), 3-25.

157. Nagata, Y.; Yamashiro, S.; Yodoi, J.; Lloyd, K. O.; Shiku, H.; Furukawa, K., Expression cloning of beta 1,4 N-acetylgalactosaminyltransferase cDNAs that determine the expression of GM2 and GD2 gangliosides. *J Biol Chem* **1992,** *267* (17), 12082-9.

158. Nagata, Y.; Yamashiro, S.; Yodoi, J.; Lloyd, K. O.; Shiku, H.; Furukawa, K., Expression cloning of beta 1,4 N-acetylgalactosaminyltransferase cDNAs that determine the expression of GM2 and GD2 gangliosides. *J Biol Chem* **1994,** *269* (9), 7045.

159. Nakagawa, T.; Tani, M.; Kita, K.; Ito, M., Preparation of fluorescence-labeled GM1 and sphingomyelin by the reverse hydrolysis reaction of sphingolipid ceramide N-deacylase as substrates for assay of sphingolipid-degrading enzymes and for detection of sphingolipid-binding proteins. *J Biochem* **1999,** *126* (3), 604-11.

160. Negroni, E.; Chigorno, V.; Tettamanti, G.; Sonnino, S., Evaluation of the efficiency of an assay procedure for gangliosides in human serum. *Glycoconj J* **1996,** *13* (3), 347-52.

161. Neuenhofer, S.; Schwarzmann, G.; Egge, H.; Sandhoff, K., Synthesis of lysogangliosides. *Biochemistry* **1985,** *24* (2), 525-532.

162. Neville, D. C.; Coquard, V.; Priestman, D. A.; te Vruchte, D. J.; Sillence, D. J.; Dwek, R. A.; Platt, F. M.; Butters, T. D., Analysis of fluorescently labeled glycosphingolipid-derived oligosaccharides following ceramide glycanase digestion and anthranilic acid labeling. *Anal Biochem* **2004,** *331* (2), 275-82.

163. Nicolson, G. L., The Fluid-Mosaic Model of Membrane Structure: still relevant to understanding the structure, function and dynamics of biological membranes after more than 40 years. *Biochim Biophys Acta* **2014,** *1838* (6), 1451-66.

164. Nilsson, O.; Svennerholm, L., Accumulation of glucosylceramide and glucosylsphingosine (psychosine) in cerebrum and cerebellum in infantile and juvenile Gaucher disease. *J Neurochem* **1982,** *39* (3), 709-18.

165. Novak, J.; Kriston-Pal, E.; Czibula, A.; Deak, M.; Kovacs, L.; Monostori, E.; Fajka-Boja, R., GM1 controlled lateral segregation of tyrosine kinase Lck

predispose T-cells to cell-derived galectin-1-induced apoptosis. *Mol Immunol* **2014,** *57* (2), 302-9.

166. O'Brien, J. P.; Brodbelt, J. S., Structural characterization of gangliosides and glycolipids via ultraviolet photodissociation mass spectrometry. *Anal Chem* **2013,** *85* (21), 10399-407.

167. Ogawa-Goto, K.; Funamoto, N.; Abe, T.; Nagashima, K., Different ceramide compositions of gangliosides between human motor and sensory nerves. *J Neurochem* **1990,** *55* (5), 1486-93.

168. Ohara, K.; Sano, M.; Kondo, A.; Kato, I., Two-dimensional mapping by high-performance liquid chromatography of pyridylamino oligosaccharides from various glycosphingolipids. *J Chromatogr* **1991,** *586* (1), 35-41.

169. Ohmi, Y.; Ohkawa, Y.; Tajima, O.; Sugiura, Y.; Furukawa, K.; Furukawa, K., Ganglioside deficiency causes inflammation and neurodegeneration via the activation of complement system in the spinal cord. *J Neuroinflammation* **2014,** *11*, 61.

170. Ohmi, Y.; Tajima, O.; Ohkawa, Y.; Yamauchi, Y.; Sugiura, Y.; Furukawa, K.; Furukawa, K., Gangliosides are essential in the protection of inflammation and neurodegeneration via maintenance of lipid rafts: elucidation by a series of ganglioside-deficient mutant mice. *J Neurochem* **2011,** *116* (5), 926-35.

171. Oikawa, N.; Matsubara, T.; Fukuda, R.; Yasumori, H.; Hatsuta, H.; Murayama, S.; Sato, T.; Suzuki, A.; Yanagisawa, K., Imbalance in fatty-acid-chain length of gangliosides triggers Alzheimer amyloid deposition in the precuneus. *PLoS One* **2015,** *10* (3), e0121356.

172. Olling, A.; Breimer, M. E.; Peltomaa, E.; Samuelsson, B. E.; Ghardashkhani, S., Electrospray ionization and collision-induced dissociation time-of-flight mass spectrometry of neutral glycosphingolipids. *Rapid Commun Mass Spectrom* **1998,** *12* (10), 637-45.

173. Olsen, B. A., Hydrophilic interaction chromatography using amino and silica columns for the determination of polar pharmaceuticals and impurities. *J Chromatogr A* **2001,** *913* (1-2), 113-22.

174. Orekhov, A. N.; Tertov, V. V.; Mukhin, D. N., Desialylated low density lipoprotein--naturally occurring modified lipoprotein with atherogenic potency. *Atherosclerosis* **1991,** *86* (2-3), 153-61.

175. Orihuela, R.; McPherson, C. A.; Harry, G. J., Microglial M1/M2 polarization and metabolic states. *Br J Pharmacol* **2016,** *173* (4), 649-65.

176. Ozawa, H.; Kotani, M.; Kawashima, I.; Tai, T., Generation of one set of monoclonal antibodies specific for b-pathway ganglio-series gangliosides. *Biochim Biophys Acta* **1992,** *1123* (2), 184-90.

177. Packard, R. R.; Libby, P., Inflammation in atherosclerosis: from vascular biology to biomarker discovery and risk prediction. *Clin Chem* **2008,** *54* (1), 24-38.

178. Palmano, K.; Rowan, A.; Guillermo, R.; Guan, J.; McJarrow, P., The role of gangliosides in neurodevelopment. *Nutrients* **2015,** *7* (5), 3891-913.

179. Pan, B.; Fromholt, S. E.; Hess, E. J.; Crawford, T. O.; Griffin, J. W.; Sheikh, K. A.; Schnaar, R. L., Myelin-associated glycoprotein and complementary axonal ligands, gangliosides, mediate axon stability in the CNS and PNS: neuropathology

and behavioral deficits in single- and double-null mice. *Exp Neurol* **2005,** *195* (1), 208-17.

180. Pan, X.; De Aragao, C. B. P.; Velasco-Martin, J. P.; Priestman, D. A.; Wu, H. Y.; Takahashi, K.; Yamaguchi, K.; Sturiale, L.; Garozzo, D.; Platt, F. M.; Lamarche-Vane, N.; Morales, C. R.; Miyagi, T.; Pshezhetsky, A. V., Neuraminidases 3 and 4 regulate neuronal function by catabolizing brain gangliosides. *FASEB J* **2017,** *31* (8), 3467-3483.

181. Pande, G., The role of membrane lipids in regulation of integrin functions. *Curr Opin Cell Biol* **2000,** *12* (5), 569-74.

182. Park, H.; Zhou, Y.; Costello, C. E., Direct analysis of sialylated or sulfated glycosphingolipids and other polar and neutral lipids using TLC-MS interfaces. *J Lipid Res* **2014,** *55* (4), 773-81.

183. Pastrana, J. L.; Sha, X.; Virtue, A.; Mai, J.; Cueto, R.; Lee, I. A.; Wang, H.; Yang, X. F., Regulatory T cells and Atherosclerosis. *J Clin Exp Cardiolog* **2012,** *2012* (Suppl 12), 2.

184. Perry, V. H.; Teeling, J., Microglia and macrophages of the central nervous system: the contribution of microglia priming and systemic inflammation to chronic neurodegeneration. *Semin Immunopathol* **2013,** *35* (5), 601-12.

185. Pilatte, Y.; Bignon, J.; Lambre, C. R., Sialic acids as important molecules in the regulation of the immune system: pathophysiological implications of sialidases in immunity. *Glycobiology* **1993,** *3* (3), 201-18.

186. Pinto, W. J.; Srinivasan, B.; Shepherd, S.; Schmidt, A.; Dickson, R. C.; Lester, R. L., Sphingolipid long-chain-base auxotrophs of Saccharomyces cerevisiae:

genetics, physiology, and a method for their selection. *J Bacteriol* **1992,** *174* (8), 2565-74.

187. Piszkiewicz, D.; Bruice, T. C., Glycoside hydrolysis. II. Intramolecular carboxyl and acetamido group catalysis in .beta.-glycoside hydrolysis. *Journal of the American Chemical Society* **1968,** *90* (8), 2156-2163.

188. Posse de Chaves, E.; Sipione, S., Sphingolipids and gangliosides of the nervous system in membrane function and dysfunction. *FEBS Lett* **2010,** *584* (9), 1748-59.

189. Pyo, H.; Joe, E.; Jung, S.; Lee, S. H.; Jou, I., Gangliosides activate cultured rat brain microglia. *J Biol Chem* **1999,** *274* (49), 34584-9.

190. Quehenberger, O.; Armando, A. M.; Brown, A. H.; Milne, S. B.; Myers, D. S.; Merrill, A. H.; Bandyopadhyay, S.; Jones, K. N.; Kelly, S.; Shaner, R. L.; Sullards, C. M.; Wang, E.; Murphy, R. C.; Barkley, R. M.; Leiker, T. J.; Raetz, C. R.; Guan, Z.; Laird, G. M.; Six, D. A.; Russell, D. W.; McDonald, J. G.; Subramaniam, S.; Fahy, E.; Dennis, E. A., Lipidomics reveals a remarkable diversity of lipids in human plasma. *J Lipid Res* **2010,** *51* (11), 3299-305.

191. Rao, C. S.; Lin, X.; Pike, H. M.; Molotkovsky, J. G.; Brown, R. E., Glycolipid transfer protein mediated transfer of glycosphingolipids between membranes: a model for action based on kinetic and thermodynamic analyses. *Biochemistry* **2004,** *43* (43), 13805-15.

192. Regina Todeschini, A.; Hakomori, S. I., Functional role of glycosphingolipids and gangliosides in control of cell adhesion, motility, and growth, through glycosynaptic microdomains. *Biochim Biophys Acta* **2008,** *1780* (3), 421-33.

193. Rockendorf, N.; Bade, S.; Hirst, T. R.; Gorris, H. H.; Frey, A., Synthesis of a fluorescent ganglioside GM1 derivative and screening of a synthetic peptide library for GM1 binding sequence motifs. *Bioconjug Chem* **2007,** *18* (2), 573-8.

194. Rohlfing, A.; Muthing, J.; Pohlentz, G.; Distler, U.; Peter-Katalinic, J.; Berkenkamp, S.; Dreisewerd, K., IR-MALDI-MS analysis of HPTLC-separated phospholipid mixtures directly from the TLC plate. *Anal Chem* **2007,** *79* (15), 5793-808.

195. Rosengren, B.; Mansson, J. E.; Svennerholm, L., Composition of gangliosides and neutral glycosphingolipids of brain in classical Tay-Sachs and Sandhoff disease: more lyso-GM2 in Sandhoff disease? *J Neurochem* **1987,** *49* (3), 834-40.

196. Rossjohn, J.; Pellicci, D. G.; Patel, O.; Gapin, L.; Godfrey, D. I., Recognition of CD1d-restricted antigens by natural killer T cells. *Nat Rev Immunol* **2012,** *12* (12), 845-57.

197. Rueda, R., The role of dietary gangliosides on immunity and the prevention of infection. *Br J Nutr* **2007,** *98 Suppl 1*, S68-73.

198. Ruelland, A.; Gallou, G.; Legras, B.; Paillard, F.; Cloarec, L., LDL sialic acid content in patients with coronary artery disease. *Clin Chim Acta* **1993,** *221* (1-2), 127-33.

199. Ruhaak, L. R.; Zauner, G.; Huhn, C.; Bruggink, C.; Deelder, A. M.; Wuhrer, M., Glycan labeling strategies and their use in identification and quantification. *Anal Bioanal Chem* **2010,** *397* (8), 3457-81.

200. Saito, M.; Sugiyama, K., Characterization of nuclear gangliosides in rat brain: concentration, composition, and developmental changes. *Arch Biochem Biophys* **2002,** *398* (2), 153-9.

201. Saito, M.; Wu, G.; Hui, M.; Masiello, K.; Dobrenis, K.; Ledeen, R. W.; Saito, M., Ganglioside accumulation in activated glia in the developing brain: comparison between WT and GalNAcT KO mice. *J Lipid Res* **2015,** *56* (8), 1434-48.

202. Salas, A.; Shimaoka, M.; Kogan, A. N.; Harwood, C.; von Andrian, U. H.; Springer, T. A., Rolling adhesion through an extended conformation of integrin alphaLbeta2 and relation to alpha I and beta I-like domain interaction. *Immunity* **2004,** *20* (4), 393-406.

203. Sandbhor, M. S.; Soya, N.; Albohy, A.; Zheng, R. B.; Cartmell, J.; Bundle, D. R.; Klassen, J. S.; Cairo, C. W., Substrate recognition of the membrane-associated sialidase NEU3 requires a hydrophobic aglycone. *Biochemistry* **2011,** *50* (32), 6753-62.

204. Sango, K.; Yamanaka, S.; Hoffmann, A.; Okuda, Y.; Grinberg, A.; Westphal, H.; McDonald, M. P.; Crawley, J. N.; Sandhoff, K.; Suzuki, K.; Proia, R. L., Mouse models of Tay-Sachs and Sandhoff diseases differ in neurologic phenotype and ganglioside metabolism. *Nat Genet* **1995,** *11* (2), 170-6.

205. Scandroglio, F.; Loberto, N.; Valsecchi, M.; Chigorno, V.; Prinetti, A.; Sonnino, S., Thin layer chromatography of gangliosides. *Glycoconj J* **2009,** *26* (8), 961-73.

206. Schauer, R.; Srinivasan, G. V.; Coddeville, B.; Zanetta, J. P.; Guerardel, Y., Low incidence of N-glycolylneuraminic acid in birds and reptiles and its absence in the platypus. *Carbohydr Res* **2009,** *344* (12), 1494-500.

207. Schengrund, C. L., Gangliosides: glycosphingolipids essential for normal neural development and function. *Trends Biochem Sci* **2015,** *40* (7), 397-406.

208. Scherer, M.; Bottcher, A.; Schmitz, G.; Liebisch, G., Sphingolipid profiling of human plasma and FPLC-separated lipoprotein fractions by hydrophilic interaction chromatography tandem mass spectrometry. *Biochim Biophys Acta* **2011,** *1811* (2), 68-75.

209. Scherer, M.; Leuthauser-Jaschinski, K.; Ecker, J.; Schmitz, G.; Liebisch, G., A rapid and quantitative LC-MS/MS method to profile sphingolipids. *J Lipid Res* **2010,** *51* (7), 2001-11.

210. Schmelzer, K.; Fahy, E.; Subramaniam, S.; Dennis, E. A., The lipid maps initiative in lipidomics. *Methods Enzymol* **2007,** *432*, 171-83.

211. Schnaar, R. L., Brain gangliosides in axon-myelin stability and axon regeneration. *FEBS Lett* **2010,** *584* (9), 1741-7.

212. Schnaar, R. L., Isolation of glycosphingolipids. *Methods Enzymol* **1994,** *230*, 348-70.

213. Schnaar, R. L.; Fromholt, S. E.; Gong, Y.; Vyas, A. A.; Laroy, W.; Wayman, D. M.; Heffer-Lauc, M.; Ito, H.; Ishida, H.; Kiso, M.; Griffin, J. W.; Shiekh, K. A., Immunoglobulin G-class mouse monoclonal antibodies to major brain gangliosides. *Anal Biochem* **2002,** *302* (2), 276-84.

214. Schnaar, R. L.; Gerardy-Schahn, R.; Hildebrandt, H., Sialic acids in the brain: gangliosides and polysialic acid in nervous system development, stability, disease, and regeneration. *Physiol Rev* **2014,** *94* (2), 461-518.

215. Schwarzmann, G.; Wendeler, M.; Sandhoff, K., Synthesis of novel NBD-GM1 and NBD-GM2 for the transfer activity of GM2-activator protein by a FRET-based assay system. *Glycobiology* **2005,** *15* (12), 1302-11.

216. Senn, H. J.; Orth, M.; Fitzke, E.; Wieland, H.; Gerok, W., Gangliosides in normal human serum. Concentration, pattern and transport by lipoproteins. *Eur J Biochem* **1989,** *181* (3), 657-62.

217. Seyrantepe, V.; Landry, K.; Trudel, S.; Hassan, J. A.; Morales, C. R.; Pshezhetsky, A. V., Neu4, a novel human lysosomal lumen sialidase, confers normal phenotype to sialidosis and galactosialidosis cells. *J Biol Chem* **2004,** *279* (35), 37021-9.

218. Seyrantepe, V.; Lema, P.; Caqueret, A.; Dridi, L.; Bel Hadj, S.; Carpentier, S.; Boucher, F.; Levade, T.; Carmant, L.; Gravel, R. A.; Hamel, E.; Vachon, P.; Di Cristo, G.; Michaud, J. L.; Morales, C. R.; Pshezhetsky, A. V., Mice doubly-deficient in lysosomal hexosaminidase A and neuraminidase 4 show epileptic crises and rapid neuronal loss. *PLoS Genet* **2010,** *6* (9), e1001118.

219. Shaner, R. L.; Allegood, J. C.; Park, H.; Wang, E.; Kelly, S.; Haynes, C. A.; Sullards, M. C.; Merrill, A. H., Jr., Quantitative analysis of sphingolipids for lipidomics using triple quadrupole and quadrupole linear ion trap mass spectrometers. *J Lipid Res* **2009,** *50* (8), 1692-707.

220. Sharma, D. K.; Brown, J. C.; Cheng, Z.; Holicky, E. L.; Marks, D. L.; Pagano, R. E., The glycosphingolipid, lactosylceramide, regulates beta1-integrin clustering and endocytosis. *Cancer Res* **2005,** *65* (18), 8233-41.

221. Sheikh, K. A.; Sun, J.; Liu, Y.; Kawai, H.; Crawford, T. O.; Proia, R. L.; Griffin, J. W.; Schnaar, R. L., Mice lacking complex gangliosides develop Wallerian degeneration and myelination defects. *Proc Natl Acad Sci U S A* **1999,** *96* (13), 7532-7.

222. Shrestha, D.; Exley, M. A.; Vereb, G.; Szollosi, J.; Jenei, A., CD1d favors MHC neighborhood, GM1 ganglioside proximity and low detergent sensitive membrane regions on the surface of B lymphocytes. *Biochim Biophys Acta* **2014,** *1840* (1), 667-80.

223. Sieve, I.; Ricke-Hoch, M.; Kasten, M.; Battmer, K.; Stapel, B.; Falk, C. S.; Leisegang, M. S.; Haverich, A.; Scherr, M.; Hilfiker-Kleiner, D., A positive feedback loop between IL-1beta, LPS and NEU1 may promote atherosclerosis by enhancing a pro-inflammatory state in monocytes and macrophages. *Vascul Pharmacol* **2018,** *103-105*, 16-28.

224. Smith, J.; Mittermayr, S.; Varadi, C.; Bones, J., Quantitative glycomics using liquid phase separations coupled to mass spectrometry. *Analyst* **2017,** *142* (5), 700-720.

225. Smith, R. J.; Justen, J. M.; Sam, L. M., Function and stimulus-specific effects of phorbol 12-myristate 13-acetate on human polymorphonuclear neutrophils: autoregulatory role for protein kinase C in signal transduction. *Inflammation* **1988,** *12* (6), 597-611.

226. Sommer, U.; Herscovitz, H.; Welty, F. K.; Costello, C. E., LC-MS-based method for the qualitative and quantitative analysis of complex lipid mixtures. *J Lipid Res* **2006,** *47* (4), 804-14.

227. Song, X.; Ju, H.; Lasanajak, Y.; Kudelka, M. R.; Smith, D. F.; Cummings, R. D., Oxidative release of natural glycans for functional glycomics. *Nat Methods* **2016,** *13* (6), 528-34.

228. Sonnino, S.; Chigorno, V., Ganglioside molecular species containing C18- and C20-sphingosine in mammalian nervous tissues and neuronal cell cultures. *Biochim Biophys Acta* **2000,** *1469* (2), 63-77.

229. Spector, A. A.; Yorek, M. A., Membrane lipid composition and cellular function. *J Lipid Res* **1985,** *26* (9), 1015-35.

230. Spitz, C.; Winkels, H.; Burger, C.; Weber, C.; Lutgens, E.; Hansson, G. K.; Gerdes, N., Regulatory T cells in atherosclerosis: critical immune regulatory function and therapeutic potential. *Cell Mol Life Sci* **2016,** *73* (5), 901-22.

231. Sturgill, E. R.; Aoki, K.; Lopez, P. H.; Colacurcio, D.; Vajn, K.; Lorenzini, I.; Majic, S.; Yang, W. H.; Heffer, M.; Tiemeyer, M.; Marth, J. D.; Schnaar, R. L., Biosynthesis of the major brain gangliosides GD1a and GT1b. *Glycobiology* **2012,** *22* (10), 1289-301.

232. Sugiura, Y.; Shimma, S.; Konishi, Y.; Yamada, M. K.; Setou, M., Imaging mass spectrometry technology and application on ganglioside study; visualization of age-dependent accumulation of C20-ganglioside molecular species in the mouse hippocampus. *PLoS One* **2008,** *3* (9), e3232.

233. Sullards, M. C.; Allegood, J. C.; Kelly, S.; Wang, E.; Haynes, C. A.; Park, H.; Chen, Y.; Merrill, A. H., Jr., Structure-specific, quantitative methods for analysis of sphingolipids by liquid chromatography-tandem mass spectrometry: "inside-out" sphingolipidomics. *Methods Enzymol* **2007,** *432*, 83-115.

234. Suzuki, A.; Suzuki, M.; Ito, E.; Nitta, T.; Inokuchi, J. I., Mass Spectrometry of Gangliosides. *Methods Mol Biol* **2018,** *1804*, 207-221.

235. Suzuki, Y., Sialobiology of influenza: molecular mechanism of host range variation of influenza viruses. *Biol Pharm Bull* **2005,** *28* (3), 399-408.

236. Svennerholm, L., Designation and schematic structure of gangliosides and allied glycosphingolipids. *Prog Brain Res* **1994,** *101*, XI-XIV.

237. Svennerholm, L.; Fredman, P., A procedure for the quantitative isolation of brain gangliosides. *Biochim Biophys Acta* **1980,** *617* (1), 97-109.

238. Takamiya, K.; Yamamoto, A.; Furukawa, K.; Yamashiro, S.; Shin, M.; Okada, M.; Fukumoto, S.; Haraguchi, M.; Takeda, N.; Fujimura, K.; Sakae, M.; Kishikawa, M.; Shiku, H.; Furukawa, K.; Aizawa, S., Mice with disrupted GM2/GD2 synthase gene lack complex gangliosides but exhibit only subtle defects in their nervous system. *Proc Natl Acad Sci U S A* **1996,** *93* (20), 10662-7.

239. Takenouchi, H.; Kiyokawa, N.; Taguchi, T.; Matsui, J.; Katagiri, Y. U.; Okita, H.; Okuda, K.; Fujimoto, J., Shiga toxin binding to globotriaosyl ceramide induces intracellular signals that mediate cytoskeleton remodeling in human renal carcinoma-derived cells. *J Cell Sci* **2004,** *117* (Pt 17), 3911-22.

240. Taketomi, T.; Hara, A.; Uemura, K.; Sugiyama, E., Rapid method of preparation of lysoglycosphingolipids and their confirmation by delayed extraction matrix-assisted laser desorption ionization time-of-flight mass spectrometry. *J Biochem* **1996,** *120* (3), 573-9.

241. Tanaka, K.; Miyazawa, M.; Mikami, M.; Aoki, D.; Kiguchi, K.; Iwamori, M., Enhanced expression of unique gangliosides with GM2-determinant in human uterine cervical carcinoma-derived cell lines. *Glycoconj J* **2016,** *33* (5), 745-54.

242. Tangvoranuntakul, P.; Gagneux, P.; Diaz, S.; Bardor, M.; Varki, N.; Varki, A.; Muchmore, E., Human uptake and incorporation of an immunogenic nonhuman dietary sialic acid. *Proc Natl Acad Sci U S A* **2003,** *100* (21), 12045-50.

243. Tauber, R.; Park, C. S.; Reutter, W., Intramolecular heterogeneity of degradation in plasma membrane glycoproteins: evidence for a general characteristic. *Proc Natl Acad Sci U S A* **1983,** *80* (13), 4026-9.

244. Tettamanti, G., Ganglioside/glycosphingolipid turnover: new concepts. *Glycoconj J* **2004,** *20* (5), 301-17.

245. Tiralongo, J., Chapter 29 - Sialic acid-specific microbial lectins. In *Microbial Glycobiology*, Holst, O.; Brennan, P. J.; Itzstein, M. v.; Moran, A. P., Eds. Academic Press: San Diego, 2010; pp 585-598.

246. Torretta, E.; Vasso, M.; Fania, C.; Capitanio, D.; Bergante, S.; Piccoli, M.; Tettamanti, G.; Anastasia, L.; Gelfi, C., Application of direct HPTLC-MALDI for the qualitative and quantitative profiling of neutral and acidic glycosphingolipids: the case of NEU3 overexpressing C2C12 murine myoblasts. *Electrophoresis* **2014,** *35* (9), 1319-28.

247. Touboul, D.; Brunelle, A.; Laprevote, O., Mass spectrometry imaging: Towards a lipid microscope? *Biochimie* **2011,** *93* (1), 113-9.

248. Tsai, B.; Gilbert, J. M.; Stehle, T.; Lencer, W.; Benjamin, T. L.; Rapoport, T. A., Gangliosides are receptors for murine polyoma virus and SV40. *EMBO J* **2003,** *22* (17), 4346-55.

249. Tu, J.; Yin, Y.; Xu, M.; Wang, R.; Zhu, Z.-J., Absolute quantitative lipidomics reveals lipidome-wide alterations in aging brain. *Metabolomics* **2017,** *14* (1), 5.

250. Tumanov, S.; Kamphorst, J. J., Recent advances in expanding the coverage of the lipidome. *Curr Opin Biotechnol* **2017,** *43*, 127-133.

251. Ulmer, C. Z.; Patterson, R. E.; Koelmel, J. P.; Garrett, T. J.; Yost, R. A., A Robust Lipidomics Workflow for Mammalian Cells, Plasma, and Tissue Using Liquid-Chromatography High-Resolution Tandem Mass Spectrometry. *Methods Mol Biol* **2017,** *1609*, 91-106.

252. Ulmer, C. Z.; Yost, R. A.; Chen, J.; Mathews, C. E.; Garrett, T. J., Liquid Chromatography-Mass Spectrometry Metabolic and Lipidomic Sample Preparation Workflow for Suspension-Cultured Mammalian Cells using Jurkat T lymphocyte Cells. *J Proteomics Bioinform* **2015,** *8* (6), 126-132.

253. van Kooyk, Y.; Figdor, C. G., Avidity regulation of integrins: the driving force in leukocyte adhesion. *Curr Opin Cell Biol* **2000,** *12* (5), 542-7.

254. van Meer, G.; Voelker, D. R.; Feigenson, G. W., Membrane lipids: where they are and how they behave. *Nat Rev Mol Cell Biol* **2008,** *9* (2), 112-24.

255. Varki, A., Evolutionary forces shaping the Golgi glycosylation machinery: why cell surface glycans are universal to living cells. *Cold Spring Harb Perspect Biol* **2011,** *3* (6).

256. Varki, A.; Cummings, R. D.; Aebi, M.; Packer, N. H.; Seeberger, P. H.; Esko, J. D.; Stanley, P.; Hart, G.; Darvill, A.; Kinoshita, T.; Prestegard, J. J.; Schnaar, R. L.; Freeze, H. H.; Marth, J. D.; Bertozzi, C. R.; Etzler, M. E.; Frank, M.; Vliegenthart, J. F.; Lutteke, T.; Perez, S.; Bolton, E.; Rudd, P.; Paulson, J.; Kanehisa, M.; Toukach, P.; Aoki-Kinoshita, K. F.; Dell, A.; Narimatsu, H.; York, W.; Taniguchi, N.; Kornfeld, S., Symbol Nomenclature for Graphical Representations of Glycans. *Glycobiology* **2015,** *25* (12), 1323-4.

257. Varki, N. M.; Varki, A., Diversity in cell surface sialic acid presentations: implications for biology and disease. *Lab Invest* **2007,** *87* (9), 851-7.

258. Vawter, M. P., Dysregulation of the neural cell adhesion molecule and neuropsychiatric disorders. *Eur J Pharmacol* **2000,** *405* (1-3), 385-95.

259. Veillon, L.; Go, S.; Matsuyama, W.; Suzuki, A.; Nagasaki, M.; Yatomi, Y.; Inokuchi, J., Identification of Ganglioside GM3 Molecular Species in Human Serum Associated with Risk Factors of Metabolic Syndrome. *PLoS One* **2015,** *10* (6), e0129645.

260. Vieira, D. B.; Thur, K.; Sultana, S.; Priestman, D.; van der Spoel, A. C., Verification and refinement of cellular glycosphingolipid profiles using HPLC. *Biochem Cell Biol* **2015,** *93* (6), 581-6.

261. Vlckova, H.; Jezkova, K.; Stetkova, K.; Tomsikova, H.; Solich, P.; Novakova, L., Study of the retention behavior of small polar molecules on different types of stationary phases used in hydrophilic interaction liquid chromatography. *J Sep Sci* **2014,** *37* (11), 1297-307.

262. Wang, P.; Zhang, J.; Bian, H.; Wu, P.; Kuvelkar, R.; Kung, T. T.; Crawley, Y.; Egan, R. W.; Billah, M. M., Induction of lysosomal and plasma membrane-bound sialidases in human T-cells via T-cell receptor. *Biochem J* **2004,** *380* (Pt 2), 425-33.

263. Wang, W. Q.; Gustafson, A., Ganglioside extraction from erythrocytes: a comparison study. *Acta Chem Scand* **1995,** *49* (12), 929-36.

264. Wang, Y.; Yamaguchi, K.; Wada, T.; Hata, K.; Zhao, X.; Fujimoto, T.; Miyagi, T., A close association of the ganglioside-specific sialidase Neu3 with caveolin in membrane microdomains. *J Biol Chem* **2002,** *277* (29), 26252-9.

265. Weishaupt, N.; Caughlin, S.; Yeung, K. K.; Whitehead, S. N., Differential Anatomical Expression of Ganglioside GM1 Species Containing d18:1 or d20:1 Sphingosine Detected by MALDI Imaging Mass Spectrometry in Mature Rat Brain. *Front Neuroanat* **2015,** *9*, 155.

266. Wells, T. N. C.; Proudfoot, A. E. I.; Power, C. A., Chemokine receptors and their role in leukocyte activation. *Immunology Letters* **1999,** *65* (1), 35-40.

267. Wickramasinghe, S.; Medrano, J. F., Primer on genes encoding enzymes in sialic acid metabolism in mammals. *Biochimie* **2011,** *93* (10), 1641-1646.

268. Williams, R. D.; Wang, E.; Merrill, A. H., Jr., Enzymology of long-chain base synthesis by liver: characterization of serine palmitoyltransferase in rat liver microsomes. *Arch Biochem Biophys* **1984,** *228* (1), 282-91.

269. Wing, D. R.; Garner, B.; Hunnam, V.; Reinkensmeier, G.; Andersson, U.; Harvey, D. J.; Dwek, R. A.; Platt, F. M.; Butters, T. D., High-performance liquid chromatography analysis of ganglioside carbohydrates at the picomole level after

ceramide glycanase digestion and fluorescent labeling with 2-aminobenzamide. *Anal Biochem* **2001,** *298* (2), 207-17.

270. Winograd, N.; Garrison, B. J., Biological cluster mass spectrometry. *Annu Rev Phys Chem* **2010,** *61*, 305-22.

271. Wong, M.; Xu, G.; Park, D.; Barboza, M.; Lebrilla, C. B., Intact glycosphingolipidomic analysis of the cell membrane during differentiation yields extensive glycan and lipid changes. *Sci Rep* **2018,** *8* (1), 10993.

272. Xu, X.; Monjusho, H.; Inagaki, M.; Hama, Y.; Yamaguchi, K.; Sakaguchi, K.; Iwamori, M.; Okino, N.; Ito, M., Fucosyl-GM1a, an endoglycoceramidase-resistant ganglioside of porcine brain. *J Biochem* **2007,** *141* (1), 1-7.

273. Yamashita, T.; Hashiramoto, A.; Haluzik, M.; Mizukami, H.; Beck, S.; Norton, A.; Kono, M.; Tsuji, S.; Daniotti, J. L.; Werth, N.; Sandhoff, R.; Sandhoff, K.; Proia, R. L., Enhanced insulin sensitivity in mice lacking ganglioside GM3. *Proc Natl Acad Sci U S A* **2003,** *100* (6), 3445-9.

274. Yamashita, T.; Wu, Y. P.; Sandhoff, R.; Werth, N.; Mizukami, H.; Ellis, J. M.; Dupree, J. L.; Geyer, R.; Sandhoff, K.; Proia, R. L., Interruption of ganglioside synthesis produces central nervous system degeneration and altered axon-glial interactions. *Proc Natl Acad Sci U S A* **2005,** *102* (8), 2725-30.

275. Yanagisawa, K., GM1 ganglioside and Alzheimer's disease. *Glycoconj J* **2015,** *32* (3-4), 87-91.

276. Yang, L. J.; Zeller, C. B.; Shaper, N. L.; Kiso, M.; Hasegawa, A.; Shapiro, R. E.; Schnaar, R. L., Gangliosides are neuronal ligands for myelin-associated glycoprotein. *Proc Natl Acad Sci U S A* **1996,** *93* (2), 814-8.

277. Yoshida, Y.; Furukawa, J. I.; Naito, S.; Higashino, K.; Numata, Y.; Shinohara, Y., Quantitative analysis of total serum glycome in human and mouse. *Proteomics* **2016,** *16* (21), 2747-2758.

278. Yu, R. K.; Macala, L. J.; Taki, T.; Weinfield, H. M.; Yu, F. S., Developmental changes in ganglioside composition and synthesis in embryonic rat brain. *J Neurochem* **1988,** *50* (6), 1825-9.

279. Yu, R. K.; Nakatani, Y.; Yanagisawa, M., The role of glycosphingolipid metabolism in the developing brain. *J Lipid Res* **2009,** *50 Suppl*, S440-5.

280. Yu, R. K.; Schengrund, C.-L., *Glycobiology of the nervous system*. New York, NY : Springer, 2014.: 2014.

281. Yu, R. K.; Tsai, Y. T.; Ariga, T.; Yanagisawa, M., Structures, biosynthesis, and functions of gangliosides--an overview. *J Oleo Sci* **2011,** *60* (10), 537-44.

282. Zama, K.; Hayashi, Y.; Ito, S.; Hirabayashi, Y.; Inoue, T.; Ohno, K.; Okino, N.; Ito, M., Simultaneous quantification of glucosylceramide and galactosylceramide by normal-phase HPLC using O-phtalaldehyde derivatives prepared with sphingolipid ceramide N-deacylase. *Glycobiology* **2009,** *19* (7), 767-75.

283. Zamfir, A. D.; Vukelic, Z.; Schneider, A.; Sisu, E.; Dinca, N.; Ingendoh, A., A novel approach for ganglioside structural analysis based on electrospray multiple-stage mass spectrometry. *J Biomol Tech* **2007,** *18* (4), 188-93.

284. Zanchetti, G.; Colombi, P.; Manzoni, M.; Anastasia, L.; Caimi, L.; Borsani, G.; Venerando, B.; Tettamanti, G.; Preti, A.; Monti, E.; Bresciani, R., Sialidase NEU3 is a peripheral membrane protein localized on the cell surface and in endosomal structures. *Biochem J* **2007,** *408* (2), 211-9.

285. Zarbock, A.; Lowell, C. A.; Ley, K., Spleen tyrosine kinase Syk is necessary for E-selectin-induced alpha(L)beta(2) integrin-mediated rolling on intercellular adhesion molecule-1. *Immunity* **2007,** *26* (6), 773-83.

286. Zhang, T.; Watson, D. G., A short review of applications of liquid chromatography mass spectrometry based metabolomics techniques to the analysis of human urine. *Analyst* **2015,** *140* (9), 2907-15.

287. Zhang, Y.; Albohy, A.; Zou, Y.; Smutova, V.; Pshezhetsky, A. V.; Cairo, C. W., Identification of selective inhibitors for human neuraminidase isoenzymes using C4,C7-modified 2-deoxy-2,3-didehydro-N-acetylneuraminic acid (DANA) analogues. *J Med Chem* **2013,** *56* (7), 2948-58.

288. Zhang, Y.; Wang, J.; Liu, J.; Han, J.; Xiong, S.; Yong, W.; Zhao, Z., Combination of ESI and MALDI mass spectrometry for qualitative, semi-quantitative and in situ analysis of gangliosides in brain. *Sci Rep* **2016,** *6*, 25289.

289. Zhu, T.; Xu, L.; Xu, X.; Wang, Z.; Zhu, J.; Xie, Q.; Zhang, B.; Wang, Y.; Ju, L.; He, Y.; Ye, X.; Zhou, D.; Li, Y., Analysis of breast cancer-associated glycosphingolipids using electrospray ionization-linear ion trap quadrupole mass spectrometry. *Carbohydr Res* **2015,** *402*, 189-99.

290. Zhuo, D.; Li, X.; Guan, F., Biological Roles of Aberrantly Expressed Glycosphingolipids and Related Enzymes in Human Cancer Development and Progression. *Front Physiol* **2018,** *9*, 466.

APPENDIX A: SUPPORTING INFORMATION FOR CHAPTER 2
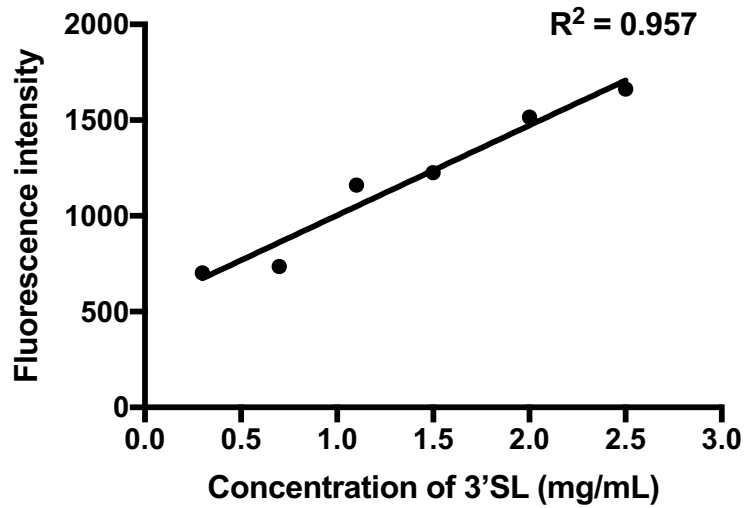
Figure A– 1. Calibration curve of serial dilutions of 2AA labeled 3-sialyllactose (3'-SL) vs fluorescence intensity. A representative linear calibration curve of a range of different concentrations of 3'SL in mg/mL against fluorescence intensity obtained for each concentration. Fluorescence was measured by monitoring at an excitation wavelength of 320 nm and an emission wavelength of 420 nm. The curve was linear over a range of different concentrations. This calibration curve was used to extrapolate the concentration of an unknown sample of ganglioside GM3 after EGCase digestion at 37 °C for 18 hours in a reaction buffer (pH 5.2), followed by 2-AA labeling. Using the value of this concentration, the specific activity of the enzyme was calculated for every new batch of enzyme produced.
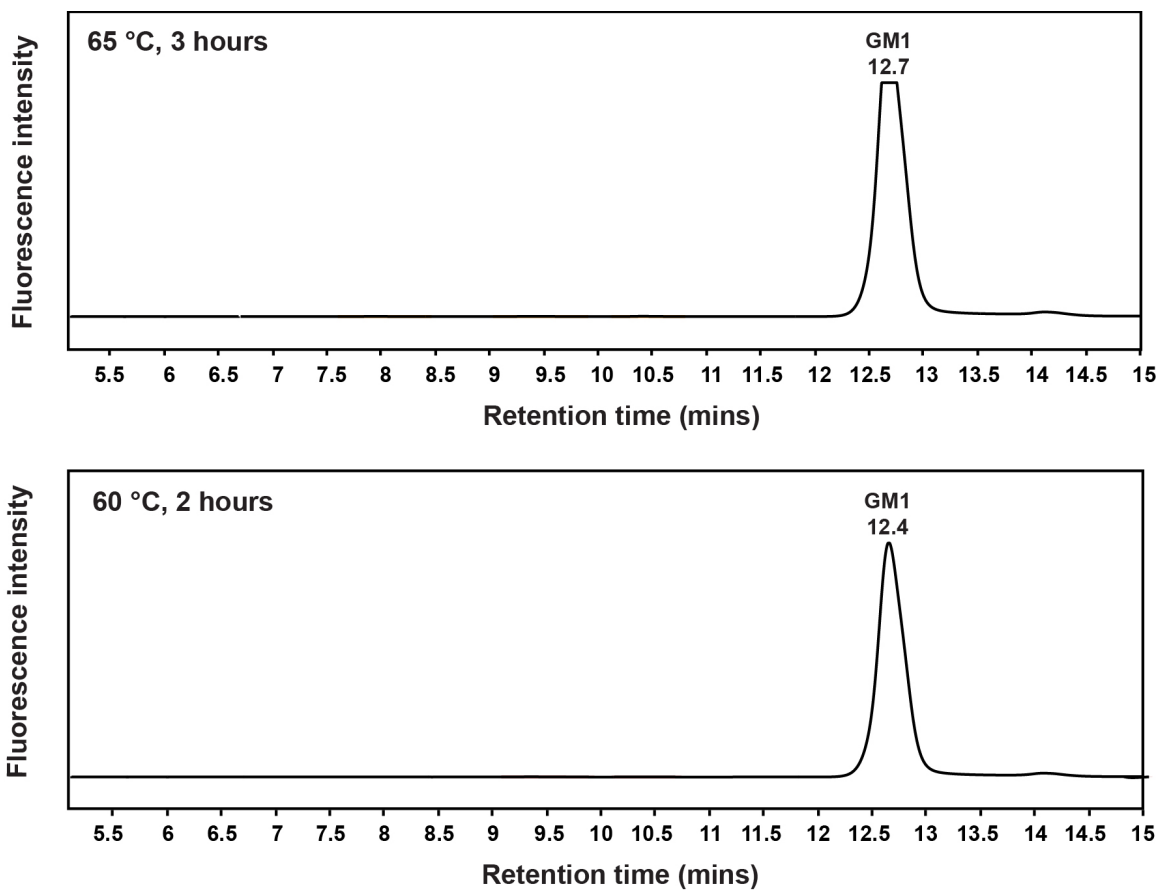
Figure A–2. Chromatogram showing 2-AA labeled GM1-glycan. Standard ganglioside GM1 was subjected to EGCase digestion at 37 °C for 18 hours in a reaction buffer (pH 5.2), followed by 2-AA labeling of GM1-glycan at 65 °C for 3 hours and 60 °C for 2 hours. Only one single peak was observed for GM1-glycan, confirming no loss of sialic acid under digestion and labeling conditions.
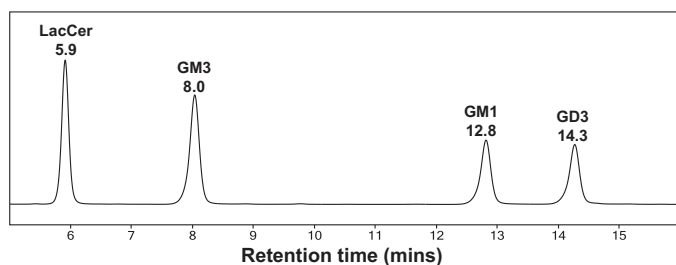
1	Area	% of Total Area
LacCer	3726752.5	29.78754031
GM3	4141856.52	33.10542303
GM1	2280339.05	18.22650991
GD3	2362163.83	18.88052676
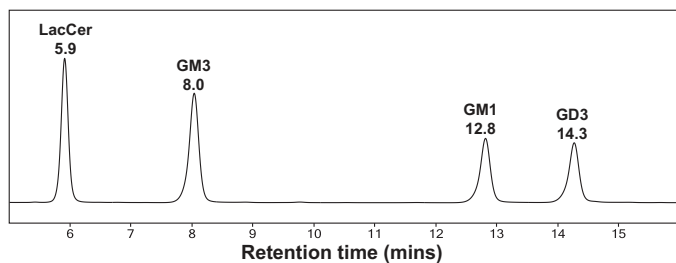
2	Area	% of Total Area
LacCer	3727989.35	29.65290151
GM3	4176123.95	33.21742113
GM1	2286200.99	18.18473349
GD3	2381775.32	18.94494387
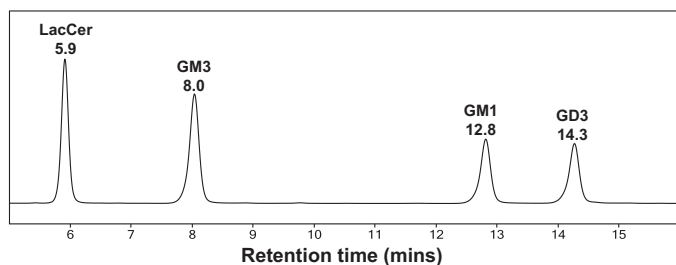
3	Area	% of Total Area
LacCer	3665651.42	29.29999958
GM3	4151283.85	33.18171891
GM1	2306925.85	18.43954012
GD3	2386894.76	19.07874139

Figure A– 3. Percent recovery of a standard GSL mixture containing LacCer, GM3, GM1, and GD3.

A mixture of LacCer, GM3, GM1, and GD3 containing approximately equal amounts of each GSL was subjected to EGCase I digestion at 37 °C for 18 hours followed by 2-AA labeling. Three replicate chromatograms of samples subjected to SepPak C18 and Discovery DPA-6S amide-HILIC clean up (C18 + HILIC) shown here. The fluorescent peak areas of each GSL are represented as a percent of the total fluorescence peak area of all GSLs in the mixture. Values represent mean ± standard error of mean (SEM) of triplicate measurements (n = 3).
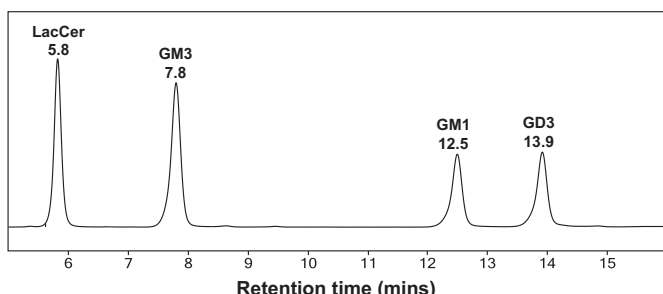
1	Area	% of Total Area
LacCer	6112880.27	30.39658271
GM3	6304607.79	31.34995676
GM1	3958828.5	19.68545966
GD3	3734102.85	18.56800086
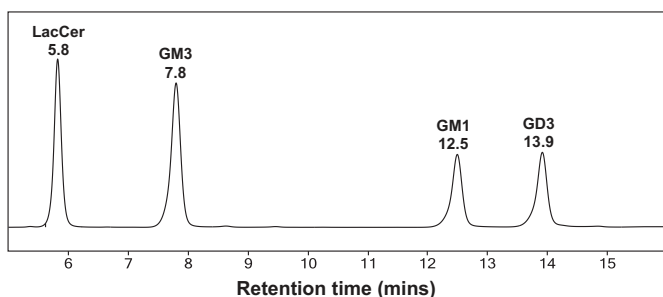
2	Area	% of Total Area
LacCer	5915101.64	29.75277794
GM3	6289480.49	31.63589196
GM1	3957801.63	19.90761955
GD3	3718454.43	18.70371055
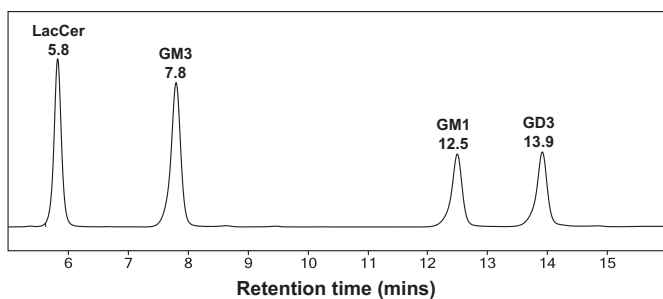
3	Area	% of Total Area
LacCer	5943598.53	29.78268324
GM3	6332050.04	31.72916873
GM1	3942874.82	19.75728866
GD3	3738034.86	18.73085937

Figure A– 4. Percent recovery of a standard GSL mixture containing LacCer, GM3, GM1, and GD3.

A mixture of LacCer, GM3, GM1, and GD3 containing approximately equal amounts of each GSL was subjected to EGCase I digestion at 37 °C for 18 hours followed by 2-AA labeling. Three replicate chromatograms of samples subjected to only Discovery DPA-6S amide-HILIC clean up (Only HILIC) are shown here. The fluorescent peak areas of each GSL are represented as a percent of the total fluorescence peak area of all GSLs in the mixture. Values represent mean ± standard error of mean (SEM) of triplicate measurements (n = 3).
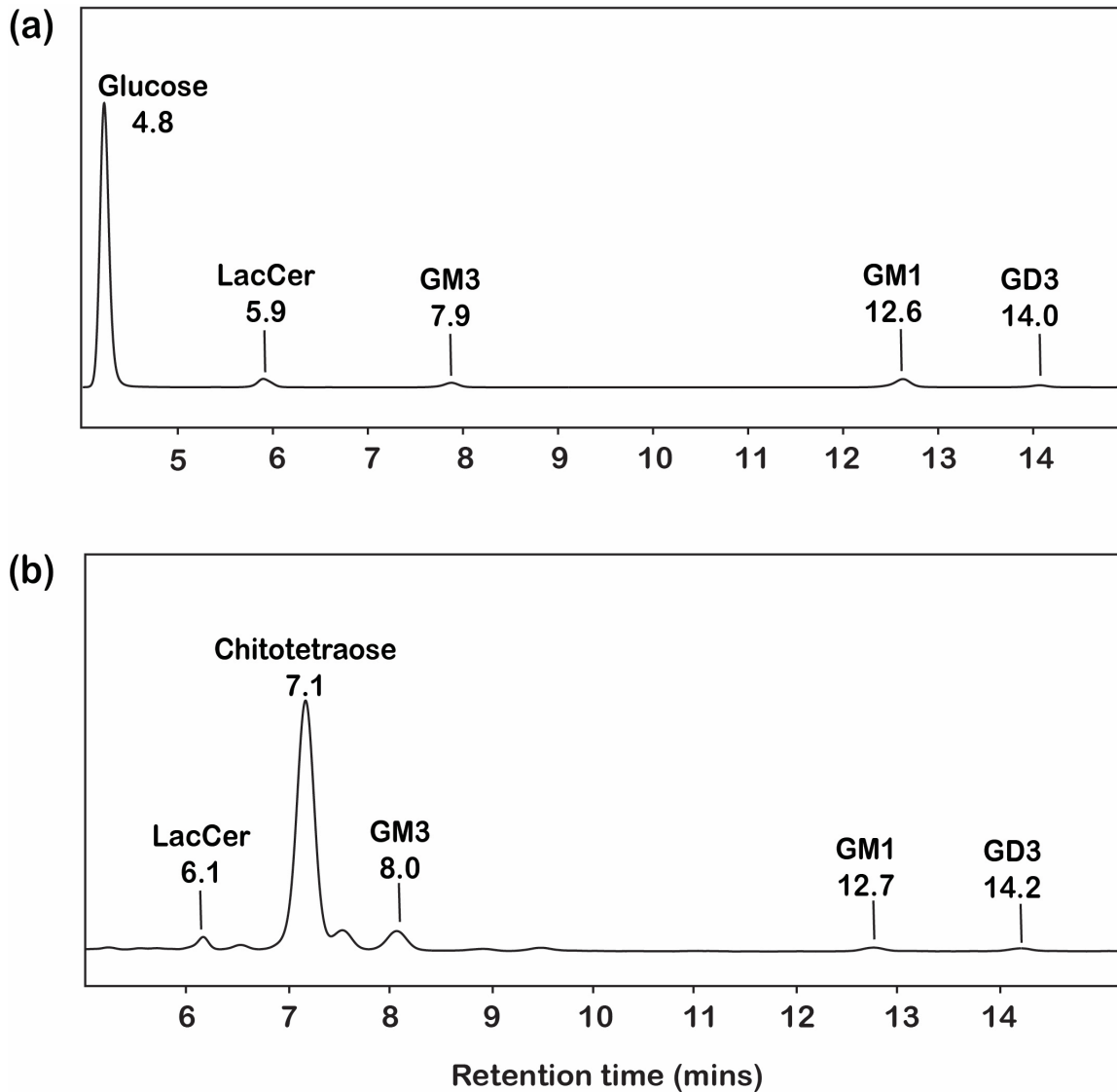
Figure A– 5. Selection of internal standard. A standard mixture of commercially available GLSs LacCer, GM3, GM1, and GD3 was subjected to EGCase digestion at 37 °C for 18 hours, followed by 2-AA labeling at 80 °C for 45 min. Prior to labeling, (a) glucose and (b) chitotetraose were added to see their separation in a complex mixture of GSLs. Glucose eluted earliest at ~ 4.8 min, and chitotetraose at ~ 7.1 min, very close to GM3. Glucose, being a glycan component of naturally occurring GSLs, was eliminated from the list of internal standard. Chitotetraose was still kept under consideration.

(a)

	Area	Area %	Conc (ug/ml)
Internal Standard	202136.54	100	0.05
LacCer	123074.87	60.886997	0.030443499
GM3	35513.1	17.568867	0.008784434
GM2	42863.42	21.205181	0.010602591
GM1	978429.3	484.04376	0.242021878
Fucosyl GM1	302260.63	149.5329	0.07476645
GD1a	906708.83	448.56256	0.224281278
GD1b	269117.3	133.13639	0.066568197
Fucosyl-GD1	44253.49	21.89287	0.010946435
GT1	90095.83	44.571768	0.022285884

(b)

	Area	Area %	Conc (ug/ml)
Internal Standard	396162.85	100	0.1
LacCer	136274.73	34.398665	0.034398665
GM3	46518.98	11.742388	0.011742388
GM2	32688.51	8.251281	0.008251281
GM1	1092525.8	275.77695	0.275776951
Fucosyl GM1	324421.5	81.890945	0.081890945
GD1a	1033656.9	260.91716	0.260917158
GD1b	247086.62	62.369962	0.062369962
Fucosyl-GD1	39982.49	10.092438	0.010092438
GT1	87579.74	22.107005	0.022107005

(c)

	Area	Area %	Conc (ug/ml)
Internal Standard	580265.79	100	0.15
LacCer	140647.33	24.238432	0.036357648
GM3	25707.23	4.4302508	0.006645376
GM2	38629.51	6.6572096	0.009985814
GM1	799681.78	137.81301	0.206719522
Fucosyl GM1	237428.85	40.917258	0.061375887
GD1a	597690.45	103.00288	0.154504313
GD1b	185580.82	31.982037	0.047973056
Fucosyl-GD1	29454.85	5.0760962	0.007614144
GT1	51088.5	8.8043274	0.013206491

Figure A–6. Glycosphingolipid (GSL) profiling in porcine brain. Three biological replicates, (a), (b), and (c) showing HPLC separation of 2-AA labeled oligosaccharides generated from EGCase digestion of GSLs extracted from porcine brain. For each run, 10 μL of brain homogenate (~ 2 mg wet tissue weight) were subjected to a chloroform-methanol-water extraction, as outlined in the Material and Methods Section. Dry GSL extract, ~ 0.5 mg, was subjected to enzyme cleavage and labeling. The GSLs identified were LacCer, GM3, GM2, GM1, Fucosyl-GM1, GD1a, GD1b, Fucosyl GD1, and GT1. Peak assignment was performed based on commercially available standards and further confirmed by HR-ESI-MS. Quantification was performed based on the amount of internal standard (IS*) maltose added, i.e., 0.05, 0.1 and 0.15 μg/mL in this case.
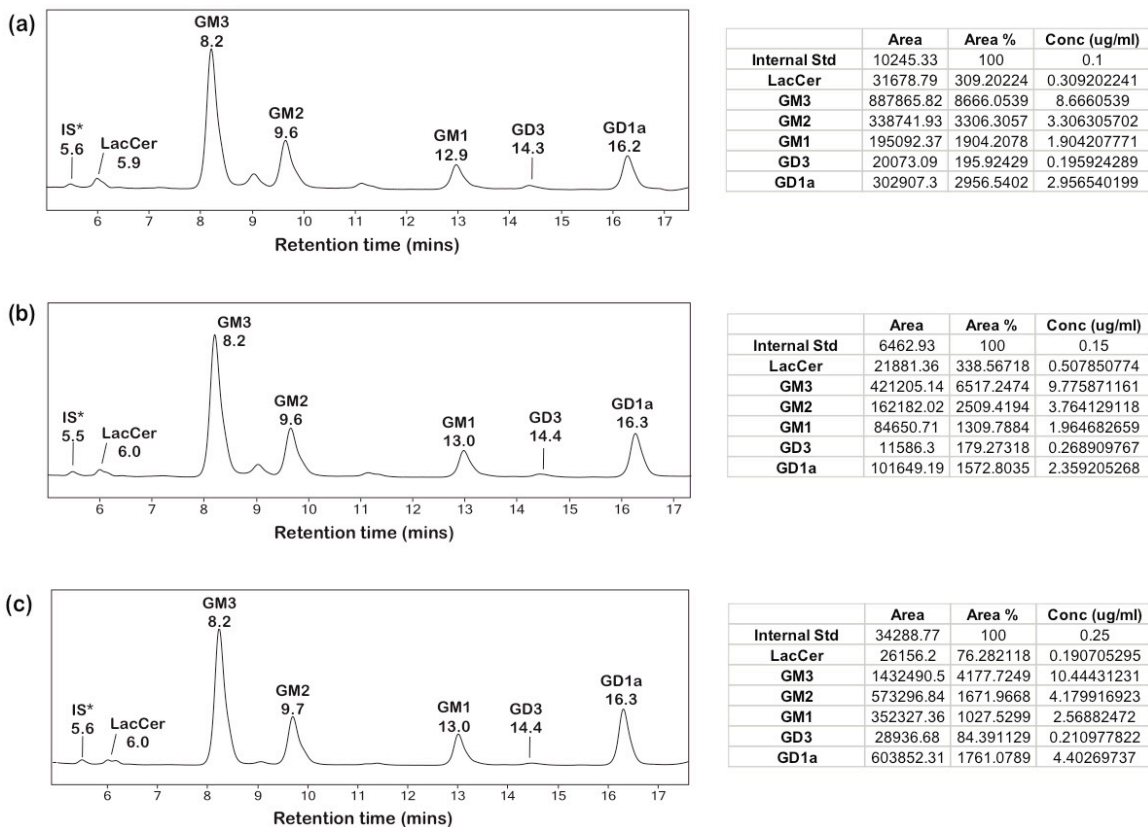
Figure A–7. Glycosphingolipid (GSL) profiling in Jurkat T-cells. Three biological replicates, (a), (b), and (c) showing HPLC separation of 2-AA labeled oligosaccharides generated from EGCase digestion of GSLs extracted from Jurkat T-cells. For each run, 1 x 10^6 cells were subjected to chloroform-methanol-water extraction, as outlined in the Materisl and Methods Section. Dry GSL extract, ~ 0.5 mg, was subjected to enzyme cleavage and labeling. The GSLs identified were LacCer, GM3, GM2, GM1, GD3, and GD1a, Peak assignment was performed based on commercially available standards and further confirmed by HR-ESI-MS. Quantification was performed based on the amount of internal standard (IS*) maltose added, i.e., 0.1, 0.15 and 0.25 µg/mL in this case.
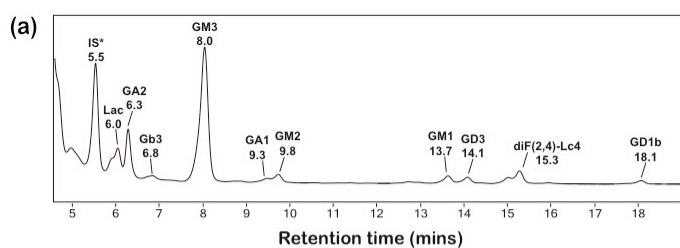
Run 1	Area	Area percentage	Conc (ug/ml)
IS	308330.92	100	0.143
LacCer	105303.93	34.15289326	0.048838637
GA2	124394.13	40.34435794	0.057692432
Gb3	16132.03	5.232050681	0.007481832
GM3	600771.76	194.8464202	0.278630381
GM2	17576.39	5.700495429	0.008151708
GA1	35301.14	11.44910799	0.016372224
GM1	33351.13	10.81666737	0.015467834
GD3	28065.48	9.102389082	0.013016416
diF(2,4)-Lc4	75881.54	24.61042182	0.035192903
GD1b	16309.7	5.289673835	0.007564234
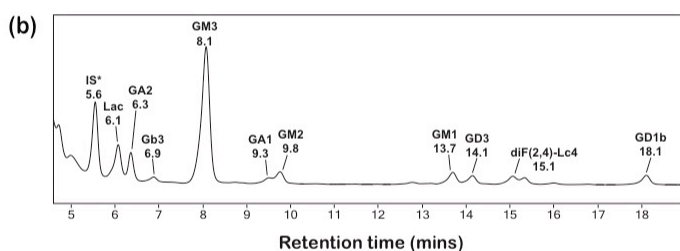
Run 2	Area	Area percentage	Conc (ug/ml)
IS	291264.13	100	0.143
LacCer	162920.62	55.93569658	0.079988046
GA2	103199.59	35.43161666	0.050667212
Gb3	27208.74	9.341603444	0.013358493
GM3	863860.87	296.5902015	0.424123988
GM2	34127.31	11.71696288	0.016755257
GA1	75150.81	25.80160145	0.03689629
GM1	73273.29	25.15699067	0.035974497
GD3	55304.04	18.9875904	0.027152254
diF(2,4)-Lc4	91349.67	31.36317198	0.044849336
GD1b	65868.21	22.61459727	0.032338874
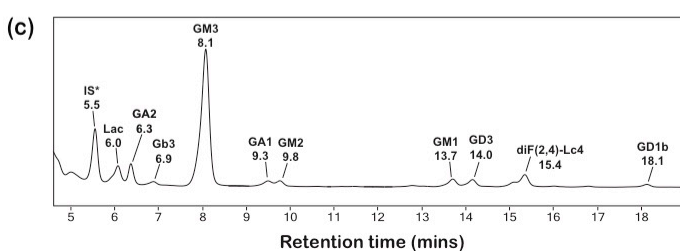
Run 3	Area	Area percentage	Conc (ug/ml)
IS	324627.36	100	0.143
LacCer	135165.64	41.63716823	0.059541151
GA2	114635.89	35.31307096	0.050497691
Gb3	31846.59	9.810198992	0.014028585
GM3	1325014.28	408.1646969	0.583675517
GM2	56191.34	17.30948987	0.024752571
GA1	48833.29	15.04287562	0.021511312
GM1	74903.4	23.0736559	0.032995328
GD3	72311.62	22.27526971	0.031853636
diF(2,4)-Lc4	112240.57	34.5752034	0.049442541
GD1b	31399.83	9.672576581	0.013831785

Figure A–8. Glycosphingolipid (GSL) profiling in normal human serum. Three biological replicates, (a), (b), and (c) showing HPLC separation of 2-AA labeled oligosaccharides generated from EGCase digestion of GSLs extracted from serum. For each run, 50 µL aliquots of serum were subjected to a chloroform-methanol-water extraction, as outlined in the Materials and Methods section. Dry GSL extract, ~ 0.5 mg, was subjected to enzyme cleavage and labeling. The GSLs identified were LacCer, Gb3, GA2, GM3, GA1, GM3, GM1, GD3, diFuc(1,4)-Lc4, and GD1b, Peak assignment was performed based on commercially available standards and further confirmed by HR-ESI-MS. Quantification was performed based on the amount of internal standard (IS*) maltose added, i.e., 0.143 µg/mL in this case.

Run 1	Area	Area percentage	Conc (ug/ml)
IS	255498.92	100	0.143
LacCer	195004.52	76.32303103	0.109141934
GA2	100968.76	39.51827272	0.05651113
Gb3	25329.33	9.913673999	0.014176554
GM3	967817.33	378.7950767	0.54167696
GM2	54584.84	21.36401986	0.030550548
GA1	58766.77	23.00078998	0.03289113
GM1	68262.74	26.717428	0.038205922
GD3	59370.14	23.23694362	0.033228829
diF(2,4)-Lc4	89589.41	35.06449655	0.05014223
GD1b	40731.29	15.94186386	0.022796865
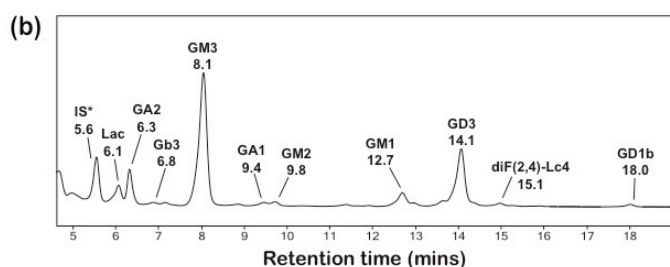
Run 2	Area	Area percentage	Conc (ug/ml)
IS	298099.97	100	0.143
LacCer	125824.09	42.20868925	0.060358426
GA2	189223.49	63.47652098	0.090771425
Gb3	21967.93	7.369316408	0.010538122
GM3	718933.17	241.1718357	0.344875725
GM2	45507.83	15.26596262	0.021830327
GA1	32185.97	10.79703899	0.015439766
GM1	35926.76	12.05191668	0.017234241
GD3	36184.13	12.13825349	0.017357702
diF(2,4)-Lc4	125020.86	41.93923938	0.059973112
GD1b	16796.22	5.634425257	0.008057228
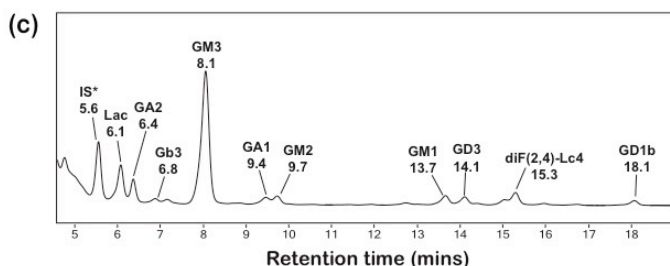
Run 3	Area	Area percentage	Conc (ug/ml)
IS	297565.72	100	0.143
LacCer	141695.52	47.61822699	0.068094065
GA2	219383.4	73.72603269	0.105428227
Gb3	20918.57	7.029899143	0.010052756
GM3	1364022.61	458.3937323	0.655503037
GM2	36776.19	12.35901434	0.017673391
GA1	39639.35	13.3212085	0.019049328
GM1	153929.38	51.72954062	0.073973243
GD3	643035.38	216.0986084	0.30902101
diF(2,4)-Lc4	31704.18	10.65451356	0.015235954
GD1b	29159.16	9.799233595	0.014012904

Figure A–9. Glycosphingolipid (GSL) profiling in serum from HD patients. Three biological replicates, (a), (b), and (c) showing HPLC separation of 2-AA labeled oligosaccharides generated from EGCase digestion of GSLs extracted from serum. For each run, 50 μL aliquots of serum were subjected to a chloroform-methanol-water extraction, as outlined in the Materials and Methods section. Dry GSL extract, ~ 0.5 mg, was subjected to enzyme cleavage and labeling. The GSLs identified were LacCer, Gb3, GA2, GM3, GA1, GM3, GM1, GD3, diFuc(1,4)-Lc4, and GD1b, Peak assignment was performed based on commercially available standards and further confirmed by HR-ESI-MS. Quantification was performed based on the amount of internal standard (IS*) maltose added, i.e., 0.143 μg/mL in this case.

Figure A–10. High Resolution-Electrospray Ionization Mass Spectrometry (HR-ESI-MS) of glycosphingolipids (GSLs) HR-ESI-MS spectra of 2-AA labeled (a) singly charged species of diF(2,4)-Lc4, (b) doubly charged species of Fuc-GD1, and (c) singly and double charged species of Fuc-GM1.
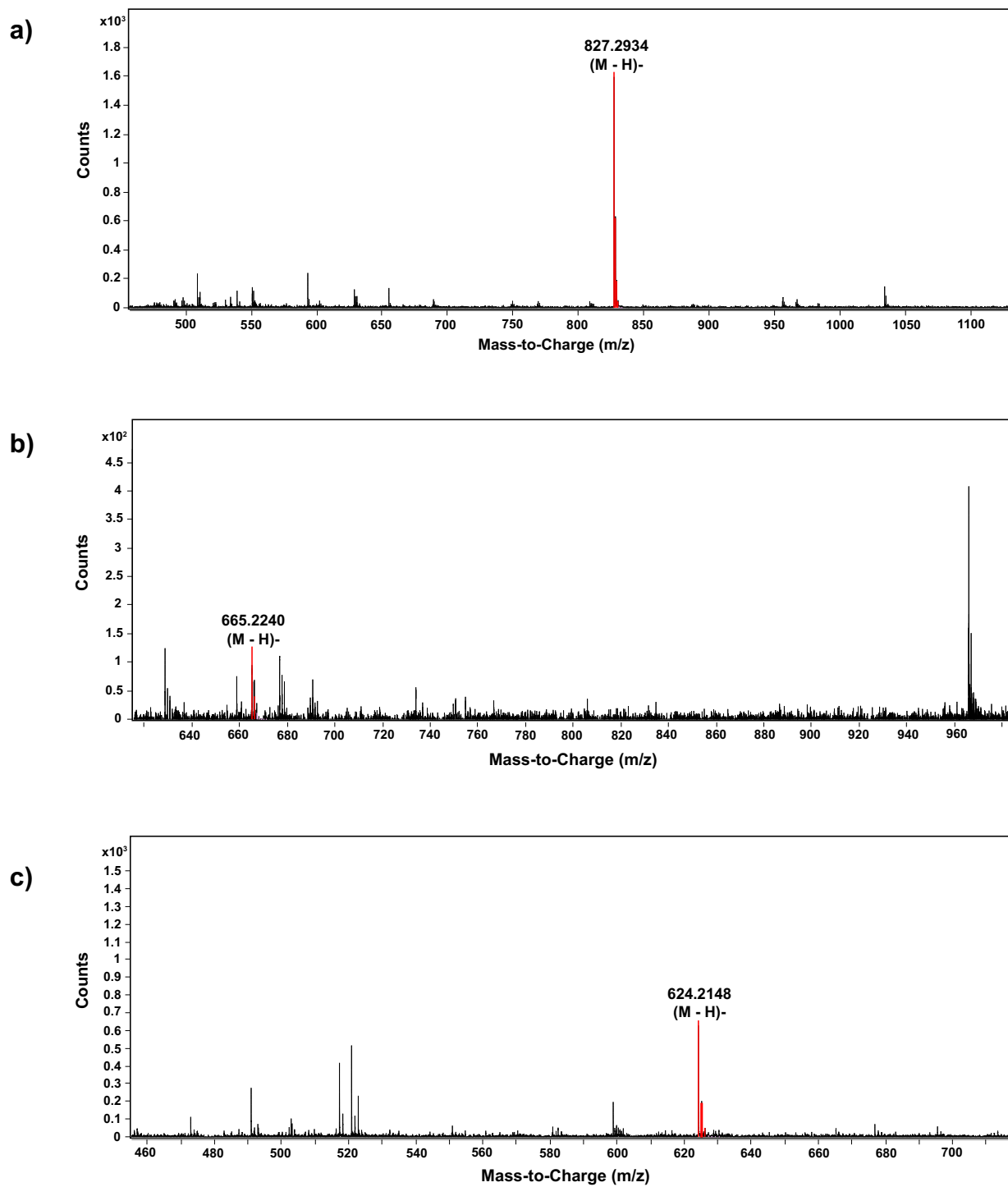
Figure A–11. High Resolution-Electrospray Ionization Mass Spectrometry (HR-ESI-MS) of glycosphingolipids (GSLs) HR-ESI-MS spectra of 2-AA labeled (a) singly charged species GA1, (b) singly charged species GA2, and (c) singly charged species Gb3.
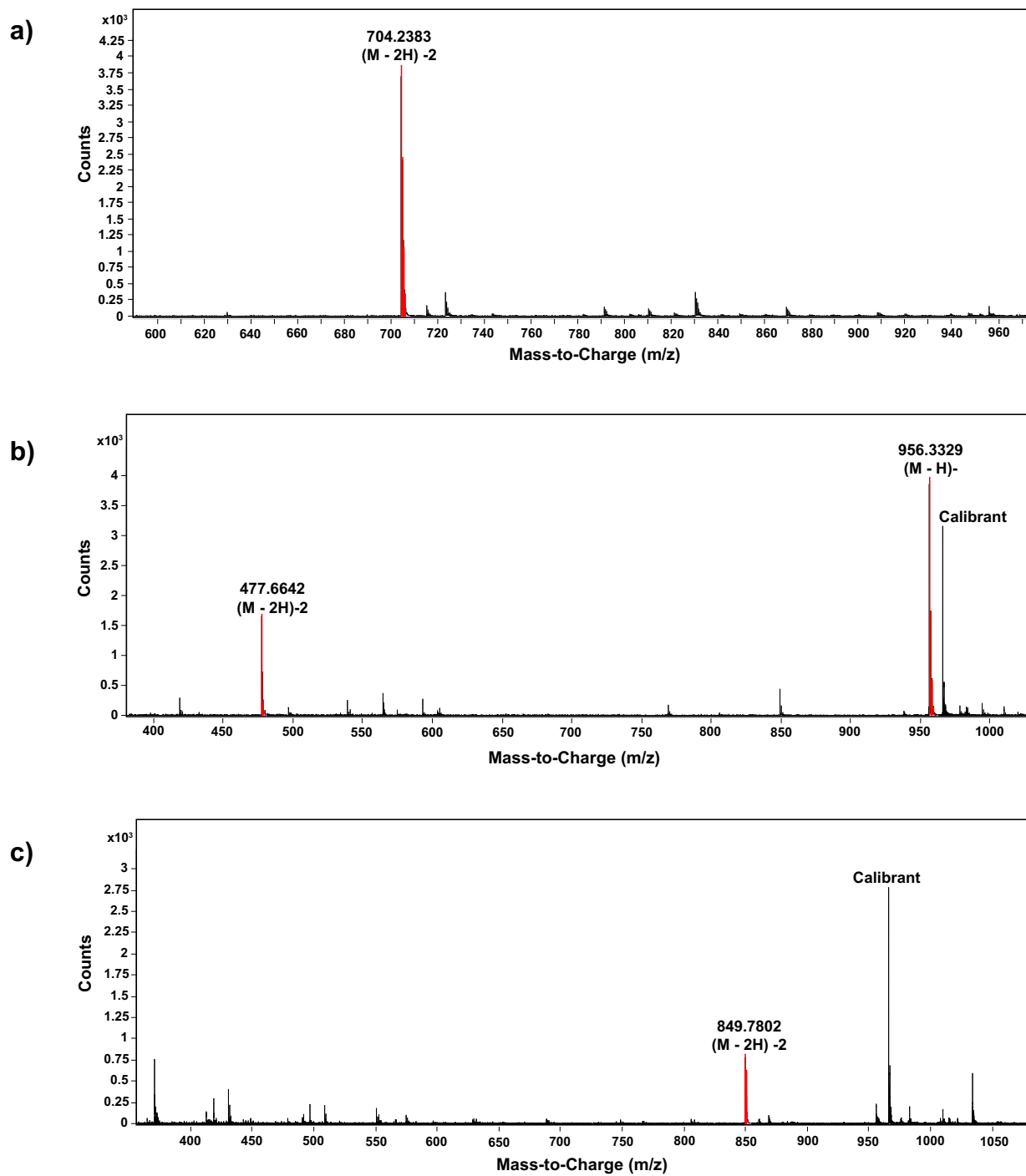
Figure A–12. High Resolution-Electrospray Ionization Mass Spectrometry (HR-ESI-MS) of glycosphingolipids (GSLs) HR-ESI-MS spectra of 2-AA labeled (a) doubly charged species of GD1, (b) singly and doubly charged species of GM2, and (c) doubly charged species of GT1.

Table A–1. Compound report showing all GSLs detected in human serum (normal and Huntington's patients) by HR-ESI-MS.

Glycosphingolipid	Target Mass	Mass detected
LacCer	463.1690	463.1683
GA2	666.2483	666.2454
Gb3	625.2218	625.2212
GM3	754.2544	754.2639
GM2	957.3438	957.3425
GA1	828.3012	828.3004
GM1	1119.3966	1119.3948
GD3	1045.3598	1045.3579
diF(2,4)-nLc4	1120.4170	1120.4166
GD1	1410.4920	1410.4861

Table A–2. Compound report showing all GSLs detected in porcine brain by HR-ESI-MS.

Glycosphingolipid	Target Mass	Mass detected
LacCer	463.1690	463.1687
GM3	754.2544	754.2632
GM2	957.3438	957.3447
GM1	1119.3966	1119.3956
Fucosyl-GM1	1265.4545	1265.4538
GD1a	1410.4920	1410.4913
GD1b	1410.4920	1410.4904
GT1a	1701.5874	1701.5854
GT1b	1701.5874	1701.5874

Table A–3. Compound report showing all GSLs detected in Jurkat T-cells by HR-ESI-MS.

Glycosphingolipid	Target Mass	Mass detected
LacCer	463.1690	463.1693
GM3	754.2544	754.2645
GM2	957.3438	957.3424
GM1	1119.3966	1119.3967
GD3	1045.3598	1045.3601
GD1	1410.4920	1410.4901

APPENDIX B: SUPPORTING INFORMATION FOR CHAPTER 4

Figure B– 1. MALDI-MS analysis of intact , standard ganglioside GD3

Figure B– 2. MALDI-MS analysis of intact, standard ganglioside GM3

D:\Data\MSService\2018\201802\180206_Chakraberty_Cairo\GM1\0_B5\1\1SRef

Comment 1   GM1, DHB, RP_300-5k_DHB, SS plate
Comment 2

GM1, DHB, RP_300-5k_DHB, SS plate

Intens. [a.u.] x10⁴

1523.89
1528.86
1550.89
1566.88
1568.89
1584.86
1590.89
1596.92
1618.93

28

m/z
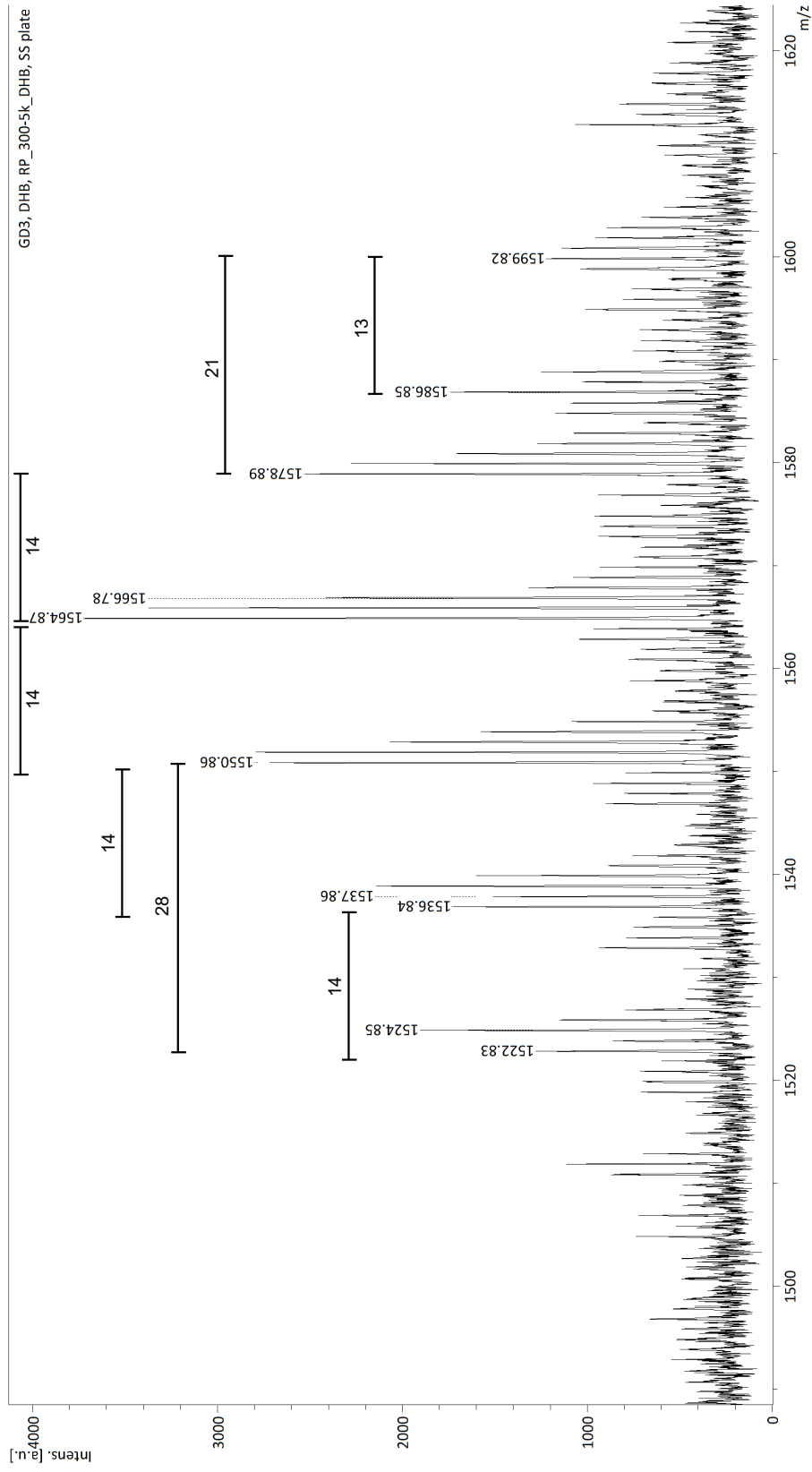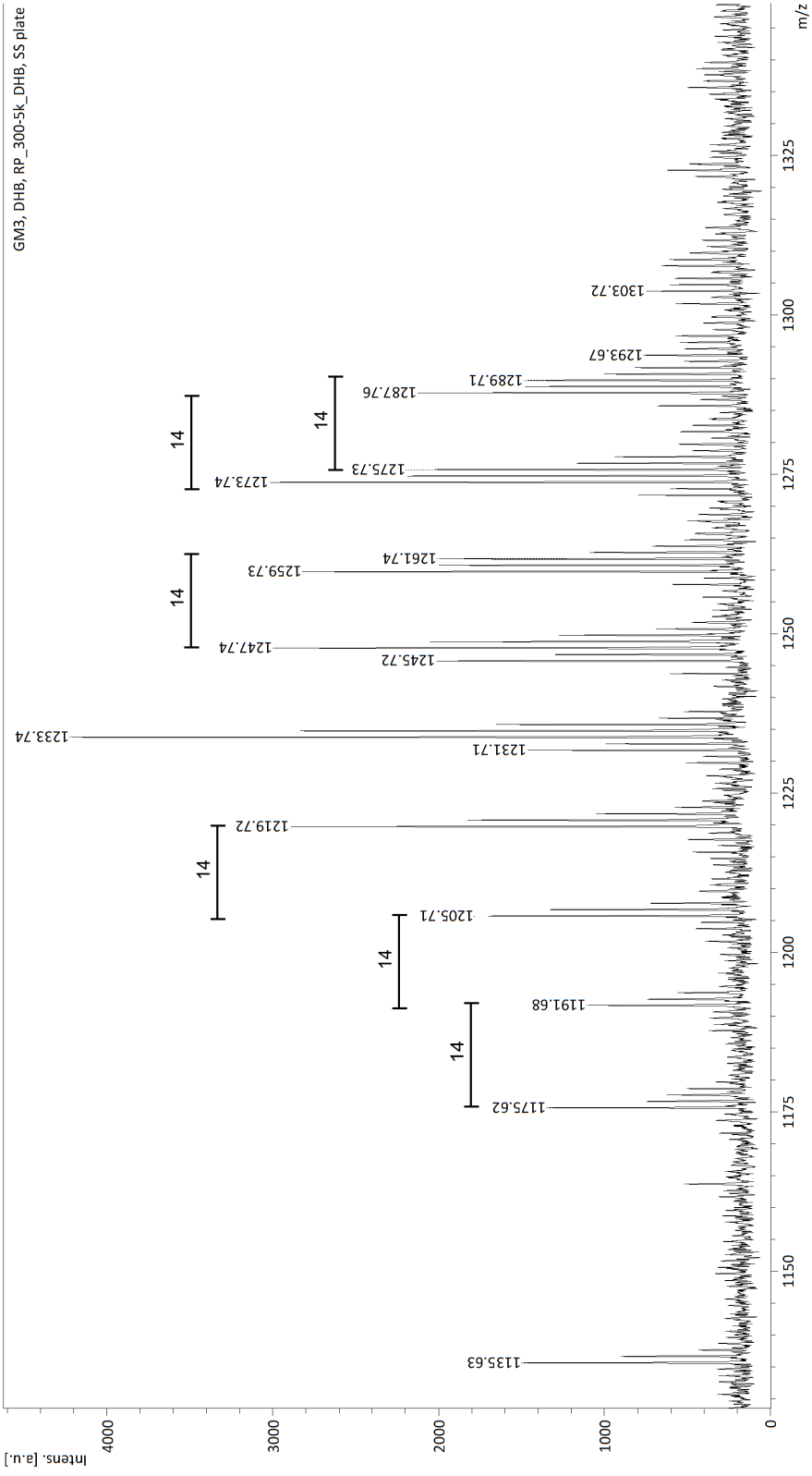
Mass Spectometry Facility, University of Alberta   Phone: 1-780-492-5577   http://www.chem.ualberta.ca/~massspec/

Figure B– 3. MALDI-MS analysis of intact, standard ganglioside GM1

1	Area	Area percent
GM3-C16	5048587	47.2075786
GM3-C17	591032.18	5.52653606
GM3-C18	2198705.77	20.5593319
GD3-C16	210865.09	1.97172601
GD3-C17	450731.46	4.2146329
GD3-C18	67720.98	0.6332353
GM1-C18	1877751.38	17.5581991
GM1-C20	249047.89	2.32876008

2	Area	Area percent
GM3-C16	5187816.91	48.4706264
GM3-C17	641240.91	5.99121926
GM3-C18	1999742.15	18.6839197
GD3-C16	233469.51	2.18134402
GD3-C17	450471.54	4.20882967
GD3-C18	72697.75	0.67922703
GM1-C18	1860364.55	17.3816919
GM1-C20	257208.58	2.40314205

3	Area	Area percent
GM3-C16	4646176.84	47.9718666
GM3-C17	576324.33	5.95055997
GM3-C18	1834452	18.9407527
GD3-C16	205627.7	2.12311002
GD3-C17	403487.05	4.16601167
GD3-C18	67946.14	0.70154522
GM1-C18	1709723.99	17.6529336
GM1-C20	241473.65	2.49322015

Figure B– 4. Percent recovery of a standard GSL mixture containing GM3, GM1 and GD3. A mixture of GM3, GM1 and GD3 containing approximately equal amounts of GM3, GM1 and half that amount of GD3, was subjected to SA_SCD digestion at 37 °C for 18 hours followed by RapiFluor-MS labeling. Three replicate chromatograms of samples subjected to only HILIC-elution (Only HILIC), are shown here. An appropriate amount of external standard (ES*) was added. The fluorescent peak area of each *l*-GSL in the mixture is represented as a percent of fluorescence peak area of ES*. Values represent mean ± standard error of mean (SEM) of triplicate measurement (n = 3).

258

1	Area	Area percent
GM3-C16	3111851.81	51.4592082
GM3-C17	371101.07	6.13672128
GM3-C18	973769.66	16.1027641
GD3-C16	139364.09	2.30459744
GD3-C17	279449.7	4.62112632
GD3-C18	32589.04	0.5389094
GM1-C18	1001011.27	16.5532456
GM1-C20	138083.9	2.28342755

2	Area	Area percent
GM3-C16	2915683.33	50.789007
GM3-C17	347851.74	6.05931525
GM3-C18	951887.64	16.5811656
GD3-C16	128743.09	2.24260764
GD3-C17	261830.96	4.56089807
GD3-C18	38223.03	0.66581639
GM1-C18	965684.09	16.8214893
GM1-C20	130872.52	2.2797007

3	Area	Area percent
GM3-C16	2616357.43	50.1786924
GM3-C17	319929.29	6.13587167
GM3-C18	874609.2	16.7739872
GD3-C16	119451.52	2.29094122
GD3-C17	236093.07	4.52799048
GD3-C18	34906.57	0.66946741
GM1-C18	886879.97	17.0093263
GM1-C20	125853.48	2.41372336

Figure B– 5. Percent recovery of a standard GSL mixture containing GM3, GM1 and GD3. A mixture of GM3, GM1 and GD3 containing approximately equal amounts of GM3, GM1 and half that amount of GD3, was subjected to SA_SCD digestion at 37 °C for 18 hours followed by RapiFluor-MS labeling. Three replicate chromatograms of samples subjected to SepPak C18 and HILIC-elution (C18 + HILIC), are shown here. An appropriate amount of external standard (ES*) was added. The fluorescent peak area of each *l*-GSL in the mixture is represented as a percent of fluorescence peak area of ES*. Values represent mean ± standard error of mean (SEM) of triplicate measurement (n = 3).
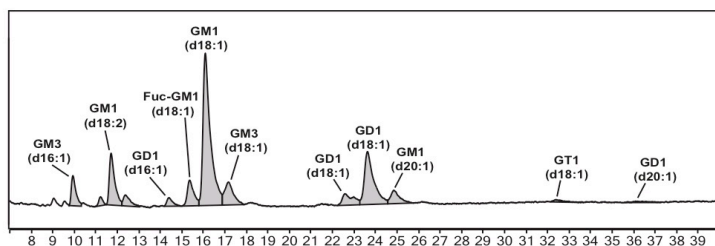
Run 1	Area	Area Percentage	Amount (ug/mL)
ES*	287906.89	100	0.693
GM3 (d16:1)	37414.73	12.9954271	0.09005831
GM1 (d18:2)	76407.14	26.53883691	0.18391414
GD1 (d16:1)	13683.61	4.752790043	0.032936835
Fuc-GM1 (d18:1)	45596.93	15.83738757	0.109753096
GM1 (d18:1)	309401.18	107.4657088	0.744737362
GM3 (d18:1)	55497.86	19.27632229	0.133584913
GD1 (d18:1)	34517.94	11.98927195	0.083085655
GD1 (d18:1)	134590.24	46.74783573	0.323962502
GM1 (d20:1)	32540.22	11.30234153	0.078325227
GT1 (d18:1)	6696.16	2.325807486	0.016117846
GD1 (d20:1)	5995.2	2.082339884	0.014430615
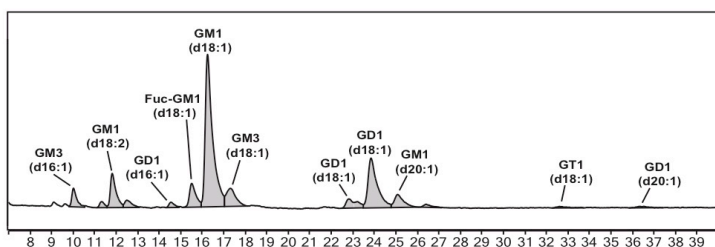
Run 2	Area	Area Percentage	Amount (ug/mL)
ES*	274390.29	100	0.52
GM3 (d16:1)	46891.32	17.0892782	0.088864247
GM1 (d18:2)	99605.83	36.30078528	0.188764083
GD1 (d16:1)	14781.58	5.387063806	0.028012732
Fuc-GM1 (d18:1)	79516.51	28.97934544	0.150692596
GM1 (d18:1)	581758.75	212.0187088	1.102497286
GM3 (d18:1)	88853.12	32.38202052	0.168386507
GD1 (d18:1)	52096.26	18.98618934	0.098728185
GD1 (d18:1)	236095.98	86.04385381	0.44742804
GM1 (d20:1)	61639.68	22.46423516	0.116814023
GT1 (d18:1)	8397.38	3.060377975	0.015913965
GD1 (d20:1)	8583.52	3.128215652	0.016266721
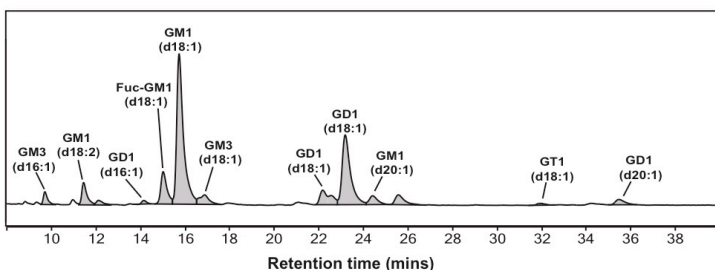
Run 3	Area	Area Percentage	Amount (ug/mL)
ES*	1216396.86	100	1.25
GM3 (d16:1)	64684.72	5.317731583	0.066471645
GM1 (d18:2)	137638.67	11.31527666	0.141440958
GD1 (d16:1)	18655.08	1.533634344	0.019170429
Fuc-GM1 (d18:1)	235177.26	19.33392528	0.241674066
GM1 (d18:1)	1216997.78	100.0494016	1.250617521
GM3 (d18:1)	111605.32	9.175074655	0.114688433
GD1 (d18:1)	104357.32	8.57921649	0.107240206
GD1 (d18:1)	699386.09	57.49653859	0.718706732
GM1 (d20:1)	88510.01	7.276408951	0.090955112
GT1 (d18:1)	18337.57	1.507531843	0.018844148
GD1 (d20:1)	60183.36	4.947674725	0.061845934
Fuc-GD1 (d18:1)	34054.19	2.799595356	0.034994942
GM3(d20:1)	108989.53	8.960030528	0.112000382

Figure B– 6. Lyso-glycosphingolipid (*l*-GSL) profiling in porcine brain. Three biological replicates showing HPLC separation of RapiFluor-MS labeled *l*-GSLs generated from SA_SCD digestion of GSLs extracted from porcine brain. For each run, 30 μL of brain homogenate (~ 6 mg wet tissue weight) was subjected to chloroform-methanol-water extraction as outlined in the Materials and Methods section. Dry GSL extract, ~ 1.5 mg, was subjected to enzyme cleavage and labeling. The *l*-GSLs identified were (d16:1), and (d18:1) forms of GM3; (d18:1), (d20:1) and (d18:2) forms of GM1, (d18:1) form of Fucosyl-GM1, GT1, and finally (d18:1) and (d20:1) forms of GD1. Peak assignment was performed based on commercially available standards and further confirmed by HR-ESI-MS. Quantification was performed based on the amount of external standard (ES*) added, i.e., 0.693, 0.52 and 1.25 μg/mL in this case.
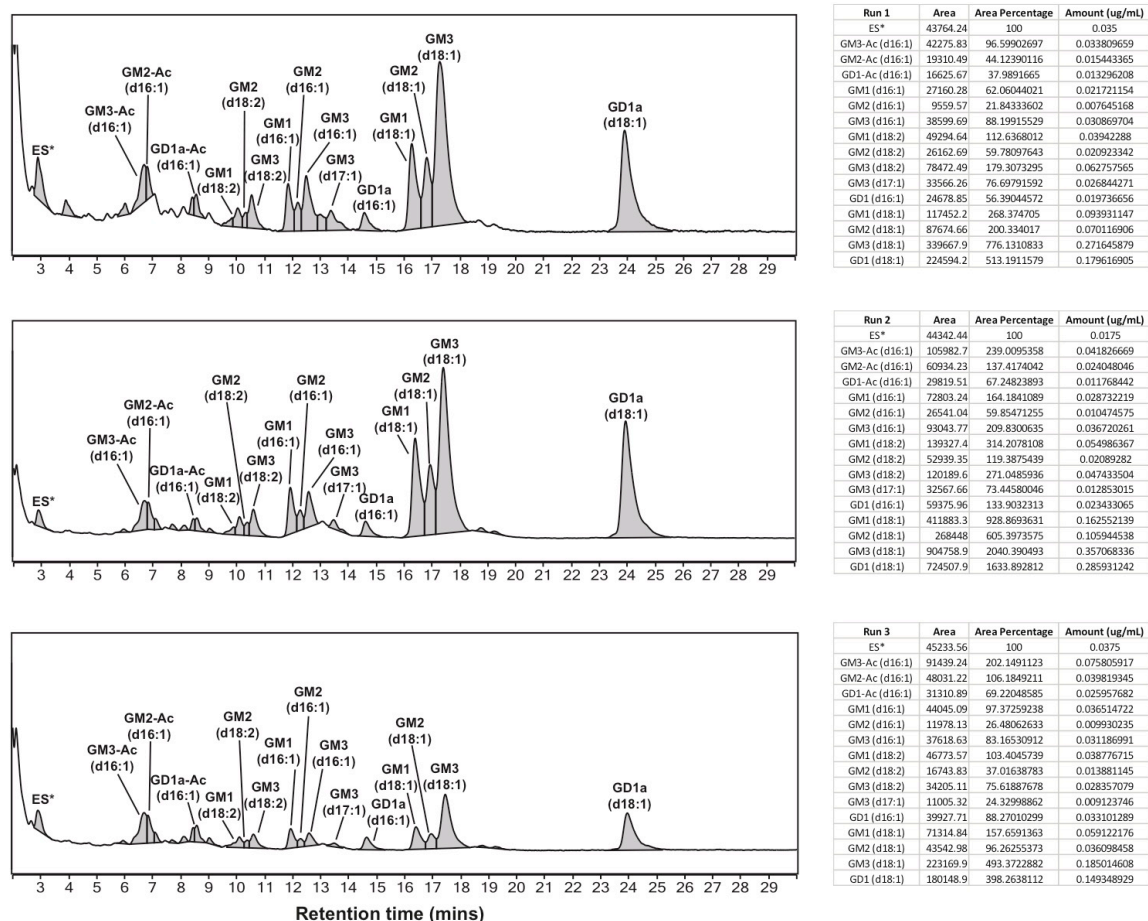
Figure B– 7. Lyso-glycosphingolipid (*l*-GSL) profiling in Jurkat T cells. Three biological replicates showing HPLC separation of RapiFluor-MS labeled *l*-GSLs generated from SA_SCD digestion of GSLs extracted from Jurkat T cells. For each run, ~1 x 10^7 cells was subjected to chloroform-methanol-water extraction as outlined in the Materials and Methods section. Dry GSL extract, ~ 1.5 mg, was subjected to enzyme cleavage and labeling. The *l*-GSLs identified were (d16:1), (d18:2) and (d18:1) forms of GM3; (d18:1), (d16:1) and (d18:2) forms of GM1, (d18:1), (d16:1) and (d18:2) forms of GM2, (d16:1) and (d18:1) forms of GD1a, and finally (d16:1) forms of acetylated GM3, GD1a and GM2. Peak assignment was performed based on commercially available standards and further confirmed by HR-ESI-MS. Quantification was performed based on the amount of external standard (ES*) added, i.e., 0.035, 0.0175 and 0.0375 µg/mL in this case.

Run 1	Area	Area Percentage	Amount (ug/mL)
ES*	43764.24	100	0.035
GM3-Ac (d16:1)	42275.83	96.59902697	0.033809659
GM2-Ac (d16:1)	19310.49	44.12390116	0.015443365
GD1-Ac (d16:1)	16625.67	37.9891665	0.013296208
GM1 (d16:1)	27160.28	62.06044021	0.021721154
GM2 (d16:1)	9559.57	21.84333602	0.007645168
GM3 (d16:1)	38599.69	88.19915529	0.030869704
GM1 (d18:2)	49294.64	112.6368012	0.03942288
GM2 (d18:2)	26162.69	59.78097643	0.020923342
GM3 (d18:2)	78472.49	179.3073295	0.062757565
GM3 (d17:1)	33566.26	76.69791592	0.026844271
GD1 (d16:1)	24678.85	56.39044572	0.019736656
GM1 (d18:1)	117452.2	268.374705	0.093931147
GM2 (d18:1)	87674.66	200.334017	0.070116906
GM3 (d18:1)	339667.9	776.1310833	0.271645879
GD1 (d18:1)	224594.2	513.1911579	0.179616905

Run 2	Area	Area Percentage	Amount (ug/mL)
ES*	44342.44	100	0.0175
GM3-Ac (d16:1)	105982.7	239.0095358	0.041826669
GM2-Ac (d16:1)	60934.23	137.4174042	0.024048046
GD1-Ac (d16:1)	29819.51	67.24823893	0.011768442
GM1 (d16:1)	72803.24	164.1841089	0.028732219
GM2 (d16:1)	26541.04	59.85471255	0.010474575
GM3 (d16:1)	93043.77	209.8300635	0.036720261
GM1 (d18:2)	139327.4	314.2078108	0.054986367
GM2 (d18:2)	52939.35	119.3875439	0.02089282
GM3 (d18:2)	120189.6	271.0485936	0.047433504
GM3 (d17:1)	32567.66	73.44580046	0.012853015
GD1 (d16:1)	59375.96	133.9032313	0.023433065
GM1 (d18:1)	411883.3	928.8693631	0.162552139
GM2 (d18:1)	268448	605.3973575	0.105944538
GM3 (d18:1)	904758.9	2040.390493	0.357068336
GD1 (d18:1)	724507.9	1633.892812	0.285931242

Run 3	Area	Area Percentage	Amount (ug/mL)
ES*	45233.56	100	0.0375
GM3-Ac (d16:1)	91439.24	202.1491123	0.075805917
GM2-Ac (d16:1)	48031.22	106.1849211	0.039819345
GD1-Ac (d16:1)	31310.89	69.22048585	0.025957682
GM1 (d16:1)	44045.09	97.37259238	0.036514722
GM2 (d16:1)	11978.13	26.48062633	0.009930235
GM3 (d16:1)	37618.63	83.16530912	0.031186991
GM1 (d18:2)	46773.57	103.4045739	0.038776715
GM2 (d18:2)	16743.83	37.01638783	0.013881145
GM3 (d18:2)	34205.11	75.61887678	0.028357079
GM3 (d17:1)	11005.32	24.32998862	0.009123746
GD1 (d16:1)	39927.71	88.27010299	0.033101289
GM1 (d18:1)	71314.84	157.6591363	0.059122176
GM2 (d18:1)	43542.98	96.26255373	0.036098458
GM3 (d18:1)	223169.9	493.3722882	0.185014608
GD1 (d18:1)	180148.9	398.2638112	0.149348929

a)

Run 1	Area	Area Percentage	Amount (ug/mL)
ES*	271741.8	100	1.05
diF(2,4)-Lc4 (d16:1)	12701.97	4.674279384	0.049079934
GM1 (d16:1)	15919.2	5.85820848	0.061511189
GM2 (d16:1)	54824.43	20.17519352	0.211839532
GM3 (d16:1)	271217.9	99.80721772	1.047975786
GM1 (d18:2)	159436.4	58.67200472	0.61605605
GM3 (d17:1)	47477.21	17.47144293	0.183450151
GD3 (d16:1)	23753.2	8.741092371	0.09178147
GD1b (d16:1)	19447.66	7.1566691	0.075145026
GM3 (d18:1)	152632.6	56.16824914	0.589766616
GD3 (d18:1)	23014.33	8.469190862	0.088926504

b)

Run 2	Area	Area Percentage	Amount (ug/mL)
ES*	313830.9	100	1.05
diF(2,4)-Lc4 (d16:1)	34821.02	11.09547353	0.116502472
GM1 (d16:1)	21268.07	6.776921173	0.071157672
GM2 (d16:1)	70422.34	22.43958418	0.235615634
GM3 (d16:1)	291149.5	92.77272796	0.974113644
GM1 (d18:2)	224641.6	71.58047491	0.751594987
GM3 (d17:1)	65137.22	20.7555178	0.217932937
GD3 (d16:1)	39532.68	12.59681091	0.132266515
GD1b (d16:1)	24576.18	7.831027197	0.082225786
GM3 (d18:1)	168728.4	53.7641072	0.564523126
GD3 (d18:1)	32452.96	10.34090784	0.108579532

c)

Run 3	Area	Area Percentage	Amount (ug/mL)
ES*	216322	100	1.05
diF(2,4)-Lc4 (d16:1)	15378.67	7.109157706	0.074646156
GM1 (d16:1)	11328.62	5.236925311	0.054987716
GM2 (d16:1)	46540.9	21.5146432	0.225903754
GM3 (d16:1)	117089.5	54.1274148	0.568337855
GM1 (d18:2)	89963.15	41.5876159	0.436669967
GM3 (d17:1)	27476.07	12.70146994	0.133365434
GD3 (d16:1)	20390.61	9.426046739	0.098973491
GD1b (d16:1)	13659.18	6.314282363	0.066299965
GM3 (d18:1)	84522.97	39.0727627	0.410264008
GD3 (d18:1)	21788.17	10.07210225	0.105757074

Figure B– 8. Lyso-glycosphingolipid (*l*-GSL) profiling in serum from normal individuals. Three biological replicates showing HPLC separation of RapiFluor-MS labeled *l*-GSLs generated from SA_SCD digestion of GSLs extracted from control serum. For each run, 150 µL was subjected to chloroform-methanol-water extraction as outlined in the Materials and Methods section. Dry GSL extract, ~ 1.5 mg, was subjected to enzyme cleavage and labeling. The *l*-GSLs identified were (d16:1), (d17:1) and (d18:1) forms of GM3; (d18:2), and (d16:1) forms of GM1; (d16:1) form of GM2, (d16:1) and (d18:1) forms of GD3, and finally (d16:1) form of diF(2,4)-Lc4. Peak assignment was performed based on commercially available standards and further confirmed by HR-ESI-MS. Quantification was performed based on the amount of external standard (ES*) added, i.e.,1.05 µg/mL in this case.

| Run 1	Area	Area Percentage	Amount (ug/mL)
ES*	194600.9	100	1.05
diF(2,4)-Lc4 (d16:1)	6497.52	3.338895144	0.035058399
GM1 (d16:1)	11894.42	6.112212225	0.064178228
GM2 (d16:1)	45526.34	23.39472222	0.245644583
GM3 (d16:1)	208875	107.3350534	1.127018061
GM1 (d18:2)	130078.5	66.84371449	0.701859002
GM3 (d17:1)	37125.09	19.07755308	0.200314307
GD3 (d16:1)	26601.67	13.6698597	0.143533527
GD1b (d16:1)	15298.11	7.861274023	0.082543377
GM3 (d18:1)	120315.1	61.82659998	0.6491793
GD3 (d18:1)	27141.27	13.94714516	0.146445024

Run 2	Area	Area Percentage	Amount (ug/mL)
ES*	213726.6	100	1.05
diF(2,4)-Lc4 (d16:1)	13652.4	6.387787612	0.06707177
GM1 (d16:1)	15771.77	7.37941439	0.077483851
GM2 (d16:1)	84832	39.69183431	0.41676426
GM3 (d16:1)	230005.5	107.6166989	1.129975338
GM1 (d18:2)	225712.2	105.607922	1.108883181
GM3 (d17:1)	70522.85	32.99676156	0.346465996
GD3 (d16:1)	33164.99	15.517485	0.162933593
GD1b (d16:1)	24187.12	11.31685165	0.118826942
GM3 (d18:1)	403743.3	188.9064523	1.98351775
GD3 (d18:1)	74313.6	34.77040619	0.365089265

Run 3	Area	Area Percentage	Amount (ug/mL)
ES*	225414.6	100	4.95
diF(2,4)-Lc4 (d16:1)	3198.95	1.41914049	0.070247454
GM1 (d16:1)	2887.49	1.280968434	0.063407937
GM2 (d16:1)	20745.94	9.203458463	0.455571194
GM3 (d16:1)	33506.74	14.86449348	0.735792427
GM1 (d18:2)	17112.24	7.591451149	0.375776832
GM3 (d17:1)	3147.62	1.396369117	0.069120271
GD3 (d16:1)	3053.28	1.354517349	0.067048609
GD1b (d16:1)	1413.79	0.627195371	0.031046171
GM3 (d18:1)	16318.89	7.239499693	0.358355235
GD3 (d18:1)	4648.53	2.06221327	0.102079557

Figure B– 9. Lyso-glycosphingolipid (*l*-GSL) profiling in serum from Huntington's disease patients.
Three biological replicates showing HPLC separation of RapiFluor-MS labeled *l*-GSLs generated from SA_SCD digestion of GSLs extracted from HD-patient serum. For each run, 150 μL was subjected to chloroform-methanol-water extraction as outlined in the Materials and Methods section. Dry GSL extract, ~ 1.5 mg, was subjected to enzyme cleavage and labeling. The *l*-GSLs identified were (d16:1), (d17:1) and (d18:1) forms of GM3; (d18:2), and (d16:1) forms of GM1; (d16:1) form of GM2, (d16:1) and (d18:1) forms of GD3, and finally (d16:1) form of diF(2,4)-Lc4. Peak assignment was performed based on commercially available standards and further confirmed by HR-ESI-MS. Quantification was performed based on the amount of external standard (ES*) added, i.e., 1.05 μg/mL and 4.95 μg/mL in this case.
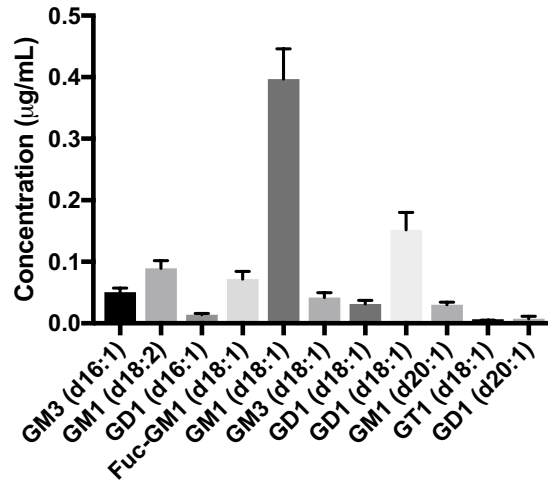
Figure B– 10. Comparison of *l*-GSL composition in porcine brain. Peak heights were considered for quantification in this data set. Absolute concentrations were calculated based on the concentration of external standard added. Only small differences in amounts of each chain length were observed between control and diseased samples, none of the changes observed were significant. Values represent mean and standard error of mean (SEM) of triplicate measurements; n=3.
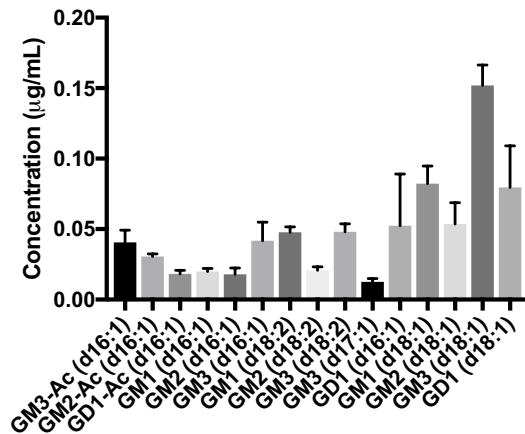
Figure B– 11. Comparison of *l*-GSL composition in Jurkat T cells. Peak heights were considered for quantification in this data set. Absolute concentrations were calculated based on the concentration of external standard added. Only small differences in amounts of each chain length were observed between control and diseased samples, none of the changes observed were significant. Values represent mean and standard error of mean (SEM) of triplicate measurements; n=3.
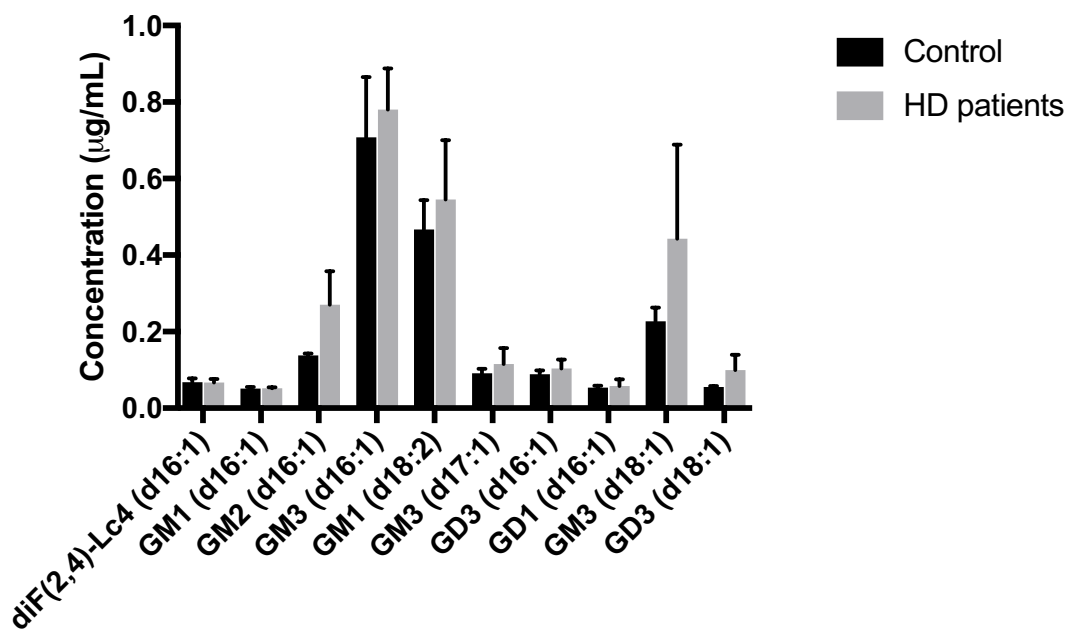
Figure B– 12. Comparison of *l*-GSL composition in serum from normal individuals (control) and individuals suffering from Huntington's disease (HD patients). Peak heights were considered for quantification in this data set. Absolute concentrations were calculated based on the concentration of external standard added. Only small differences in amounts of each chain length were observed between control and diseased samples, none of the changes observed were significant. Values represent mean and standard error of mean (SEM) of triplicate measurements; n=3.

Table B– 1. Comparison of percent composition of major GSLs in normal human serum identified independently in the EGCase and SCDase assays. [10]

Glycosphingolipid (GSL)	EGCase (% of total GSL composition)	SCDase (% of total GSL composition)
diF(2,4)-Lc4	6.2 ± 0.5	2.9 ± 0.6
GM1	3.8 ± 0.5	23.5 ± 0.9
GM2	2.2 ± 0.3	8 ± 1
GM3	59.6 ± 3.3	55.2 ± 2.7
GD3	3.3 ± 0.3	7.6 ± 0.9
GD1	2.4 ± 0.9	2.7 ± 0.2
LacCer	9 ± 1	n.d.
GA2	8 ± 2	n.d.
Gb3	1.6 ± 0.1	n.d.
GA1	3.5± 0.7	n.d.
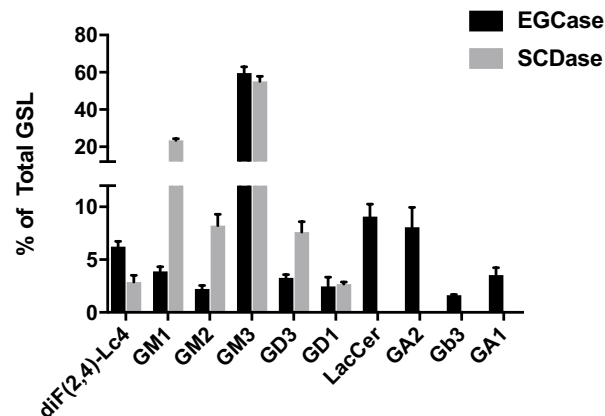
Figure B– 13. Comparison of percent composition of GSLs identified in normal human serum using EGCase and SCDase methods. Relative percentages of diF(2,4)-Lc4, GM1, GM2, GM3, GD3, GD1, LacCer, GA2, Gb3, and GA1 identified in normal human serum from glycan analysis (EGCase method)

---

[10] Values represent the mean ± standard error of the mean of triplicate measurements, n = 3; n.d.- Not detected
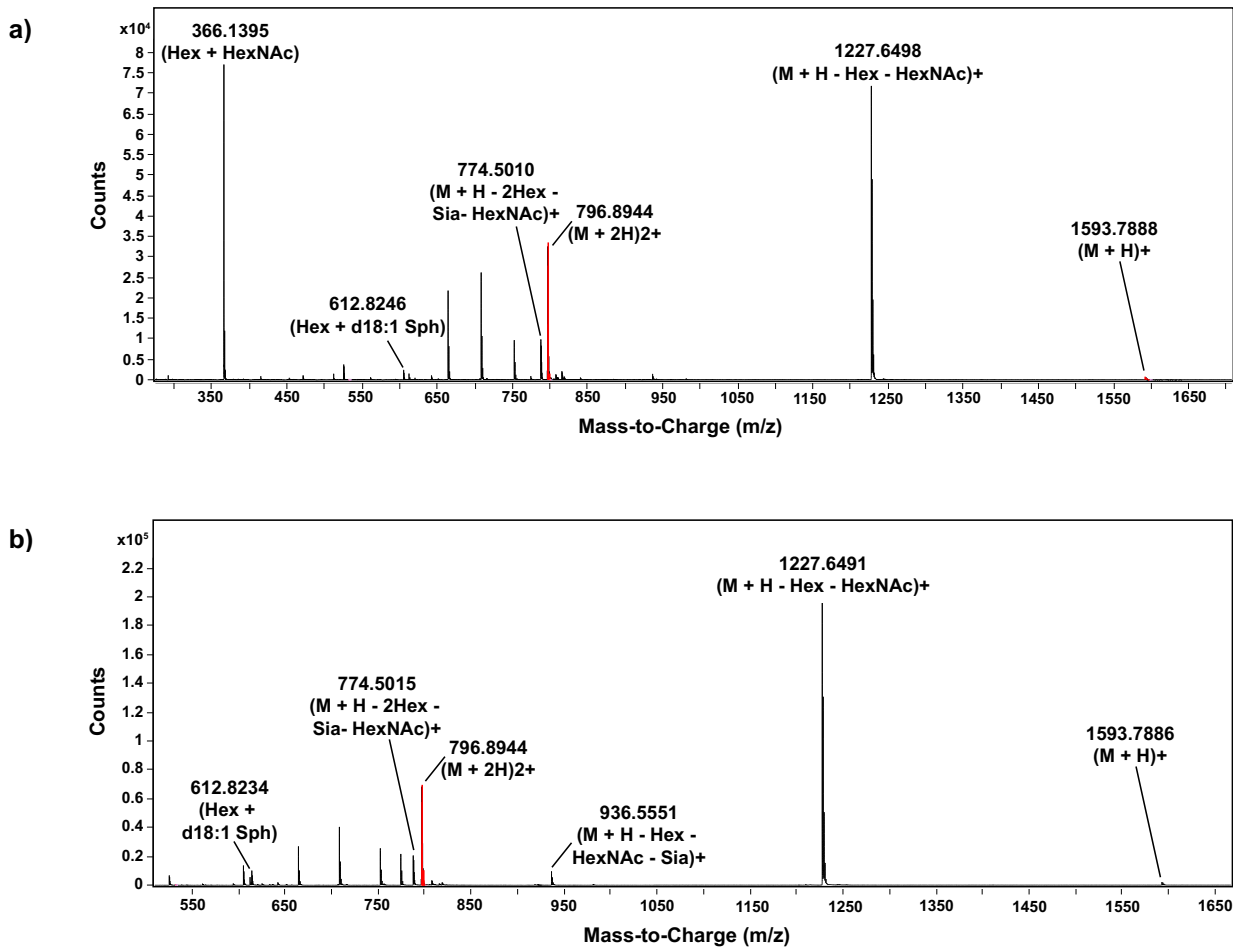
Figure B– 14. Fragmentation pattern of RapiFluor-MS labeled GM1 (d18:1). (a) Fragmentation of GM1 (d18:1) in porcine brain shows the singly charged parent ion at m/z value of 1593.7888 and its corresponding doubly charged species at m/z value 796.8944. Strong fragments of the parent ion are seen at 1227.6498 due to the loss of a galactose (Hex) and N-acetylhexosamine (HexNAc). This is followed by the loss of a Sialic acid (Sia) at 936.5551. A weak fragment isseen at 774.5010 after the loss of 2 Hex, one Sia and HexNAc each. Finally, the (d18:1) Sph chain is seen at 612.8246. This fragmentation pattern was compared to (d18:1) from standard GM1 shown in (b), indicating the same fragmentation pattern.
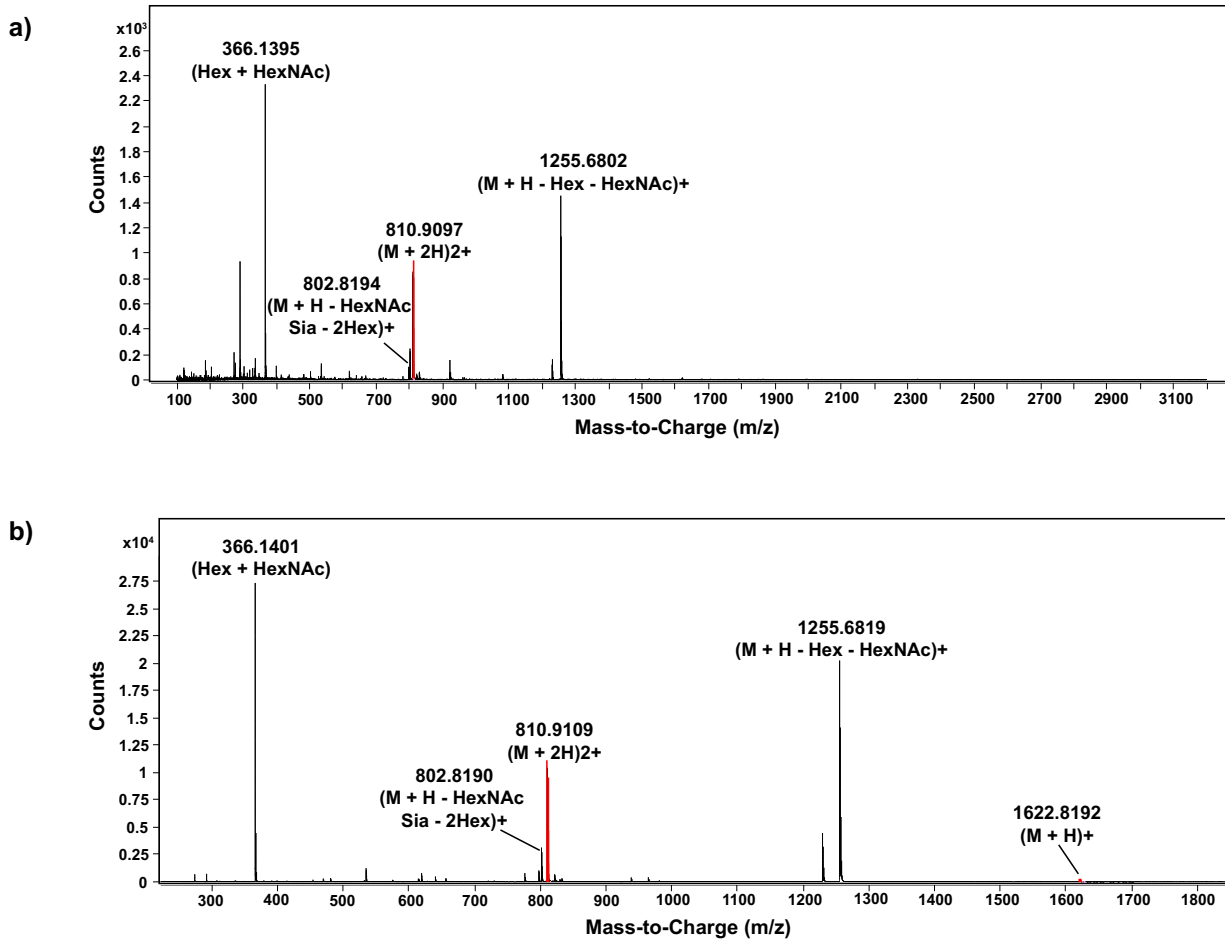
Figure B– 15. Fragmentation pattern of RapiFluor-MS labeled GM1 (d20:1). (a) Fragmentation of

GM1 (d20:1) in porcine brain shows the doubly charged parent ion at m/z value of 810.9097, which would

show the singly charged species to be at 1622.8194. Strong fragments of the singly charged parent ion are

seen at 1255.6802 due to the loss of a galactose (Hex) and N-acetylhexosamine (HexNAc). A weak

fragment isseen at 802.8194 after the loss of 2 Hex, and one Sia and HexNAc each. A complete fragment of

a Hex and HexNAc is seen at 366.1401. This fragmentation pattern was compared to (d20:1) from standard

GM1 shown in (b), indicating the same fragmentation pattern. The singly charged parent ion was visible in

this case, even though it was at very low counts. Bulkier gangliosides tend to fragment better, which is why

usually they would appear at the doubly charged species than singly charged. Additionally, it also depends

on the quantities of the analyte in a biological sample; if it's very low then it's unlikely that the parent ion

would show up as a singly charged species. Thus, based on the relative abundance (%), which is 10 times

higher in case of the standard GM1 (d20:1), it is not surprising that the singly charged species was not visible in porcine brain.
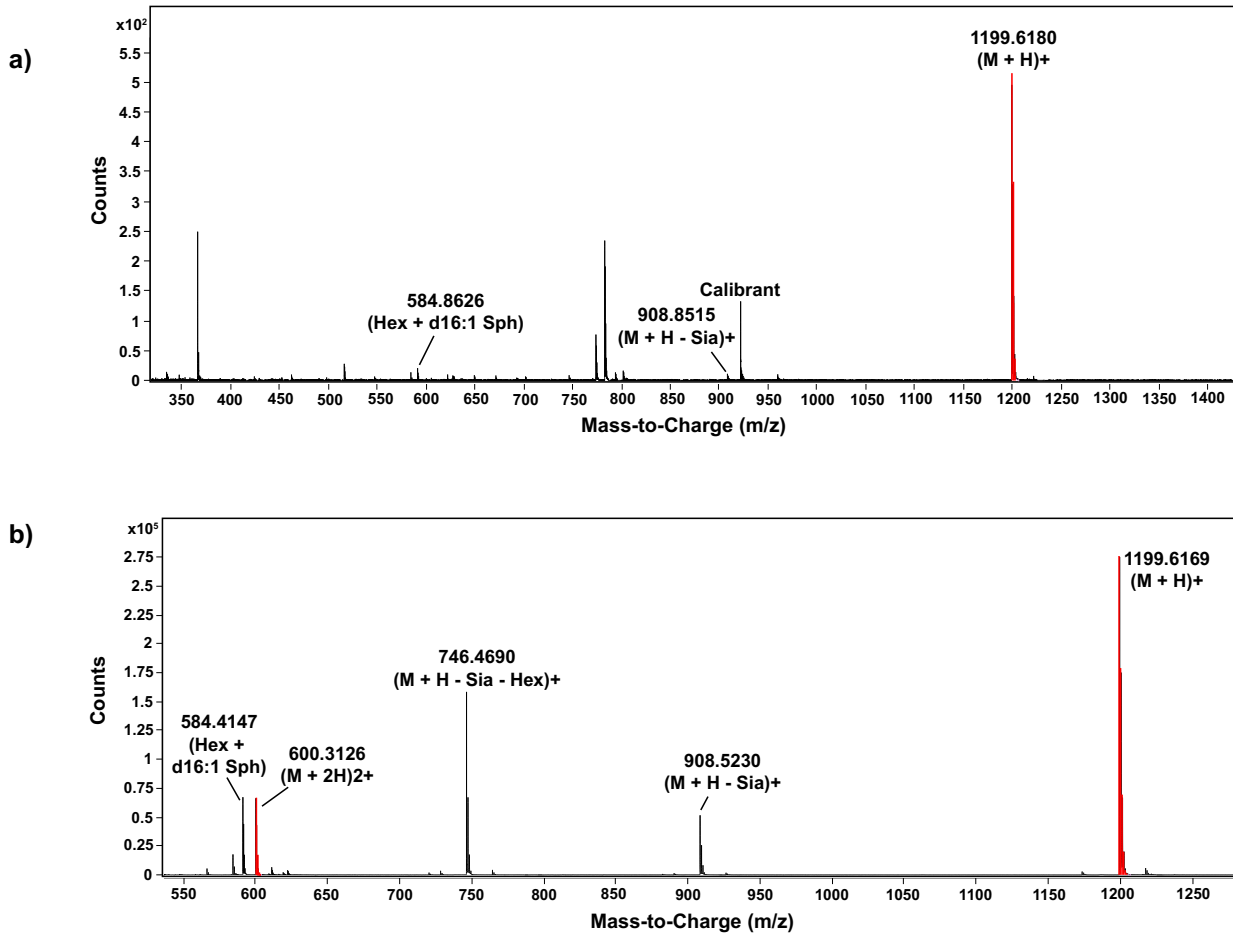
Figure B– 16. Fragmentation pattern of RapiFluor-MS labeled GM3 (d16:1). (a) Fragmentation of GM3 (d16:1) in human serum shows the singly charged parent ion at m/z value of 1199.6180. Weak fragments of the singly charged parent ion are seen at 908.5245 due to the loss of a Sialic acid (Sia), followed by the loss of a hexose (Hex) at 746.4681. Finally, the (d16:1) Sph chain is seen at 584.8626. This fragmentation pattern was compared to (d16:1) from standard GM3 shown in (b), indicating the same fragmentation pattern. The doubly charged parent ion was visible in this case, at lower counts than the singly charged species. Gangliosides that are smaller in size with less number of oligosaccharide residues, they tend to show up mostly as the singly charged species, with low counts of doubly charged species. Additionally, it also depends on the quantities of the analyte in a biological sample; if it's very low then it's

unlikely that the parent ion would show up as a singly charged species. Thus, based on the relative abundance (%), which is 3 orders of magnitude higher in case of the standard GM3 (d16:1), it is not surprising that the doubly charged species was not visible
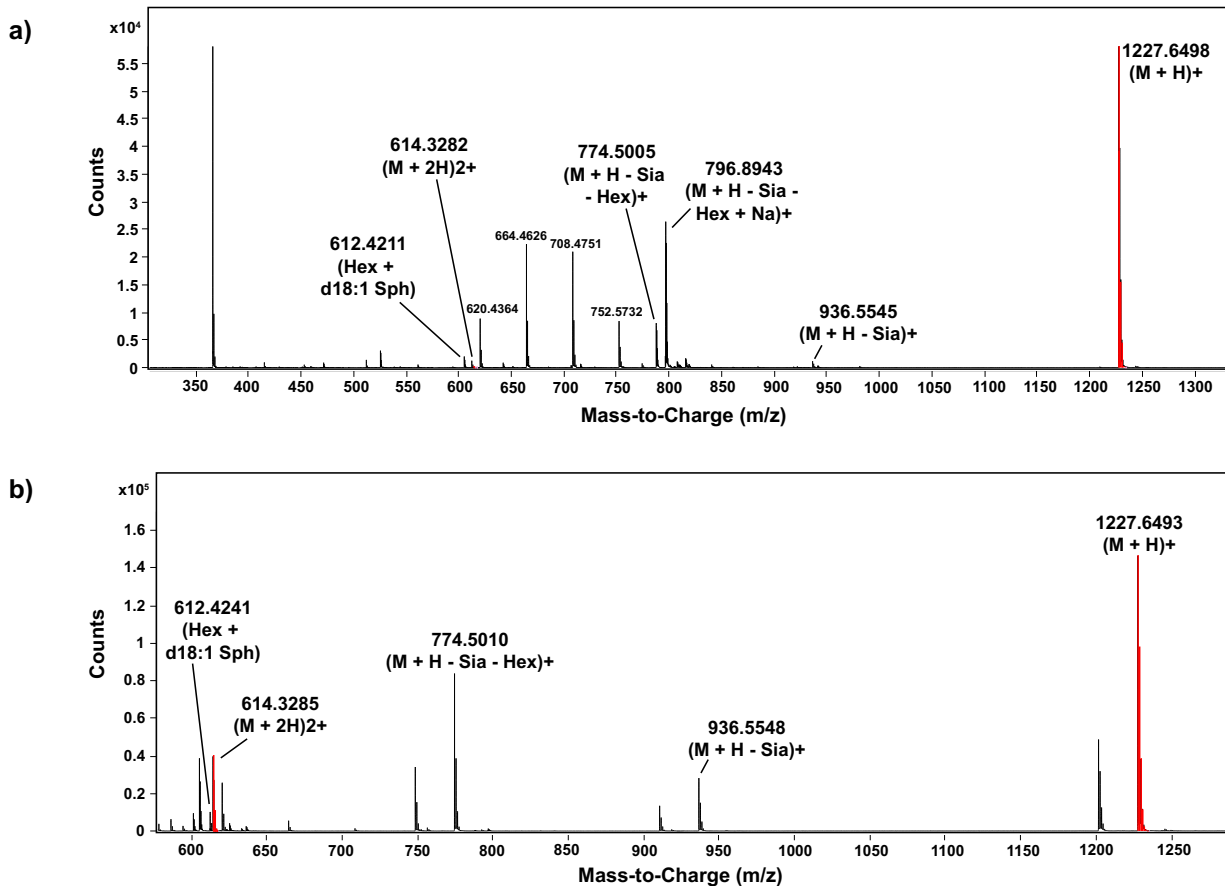

Figure B– 17. Fragmentation pattern of RapiFluor-MS labeled GM3 (d18:1). (a) Fragmentation of GM3 (d18:1) in porcine brain shows the singly charged parent ion at m/z value of 1227.6498. Strong fragments of the singly charged parent ion are seen at 936.5545 due to the loss of a Sialic acid (Sia), followed by the loss of a hexose (Hex) at 774.5005, and its corresponding sodium (Na) adduct at 796.8943. The double charged species is seen at 614.3282, and finally, the (d18:1) Sph chain is seen at 612.4211. There are fragments at 620.4364, 664.4625, 708.4751, 752.5732, all 44 apart that could be due to presence of some residual polymer from a detergent in the enzyme reaction buffer. This fragmentation pattern was compared to (d18:1) from standard GM3 shown in (b), indicating the same fragmentation pattern. The difference in relative abundance between the standard GM3 (d18:1) and porcine brain (d18:1) was one

order of magnitude, hence it was easier to see the entire fragmentation pattern in this case compared to the

ones where there is a large difference of a few orders of magnitude. (as seen in Figure SI 4–13)
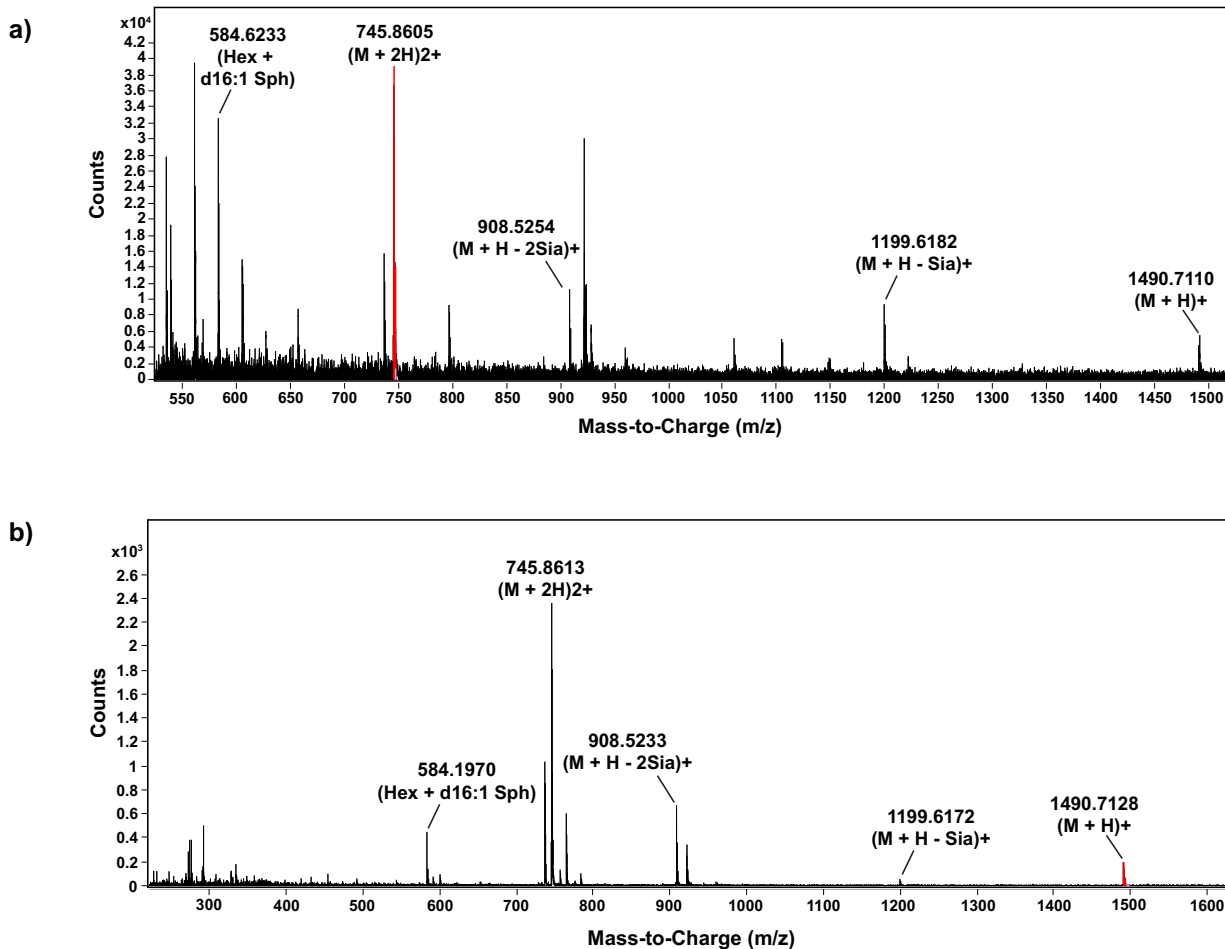

Figure B– 18. Fragmentation pattern of RapiFluor-MS labeled GD3 (d16:1). (a) Fragmentation of GD3

(d16:1) in human serum shows the singly charged parent ion at m/z value of 1490.7110. Strong fragments

of the singly charged parent ion are seen at 1199.6182 due to the loss of a Sialic acid (Sia), followed by the

loss of another Sia at 908.5254. The doubly charged species is seen at 745.8605, and finally, the (d16:1)

Sph chain is seen at 584.6233. This fragmentation pattern was compared to (d16:1) from standard GD3

shown in (b), indicating the same fragmentation pattern.
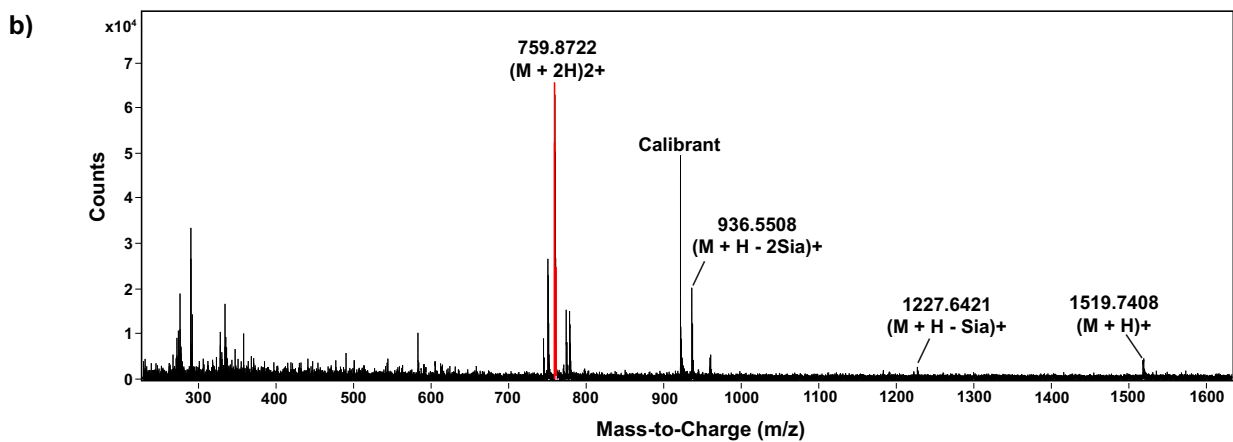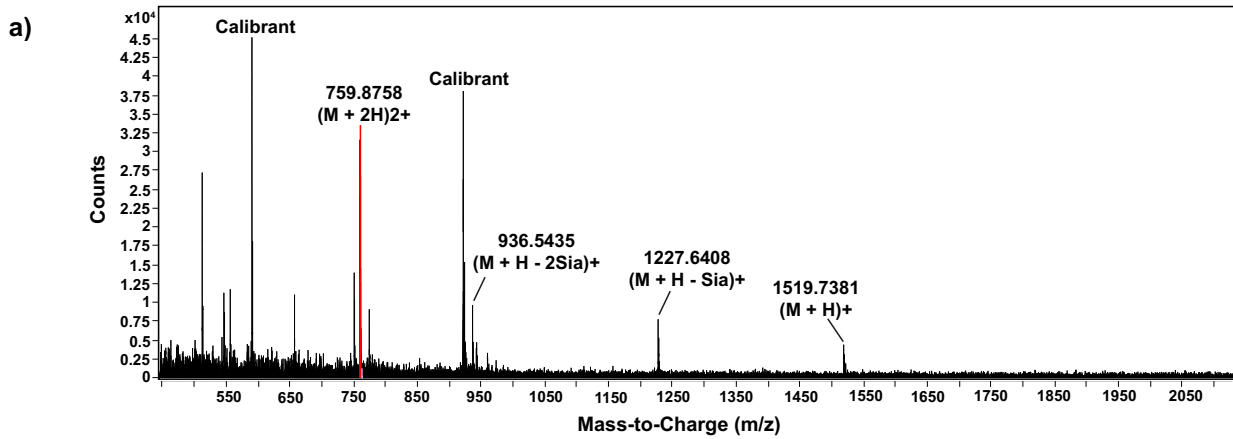
Figure B– 19. Fragmentation pattern of RapiFluor-MS labeled GD3 (d18:1). (a) Fragmentation of GD3 (d18:1) in human serum shows the singly charged parent ion at m/z value of 1519.7381. Strong fragments of the singly charged parent ion are seen at 1227.6408 due to the loss of a Sialic acid (Sia), followed by the loss of another Sia at 936.5435. The doubly charged species is seen at 759.8758. This fragmentation pattern was compared to (d16:1) from standard GD3 shown in (b), indicating the same fragmentation pattern. Neither of the two samples showed the (d18:1) Sph chain fragment, perhaps because it was a much weaker fragment with very low relative abundance, compared to the others.
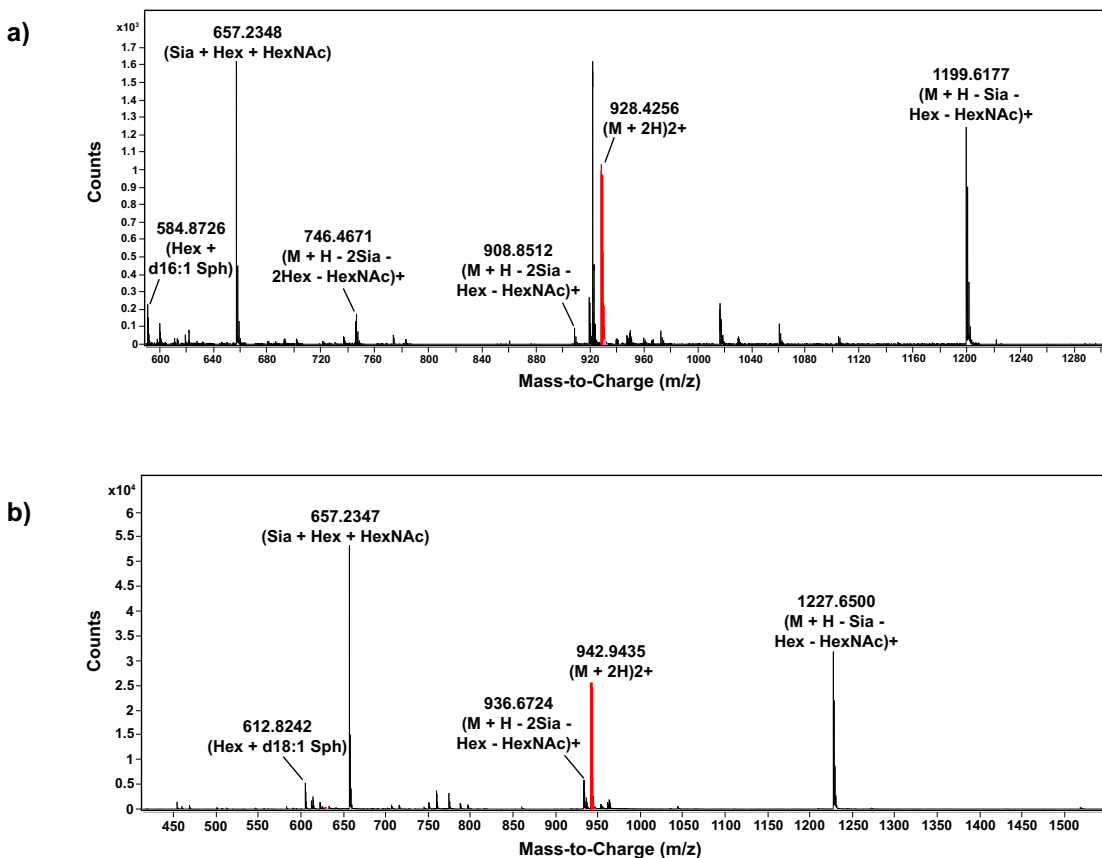
Figure B– 20. Fragmentation pattern of RapiFluor-MS labeled GD1 (d16:1) and GD1 (d18:1) (a) Fragmentation of GD1 (d16:1) in human serum shows the doubly charged parent ion at m/z value of 928.4256. The corresponding singly charged species would be at 1856.8512. Strong fragments of the singly charged parent ion were seen after the loss of a Sialic acid (Sia), N-acetylglucosamine (HexNAc), and a galactose (Hex) at 1199.6177. This was followed by another loss of a Sialic acid (Sia) at 908.8512, and another loss of Hex at 746.4671. Finally, the (d16:1) Sph chain fragment was seen at m/z value 584.8726. The complete fragment of one Sia, one Hex and one HexNAc is seen at 657.2348, which when added to 1199.6177, gives the singly charged parent ion at m/z value 1856.8525. (b) Fragmentation of GD1 (d18:1) in Jurkat T cells shows the doubly charged parent ion at m/z value of 942.9435. The corresponding singly charged species would be at 1884.8870. Strong fragments of the singly charged parent ion were seen after the loss of a Sialic acid (Sia), N-acetylglucosamine (HexNAc), and a galactose (Hex) at 1227.6500. This was followed by another loss of a Sialic acid (Sia) at 936.6724. Finally, the (d18:1) Sph chain fragment was

seen at m/z value 612.8242. The complete fragment of one Sia, one Hex and one HexNAc is seen at 657.2347, which when added to 1227.6500, gives the singly charged parent ion at m/z value 1884.8847
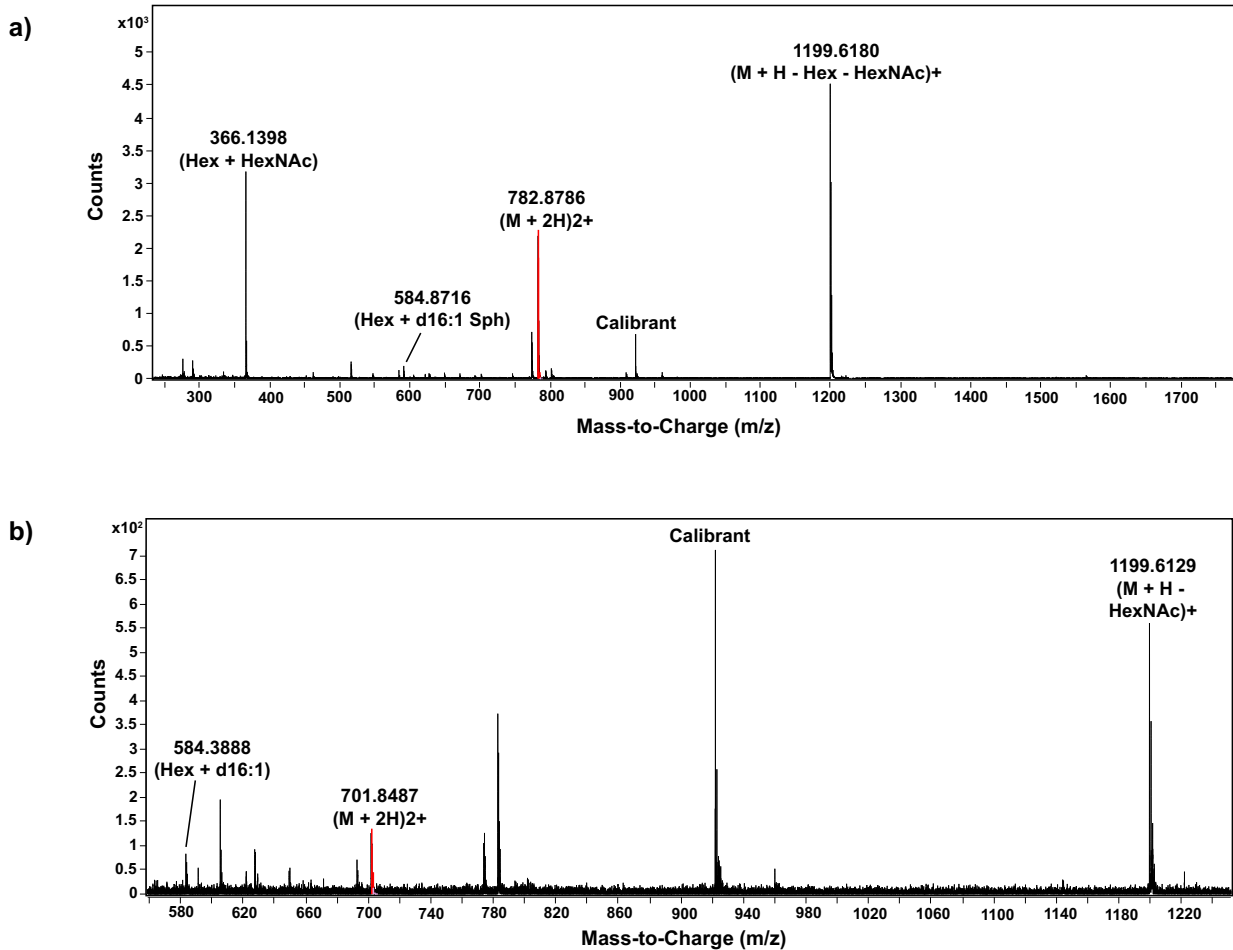
Figure B– 21. Fragmentation pattern of RapiFluor-MS labeled GM1 (d16:1) and GM2 (d16:1) (a) Fragmentation of GM1 (d16:1) in human serum shows the doubly charged parent ion at m/z value of 782.8786. The corresponding singly charged species would be at 1565.7572. Strong fragments of the singly charged parent ion were seen after the loss of a N-acetylglucosamine (HexNAc), and a galactose (Hex) at 1199.6180. The doubly charged species is seen at 782.8786. Finally, the (d16:1) Sph chain fragment was seen at m/z value 584.8716. The complete fragment of one Hex and one HexNAc is seen at 366.1398, which when added to 1199.6180, gives the singly charged parent ion at m/z value 1565.7572. (b) Fragmentation of GM2 (d16:1) in Jurkat T cells shows the doubly charged parent ion at m/z value of 701.8487. The corresponding singly charged species would be at 1403.6974. Strong fragments of the singly

charged parent ion were seen after the loss of a N-acetylglucosamine (HexNAc) at 1199.6129. The (d16:1) Sph chain fragment was seen at m/z value 584.3888.
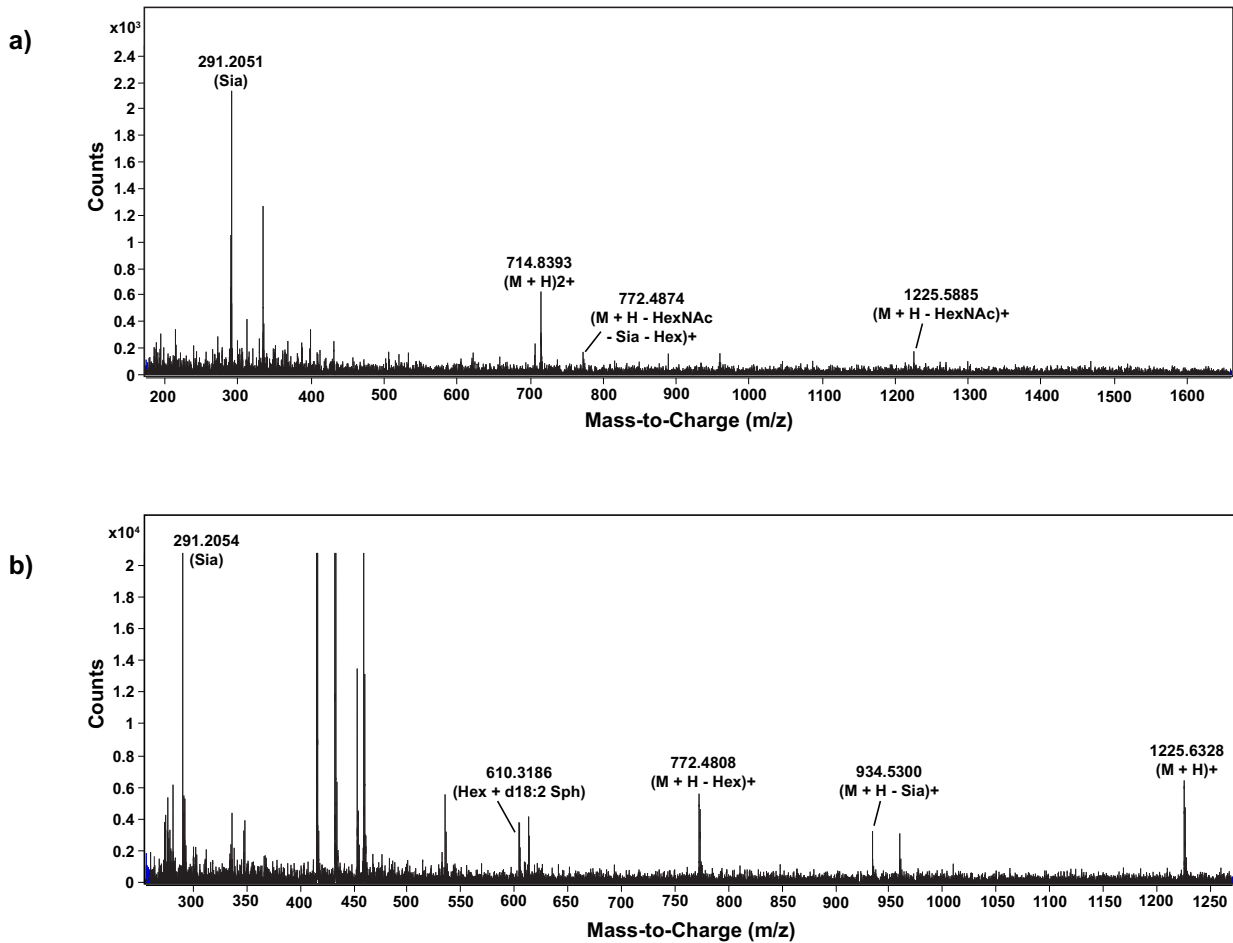
Figure B– 22. Fragmentation pattern of RapiFluor-MS labeled GM2 (d18:2) and GM3 (d18:2) (a) Fragmentation of GM2 (d18:2) in Jurkat T cells shows the doubly charged parent ion at m/z value of 714.8393. Strong fragments of the singly charged parent ion were seen after the loss of a N-acetylglucosamine (HexNAc) at 1225.5885, followed by the loss of a galactose (Hex) and Sialic acid (Sia) at 772.4874. Finally, a Sia fragment is seen at 291.2051. (b) Fragmentation of GM3 (d18:2) in Jurkat T cells shows the doubly charged parent ion at m/z value of 772.4808. The corresponding singly charged species is seen at 1225.6328. Strong fragments of the singly charged parent ion were seen after the loss of a Sia at 934.5300. The (d18:2) Sph chain fragment was seen at m/z value 610.3185, along with a Sia fragment at 291.2054.
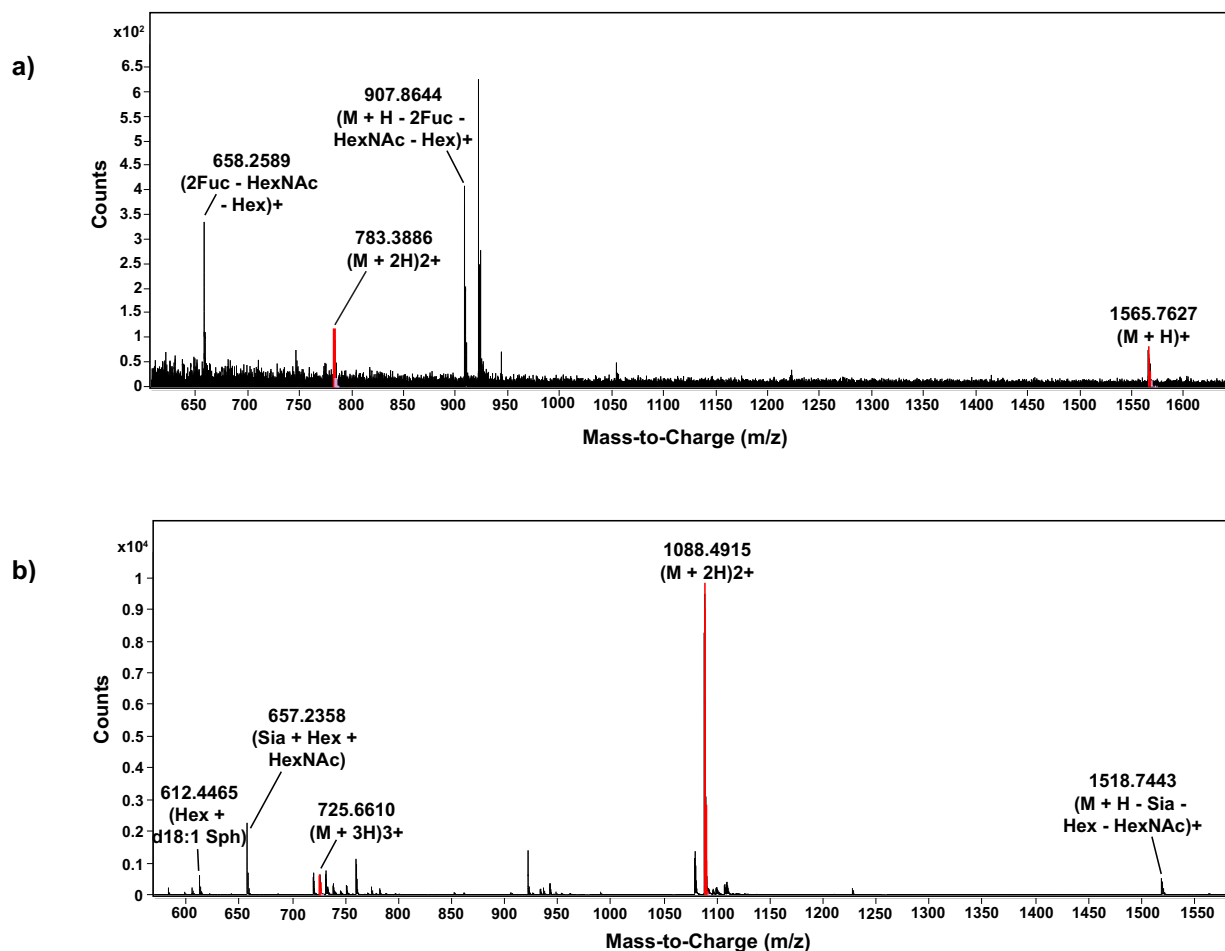
Figure B– 23. Fragmentation pattern of RapiFluor-MS labeled diF(2,4)-Lc4 (d16:1) and GT1 (d18:1)

(a) Fragmentation of diF(2,4)-Lc4 (d16:1) in human serum shows the singly charged parent ion at m/z value of 1565.7627, and the doubly charged species at 783.3886. Strong fragments of the singly charged parent ion were seen after the loss of a N-acetylglucosamine (HexNAc), a galactose (Hex) and two Fucoses (Fuc) at 907.8644. Finally, a complete fragment of HexNAc, Hex and Fuc is seen at 658.2589. (b) Fragmentation of GT1 (d18:1) in porcine brain shows the doubly charged parent ion at m/z value of 1088.4915, along with a triply charged species at 725.6610. Strong fragments of the singly charged parent ion were seen after the loss of a Sialic acid (Sia), galactose (Hex) and N-acetylhexosamine (HexNAc) at 1518.7443, and a complete fragment of Sia, Hex and HexNAc is seen at 657.2358. The (d18:1) Sph chain fragment was seen at m/z value 612.4465.

Table B– 2. Compound report showing all GSLs detected in human serum (normal and Huntington's patients) by HR-ESI-MS.

Lyso-Glycosphingolipid	Target Mass	Mass detected
diF(2,4)-nLc4 (d16:1)	1564.7634	1564.7630
GM1 (d16:1)	1563.7430	1563.7398
GM2 (d16:1)	1401.6902	1401.6848
GM3 (d16:1)	1198.6108	1198.6115
GM1 (d18:2)	1589.7730	1589.7718
GM3 (d17:1)	1212.6265	1212.6255
GD3 (d16:1)	1489.7062	1489.7065
GD1 (d16:1)	1854.8384	1854.8412
GM3 (d18:1)	1226.6430	1226.6421
GD3 (d18:1)	1517.7375	1517.7381

Table B– 3. Compound report showing all GSLs detected in Jurkat T-cells by HR-ESI-MS.

Lyso-Glycosphingolipid	Target Mass	Mass detected
GM3-Ac (d16:1)	1240.6214	1240.6187
GM2-Ac (d16:1)	1443.7008	1443.7002
GD1-Ac (d16:1)	1896.8490	1896.8479
GM1 (d16:1)	1563.7386	1563.7430
GM2 (d16:1)	1401.6908	1401.6902
GM3 (d16:1)	1198.6108	1198.6085
GM1 (d18:2)	1589.7729	1589.7721
GM2 (d18:2)	1427.6726	1427.6646
GM3 (d18:2)	1224.6346	1224.6328
GM3 (d17:1)	1212.6199	1212.6265
GD1 (d16:1)	1854.8405	1854.8384
GM1 (d18:1)	1591.7718	1591.7743
GM2 (d18:1)	1429.7207	1429.7215
GM3 (d18:1)	1226.6421	1226.6419
GD1 (d18:1)	1882.8698	1882.8697

Table B– 4. Compound report showing all GSLs detected in porcine brain by HR-ESI-MS.

Lyso-Glycosphingolipid	Target Mass	Mass detected
GM3 (d16:1)	1198.6108	1198.6105
GM1 (d18:2)	1589.7731	1589.7717
GD1 (d16:1)	1854.8384	1854.8374
Fuc-GM1 (d18:1)	1737.8322	1737.8314
GM1 (d18:1)	1591.7743	1591.7740
GM3 (d18:1)	1226.6573	1226.6564
GD1 (d18:1)	1882.8690	1882.8697
GM1 (d20:1)	1619.8046	1619.8056
GT1 (d18:1)	2173.9643	2173.9651
GD1 (d20:1)	1910.8994	1910.9010

APPENDIX C: PROTOCOLS AND DATABASES

Expression and purification of recombinant Endoglycoceramidase (EGCase)

Blake Zheng and Radhika Chakraberty

Background: A gene encoding EGCase I was identified from the works of Albrecht *et al* and synthesized by Genscript, with the vector being modified to pET30 instead of pJS119. This was then transformed into E.coli BL21 (DE3) and expressed as an N-His6-tagged protein.

Day 1:

1. Prepare culture media (1.1 L): Dissolve 27.5g LB Broth powder (BP9723-500, Miller, Granulated) in 1.1L MQ water and agitate to completely dissolve. Place 100mL of this solution in 500mL clean baffled Erlenmeyer flask and 1L of this solution in 4L clean baffled Erlenmeyer flask. Plug and cover with aluminum foil. Sterilize by autoclaving (cycle 4)

2. Prior to inoculation, add 100µL of 25 mg/mL Kanamycin into the 100mL of LB media:

3. Remove the glycerol stock from the freezer (storage box labelled as "Blake's bacterial stocks") and place on dry ice. Do not allow it to thaw. Scrape a little frozen bacteria glycerol stock onto a sterile, plastic loop and transfer to the media. Incubate at $37^{o}C$ overnight (not more than 16 hours) with shaking at 200 rpm.

Day 2:

4. Add the following into the above autoclaved scale-up media. For a 4L flask (1L media), add:

       1mL of 25 mg/mL Kanamycin

5. Grow the culture at 37 $^{\circ}C$ with shaking until the OD_{600} reaches ~ 0.8.

6. Add 1 (M) IPTG to a final concentration of 0.1mM.

7. Shake at 16 ^{o}C for 18-20 hours (overnight) at 200 rpm.

Day 3:

8. Remove the culture and spin in JLA8.1 rotor at 6000 rpm for 30 minutes. (Before you remove the culture in the centrifuge tubes, weigh an empty tube first. After you finish

spinning, pour off supernatant and collect all cell pellets into the weighed tube and then weigh the tube again, to get the wet cells' weight). Cells maybe frozen at this stage in -20 ^{o}C and used later.

Note: JLA8.1 centrifugal tubes could not be stored at -20 ^{o}C. You have to re-suspend cell pellets in PBS and transfer to a 50 mL plastic centrifugal tube and spin again. Remove the S/N and stored at a freezer. OR directly transfer the pellets to a 50 mL plastic centrifugal tube using a plastic spatula.

All centrifugation and manipulations of the protein is at 4°C.

Day 4:

Resuspesion buffer
300 mM NaCl
10mM Imidazole
0.1% Triton X-100
50 mM Tris-Cl (pH=7.5)

Wash buffer (1)
300 mM NaCl
20mM Imidazole
50 mM Tris-Cl (pH=7.5)

Wash buffer (2)
300 mM NaCl
50mM Imidazole
50 mM Tris-Cl (pH=7.5)

Elution buffer
300 mM NaCl
250mM Imidazole
50 mM Tris-Cl (pH=7.5)

Dialysis buffer
0.15M NaCl
50 mM Tris-Cl (pH=7.5)

Equilibration buffer
300 mM NaCl
50 mM Tris-Cl (pH=7.5)

9. Re-suspend cell pellets in the cold Re-suspension buffer (see the above re-suspension buffer). The ideal suspension has 10-15g of pellets (wet weight) per 100 mL solution. Re-suspend with Biorad plastic pipette, keeping suspension on ice until homogenous. Suspension should be soupy, not too thick. Otherwise, lots of foam will be found in your lysis. Alternatively, re-suspend by first breaking up the cell pellet with a

281

Teflon spatula and then passing the solution in and out of a 60 mL syringe until homogeneous. Add Roche Protease Inhibitor EDTA-free Cocktail tablets (full size, not Mini) at 1 tablet/50 mL cell extract.

10. Pass the suspension once through the Cell disrupter at 20,000 psi. Collect the supernatant on ice after cell disruption is complete.

11. Place the supernatant in ultracentrifuge Ti45 rotor and spin at 36000 rpm at 4 $^{\circ}$C for 60minutes.

12. Make Ni-NTA superflow/agarose column: Column size for a 1 L culture = 2 mL

13. Equilibrate the column with 10 column volumes of equilibration buffer with a flow rate of 0.5 mL/min (for Ni-NTA agarose) or 1mL/min (for Ni-NTA superflow). The same speed is retained for loading, washing and elution.

14. Load the supernatant onto the column. Collect Load Flow Through (LFT).

15. Wash the column with wash buffer (1) and wash buffer (2) until the protein profile returns to baseline and keep washing using 10 mL more of buffer.

16. Elute the protein with elution buffer. Optionally, you can get more pure protein if running a gradient elution. Run SDS-PAGE to confirm the purity. Measure the protein concentration at A_{280}. The protein level (mg/mL) is then calculated as follows: [protein] (mg/mL)=OD_{280}/1.2

17. Dialyze the elute against the Dialysis buffer and change once next day. Alternatively use 30 kDa MWCO ultracentrifuge filter tubes to concentrate protein. Wash 3 times with 50 mM sodium acetate buffer (pH 5.0) containing sodium cholate (1mg/mL) and store concentrated enzyme in 4 $^{\circ}$C.

Reference:

1. Comprehensive Profiling of Glycosphingolipid Glycans Using a Novel Broad Specificity Endoglycoceramidase in a High-Throughput Workflow. Simone Albrecht, Saulius Vainauskas, Henning Stöckmann, Ciara McManus, Christopher H. Taron, and Pauline M. Rudd, *Analytical Chemistry* **2016** *88* (9), 4795-4802

Expression and purification of recombinant Sphingolipid ceramide *N*-deacylase (SCDase)

Blake Zheng and Radhika Chakraberty

Background: The gene encoding the mature SA_SCD protein, which lacks its 38-residue N-terminal secretion signal sequence and from which the 277-residue C-terminal sequence has been deleted, was codon-optimized for E. coli and synthesized (Genscript Corporation). The gene sequence was subcloned into pET23b vector (Novagen, Madison, USA) using the NdeI/XhoI restriction sites and was transformed into E. coli BL21 (DE3) pLysS and expressed as an N-His6-tagged protein.

Day 1:

1. Prepare culture media (1.1 L): Dissolve 27.5g LB Broth powder (BP9723-500, Miller, Granulated) in 1.1L MQ water and agitate to completely dissolve. Place 100mL of this solution in 500mL clean baffled Erlenmeyer flask and 1L of this solution in 4L clean baffled Erlenmeyer flask. Plug and cover with aluminum foil. Sterilize by autoclaving (cycle 4)

2. Prior to inoculation, add 100µL of 100mg/mL Ampicillin (Amp) and 35mg/mL Chloramphenicol into the 100mL of LB media:

3. Remove the glycerol stock from the freezer (storage box labelled as "Blake's bacterial stocks") and place on dry ice. Do not allow it to thaw. Scrape a little frozen bacteria glycerol stock onto a sterile, plastic loop and transfer to the media. Incubate at 37°C overnight (not more than 16 hours) with shaking at 200 rpm.

Day 2:

4. Add the following into the above autoclaved scale-up media. For a 4L flask (1L media), add:
>   1mL of 100mg/mL Ampicillin (Amp)
>   1mL of 35mg/mL Chloramphenicol
>   20mL of turbid starter culture

5. Grow the culture at 37°C with shaking until the OD_{600} reaches ~ 0.8.

6. Add 1 (M) IPTG to a final concentration of 0.1mM.

7. Shake at $16\,^{o}$C for 18-20 hours (overnight) at 200 rpm.

Day 3:

8. Remove the culture and spin in JLA8.1 rotor at 6000 rpm for 30 minutes. (Before you remove the culture in the centrifuge tubes, weigh an empty tube first. After you finish spinning, pour off supernatant and collect all cell pellets into the weighed tube and then weigh the tube again, to get the wet cells' weight). Cells maybe frozen at this stage in -20 $^{\circ}$C and used later.

Note: JLA8.1 centrifugal tubes could not be stored at -20 $^{\circ}$C. You have to re-suspend cell pellets in PBS and transfer to a 50mL plastic centrifugal tube and spin again. Remove the S/N and stored at a freezer. OR directly transfer the pellets to a 50 mL plastic centrifugal tube using a plastic spatula.
All centrifugation and manipulations of the protein is at 4°C.

Day 4:

Resuspesion buffer
300 mM NaCl
10mM Imidazole
0.1% Triton X-100
50 mM Tris-Cl (pH=7.5)

Wash buffer (1)
300 mM NaCl
20mM Imidazole
50 mM Tris-Cl (pH=7.5)

Wash buffer (2)
300 mM NaCl
50mM Imidazole
50 mM Tris-Cl (pH=7.5)

Elution buffer
300 mM NaCl
250mM Imidazole
50 mM Tris-Cl (pH=7.5)

Dialysis buffer
0.15M NaCl
50 mM Tris-Cl (pH=7.5)

Equilibration buffer
300 mM NaCl
50 mM Tris-Cl (pH=7.5)

9. Re-suspend cell pellets in the cold Re-suspension buffer (see the above re-suspension buffer). The ideal suspension has 10-15g of pellets (wet weight) per 100 mL solution. Re-suspend with Biorad plastic pipette, keeping suspension on ice until homogenous. Suspension should be soupy, not too thick. Otherwise, lots of foam will be found in your lysis. Alternatively, re-suspend by first breaking up the cell pellet with a Teflon spatula and then passing the solution in and out of a 60 mL syringe until homogeneous. Add Roche Protease Inhibitor EDTA-free Cocktail tablets (full size, not Mini) at 1 tablet/50 mL cell extract.

10. Pass the suspension once through the Cell disrupter at 20,000 psi. Collect the supernatant on ice after cell disruption is complete.

11. Place the supernatant in ultracentrifuge Ti45 rotor and spin at 36000 rpm at 4 $^{\circ}$C for 60 minutes.

12. Make Ni-NTA superflow/agarose column: Column size for a 1 L culture = 2 mL

13. Equilibrate the column with 10 column volumes of equilibration buffer with a flow rate of 0.5 mL/min (for Ni-NTA agarose) or 1mL/min (for Ni-NTA superflow). The same speed is retained for loading, washing and elution.

14. Load the supernatant onto the column. Collect Load Flow Through (LFT).

15. Wash the column with wash buffer (1) and wash buffer (2) until the protein profile returns to baseline and keep washing using 10 mL more of buffer.

16. Elute the protein with elution buffer. Optionally, you can get more pure protein if running a gradient elution. Run SDS-PAGE to confirm the purity. Measure the protein concentration at A_{280}. The protein level (mg/mL) is then calculated as follows: [protein] (mg/mL)=OD_{280}/1.2

17. Dialyze the elute against the Dialysis buffer and change once next day. Alternatively use 50 kDa MWCO ultracentrifuge filter tubes to concentrate protein. Wash 3 times with 25 mM sodium acetate buffer (pH 6.0) containing 0.1% Triton X-100 and store concentrated enzyme in 4 $^{\circ}$C.

Reference:
Comprehensive characterization of sphingolipid ceramide N-deacylase for the synthesis and fatty acid remodeling of glycosphingolipids
Yun-Bin Han, Lie Wu, Jamie R. Rich, Feng-Tao Huang, Stephen G. Withers, Yan Feng & Guang-Yu Yang
Appl Microbiol Biotechnol **2015** 99, 6715–6726

Extraction and purification of glycosphingolipids (GSLs) from cells, tissues and plasma

Radhika Chakraberty

(Ganglioside GM1)
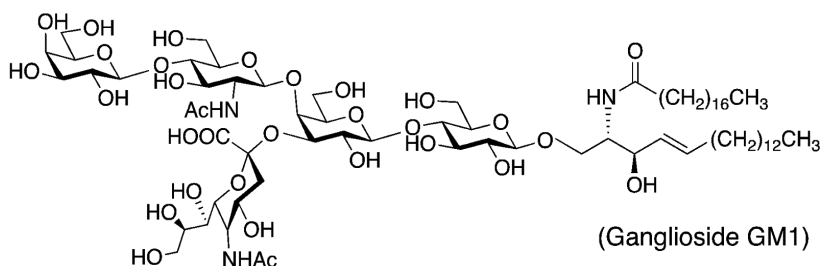
Short summary

Glycosphingolipids (GSLs) are a complex class of glycolipids that are synthesized by a large number of eukaryotic cells. This protocol describes the extraction and purification of GSLs from cell and tissue lysates and also plasma samples.

Methods

Tissue or Plasma:

1. Weigh tissue homogenate or plasma by difference.
2. Dilute tissue homogenate or plasma with 4 volumes of ice-cold water (4 mL/g based on wet tissue weight or wet weight of plasma).

3. Calculate "total aqueous volume" as follows: volume of water added + 80% of wet tissue weight. Eg: Total aqueous volume of 1 gm of tissue weight would be 4.8 mL.

4. Suspend tissue homogenously in water by aspirating with a pipet

5. Add 2.67 volumes of methanol (based on total aqueous volume), mix thoroughly, vortex and allow the mixture to come to room temperature.

6. Add 1.33 volumes of chloroform, again based on total aqueous volume. Mix thoroughly and vortex again.

Example calculation:

　　Weight of sample: 17.5 mg
　　Amount of water to add: 17.5 mg x 4 = 70 uL
　　Total Aqueous volume: (0.8 x 17.5 mg) + 70 uL = 84 uL
　　Amount of Methanol to add: 2.67 x 84 uL = 224. 28 uL
　　Amount of Chloroform to add: 1.33 x 84 uL = 111.72 uL

7. Centrifuge the suspension at 1500 rpm on a table-top centrifuge for 15 mins.

8. Transfer the supernatant to a fresh tube. Measure this volume as the "recovered extract volume". Note down the volume of supernatant as "recovered extract volume".

9. Add 0.173 volumes of water, based on the "recovered extract volume". Mix thoroughly and vortex.

10. Centrifuge this suspension at 1500 rpm for 15 min.

11. Recover the upper phase and transfer to a fresh tube. The upper phase is much more distinguishable at this step and easier to separate.

12. During the above centrifugation, equilibrate a SepPak C18 cartridge with ~ 3mL each of the following (in the given order): (i) chloroform-methanol-water (2:43:55), (ii) methanol-water (1:1), (iii) 100% methanol, (iv) methanol-water (1:1) and (v) chloroform-methanol-water (2:43:55). Each addition should be added via a 3 or 5 mL syringe and the flow should be dropwise and consistent. A waste container should be underneath the cartridge.

13. Slowly load the recovered upper phase from centrifugation onto the pre-equilibrated C18 with the waste container still underneath. Wash this with 3 mL each of (i) chloroform-methanol-water (2:43:55), (ii) methanol-water (1:1).

14. SLOWLY and CONSISTENTLY elute GSLs with 3 mL of 100% methanol into a fresh glass tube. Record the weight of the empty glass tube before elution, so as to calculate the weight of the dried extract by difference. **NOTE: Using a glass bottle is critical. Storing purified extracts in plastic tubes may lead to degradation of GSLs.**

15. Evaporate the eluate to dryness under a stream of Nitrogen gas.

16. Use dried extract as required.

Cells:

1. Culture cells according to respective protocols.

2. Remove a suspension of cells containing ~ 10^6 – 10^7 cells, from growth media into a centrifuge tube.

3. Centrifuge at 1200 rpm for 2 mins

4. Discard media and wash cell lysate with 1 mL PBS buffer (3 times)

5. Discard PBS buffer and record wet weight of cell lysate

6. Perform extraction according to the protocol mentioned above for tissues and plasma

Reagents

1. Chloroform

2. Methanol

3. PBS

Safety

1. Regular items of PPE including lab coats and safety glasses must be worn at all times

2. All organic solvents are flammable and toxic. Care must be taken while handling them, to avoid skin contact and inhalation.

3. Cells, tissues and plasma are bio-hazardous. Clean surfaces and equipment must be used at all times while handling these samples.

References

1. M, Tiemeyer M, Marth JD, Schnaar RL. **2012**. Biosynthesis of the major brain gangliosides GD1a and GT1b. Glycobiology 22:1289-1301.

Ganglioside profiling in cells and tissues using Endoglycoceramidase (EGCase)

Radhika Chakraberty
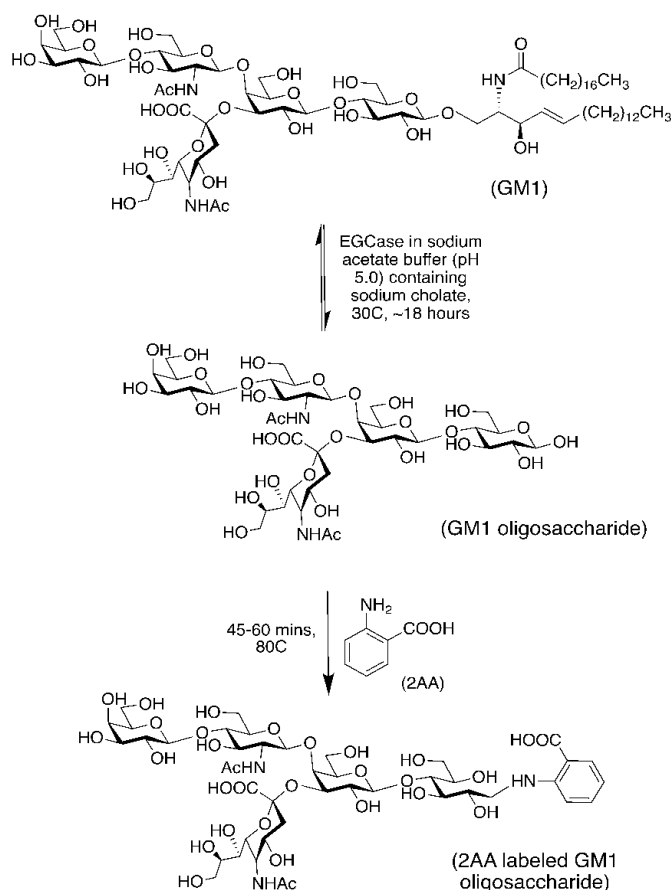
Short summary

Gangliosides belong to the class of glycosphingolipids, characterized by a carbohydrate moiety bearing 1 or more sialic acid residues along with a ceramide moiety composed of a fatty acid chain and a sphingosine base. Because of the two degrees of variability in structure of these biomolecules i.e. glycans and lipid chain, accurate analysis and quantitation of gangliosides has been very challenging. One of the ways to do this is by enzymatic modification of gangliosides using the EGCase enzyme that cleaves off the entire ceramide portion generating a free glycan. The reducing end of the glycans can be fluorescently labeled and analyzed via HPLC or LC-MS.

289

The fluorophore chosen here is Anthranilic acid (2AA), which is a common reagent used for the purpose of labeling via a simple reductive amination mechanism, using a mild reducing agent sodium cyanoborohydride.

Methods

1. **EGCase production**: Follow the detailed SOP on the group drive titled "Expression and purification of EGCase"

2. Preliminary test of enzyme activity is performed by incubating a standard GSL such as GM3 (5 μL from a 1 mg/ml stock solution) with EGCase (5 μL), in reaction buffer (50 mM sodium acetate, pH 5.0, containing sodium cholate), keeping total volume of reaction mixture ~30 μL.

a.   Incubate the reaction mixture for 60 mins at 30°C

b.   Remove from incubation and spot on TLC plate. Wait till the spots are dry.

c.   TLC plate is developed with solvent mixture AcOH : n-Butanol : 0.25% $CaCl_2$ in the ratio (1:2:1)

d.   Dry the TLC plate and stain with Orcinol-sulphuric acid staining solution to visualize spots for reactant GM3 and product 3'-sialyllactose

3.   To calculate specific activity of EGCase, test using 3'SL, which is the digestion product of GM3. Taking serial dilutions of 3'SL, label each sample with 20 μL of 2-aminobenzoic acid or anthranilic acid (2AA) [fluorophore mixture recipe is provided in the reagents section], at 80°C for 45 mins.

a.   Post labelling clean-up using Discovery DPA-6S amide HILIC columns:

1. equilibrate with 2 x 1 mL 100% acetonitrile.

2. dilute sample with 1 mL of 97:3 Acetonitrile to water.

3. load sample onto column 1 mL at a time.

4. wash column with 4 x 1 mL of 99:1 Acetonitrile to water.

5. wash column with 0.5 mL of 97:3 Acetonitrile to water

6. elute the products into a new epitube with 2 x 0.6 mL 100% water

b.   Measure fluorescence intensity of each of the serially diluted 3'SL solutions on a plate reader, to obtain a calibration curve of fluorescence intensity vs concentration.

c.   Take an unknown amount of GM3, incubate it with EGCase as mentioned above for 60 mins. Label with 2AA following the same labelling and clean-up protocol as above.

d.   Measure fluorescence intensity for this unknown concentration of GM3. Using the 3'SL calibration curve and observed intensity for GM3, calculate the concentration of 3'SL released by EGCase. Report specific activity in Units/ml (U/ml).

4.   **Pig brain homogenization**: ~ 6 g of pig brain tissue is homogenized in 30 ml (w/v ratio is 1:5) of solvent (4 ml methanol + 2 ml chloroform + 1.5 ml water) using the homogenizer in Biological services (Gareth's lab). Aliquots of homogenate stored in -80°C.

5.   **Extraction of gangliosides**: Follow detailed SOP on the group drive (Extraction and purification of glycosphingolipids from cells, tissues and plasma) . Amount of starting material required is as follows:

   a. 1×10^6 cells (Jurkat, PC3, Raji, HeLa)

   b. 10 µL pig/mouse brain homogenate

   c. 50 µL human/mouse plasma

6.   The dried extract is re-dissolved in minimum amount of methanol. The final extracts are again dried and dissolved in the EGCase reaction buffer (start with 50 uL and see if it dissolves, add 50 uL more if necessary) . Appropriate volume of EGCase (10 uL) is added to the reaction mixture and gangliosides are incubated at 30°C for ~18 hours to release the corresponding glycans.

7.   Appropriate amount of internal standard (Maltose) is spiked into each of the samples (depending on the amount of tissue used or number of cells used and the dry weight of extract). The mixture is then labeled with 2AA (20 uL), and incubated at 80°C for 45 minutes, and then cleaned-up in the same manner using Discovery DPA-6S amide HILIC columns as mentioned above (Step 3 a)).

8.   The final eluents are reduced under vacuum (dry on a speed vac) and submitted for LC-MS analysis.

9.   LC-MS is carried out using a Normal phase column (Accucore-150-Amide-HILIC, 2.6 µm, 2.1 x 150 mm, Thermo Fisher). The fluorescence detector is set to monitor at excitation 320 nm, emission 420 nm and all chromatography is performed at 40°C. The binary solvent system follows a linear gradient with a flow rate of 0.4 ml/min (Solvent A: 100 mM ammonium formate, pH 4.45; Solvent B: 100% acetonitrile). Flow was split ~ 50:50 between fluorescence and mass spectrometry (MS) detectors. MS was used to assign and confirm the identity of fluorescent peaks. Mass spectra were acquired in negative mode using an Agilent 6220 Accurate-Mass TOF HPLC/MS system with a dual spray electrospray ionization source along with a secondary reference sprayer for a reference mass solution. Data analysis was performed using the Agilent MassHunter Qualitative Analysis software package version B.07.01. The gradient conditions are given in the following table.

MCP: 650V; PMT: 859V
Fragmentor: 140V, Source: 3800V

FLD: Excitation 320nm, Emission 420nm
Gradient:

Time (min)	0	1	1.5	6.5	41.5	43.5	44	50
% B	90	90	75	75	45	45	90	90

Reagents

1. Reaction buffer: 50 mM sodium acetate (pH 5.0) containing sodium cholate (1 mg/ml)

2. 2AA fluorescent mixture: 30 mg anthranilic acid, 20 mg boric acid, 40 mg sodium acetate, 45 mg sodium cyanoborohydride dissolved in 1 ml methanol. Make sure pH of labeling solution is ~5.2. Best to only use within a week of preparation.

3. Methanol

4. Acetonitrile

5. n-Butanol

6. Chloroform

7. Acetic acid

8. Sulphuric acid

Safety

1. Regular items of PPE including lab coats and safety glasses must be worn at all times

2. All organic solvents are flammable and toxic. Care must be taken while handling them, to avoid skin contact and inhalation.

3. Acetic acid may cause serious burns, wash with a lot of water in case of any spills.

4. Cells and tissues are bio-hazardous. Clean surfaces and equipment must be used at all times while handling these samples.

References

1. Neville DC, Coquard V, Priestman DA, te Vruchte DJ, Sillence DJ, Dwek RA, Platt FM, ButtersTD. **2004**. Analysis of fluorescently labeled glycosphingolipid-derived oligosaccharidesfollowing ceramide glycanase digestion and anthranilic acid labeling. Anal Biochem 331:275-282

2. M, Tiemeyer M, Marth JD, Schnaar RL. **2012**. Biosynthesis of the major brain gangliosides GD1a and GT1b. Glycobiology 22:1289-1301.

Ganglioside profiling in cells, tissues and plasma using Sphingolipid ceramide *N*-deacylase (SCDase)

Radhika Chakraberty
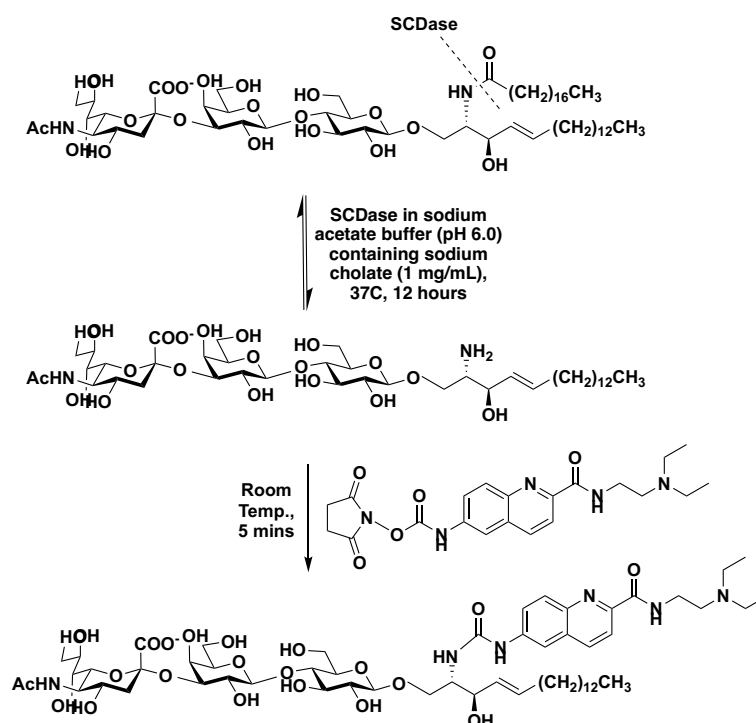
Short summary

Gangliosides belong to the class of glycosphingolipids, characterized by a carbohydrate moiety bearing 1 or more sialic acid residues along with a ceramide moiety composed of a fatty acid chain and a sphingosine base. Because of the two degrees of variability in structure of these biomolecules i.e. glycans and lipid chain, accurate analysis and quantitation of gangliosides has been very challenging. One of the ways to do this is by enzymatic modification of gangliosides using the SCDase enzyme that cleaves off the fatty acid chain of the ceramide moetiy, generating a lyso-ganglioside bearing a free primary amine residue. This primary amine is then labelled with a fluorophore and analyzed by HPLC or LC-MS. This method gives us information about the sphingosine chain of gangliosides, a complementary method to the already established EGCase method in our lab, that gives us information about the glycan/carbohydrate moeity of gangliosides.

The fluorophore chosen here is RapiFluor-MS, generously supplied by Waters Corporation. RapiFluor is designed specifically to be used in Mass Spectrometry analysis because of the tertiary amine group that is highly sensitive in positive mode MS analysis. The labeling reaction is a quick and simple amine coupling between the primary amine of lyso-gangliosides and the NHS ester group on RapiFluor.

Methods

1. **SCDase production**: Follow the detailed SOP on the group drive titled "Expression and purification of SCDase"

2. Preliminary test of enzyme activity is performed by incubating a commerially available standard GSL such as GM3 (5 µL from a 1 mg/mL stock solution) with SCDase (5 uL), in reaction buffer (25 mM sodium acetate, pH 6.0, containing sodium cholate), keeping total volume of reaction mixture ~30 uL.

a. Incubate the reaction mixture for 1-2 hours at 37 °C

b. Remove from incubation and spot on TLC plate. Wait till the spots are dry.

c. TLC plate is developed with solvent mixture AcOH : n-Butanol : 0.25% $CaCl_2$ in the ratio (1:2:1)

d. Dry the TLC plate and stain with Orcinol-sulphuric acid staining solution to visualize spots for reactant GM3 and product lyso-GM3.

3. To calculate specific activity of SCDase, test using a standard ganglioside such as GM3 and GM1. Taking a known amount of a commercially available standard , incubate it with SCDase and monitor the reaction completion over time. Time points taken: 2, 6, 10, 14, 24, 36 hours. After each time point, the lyso products in the reaction mixture are labelled with 12 µL RapiFluor (fluorophore mixture recipe provided in the reagents section) for 5 mins at room temperature.

a. Post labelling clean-up using GlycoWorks HILIC µElution plate (Waters Corporation):

1. prep column with 200 µL MQ water

2. equilibrate wit 200 µL or 15:85 MQ water:acetonitrile

3. load 400 µL sample onto column

4. wash column with 2 x 600 µL of 1:9:90 of formic acid: MQ water: acetonitrile

5. elute products with 4 x 30 µL of 200 mM ammonium acetate in 5% acetonitrile

b. Spike in a known amount (µg) of external standard (details of external standard provided in reagents section), that has already been labelled with RapiFluor previously and run this on the LC-MS

c. Plot FLD peak area vs Time

d. Using the fluorescence peak areas of external standard and lyso-product, calculate the amount of product generated at each time point in μg in the following way:

1. Take peak are of external standard as a 100%

2. Express peak areas of lyso products as a percentage of this

3. Calculate the absolute amount of lyso product from the known amount of external standard initially spiked in

Convert the absolute amount to μmole, express that as a concentration value i.e. μmole /mL (volume of the reaction mixture) to express specific enyme activity in μmol/hour/mL or U/mL.

4. **Pig brain homogenization**: ~ 6 g of pig brain tissue is homogenized in 30 ml (w/v ratio is 1:5) of solvent (4 ml methanol + 2 ml chloroform + 1.5 ml water) using the homogenizer in Biological services (Gareth's lab, Biological Services). Aliquots of homogenate stored in -80°C.

5. **Extraction of gangliosides**: Follow detailed SOP on the group drive titled "Extraction and purification of glycosphingolipids from cells, tissues and plasma". Amount of starting material required is as follows:

a. 1×10^7 cells (Jurkat tested)

b. 30 μL pig brain homogenate

c. 200 μL human plasma

6. The dried extract is re-dissolved in minimum amount of methanol. The final extracts are again dried under nitrogen gas and dissolved in the SCDase reaction buffer. Appropriate volume of SCDase is added to the reaction mixture and gangliosides are incubated at 37°C for ~14 hours (depending on specific activity found in Step 3) to release the corresponding lyso-gangliosides.

7. The mixture is then labeled with RapiFluor (12 μL), and kept at room temperature for 5 minutes, and then cleaned-up in the same manner using GlycoWorks HILIC μElution plate as mentioned above (Step 3 a). A known amount of external standard is spiked in before LC-MS analysis.

8. LC-MS is carried out using a Mixed mode column (Dionex/Thermo Fisher, GlycanPAC AXR-1, 1.9 um, 2.1 x 150 mm). The fluorescence detector is set to monitor at excitation 265 nm, emission 465 nm and all chromatography is performed at 50°C. The binary solvent system followed a linear gradient with a flow rate of 0.4 mL min^{-1} (Solvent A: dd Water; Solvent B: 50 mM ammonium formate, pH 4.45 in 40:60 water/acetonitrile). Flow was split ~ 50:50 between fluorescence and mass spectrometry (MS) detectors. MS was used to assign and confirm the identity of fluorescent peaks. Mass spectra were acquired in negative mode using an Agilent 6220 Accurate-Mass TOF

HPLC/MS system with a dual spray electrospray ionization source along with a secondary reference sprayer for a reference mass solution. Data analysis was performed using the Agilent MassHunter Qualitative Analysis software package version B.07.01. The gradient conditions are given in the following table.

MCP: 650V; PMT: 850V
Fragmentor: 150V, Source: 4000V
FLD: Excitation 265nm, Emission 425nm
Gradient:

Time (min)	0	1	43	53	55	56	60
% B	50	50	65	100	100	50	50

Reagents

1. SCDase Reaction buffer: 25 mM sodium acetate (pH 6.0) containing sodium cholate (1 mg/ml)

2. RapiFluor fluorescent mixture: 9 mg GlycoWorks RapiFluor-MS reagent powder in 131 uL of GlycoWorks Reagent solvent anhydrous DMF. Weigh out as much as required per run and use immediately. Storing RapiFluor in solution decreases labeling efficiency over time. (Store dried powder in a dessicator after opening package)

3. Methanol

4. Acetonitrile

5. n-Butanol

6. Chloroform

7. Acetic acid

8. Sulphuric acid

9. External standard i.e. Lactose-NH_2 synthesis shown below. This is labelled separately according to the aforementioned labeling and clean-up protocols. Finally, a known amount of this is spiked in to the bilogical samples for testing.

Safety

1. Regular items of PPE including lab coats and safety glasses must be worn at all times

2. All organic solvents are flammable and toxic. Care must be taken while handling them, to avoid skin contact and inhalation.

3. Acetic acid may cause serious burns, wash with a lot of water in case of any spills.

4. Cells and tissues are bio-hazardous. Clean surfaces and equipment must be used at all times while handling these samples.

External Standard (synthesized by Dr. Gour Chand Daskhan)
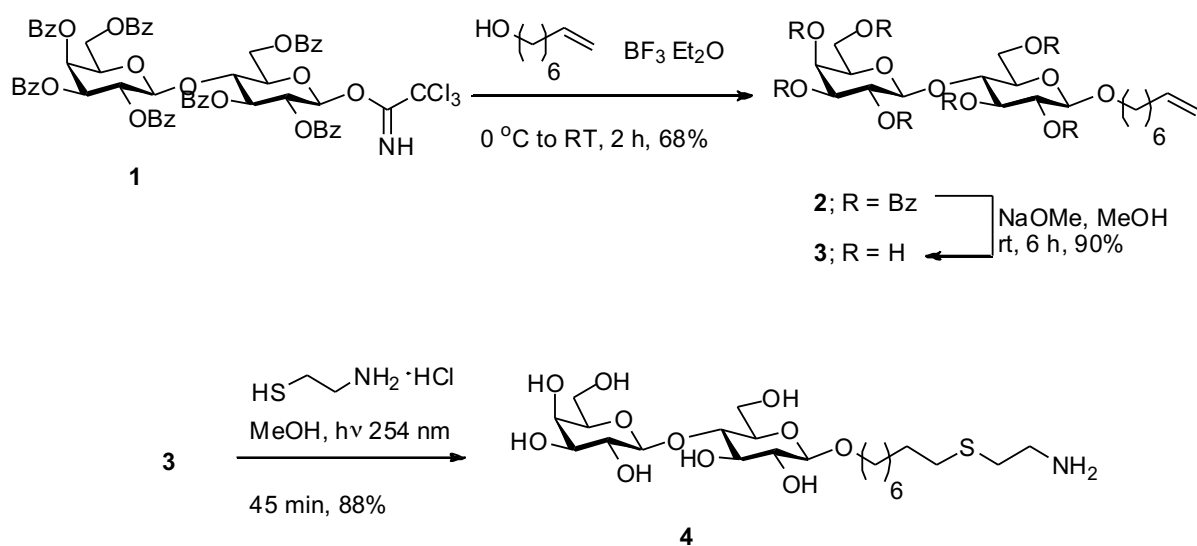
EXPERIMENTAL PROCEDURES
1-octyl-b-D-galactopyranosyl-(1→4)-b-D-glucopyranoside (3)
A mixture of trichloroacetimidate 1 (510 mg, 0.42 mmol), 1-ocyl alcohol (0.1 mL, 0.84 mmol) and powdered molecular sieves was suspended in dry CH_2Cl_2 (10 mL) and stirred at RT for 1 h. The solution was cooled to $0^{\circ}C$, and boron trifluoride diethyl etherate (59 µL, 0.42 mmol) were added slowly to the reaction mixture. After stirring the reaction mixture at $0^0 C$ for 2 h, Et3N (1 mL) was added and the mixture was filtered through Celite. The filtrate was concentrated, and the resulting residue was subjected to flash chromatography (2:1 v/v hexane/EtOAc) to afford protected derivative 2 (340 mg, 68%). NaOMe (1.0 m, few drops) was added to a solution of 2 (340 mg, 0.28 mmol) in dry MeOH (10 mL). After stirring at RT overnight, the solution was neutralized with Amberlite IR120 H+ ion-exchange resin. The solution was filtered and the filtrate was concentrated to afford 3 as a white solid (120 mg, 92 %) as white foam after C_{18} Sep-pak chromatography purification using eluent system H_2O to $MeOH/H_2O$ (1:9) and lyophilization. HRMS (ESI): m/z [M+H]+ calcd for C20H36O11: 553.2630, found: 553.2628.

8-[(2-Aminoethyl)thiol)]-1-octyl-b-D-galactopyranosyl-(1→4)-b-D-glucopyranoside (4)

Compound **3** (10 mg, 0.24 mmol) and cysteamine hydrochloride salt (27.2 mg, 0.024 mmol) were dissolved in anhydrous MeOH (0.5 mL) in a quartz tube. The solution was degassed and the tube was filled with argon. The reaction mixture was irradiated under UV light for 1 h, the solution was concreted and the crude mixture was purified by C_{18} sep-pak chromatography using gradient elution (0.5% aq AcOH to 1:8 v/v MeOH/0.5% aq AcOH) followed by treatment with HO$^-$ resin afforded the corresponding amine **4** (10.4 mg, 89 %). ^{1}H NMR (600 MHz, D$_2$O): δ 4.43 (d, J = 7.8, 1H), 4.40 (d, J = 7.8, 1H), 3.93 (dd, J = 10.8, 1.2 Hz, 1H), 3.88-3.85 (m, 2H), 3.75 (dd, J = 10.8, 4,2 Hz, 1H), 3.72 (dd, J = 10.8, 4.2 Hz, 1H), 3.69-3.67 (m, 2H), 3.66-3.59 (m, 4H), 3.55-3.54 (m, 1H), 3.50 (dd, J = 9.6, 7.8 Hz, 1H), 3.26 (t, J = 8.4 Hz, 1H), 3.09 (t, J = 6.6 Hz, 2H), 2.76 (t, J = 6.6 Hz, 2H), 2.55 (t, J = 7.2 Hz, 2H), 1.59-1.53 (m, 4H), 1.35-1.28 (m, 8H); ^{13}C NMR (126 MHz, D$_2$O): δ 103.9, 102.9, 79.4, 76.3, 75.5, 75.4, 73.8, 73.5, 71.9, 71.7, 62.0, 61.1, 39.3, 31.7, 29.6, 29.5, 29.2, 29.1, 28.8, 28.7, 25.9, 24.0. HRMS (ESI): m/z [M+H]+ calcd for C22H43NO11S: 530.2630, found: 530.2629.

Table F– 1. Compound search database for 2AA labeled glycans

Formula		Mass	Compound
C19H29N1O12		463.169	2AA-LacCer
C25H39NO17		625.2218	Gb3
C32H48N2O21		796.275	2AA-Ac-GM3
C30H46N2O20		754.26439	2AA-GM3
C40H61N3O26		999.3543	2AA-Ac-GM2
C38H59N3O25		957.3438	2AA-GM2
C46H71N3O31		1161.4072	2AA-Ac-GM1
C44H69N3O30		1119.3966	2AA-GM1
C43H65N3O29		1087.3704	2AA-Ac-GD3
C41H63N3O28		1045.3598	2AA-GD3
C54H82N4O37		1378.4658	2AA-Ac-GT3
C52H80N4O36		1336.4552	2AA-GT3
C57H88N4O39		1452.5026	2AA-Ac-GD1a
C55H86N4O38		1410.492	2AA-GD1a
C68H105N5O47		1743.598	2AA-Ac-GT1b
C66H103N5O46		1701.5874	2AA-GT1b
C27H42N2O17		666.2483	2AA-GA2
C33H52N2O22		828.3012	2AA-GA1
C57H88N4O39		1452.5026	2AA-Ac-GD1
C55H86N4O38		1410.492	2AA-GD1
C51H78N4O34		1290.4497	2AA-Ac-GD2
C49H76N4O33		1248.4392	2AA-GD2
C24H36N2O15		592.2116	2AA-GM4
C62H95N5O42		1581.5452	2AA-Ac-GT2
C60H93N5O41		1539.5346	2AA-GT2
C79H122N6O55		2034.6934	2AA-Ac-GQ1b
C77H120N6O54		1992.6828	2AA-GQ1b
C12H18N1O6		272.1134	2AA-Gal
C12H17N1S1O9		351.0624	2AA-GAL-Sulfatide
C90H139N7O63		2325.7888	2AA-Ac-GP1b
C88H137N7O62		2283.7783	2AA-GP1b
C42H71N3O32		1129.4021	2AA-Ac-GM1Gc
C44H69N3O31		1135.3915	2AA-GM1Gc
C57H88N4O40		1468.4975	2AA-Ac-GD1aGc
C55H86N4O39		1462.4869	2AA-GD1aGc
C68H105N5O48		1759.5929	2AA-Ac-GT1bGc
C66H103N5O47		1717.5823	2AA-GT1bGc
C40H61N3O27		1015.3492	2AA-Ac-GM2Gc
C38H59N3O26		973.3387	2AA-GM2Gc
C42H65N3O30		1091.3653	2AA-Ac-GD3Gc

Formula	Mass	Compound
C41H63N3O29	1061.3547	2AA-GD3Gc
C32H48N2O22	812.2699	2AA-Ac-GM3Gc
C30H46N2O21	770.2593	2AA-GM3Gc
C62H95N5O43	1597.5401	2AA-Ac-GT2Gc
C60H93N5O42	1555.5295	2AA-GT2Gc
C54H82N4O38	1394.4607	2AA-Ac-GT3Gc
C52H80N4O37	1352.4501	2AA-GT3Gc
C79H122N6O56	2050.6883	2AA-Ac-GQ1bGc
C77H120N6O55	2008.6778	2AA-GQ1bGc
C90H139N7O64	2341.7837	2AA-Ac-GP1bGc
C88H137N7O63	2299.7732	2AA-GP1bGc
C52H81N3O35	1307.4651	2AA-Ac-Fucosyl GM1
C50H79N3O34	1265.4545	2AA-Fucosyl GM1
C23H39N1O16	585.2269	2AA-Fucosyl lactose
C61H96N4O42	1556.5499	2AA-Fucosyl-GD1a
C72H113N5O50	1847.6453	2AA-Fucosyl-GT1a
C63H98N4O43	1598.5605	2AA-Fucosyl-Ac-GD1a
C83H130N6O58	2138.7407	2AA-Fucosyl-GQ1b
C45H72N2O30	1120.417	2AA-FFHHHN

Table F– 2. Compound search database for RapiFluor labeled lyso-gangliosides

Formula		Mass	Compound
C58H92N6O23		1240.6214	GM3-Ac-C16
C56H90N6O22		1198.6108	GM3-C16
C59H94N6O23		1254.637	GM3-Ac-C17
C57H92N6O22		1212.6265	GM3-C17
C60H96N6O23		1268.6527	GM3-Ac-C18
C58H94N6O22		1226.6421	GM3-C18
C58H92N6O22		1224.6265	GM3-C18 (d18:2)
C54H84N6O23		1184.5588	GM3-Ac-C12
C52H82N6O22		1142.5482	GM3-C12
C55H86N6O23		1198.5744	GM3-Ac-C13
C53H84N6O22		1156.5639	GM3-C13
C56H88N6O23		1212.5901	GM3-Ac-C14
C54H86N6O22		1170.5795	GM3-C14
C57H90N6O23		1226.6057	GM3-Ac-C15
C55H88N6O22		1184.5952	GM3-C15
C61H98N6O23		1282.6683	GM3-Ac-C19
C59H96N6O22		1240.6578	GM3-C19
C62H100N6O23		1296.684	GM3-Ac-C20

C60H98N6O22	1254.6734	GM3-C20
C63H102N6O23	1310.6996	GM3-Ac-C21
C61H100N6O22	1268.6891	GM3-C21
C64H104N6O23	1324.7153	GM3-Ac-C22
C62H102N6O22	1282.7047	GM3-C22
C65H106N6O23	1338.7309	GM3-Ac-C23
C63H104N6O22	1296.7204	GM3-C23
C66H108N6O23	1352.7466	GM3-Ac-C24
C64H106N6O22	1310.736	GM3-C24
C67H110N6O23	1366.7622	GM3-Ac-C25
C65H108N6O22	1324.7517	GM3-C25
C41H65N5O14	851.4528	LacCer-C12
C42H67N5O14	865.4685	LacCer-C13
C43H69N5O14	879.4841	LacCer-C14
C44H71N5O14	893.4998	LacCer-C15
C45H73N5O14	907.5154	LacCer-C16
C46H75N5O14	921.5311	LacCer-C17
C47H77N5O14	935.5467	LacCer-C18
C48H79N5O14	961.5624	LacCer-C19
C49H81N5O14	975.578	LacCer-C20
C50H83N5O14	989.5937	LacCer-C21
C51H85N5O14	1003.6093	LacCer-C22
C52H87N5O14	1017.625	LacCer-C23
C53H89N5O14	1031.6406	LacCer-C24
C54H91N5O14	1045.6563	LacCer-C25
C68H107N7O33	1549.691	GM1-Ac-C12
C66H105N7O32	1507.6804	GM1-C12
C69H109N7O33	1563.7066	GM1-Ac-C13
C67H107N7O32	1521.6961	GM1-C13
C70H111N7O33	1577.7223	GM1-Ac-C14
C68H109N7O32	1535.7117	GM1-C14
C71H113N7O33	1591.7379	GM1-Ac-C15
C69H111N7O32	1549.7274	GM1-C15
C72H115N7O33	1605.7536	GM1-Ac-C16
C70H113N7O32	1563.743	GM1-C16
C73H117N7O33	1619.7692	GM1-Ac-C17
C71H115N7O32	1577.7587	GM1-C17
C74H119N7O33	1633.7849	GM1-Ac-C18
C72H117N7O32	1591.7743	GM1-C18
C72H115N7O32	1598.7587	GM1-C18 (d18:2)
C75H121N7O33	1647.8005	GM1-Ac-C19

C73H119N7O32	1605.79	GM1-C19
C76H123N7O33	1661.8162	GM1-Ac-C20
C74H121N7O32	1619.8056	GM1-C20
C75H123N7O32	1633.8213	GM1-C21
C76H125N7O32	1647.8369	GM1-C22
C77H127N7O32	1661.8526	GM1-C23
C78H129N7O32	1675.8682	GM1-C24
C79H131N7O32	1689.8839	GM1-C25
C73H117N7O36	1667.754	Fuc-GM1-C13
C74H119N7O36	1681.7696	Fuc-GM1-C14
C75H121N7O36	1695.7853	Fuc-GM1-C15
C76H123N7O36	1709.8009	Fuc-GM1-C16
C77H125N7O36	1723.8166	Fuc-GM1-C17
C78H127N7O36	1737.8322	Fuc-GM1-C18
C79H129N7O36	1751.8479	Fuc-GM1-C19
C80H131N7O36	1765.8635	Fuc-GM1-C20
C81H133N7O36	1779.8792	Fuc-GM1-C21
C83H135N7O36	1805.8948	Fuc-GM1-C22
C84H137N7O36	1819.9105	Fuc-GM1-C23
C85H139N7O36	1833.9261	Fuc-GM1-C24
C86H141N7O36	1847.9418	Fuc-GM1-C25
C72H115N7O36	1653.7383	Fuc-GM1-C12
C71H113N7O31	1559.7481	GD3-Ac-C18
C69H111N7O30	1517.7375	GD3-C18
C70H111N7O31	1545.7324	GD3-Ac-C17
C68H109N7O30	1503.7219	GD3-C17
C69H109N7O31	1531.7168	GD3-Ac-C16
C67H107N7O30	1489.7062	GD3-C16
C72H115N7O31	1573.7638	GD3-Ac-C19
C70H113N7O30	1531.7532	GD3-C19
C73H117N7O31	1587.7794	GD3-Ac-C20
C71H115N7O30	1545.7688	GD3-C20
C72H117N7O30	1559.7845	GD3-C21
C74H119N7O31	1601.7951	GD3-Ac-C21
C73H119N7O30	1543.8001	GD3-C22
C75H121N7O31	1615.8107	GD3-Ac-C22
C74H121N7O30	1587.8158	GD3-C23
C76H123N7O31	1629.8264	GD3-Ac-C23
C75H123N7O30	1601.8314	GD3-C24
C77H125N7O31	1643.842	GD3-Ac-C24
C76H125N7O30	1615.8471	GD3-C25

C78H127N7O31	1657.8577	GD3-Ac-C25
C65H101N7O31	1475.6542	GD3-Ac-C12
C63H99N7O30	1433.6436	GD3-C12
C66H103N7O31	1489.6698	GD3-Ac-C13
C64H101N7O30	1447.6593	GD3-C13
C67H105N7O31	1503.6855	GD3-Ac-C14
C65H103N7O30	1461.6749	GD3-C14
C68H107N7O31	1517.7011	GD3-Ac-C15
C66H105N7O30	1475.6906	GD3-C15
C79H124N8O41	1840.7864	GD1a-Ac-C12
C77H122N8O40	1798.7758	GD1a-C12
C80H126N8O41	1854.8	GD1a-Ac-C13
C78H124N8O40	1812.7915	GD1a-C13
C81H128N8O41	1868.8177	GD1a-Ac-C14
C79H126N8O40	1826.8071	GD1a-C14
C82H130N8O41	1882.8333	GD1a-Ac-C15
C80H128N8O40	1840.8228	GD1a-C15
C83H132N8O41	1896.849	GD1a-Ac-C16
C81H130N8O40	1854.8384	GD1a-C16
C84H133N8O41	1909.8568	GD1a-Ac-C17
C82H132N8O40	1868.8541	GD1a-C17
C85H136N8O41	1924.8803	GD1a-Ac-C18
C83H134N8O40	1882.8697	GD1a-C18
C86H138N8O41	1938.8959	GD1a-Ac-C19
C84H136N8O40	1896.8854	GD1a-C19
C87H140N8O41	1952.9116	GD1a-Ac-C20
C85H138N8O40	1910.901	GD1a-C20
C86H140N8O40	1924.9167	GD1a-C21
C88H142N8O41	1966.9272	GD1a-Ac-C21
C87H142N8O40	1938.9323	GD1a-C22
C89H144N8O41	1980.9429	GD1a-Ac-C22
C88H144N8O40	1952.948	GD1a-C23
C90H146N8O41	1994.9585	GD1a-Ac-C23
C89H146N8O40	1966.9636	GD1a-C24
C91H148N8O41	2008.9742	GD1a-Ac-C24
C90H148N8O40	1980.9793	GD1a-C25
C92H150N8O41	2022.9898	GD1a-Ac-C25
C83H132N8O44	1944.8337	Fuc-GD1a-C12
C85H134N8O45	1986.8443	Fuc-Ac-GD1a-C12
C84H134N8O44	1958.8494	Fuc-GD1a-C13
C86H136N8O45	2000.86	Fuc-Ac-GD1a-C13

C85H136N8O44	1972.865	Fuc-GD1a-C14
C87H138N8O45	2014.8756	Fuc-Ac-GD1a-C14
C86H138N8O44	1986.8807	Fuc-GD1a-C15
C88H140N8O45	2028.8913	Fuc-Ac-GD1a-C15
C87H140N8O44	2000.8693	Fuc-GD1a-C16
C89H142N8O45	2042.9069	Fuc-Ac-GD1a-C16
C88H142N8O44	2014.912	Fuc-GD1a-C17
C90H144N8O45	2056.9226	Fuc-Ac-GD1a-C17
C89H144N8O44	2028.9276	Fuc-GD1a-C18
C91H146N8O45	2070.9382	Fuc-Ac-GD1a-C18
C90H146N8O44	2042.9433	Fuc-GD1a-C19
C92H148N8O45	2084.9539	Fuc-Ac-GD1a-C19
C91H148N8O44	2056.9589	Fuc-GD1a-C20
C93H150N8O45	2098.9695	Fuc-Ac-GD1a-C20
C92H150N8O44	2070.9746	Fuc-GD1a-C21
C94H152N8O45	2112.9852	Fuc-Ac-GD1a-C21
C93H152N8O44	2084.9902	Fuc-GD1a-C22
C95H154N8O45	2127.0008	Fuc-Ac-GD1a-C22
C94H154N8O44	2099.0059	Fuc-GD1a-C23
C96H156N8O45	2141.0165	Fuc-Ac-GD1a-C23
C95H156N8O44	2113.0215	Fuc-GD1a-C24
C97H158N8O45	2155.0321	Fuc-Ac-GD1a-C24
C96H158N8O44	2127.0372	Fuc-GD1a-C25
C98H160N8O45	2169.0478	Fuc-Ac-GD1a-C25
C90H141N9O49	2131.8818	GT1b-Ac-C12
C88H139N9O48	2089.8712	GT1b-C12
C91H143N9O49	2145.8975	GT1b-Ac-C13
C89H141N9O48	2103.8869	GT1b-C13
C92H145N9O49	2159.9131	GT1b-Ac-C14
C90H143N9O48	2117.9025	GT1b-C14
C93H147N9O49	2173.9288	GT1b-Ac-C15
C91H145N9O48	2131.9182	GT1b-C15
C94H149N9O49	2187.9444	GT1b-Ac-C16
C92H147N9O48	2145.9338	GT1b-C16
C95H151N9O49	2201.9601	GT1b-Ac-C17
C93H149N9O48	2159.9495	GT1b-C17
C96H153N9O49	2215.9757	GT1b-Ac-C18
C94H151N9O48	2173.9651	GT1b-C18
C97H155N9O49	2229.9914	GT1b-Ac-C19
C95H153N9O48	2187.9808	GT1b-C19
C98H157N9O49	2244.007	GT1b-Ac-C20

C96H155N9O48	2201.9964	GT1b-C20
C99H159N9O49	2258.0227	GT1b-Ac-C21
C97H157N9O48	2216.0121	GT1b-C21
C100H161N9O49	2272.0383	GT1b-Ac-C22
C98H159N9O48	2230.0277	GT1b-C22
C101H163N9O49	2286.054	GT1b-Ac-C23
C99H161N9O48	2244.0434	GT1b-C23
C102H165N9O49	2300.0696	GT1b-Ac-C24
C100H163N9O48	2258.059	GT1b-C24
C103H167N9O49	2314.0853	GT1b-Ac-C25
C101H165N9O48	2272.0747	GT1b-C25
C62H97N7O28	1387.6382	GM2-Ac-C12
C60H95N7O27	1345.6276	GM2-C12
C63H99N7O28	1401.6538	GM2-Ac-C13
C61H97N7O27	1359.6432	GM2-C13
C64H101N7O28	1415.6695	GM2-Ac-C14
C62H99N7O27	1373.6589	GM2-C14
C65H103N7O28	1429.6851	GM2-Ac-C15
C63H101N7O27	1387.6745	GM2-C15
C66H105N7O28	1443.7008	GM2-Ac-C16
C64H103N7O27	1401.6902	GM2-C16
C67H107N7O28	1457.7164	GM2-Ac-C17
C65H105N7O27	1415.7058	GM2-C17
C68H109N7O28	1471.7321	GM2-Ac-C18
C66H107N7O27	1429.7215	GM2-C18
C66H105N7O27	1427.7058	GM2-C18 (d18:2)
C69H111N7O28	1485.7477	GM2-Ac-C19
C67H109N7O27	1443.7371	GM2-C19
C70H113N7O28	1499.7634	GM2-Ac-C20
C68H111N7O27	1457.7528	GM2-C20
C59H96N6O24	1272.6476	GA1-C16
C60H98N6O24	1286.6632	GA1-C17
C61H100N6O24	1300.6789	GA1-C18
C62H102N6O24	1314.6945	GA1-C19
C63H104N6O24	1328.7102	GA1-C20
C50H80N6O17	1036.558	GM4-C16
C51H82N6O17	1050.5736	GM4-C17
C52H84N6O17	1064.5893	GM4-C18
C46H72N6O17	980.4954	GM4-C12
C47H74N6O17	994.511	GM4-C13
C48H76N6O17	1008.5267	GM4-C14

C49H78N6O17	1022.5423	GM4-C15
C53H86N6O17	1078.6049	GM4-C19
C54H88N6O17	1092.6206	GM4-C20
C55H90N6O17	1106.6362	GM4-C21
C56H92N6O17	1120.6519	GM4-C22
C57H94N6O17	1134.6675	GM4-C23
C58H96N6O17	1148.6832	GM4-C24
C59H98N6O17	1162.6988	GM4-C25
C67H108N6O32	1508.7008	2AA-FFHHHN-C12
C68H110N6O32	1522.7165	2AA-FFHHHN-C13
C69H112N6O32	1536.7321	2AA-FFHHHN-C14
C70H114N6O32	1550.7478	2AA-FFHHHN-C15
C71H116N6O32	1564.7634	2AA-FFHHHN-C16
C72H118N6O32	1578.7791	2AA-FFHHHN-C17
C73H120N6O32	1592.7947	2AA-FFHHHN-C18
C74H122N6O32	1606.8104	2AA-FFHHHN-C19
C75H124N6O32	1620.826	2AA-FFHHHN-C20
C76H126N6O32	1634.8417	2AA-FFHHHN-C21
C77H128N6O32	1648.8573	2AA-FFHHHN-C22
C78H130N6O32	1662.873	2AA-FFHHHN-C23
C79H132N6O32	1676.8886	2AA-FFHHHN-C24
C80H134N6O32	1690.9043	2AA-FFHHHN-C25
C49H78N6O19	1054.5322	GA2-C12
C50H80N6O19	1068.5478	GA2-C13
C51H82N6O19	1082.5635	GA2-C14
C52H84N6O19	1096.5791	GA2-C15
C53H86N6O19	1110.5948	GA2-C16
C54H88N6O19	1124.6104	GA2-C17
C55H90N6O19	1138.6261	GA2-C18
C56H92N6O19	1152.6417	GA2-C19
C57H94N6O19	1166.6574	GA2-C20
C58H96N6O19	1180.673	GA2-C21
C59H98N6O19	1194.6887	GA2-C22
C60H100N6O19	1208.7043	GA2-C23
C61H102N6O19	1222.72	GA2-C24
C62H104N6O19	1236.7356	GA2-C25
C47H75N5O19	1013.5056	Gb3-C12
C48H77N5O19	1027.5213	Gb3-C13
C49H79N5O19	1041.5369	Gb3-C14
C50H81N5O19	1055.5526	Gb3-C15
C51H83N5O19	1069.5682	Gb3-C16

C52H85N5O19	1083.5839	Gb3-C17
C53H87N5O19	1097.5995	Gb3-C18
C54H89N5O19	1111.6152	Gb3-C19
C55H91N5O19	1125.6308	Gb3-C20
C56H93N5O19	1139.6465	Gb3-C21
C57H95N5O19	1153.6621	Gb3-C22
C58H97N5O19	1167.6778	Gb3-C23
C59H99N5O19	1181.6934	Gb3-C24
C60H101N5O19	1195.7091	Gb3-C25